MULTIDISCIPLINARY CENTER FOR EARTHQUAKE ENGINEERING RESEARCH

A National Center of Excellence in Advanced Technology Applications

ISSN 1520-295X

Review of Energy Dissipation of Compression Members in Concentrically Braced Frames

by

Kangmin Lee and Michel Bruneau
University at Buffalo, State University of New York
Department of Civil, Structural and Environmental Engineering
Ketter Hall
Buffalo, New York 14260

Technical Report MCEER-02-0005

October 18, 2002

This research was conducted at the University at Buffalo, State University of New York and was supported by the Federal Highway Administration under contract number DTFH61-98-C-00094.

Review of Energy Dissipation of Compression Members in Concentrically Braced Frames

by

Kangmin Lee[1] and Michel Bruneau[2]

Publication Date: October 18, 2002
Submittal Date: February 1, 2002

Technical Report MCEER-02-0005

Task Number 094-C3-3

FHWA Contract Number DTFH61-98-C-00094

1 Graduate Student, Department of Civil, Structural and Environmental Engineering, University at Buffalo, State University of New York
2 Professor, Department of Civil, Structural and Environmental Engineering, University at Buffalo, State University of New York

MULTIDISCIPLINARY CENTER FOR EARTHQUAKE ENGINEERING RESEARCH
University at Buffalo, State University of New York
Red Jacket Quadrangle, Buffalo, NY 14261

Preface

The Multidisciplinary Center for Earthquake Engineering Research (MCEER) is a national center of excellence in advanced technology applications that is dedicated to the reduction of earthquake losses nationwide. Headquartered at the University at Buffalo, State University of New York, the Center was originally established by the National Science Foundation in 1986, as the National Center for Earthquake Engineering Research (NCEER).

Comprising a consortium of researchers from numerous disciplines and institutions throughout the United States, the Center's mission is to reduce earthquake losses through research and the application of advanced technologies that improve engineering, pre-earthquake planning and post-earthquake recovery strategies. Toward this end, the Center coordinates a nationwide program of multidisciplinary team research, education and outreach activities.

MCEER's research is conducted under the sponsorship of two major federal agencies, the National Science Foundation (NSF) and the Federal Highway Administration (FHWA), and the State of New York. Significant support is also derived from the Federal Emergency Management Agency (FEMA), other state governments, academic institutions, foreign governments and private industry.

The Center's Highway Project develops improved seismic design, evaluation, and retrofit methodologies and strategies for new and existing bridges and other highway structures, and for assessing the seismic performance of highway systems. The FHWA has sponsored three major contracts with MCEER under the Highway Project, two of which were initiated in 1992 and the third in 1998.

Of the two 1992 studies, one performed a series of tasks intended to improve seismic design practices for new highway bridges, tunnels, and retaining structures (MCEER Project 112). The other study focused on methodologies and approaches for assessing and improving the seismic performance of existing "typical" highway bridges and other highway system components including tunnels, retaining structures, slopes, culverts, and pavements (MCEER Project 106). These studies were conducted to:

- assess the seismic vulnerability of highway systems, structures, and components;
- develop concepts for retrofitting vulnerable highway structures and components;
- develop improved design and analysis methodologies for bridges, tunnels, and retaining structures, which include consideration of soil-structure interaction mechanisms and their influence on structural response; and
- develop, update, and recommend improved seismic design and performance criteria for new highway systems and structures.

The 1998 study, “Seismic Vulnerability of the Highway System” (FHWA Contract DTFH61-98-C-00094; known as MCEER Project 094), was initiated with the objective of performing studies to improve the seismic performance of bridge types not covered under Projects 106 or 112, and to provide extensions to system performance assessments for highway systems. Specific subjects covered under Project 094 include:

- development of formal loss estimation technologies and methodologies for highway systems;
- analysis, design, detailing, and retrofitting technologies for special bridges, including those with flexible superstructures (e.g., trusses), those supported by steel tower substructures, and cable-supported bridges (e.g., suspension and cable-stayed bridges);
- seismic response modification device technologies (e.g., hysteretic dampers, isolation bearings); and
- soil behavior, foundation behavior, and ground motion studies for large bridges.

In addition, Project 094 includes a series of special studies, addressing topics that range from non-destructive assessment of retrofitted bridge components to supporting studies intended to assist in educating the bridge engineering profession on the implementation of new seismic design and retrofitting strategies.

The research discussed in this report was performed within Project 094, Task C3-3, “Seismic Retrofit of Steel Truss Piers.” In this research, the existing experimental data on the behavior of concentrically braced frames (CBF) is reviewed to assess the extent of hysteretic energy achieved by bracing members in compression in past tests, and the extent of degradation of the compression force upon repeated cycling loading. The response of single story buildings and other case studies are also investigated to see trends in response and to develop a better understanding of the impact of some design parameters on the seismic response of CBF. While it is recognized that many parameters have an influence on the behavior of braced frames, the focus of this study is mostly on quantifying energy dissipation in compression and its effectiveness on seismic performance. Based on the experimental data review from previous tests, the normalized energy dissipation is found to typically decrease with increasing normalized displacements. The normalized degradation of the compression force envelope depends on KL/r and is particularly severe for W-shape braces. Based on dynamic analyses of a single story braced frame, a bracing member designed with bigger R and larger KL/r results in a lower normalized cumulative energy ratio in both cases.

ABSTRACT

Concentrically Braced frames (CBF) are expected to dissipate energy through yielding and post-buckling hysteresis behavior of bracing members during earthquake loads. The design and detailing requirements of seismic provisions for CBF were specified based on the premise that bracing members with low KL/r and b/t will have superior seismic performance. However, relatively few tests investigate the cyclic behavior of CBF. It is legitimate to question whether the compression member of CBF plays as significant a role as what has been typically assumed explicitly by the design provisions.

In this research, the existing experimental data is reviewed to assess the extent of hysteretic energy achieved by bracing members in compression in past tests, and the extent of degradation of the compression force upon repeated cycling loading. The response of single story buildings and other case studies are also investigated to see trends in response and to develop a better understanding of the impact of some design parameters on the seismic response of CBF. While it is recognized that many parameters have an influence on the behavior of braced frames, the focus of this study is mostly on quantifying energy dissipation in compression and its effectiveness on seismic performance.

Based on the experimental data review from previous tests, the normalized energy dissipation is found to typically decrease with increasing normalized displacements. The normalized degradation of the compression force envelope depends on KL/r and is particularly severe for W-shape braces. Based on dynamic analyses of single story braced frame, a bracing member designed with bigger R and larger KL/r result in lower normalized cumulative energy ratio in both cases.

ACKNOWLEDGEMENTS

This research was conducted by the University at Buffalo and was supported by the Federal Highway Administration under contract number DTFH61-98-C-00094 to the Multidisciplinary Center for Earthquake Engineering Research. Information generated in this report is in support of a coordinated bridge research project; some analyses refer to building examples previously analyzed by others in absence of other comparable data set for bridges.

TABLE OF CONTENTS

TABLE OF CONTENTS (continued)

LIST OF FIGURES

FIGURE **TITLE** **PAGE**

LIST OF FIGURES (continued)

FIGURE **TITLE** **PAGE**

LIST OF FIGURES (continued)

FIGURE **TITLE** **PAGE**

LIST OF TABLES

TABLE **TITLE** **PAGE**

NOTATIONS

A	Cross Sectional Area, in^2
A_g	Gross Area, in^2
B	Gross Width of the Section, in
b/t	Width-to-Thickness Ratio
C	Numerical Constant Depending on Natural Period of the Structure and Soil Type
C_e	Elastic Seismic Response Coefficient
C_r	First Buckling Load of a Bracing Member, kips
C_r'	Design (Reduced) Buckling Capacity of a Bracing Member, kips
C_r''	Compression Capacity of a Brace when the Frame Reaches it's Maximum Sway Deformation, kips
C_{rn}''	Compressive Strength reached at the Displacement δ_n, kips
$C_r''/C_r(1^{st})$	Normalized Compressive Strength Obtained the First Time the Maximum Displacement, δ_n, is reached
$C_r''/C_r(Last)$	Normalized Compressive Strength Obtained During the Last Cycle of Testing
$C_r''/C_r(1^{st}/Last)$	Ratio of $C_r''/C_r(1^{st})$ to $C_r''/C_r(Last)$
C_s	Seismic Coefficient
	Numerical Coefficient Obtained from the Test Results
D	Dead Load, kips
	Gross Depth of the Section, in
E	Modulus of Elasticity of Steel, ksi
E_C	Energy Dissipation of a Brace in Compression, kip-in
E_C / E_T	Compressive Energy Normalized by the Corresponding Tensile Energy
E_T	Energy Dissipation of a Brace in Tension, kip-in
F_y	Specified Yield Stress of Steel, ksi
F_{ye}	Expected Yield Stress of Steel, ksi
I	Seismic Importance Factor
	Moment of Inertia, in^4

KL/r	Slenderness Ratio
L	Live Load, kips
	Bracing Member Length, in
N_f	Fracture Life of Tube in Terms of Standard Cycles
P_n	Nominal Axial Strength, kips
P_{nt}	Nominal Axial Tensile Strength of a Brace, kips
Q_E	Effective Horizontal Seismic Forces Produced by the Base Shear, V
R	Structural Response Modification Factor
R_d	Reduction Factor that Accounts for Inelastic Behavior (a Value Related to the Ductile Performance of Structural Systems)
R_w	Structural System Coefficient
R_y	Ratio of the Expected Yield Strength (F_{ye}) to the Specified Yield Strength (F_y)
S	Snow Load, kips
	Seismic Site Coefficient
t	Thickness of a Section, in
T_1	Fundamental Period of a Structure, second
T_n	Natural Period of a Structure, second
T_y	Tensile Yield Load of a Brace, kips
V	Base Shear of a Structure, kips
W	Total Dead Load and Applicable Portion of Other Loads, kips
Z	Seismic Zone Factor
δ	Axial Deformation of a Brace, in
δ_B	Axial Displacement at the Theoretical Onset of Elastic Buckling of the Brace, in
δ_n	Maximum Compressive Displacement at n^{th} Cycle, in
δ_T	Axial Displacement at the Onset of Brace Yielding in Tension, in
δ/δ_B	Normalized Axial Displacement in Compression
Δ_1	Tension Deformation from the Load Reversal Point to $P_y/3$ Point
Δ_2	Tension Deformation from $P_y/3$ Point to the Unloading Point
Δ_f	Fracture Life of Tube Proposed by Lee and Goel (1987)
Δ_y	Tensile Yield Displacement of Tube

Δ^{*}_{f}	Fracture Life of Tube Proposed by Archambault et al. (1995)
Ω_O	Horizontal Seismic Overstrength Factor
Φ_c	Resistance Factor for Compression

SECTION 1

INTRODUCTION

Braced frames have been used frequently to provide lateral resistance for wind and earthquakes, particularly in the eastern United States. During earthquakes, braced frames are expected to yield and dissipate energy through post-buckling hysteresis behavior of bracing members. However, to achieve this behavior, special ductile detailing is required. Many braced frame structures designed without such ductile detailing consideration have suffered extensive damage in past earthquakes, including failure of bracing members and their connections. Seismic provisions for the analysis, design, and detailing of Concentrically Braced Frames (CBF) were gradually introduced into seismic regulations and guidelines in California in the late 1970's (SEAOC 1978) and on a nationwide basis in the early 1990's (AISC 1992). In these documents, design and detailing requirements were specified based on the premise that bracing members with low KL/r and b/t will have superior seismic performance. The philosophy was that low KL/r ensures that braces in compression can significantly contribute to energy dissipation. Upon buckling, flexure develops in the compression member and a plastic hinge eventually develops at the middle length of the brace, i.e., at the point of maximum moment. It is through the development of this plastic hinging that a member in compression can dissipate energy during earthquakes. Furthermore, in these code provisions, low b/t limits were prescribed to prevent brittle failure due to local buckling. Indeed, the reversed cyclic loading induced by earthquakes leads to repeated buckling and straightening of the material at the local buckling location, which combined with very high strains present at the tip of the local buckle, precipitate low cycle fatigue.

Although much attention has been paid to Moment Resisting Frames (MRF) after the 1994 Northridge earthquake, with a large number of tests conducted since, relatively fewer tests exist that investigate the cyclic behavior of CBF. This is surprising given the reliance imposed on compression brace energy dissipation by the existing codes and guidelines. Furthermore, given the fact that for a relatively constant plastic hinge moment capacity at mid-span of the brace, the axial force applied to brace will decrease as a function of the amplitude of buckling, resulting in strength degradation of the structural member in compression. It is legitimate to question whether the compression member plays as significant a role as what has been typically assumed explicitly by the design provisions. As a result, here, the existing experimental data is reviewed to assess the extent of hysteretic energy achieved by bracing members in compression in past tests, and the extent of degradation of the compression force upon repeated cycling loading. The response of single story buildings and other case studies are also investigated to see trends in response and to develop a better understanding of the impact of some design parameters on the seismic response of CBF.

This report is organized in six sections. SECTION 2 describes the literature review of experimental research on the behavior of bracing members and shows how experimental data have been collected and summarized, as part of the work reported here. SECTION 3 describes theoretical bracing models, the characteristics of a case study building (geometry and applied loads), and describes how bracing members were designed in this case study. SECTION 4 presents the results of limited sensitivity analyses to assess the significance of some design parameters on the seismic behavior of bracing members. In SECTION 5, the summary and conclusions of this study are presented. Finally, references are in SECTION 6.

SECTION 2

LITERATURE REVIEW

2.1 Review of Current Codes and Provisions

Regulations and guidelines for the seismic design of CBF can be found in the Recommended Lateral Force Requirements (SEAOC, 1999), NEHRP Recommended Provisions for Seismic Regulations for New Buildings (BSSC, 1997), and AISC Seismic Provisions (AISC, 1997). Conceptually, in all of these seismic provisions, the brace force that corresponds to elastic response of the structure is first calculated. It is then divided by a Structural Response Modification Factor, R, which quantifies the relative ability of a structural system to dissipate energy in a stable manner during earthquakes. Typically, MRFs have been assigned the largest response modification factor due to the ability of their energy dissipating elements (beam-to-column connections) to develop full moment-rotation hysteretic behavior, approximating very closely the ideal desirable hysteretic behavior up to large structural drifts and undergoing only slow progressive strength degradation at very large drifts (this being for a well detailed connection, obviously for a post-Northridge type detail). Generally, braced frames were assigned R factors on the order of 75% of the maximum value assigned to moment frames. This penalty is attributed mainly as a consequence of the less ideal energy dissipation provided by the compression brace, the observed pinching of the hysteretic curves of the brace frame due to the strength degradation of the compression brace, and the absence of effective strength hardening as typically occurs in moment frames.

Typically, the R factor is defined as:

$$R = R_d \, \Omega_0 \tag{2.1}$$

where R_d is a reduction factor that accounts for inelastic behavior (a value related to the ductile performance of structural systems) and Ω_0 is a reduction factor accounting empirically for inherent causes of structural overstrengths that elude accurate calculation. R values for various types of structural steel systems designed per the LRFD design philosophy (Table I-C4-1 from AISC Seimic Provisions for Structural Steel Buildings 1997, based upon similar information in the 1997 NEHRP Provisions) are shown in Table 2.1. For concentrically braced frames, Ω_0 is specified as 2.0 (it is 2.5 and 3.0 respectively for eccentrically braced frames and moment-frames).

Table 2.1 Design factors for structural steel systems (Table I-C4-1 from AISC (1997) based upon similar information in the 1997 NEHRP Provisions)

Structural Systems	R	C_d
Braced Frame Systems:		
Special Concentrically Braced Frames (SCBF)	6	5
Ordinary Concentrically Braced Frames (OCBF)	5	4½
Eccentrically Braced Frames (EBF)		
With moment connections at columns away from link	8	4
Without moment connections at columns away from link	7	4
Moment Frame Systems:		
Special Moment Frames (SMF)	8	5½
Intermediate Moment Frames (IMF)	6	5
Ordinary Moment Frames (OMF)	4	3½
Special Truss Moment Frames (STMF)	7	5½
Dual Systems with SMF Capable of Resisting 25 Percent of V:		
Special Concentrically Braced Frames (SCBF)	8	6½
Ordinary Concentrically Braced Frames (OCBF)	6	5
Eccentrically Braced Frames (EBF)		
With moment connections at columns away from link	8	4
Without moment connections at columns away from link	7	4
Dual Systems with IMF* Capable of Resisting 25 Percent of V:		
Special Concentrically Braced Frames (SCBF)	6	5
Ordinary Concentrically Braced Frames (OCBF)	5	4½

*OMF is permitted in lieu of IMF in Seismic Design Categories A, B and C.

Structural systems with large energy dissipation capacity have large R_d values and hence are assigned higher R values, resulting in design for lower forces than systems with relatively limited energy dissipation capacity. The ductility reduction factor, R_d, is therefore tied to the inelastic characteristics of a structural system, such as energy dissipation and strength degradation. A structural system designed with a high R value but having a small energy dissipation capacity can fail prematurely when yielding during an earthquake. Therefore, the values of R have been established considering these factors, coupled with engineering judgment (ATC, 1995).

It is interesting that the design requirements for CBF have changed considerably over the various editions of the AISC Seismic Provisions from 1992 up until recent changes in Supplement No. 2 of the 1997 edition of AISC Seismic Provisions (AISC, 2000) in spite of little new experimental data. This evolution is reviewed below.

2.1.1 1992 Edition of AISC Seismic Provisions

The 1992 AISC Seismic Provisions for Structural Steel Buildings included requirements for CBF designed with a R factor of 5. These requirements addressed issues related to width-to-thickness ratio, slenderness of brace members, connection requirements, and frame configuration. More specifically:

- Brace slenderness, L/r, was limited to $720/\sqrt{F_y}$.

- The width-to-thickness ratio of brace elements had to be compact or non-compact, but not slender, using the compactness requirements limits defined by the AISC Load and Resistance Factor Design Specification for Structural Steel Buildings (AISC, 1993), with the exception that more stringent requirements were specified for circular sections ($1300/F_y$) and rectangular tubes ($110/\sqrt{F_y}$).

- The design strength of bracing member in axial compression was limited to 80 % of the calculated value, $\Phi_c P_n$, to account for the strength degradation of braces subjected to repeated cyclic loading. It is noteworthy that this reduced compression strength, C_r', is close to the average value obtained when using the following equation specified by the Recommended Lateral Force Requirements and Commentary (SEAOC, 1990)

$$C_r' = \frac{C_r}{1+0.50\left(\dfrac{KL}{\pi r}\sqrt{\dfrac{0.5F_y}{E}}\right)} = \frac{C_r}{1+0.5\left(\dfrac{KL/r}{C_c}\right)} \tag{2.2}$$

where C_r' is the design (reduced) buckling capacity, C_r is the first buckling load of bracing member, KL/r is the slenderness ratio, F_y is the yield stress of brace, and E is Young's modulus. For example, for an A36 steel brace with a slenderness ratio equal to 0, C_r' = C_r. If the slenderness ratio is increased to $720/\sqrt{36} = 120$, C_r' = $0.68C_r$. Hence, the value of 0.8 specified by AISC (1992) is approximately equal to the average reduction factor over the permissible range of KL/r for this type of system (although it is not known whether this was the rationale supporting the choice of this 0.8 factor). Some equations of buckling capacity suggested by codes and recommendations are shown in Figure 2.1.

- All brace connections were required to have sufficient strength to be able to develop full yielding (i.e. A_gF_y) of the brace.

- V and Inverted-V type bracing configurations were permitted provided that the brace members were designed for at least 1.5 times the required strength otherwise specified. The beam intersected by braces had to be continuous between columns and be capable of supporting all tributary dead and live loads assuming the bracing will not be present. K bracing were permitted following design philosophy similar to that of V and Inverted-V type brace frame.

- The above requirements could be waved for low-rise buildings of two stories or less as well as in roof structures under certain conditions.

2.1.2 1997 Edition of AISC Seismic Provisions

The premise driving changes in the design requirements of braced frames in the 1997 edition of the AISC seismic provisions was that CBF possess ductility far in excess of that previously ascribed to such systems, and that energy can be effectively dissipated after the onset of global buckling only if brittle failure due to local buckling, stability problems and connection failures are prevented. As a result, a new category, Special Concentrically Braced Frames (SCBF), was added to 1997 edition of AISC Seismic Provisions (AISC, 1997). SCBF were intended to exhibit superior stable and ductile behavior during major earthquakes and the requirements for braced frames specified in the previous edition (AISC, 1992) were retained for the design of Ordinary Concentrically Braced Frames (OCBF). The new seismic provisions included the following key features:

- Higher R factor of 6 was assigned to SCBF, while a R factor of 5 was specified for the OCBF (equivalent to the R factor used for CBF in 1992 edition).

- The slenderness ratio (KL/r) limit was raised to ($1000/\sqrt{F_y}$) for SCBF, but remained ($720/\sqrt{F_y}$) for OCBF. Tang and Goel (1989) and Goel and Lee (1992) showed that the post-buckling cyclic buckling fracture life of bracing members generally increase with an increase in KL/r, which justified the increased limit while maintaining a reasonable level of compressive strength.

- The brace strength reduction factor of 0.8 was eliminated for the SCBF, because this factor was deemed to have had little influence on the seismic response of CBF when superior ductile behavior was insured (as for SCBF). This 0.8 factor however remained for the design of OCBF.

- The width-to-thickness ratio (b/t) limits remained unchanged except for the added compactness limit for angles (reduced to $52/\sqrt{F_y}$ in seismic applications).

- The ratio of the expected yield strength (F_{ye}) to the minimum specified yield strength (F_y), R_y, was added to the design connection force (A_gF_y) for both OCBF and SCBF to recognize the material overstrength of the steel grade used.

- K bracing was not permitted for SCBF because the resulting unbalanced lateral forces from the braces that would be applied at mid-height of columns for this type of system may contribute to undesirable column failures.

- The V-type and Inverted-V-type OCBF design requirements followed the provisions specified for CBF of this configuration in the 1992 edition of the AISC Seismic Provisions. However, for SCBF, the requirement that braces in V-type and Inverted-V-type braced frames be designed for at least 1.5 times the required strength was eliminated. Because columns were not required to be designed following the capacity-design philosophy, the concern was that overly-strong bracing could lead to buckling of the columns in a frame, and may thus lead to collapse. Furthermore, beams in SCBF V-type and Inverted-V-type braced frames were required to be designed for the full unbalanced forces in braces at large inelastic deformations, namely A_gF_y in the tension brace and $0.3\Phi_cP_n$ in the compression brace. Consequently to these two revisions, braced frame with these type of configurations have lighter braces, but significantly heavier beams.

2.1.3 2001 Revisions to the 1997 Edition of AISC Seismic Provisions

Recently, the 1997 edition of the AISC Seismic Provisions (AISC, 1997) was revised. Requirements for CBF were modified to simplify the provisions, as there were relatively few differences in the 1997 edition of AISC Seismic Provisions between OCBF and SCBF, and because it was believed that buildings in more severe seismic zones and having OCBF will not behave as well as desirable during earthquakes. These changes can be summarized as follows:

- The OCBF provisions, in the 1997 edition of the AISC Seismic Provisions were eliminated, except for the special dispensation (in Section 14.5) for low-rise buildings. Therefore it is the intent that SCBF be used for all braced frames where significant ductility is needed. For the special case of low and light-weight buildings where OCBF are still permitted, it was judged that satisfactory behavior could be ensured by the use of the special load combinations which were present in the AISC seismic provisions since 1992. These equations, shown in Eq. 2.3 and 2.4, magnify the seismic forces by a value equivalent to the estimated structural overstrength, which results in an effective R of about 2.5, deemed to provide sufficient strength to preclude the need for significant ductility of the system. These special load combinations are:

$$1.2D + 0.5L + 0.2S + \Omega_0 Q_E \tag{2.3}$$

$$0.9D - \Omega_0 Q_E \tag{2.4}$$

where Ω_0 is the overstrength factor, D, L, and S are the dead, live, and snow load respectively, and Q_E is the horizontal component of the specified earthquake forces.

- In all cases, the design strength of brace connections shall equal or exceed the expected tensile strength of the braces:

$$P_{nt} = R_y F_y A_g \tag{2.5}$$

where P_{nt} is the nominal tensile strength of braces, R_y is the ratio of expected yield strength F_{ye} to the minimum specified yield strength F_y, and A_g is the gross area of braces. Note that the AISC Seismic Provisions, 1997 allowed connections to be designed for either the value obtained by Eq. 2.5 or "the maximum force, indicated by analysis, that can be transferred to the brace by the system", which in the latter case could have resulted in a strength that may be less than that of the braces themselves.

- All V-type and Inverted-V-type braced frames must be designed as SCBF following the same requirements as specified for SCBF in the 1997 edition of the AISC Seismic Provisions.

- Braces with KL/r greater than $720/\sqrt{F_y}$ are not be permitted in V or Inverted-V configurations.

The above changes in AISC Seismic Provisions for CBF, from the 1992 edition to the latest 2001 revisions to the 1997 edition, are summarized in Table 2.2.

Table 2.2 Changes in AISC CBF Provisions from 1992 to 2001

Categories	1992 Edition	1997 Edition		2001 Provisions*	
		OCBF	SCBF	OCBF**	SCBF
R	5	5	6	5	6
C_r’	$0.8\Phi_c P_n$	$0.8\Phi_c P_n$	$\Phi_c P_n$	$0.8\Phi_c P_n$	$\Phi_c P_n$
$(KL/r)_{max.}$	$\frac{720}{\sqrt{F_y}}$	$\frac{720}{\sqrt{F_y}}$	$\frac{1000}{\sqrt{F_y}}$	$\frac{720}{\sqrt{F_y}}$	$\frac{1000}{\sqrt{F_y}}$
$(b/t)_{max.}$	$\frac{1300}{F_y}$ for ○ $\frac{110}{\sqrt{F_y}}$ for □	$\frac{52}{\sqrt{F_y}}$ for L $\frac{1300}{F_y}$ for ○ $\frac{110}{\sqrt{F_y}}$ for □	$\frac{52}{\sqrt{F_y}}$ for L $\frac{1300}{F_y}$ for ○ $\frac{110}{\sqrt{F_y}}$ for □	$\frac{52}{\sqrt{F_y}}$ for L $\frac{1300}{F_y}$ for ○ $\frac{110}{\sqrt{F_y}}$ for □	$\frac{52}{\sqrt{F_y}}$ for L $\frac{1300}{F_y}$ for ○ $\frac{110}{\sqrt{F_y}}$ for □
Connection Force***	$A_g F_y$	$R_y A_g F_y$	$R_y A_g F_y$	$R_y A_g F_y$	$R_y A_g F_y$

* All the provisions for OCBF were eliminated except for Low-Rise Building provision

** Low-Rise and Roof Structures only

*** Where R_y is the ratio of expected yield strength (F_{ye}) to the minimum specified yield strength (F_y)

2.2 Brace Behavior and Design Issues

From the above, it appears that until the 1997 edition of the AISC Seismic Provisions, the emphasis was on promoting stocky braces. However, there exists a compelling argument that slender braces in some instances could have desirable behavior in the perspective that elastic global buckling means no damage to braces in compression. Hence, for a brace with large slenderness ratio, there would be no need to consider C_r’ since it would provide no energy dissipation in compression and no loss of compression capacity upon repeated cyclic loading. Interestingly, Eq. (2.2) would not predict this correctly. Furthermore, in absence of plastic hinging in the middle of the brace, there is no need to be concerned about low cycle fatigue life of the brace due to local buckling at that location.

Another issue that is debatable is the relevance of the factor C_r' for braces that are stockier and do yield in compression. In that case, the capacity of the brace in compression when the entire frame reaches it's maximum sway deformation, which will be defined as C_r" here, is more relevant than C_r'. At the plastic hinge that develops in the middle of the brace, C_r" drops as deformation increases. This means that at maximum sway, when the tension brace has yielded, only a small fraction of the original compression buckling strength of the other brace is effective. This drop in axial resistance of the brace after formation of plastic hinge is more severe for slender inelastic braces.

In light of these facts, one could argue that the design provisions should accurately account for the above effects. However no data on C_r" related to KL/r could be found in the literature. Likewise, if energy dissipation is alleged to be so significant, it is surprising that the energy dissipation of braces in compression has never been quantified as part of extensive parametric experimental studies. To provide what seems to be important missing data, past experimental results are reviewed to quantify the energy dissipation of braces in compression (which is obtained by the compression force times the axial deformation as expressed graphically by the shaded area labeled E_C in Figure 2.3), and loss of compression strength, at various magnitudes of the axial deformation in compression, δ, as a function of KL/r, and for various types of structural shapes.

2.3 Experimental Data on the Hysteretic Energy and Strength Degradation of Braces

The experimental data on cyclic testing of braces have been reviewed, to the extend possible, to quantify the energy dissipation of braces in compression and loss of compression strength at various magnitudes of compressive axial displacements. For this purpose, experimental reports by Jain, Goel, and Hanson (1978), Black, Wenger, and Popov (1980), Zayas, Popov, and Mahin (1980), Astaneh-Asl, Goel, and Hanson (1982), Archambault, Tremblay, and Filiatrault (1995), Leowardi and Walpole (1996), and Walpole (1996) were collected. However, some data were excluded from review. First, bracing members tested as parts of X braced frames were not considered, because of the difficulty in accurately defining the KL/r values of these braces. Second, test specimens of hollow structural shapes built-up using double angles and or double channels welded toe-to-toe were excluded, because these were typically reported to fail at their connections, resulting in non-conventional hysteretic behavior. Third, concrete filled tubular sections were also excluded, as they were considered to be a special case beyond the scope of this study. Finally, note that in some publications (journals and conference articles), the figures were hard to read because of their small size, and the technical reports and dissertations from which these figures originated could not be easily obtained. The resulting data set considered in this study is summarized in Table 2.3, described in terms of number of braces tested for each type of structural members. Furthermore, the results of this study will be made available on the MCEER User's Network, making it possible for other investigations to expand the data set in the future.

Table 2.3 Data set reviewed

Reference	Section Types**							Total
	W	A	DA	DC	T	P	WT	
Black et al.(1980)	9	-	4	1	3	5	2	24
Zayas et al.(1980)	-	-	-	-	-	6	-	6
Lee and Goel (1987)	-	-	-	-	7*	-	-	7*
Jain et al.(1978)	-	3	-	-	6	-	-	9
Astaneh-Asl et al.(1982)	-	-	14	-	-	-	-	14
Archambault et al.(1995)	-	-	-	-	7	-	-	7
Leowardi and Walpole (1996)	3	-	-	-	-	-	-	3
Walpole(1996)	-	-	-	-	3	-	-	3
Total	12	3	18	1	26	11	2	73

* Energy dissipation could not be calculated following the method outlined in this report due to the peculiar testing sequence adapted by Lee and Goel (1987).

** Section Types

W : Wide Flange A : Single Angle T : Tube(Hollow)

P : Pipe WT : Structural Tee TC : Tube(Concrete Filled)

DA : Double Angle DC : Double Channel

Here, all quantitative information on energy dissipation and strength degradation has been generated from the hysteretic force-axial deformation curves of bracing members. A typical hysteretic curve for a brace tested under cyclic axial loading is shown in Figure 2.2. Note that in all cases, only the graphical data were available, and that quantification was achieved directly from those figures (although some were photocopied at a magnified scale to enhance precision of the readings).

2.3.1 Energy Dissipation of Brace in Compression

The energy dissipation of a brace for one compression cycle, E_C, is equal to the work produced by the compression force times the axial deformation, δ. As the compression decreases under increasing axial deformations, the energy can be obtained graphically by calculating the area under the force-axial deformation curve, as shown in Figure 2.3. Here, because the energy corresponding to each hysteretic loop is considered, note that the axial deformation in compression, δ, is measured from the point of zero member force (which may not correspond to the original zero displacement position) up to the point of maximum compressive deformation, as illustrated in Figure 2.4.

Furthermore, to facilitate comparison between results from various experiments, all results are expressed in a normalized manner. The normalized compressive energy, E_C/E_T, is obtained by dividing the compressive energy by the corresponding tensile energy, E_T, defined as the energy that would have been dissipated by the member in tension if the same maximum axial displacement was reached during unloading of the member after its elongation. This corresponding E_T is illustrated in Figure 2.3. Likewise, the axial displacements are normalized by the axial displacement value attained at the corresponding theoretical elastic buckling of the brace, δ_B. This value is defined as:

$$\delta_B = \frac{C_r L}{AE} \tag{2.6}$$

where L is the length of the specimen, A is the cross sectional area of the specimen, E is Young's modulus (=29000 ksi), and C_r is the experimental buckling load as presented in Figure 2.5.

Note that the value of δ_B is limited to δ_T to account for stocky members that yield in compression prior to buckling, where δ_T is the axial displacement attained when the brace yields in tension, and defined as:

$$\delta_T = \frac{T_y L}{AE} \tag{2.7}$$

where T_y is the tensile yield load defined as:

$$T_y = AF_y \tag{2.8}$$

and where F_y is the yield stress from the results of coupon test.

The normalized energy dissipated in compression during each hysteretic cycle is calculated for all the tests considered in this study. Detailed numerical results are provided in Appendix A for an example case; the complete set of results will be made available on the MCEER User's Network web site. A typical resulting plot of normalized energy as a function of normalized axial deformation is shown in Figure 2.6.

2.3.2 Strength Degradation of Brace in Compression

A number of manipulations were necessary to quantify the strength degradation of a brace upon repeated cycling. First, the compression excursions were extracted from the complete hysteretic force-displacement curve obtained from a test, and overlaid to start from the same zero displacement, as shown in Figure 2.5. As schematically shown in this figure, for the tests considered in the database, the magnitude of axial deformations typically increases upon subsequent cycles. In the first cycle, beyond first buckling (defined experimentally as C_r), compressive strength of the brace progressively decreases; At the point of maximum displacement for that compressive excursion, δ_1, the value of C_{r1}'' is reached, the numeral subscript indicating the cycle number. Hence, for any given cycle "n", the compressive strength C_{rn}'' is reached at the maximum displacement δ_n (note that only cycles that produce displacements exceeding the previously obtained values are considered by this procedure). These value of C_r'' are then divided by C_r for normalization. This normalized strength is labeled C_r''/C_r(first), the qualifier "first" implying "the strength obtained the first time this displacement is reached". Figure 2.7 shows a typical curve obtained following this procedure. That curve can be considered a normalized force-displacement envelope of the brace in compression. Note that notation C_r" is used to avoid confusion with the term C_r' which has been used in other codes and publications (CSA 1994 and Bruneau et al., 1998) and has a different meaning.

Strength degradation upon repeated cycling also occurs over the entire range of brace deformations, as exhibited by the force-deformation curves shown in Figure 2.5. As such, the brace compressive strength recorded during the last cycle of testing is also of interest. It can be calculated at each of the previously considered displacement points, δ_n, as shown in Figure 2.8, giving results as typically shown in Figure 2.9. This normalized strength is labeled C_r''/C_r(last), the qualifier "last" implying "the strength obtained during the last cycle of testing".

Using the same displacement points to calculate both C_r''/C_r(first) and C_r''/C_r(last) makes it possible to calculate the ratio of these values. A large ratio indicates a considerable drop in strength at a specific displacement δ/δ_B, whereas a lower ratio expresses a rather stable strength degradation from the first to last cycle. A typical result is shown in Figure 2.10. Note that in this report (and for the data on MCEER User's web site), Figures 2.6, 2.7, 2.9, and 2.10 are typically presented together for each case or group considered, as shown in Figure 2.11 for illustration purposes.

2.3.3 Fracture

Another factor that impacts behavior of braces is fracture upon local buckling. As indicated earlier, compression energy dissipation develops through plastic flexural hinging at mid-span of the brace. The large plastic curvatures that typically develop at that location can potentially lead to local buckling. Upon repeated cyclic loading, the local buckling and straightening of the material at that location induce cracks that may propagate and lead to fracture. No new models of this behavior are proposed here, but two existing models will be considered in SECTION 4 when reviewing analytical results on the behavior of braces. However, at this time, Table 2.4 reports when fractures were observed for the specimens reviewed in this study.

Table 2.4 Summary of information on the experimental data for braces

KL/r	Reference	Test ID (Type)**	$(\delta/\delta_B)_{max}$	δ_T/δ_B	δ/δ_T	Reported Local Buckling*	Reported Fracture*
0 – 40	Zayas	5(P)	12.34	0.97	12.96	X	
		6(P)	15.83	1.02	15.56	X	X
	Lee***	2(T)	3.75	1.11	3.38	X	X
		3(T)	3.47	0.80	4.34	X	X
		8(TC)	5.27	0.92	5.71		
	Jain	4(T)	18.53	1.68	11.02		
	Leowardi	3(W)	30.86	1.03	29.93		
	Walpole	3(T)	8.29	1.21	6.85		
40 – 80	Black	2(W)	29.75	1.23	24.11		
		7(W)	19.87	1.13	17.61	X	
		9(DA)	5.31	0.90	5.87	X	
		19(W)	9.68	0.98	9.84		
		21(P)	19.67	1.08	17.17	X	
	Zayas	1(P)	15.99	1.37	11.63	X	
		2(P)	12.71	1.13	11.24	X	X
		3(P)	2.75	1.55	1.77	X	X
		4(P)	4.89	1.88	2.60	X	X
	Lee***	1(T)	3.97	1.21	3.29	X	X
		4(T)	8.26	1.16	7.12	X	X
		5(T)	12.74	1.71	7.43	X	X
		6(T)	6.41	1.26	5.09	X	X
		7(T)	5.65	1.24	4.55	X	X
		9(TC)	5.09	0.74	6.86	X	X
		10(TC)	4.79	0.74	6.45	X	X
		11(TC)	9.73	0.98	9.88	X	X
		12(TC)	6.78	1.04	6.53	X	X
		13(TC)	9.26	1.11	8.33	X	X
	Jain	1(T)	22.42	1.93	11.64		
		9(T)	21.64	1.81	11.93		
	Leowardi	2(W)	30.73	1.14	26.99		
	Walpole	2(T)	16.34	1.22	13.39		
80 – 120	Black	3(W)	9.53	1.17	8.11		
		4(W)	24.28	1.22	19.94		
		5(W)	33.79	1.63	20.75		
		8(DA)	23.40	1.40	16.77	X	
		12(WT)	30.89	1.39	22.16	X	
		13(WT)	29.26	1.39	21.12		
		14(P)	13.25	1.28	10.32		
		15(P)	25.41	1.38	18.39		
		16(P)	48.41	1.23	39.30		
		17(T)	20.11	1.73	11.65		
		18(T)	17.77	1.87	9.52		
		20(DA)	11.19	1.55	7.21		X(Stitch)
		22(T)	10.68	2.44	4.37		
		23(W)	13.42	1.00	13.37		
		24(P)	11.58	1.42	8.14		

Table 2.4 Summary of information on the experimental data for braces (continued)

KL/r	Reference	Test ID (Type)**	$(\delta/\delta_B)_{max}$	δ_T/δ_B	δ/δ_T	Reported Local Buckling*	Reported Fracture*
80 – 120	Jain	6(T)	37.67	3.04	12.40		
		12A(T)	43.02	3.66	11.75		
		15(T)	14.21	1.13	12.63		
		2L(A)	86.65	7.33	11.82		
		3L(A)	56.81	4.72	12.03		
	Astaneh-Asl	2(DA)	18.84	2.95	3.31	X	X
		3(DA)	27.71	1.81	15.28		
		5(DA)	17.61	1.44	12.20		
		8(DA)	28.66	1.55	18.50	X	
		16(DA)	13.42	1.67	8.03		X(Gusset)
	Archambault	1B(T)	28.18	2.53	9.52	X	X
		1QB(T)	19.31	1.75	11.05	X	X
		2B(T)	32.75	2.27	14.41	X	X
		4B(T)	25.78	2.23	11.55	X	X
		4QB(T)	23.52	2.23	10.38	X	X
		5B(T)	42.62	2.59	16.44	X	X
	Leowardi	1(W)	45.86	0.98	46.79		
	Walpole	1(T)	23.46	1.54	15.27		
120 – 160	Black	1(W)	38.02	2.58	14.76		
		6(W)	32.66	1.84	17.78		
		10(DA)	28.88	2.29	12.63		
		11(DC)	41.03	1.72	23.90		
	Jain	4L(A)	94.39	7.80	12.10		
	Astaneh-Asl	4(DA)	66.34	3.10	21.42		X
		6(DA)	77.96	2.59	30.08		X
		10(DA)	23.90	2.15	11.10		X(Gusset)
		11(DA)	36.05	2.95	12.20		
		13(DA)	78.20	2.85	27.40		
	Archambault	3B(T)	77.38	3.85	20.10	X	X
160 – 200	Astaneh-Asl	1(DA)	42.55	2.49	17.09		
		9(DA)	106.25	5.29	20.08		
		15(DA)	65.19	4.70	13.86		
		18(DA)	67.35	3.74	18.03		X(Gusset)

* No check(X) means that it was not reported either because of good behavior or omission by researcher.

** Section Types: W=Wide Flange; A=Single Angle; T=Tube(Hollow); P= Pipe; WT= Structural Tee; DA= Double Angle; DC= Double Channel; TC=Tube(Concrete Filled)

*** Not considered in this study

**** Note: Ratios (δ/δ_B), (δ_T/δ_B), and (δ/δ_T) calculated by authors of this report.

2.4 Observations on Behavior

All results are presented, grouped over ranges of KL/r values, in Figures 2.11 to 2.15, showing the large scatter in data. The thicker line in these figures represents the average of all curves in each figure. Results are then presented again in Figure 2.16 to 2.26, but grouped per type of cross sections, namely for braces made of square hollow structural shapes (HSS) (a.k.a. tubes), W-shape, and double angles back-to-back. Results were also prepared for other types of cross-section, but are less conclusive due to sparseness of data; these are included in Appendix B for completeness. Typical results for some individual test results are also included in Appendix B to illustrate a sample from the complete data set to be included on the aforementioned MCEER web site. Finally, the obtained average curves, as a function of KL/r, are grouped and summarized in Figure 2.27 for all types of cross-sections, and in Figures 2.28 to 2.30 respectively for W-shapes, square HSS, and double-angles back to back. Note that the average curves were computed over the entire range of δ/δ_B for which at least one specimen was tested; a resulting peculiarity of this decision is that the line of average results is sometimes seen to increase in a jagged manner as weaker specimens were not pushed to the same large δ/δ_B as the stronger specimens.

A number of observations can be made from these figures. First, while the normalized energy dissipation E_C/E_T typically decreases with increasing normalized displacements δ/δ_B, the ratios are consistently smaller for larger KL/r values. This is not surprising as members with smaller KL/r typically have a larger inertia, and thus larger plastic modulus, which translates in a larger plastic moment and energy dissipation at the mid-length plastic hinge. However, it is noteworthy that braces having KL/r in the 80-120 range do not have significantly more normalized energy dissipation in compression than those having a slenderness in excess of 120. This is significant considering the large number of braced frames designed and built with braces having a KL/r of approximately 100. The rapid drop in energy dissipation effectiveness (down to 0.3 or less for braces having KL/r above 80) as the normalized displacement approximately exceed 3 is also significant; this suggests that reliance on the compression brace to dissipate seismic energy, while effective at very low KL/r, may be overly optimistic for the slenderness more commonly encountered in practice.

As a minor point, it is observed that a few values of E_C/E_T counter-intuitively exceed 1.0 at low magnitudes of displacement. Closer scrutiny of the 7 specimens for which this was noted revealed this to be a consequence of errors introduced due to: (i) an initial near vertical returning down-slope segment of the hysteretic loops, and; (ii) the difficulty in accurately graphically reading the data or calculating Young's Modulus. In addition, as shown in Figure 2.31, for Specimen 9 by Black et al. (1980), the experimentally obtained buckling strength exceeded the tensile yield strength (A_gF_y calculated with the experimentally obtained F_y value) for reasons unexplained by the authors.

Reduction in the normalized C_r''/C_r(first) envelope is particularly severe for the W-shape braces, again having KL/r above 80 dropping to approximately 0.2 when the normalized displacements exceed 5. However, behavior is not significantly worse for KL/r in the 120 to 160 range. In that perspective, tubes perform significantly better, over all slenderness range. The performance of double-angle braces is in between these two extremes. Observation of the results for C_r''/C_r(last) and C_r''/C_r(first/last) show that the compression capacity at low δ/δ_B values drops rapidly upon repeated cycling, and that C_r''/C_r(first) is effectively equal to C_r''/C_r(last) at normalized displacements above 3 in most instances.

Hence, considering that a brace with KL/r of 80 has a buckling load equal to 60% of yielding tensile force, when the braced bent will have reached its expected displacement ductility of 3 to 4 ($4\delta_T = 4\ (\delta_B/0.6) = 6.7\delta_B$), the brace compression strength will have already dropped considerably to approximately 20% of its original buckling strength (40% for square HSS).

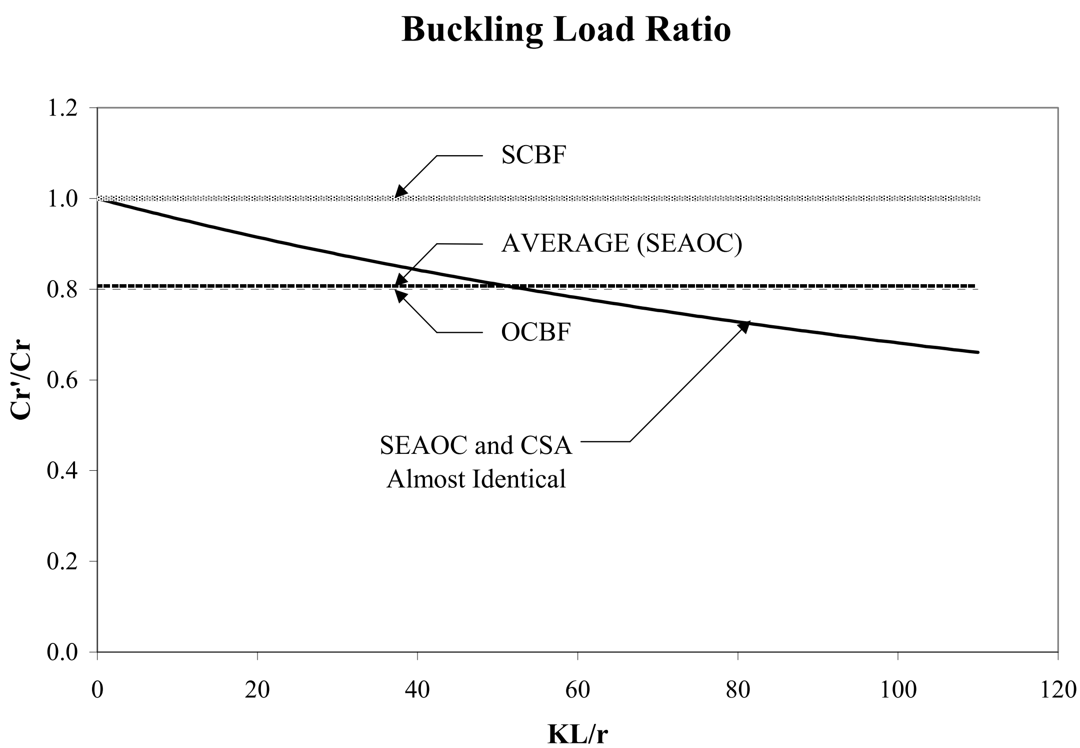

Figure 2.1 Equations of buckling capacity

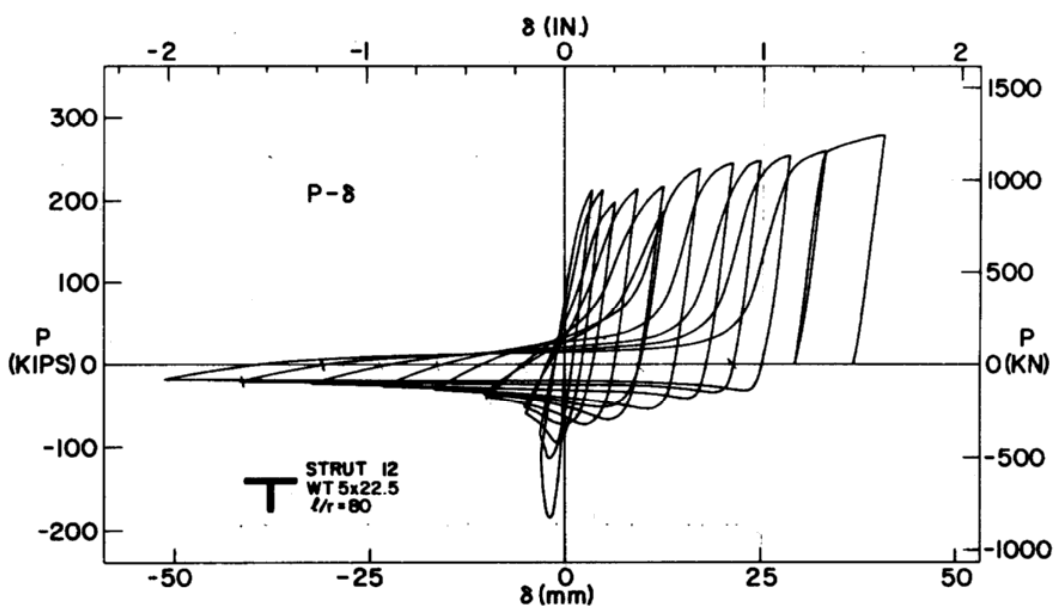

Figure 2.2 Sample hysteresis of a brace under cyclic axial loading (Black et al., 1980)

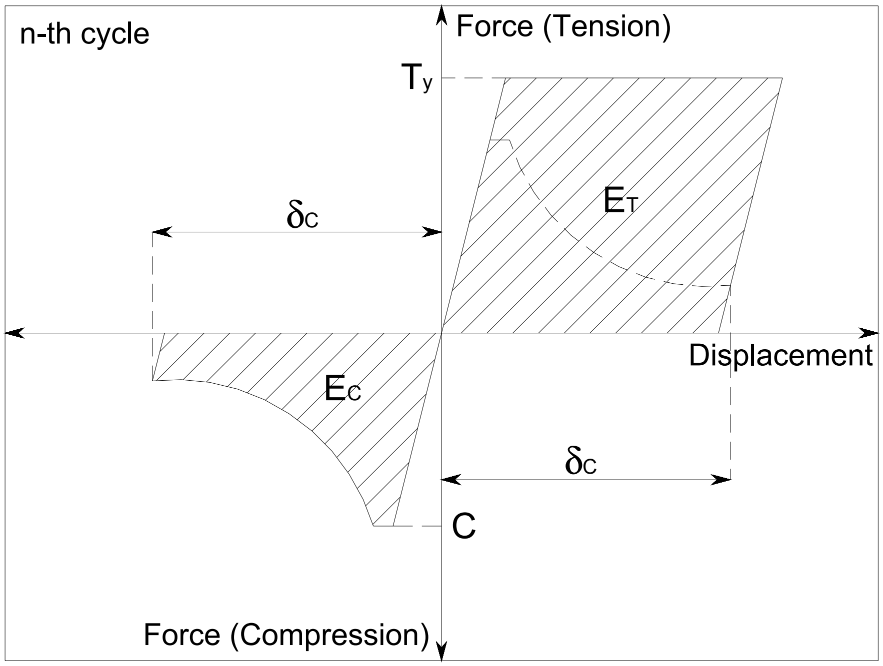

Figure 2.3 Definition of dissipated energy ratio, E_C / E_T

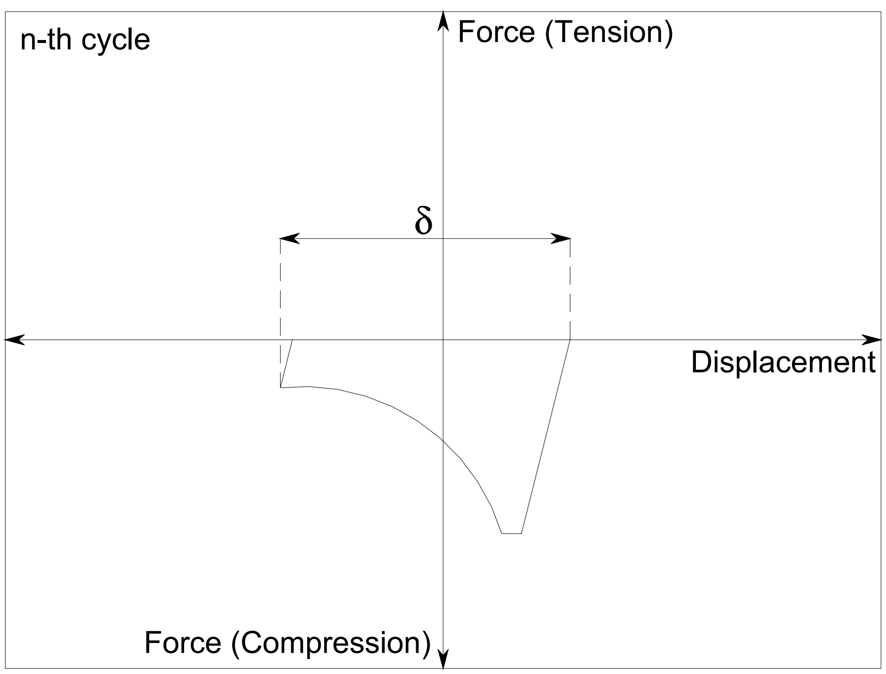

Figure 2.4 Definition of axial displacement, δ

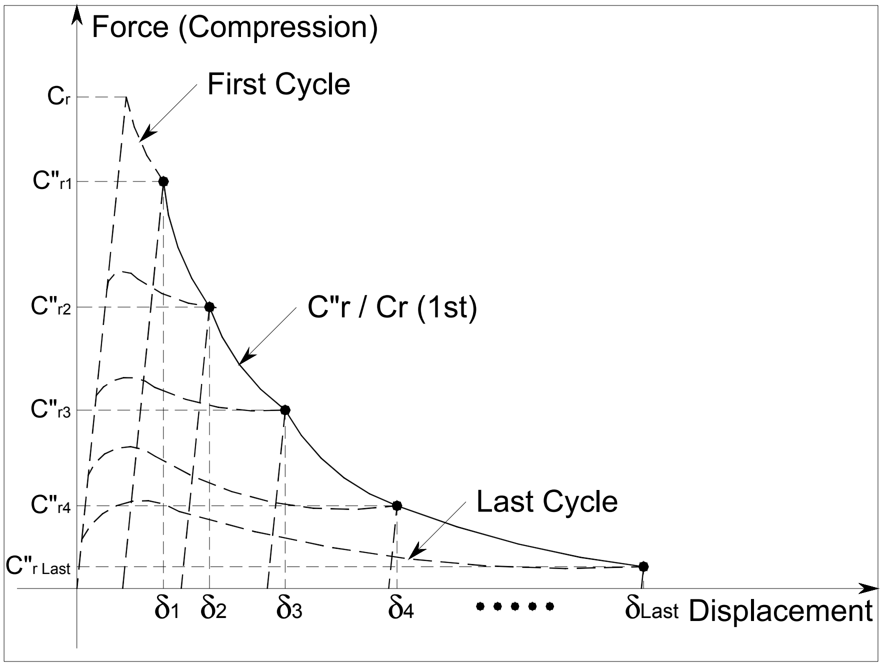

Figure 2.5 Definition of normalized buckling capacity, C_r" / C_r (1^{st})

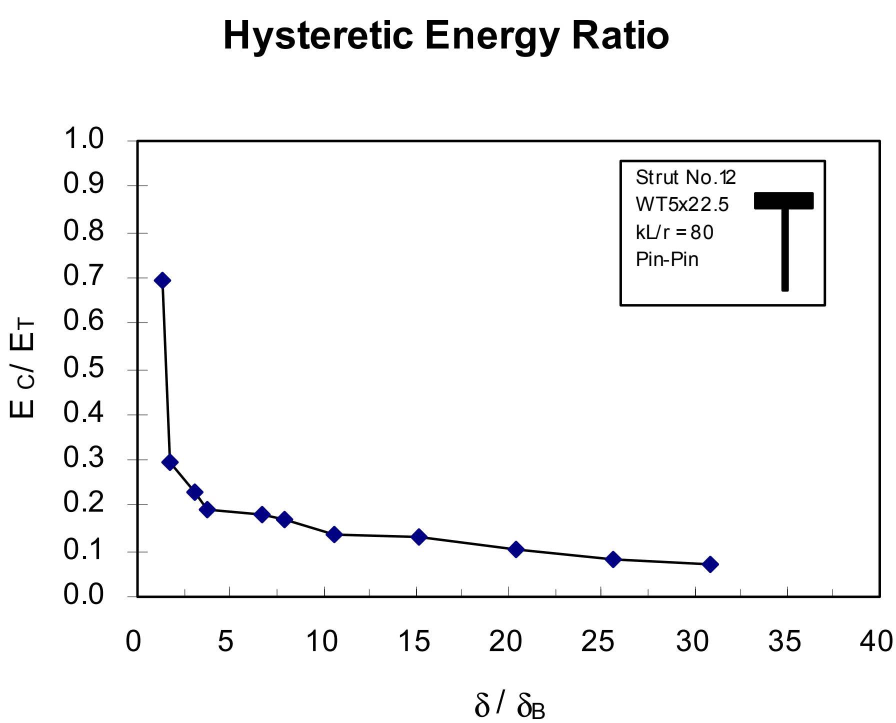

Figure 2.6 Example of normalized hysteretic energy data

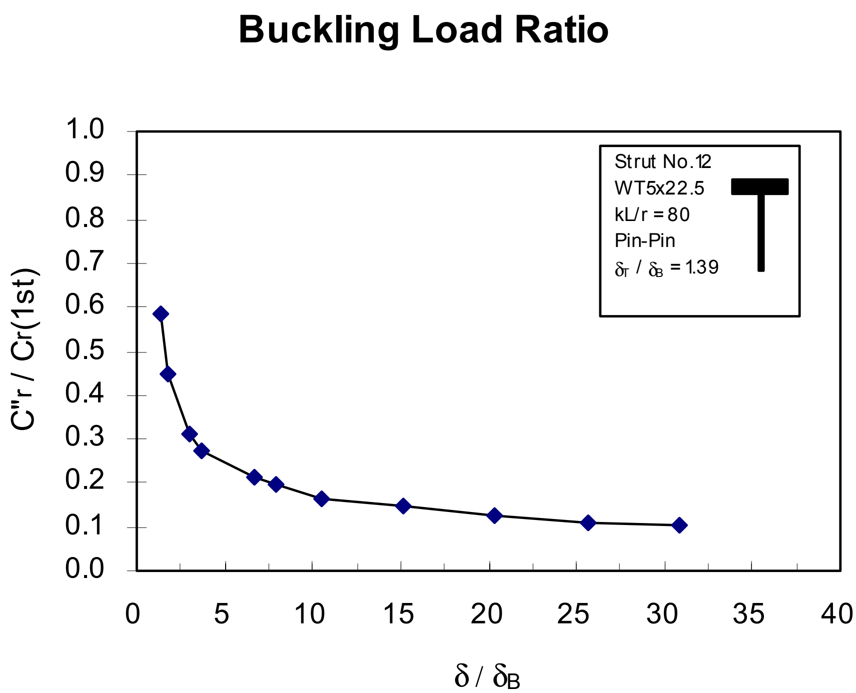

Figure 2.7 Example of normalized maximum compression strength reached upon repeated cycling data, C_r” / C_r (1^{st})

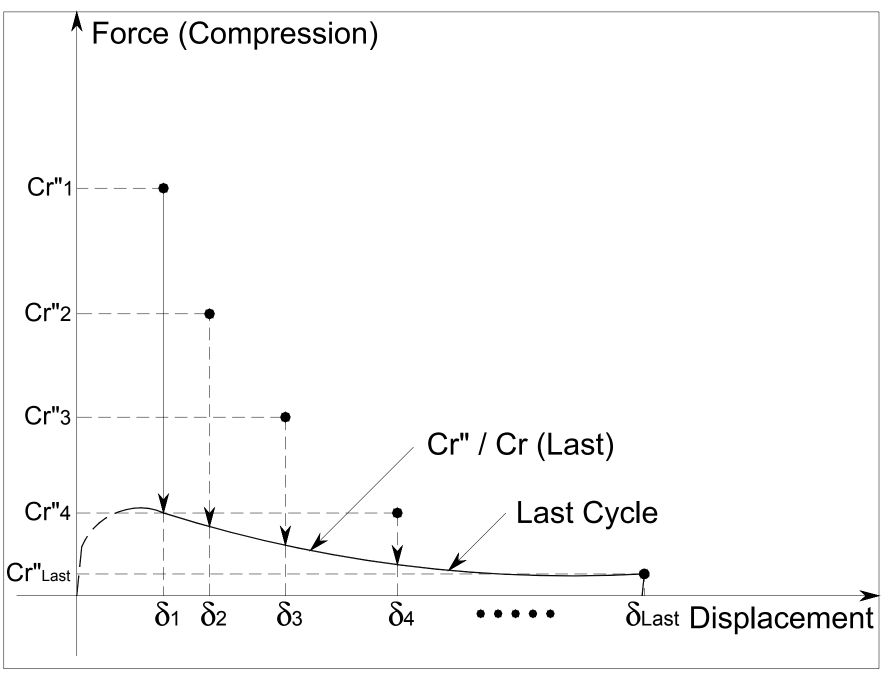

Figure 2.8 Definition of normalized buckling capacity, Cr” / Cr (Last)

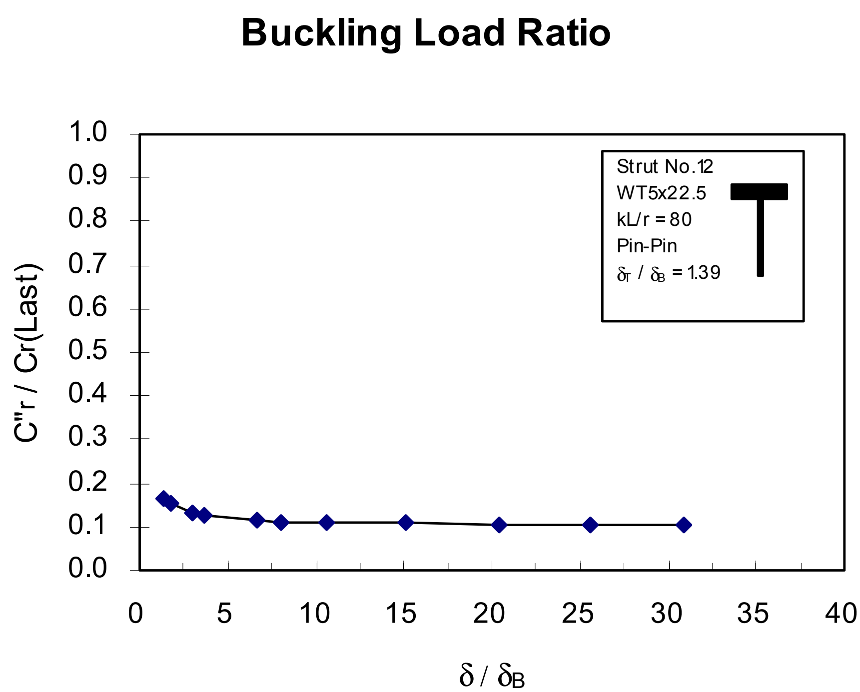

Figure 2.9 Example of normalized maximum compression strength reached upon repeated cycling data, C_r" / C_r (Last)

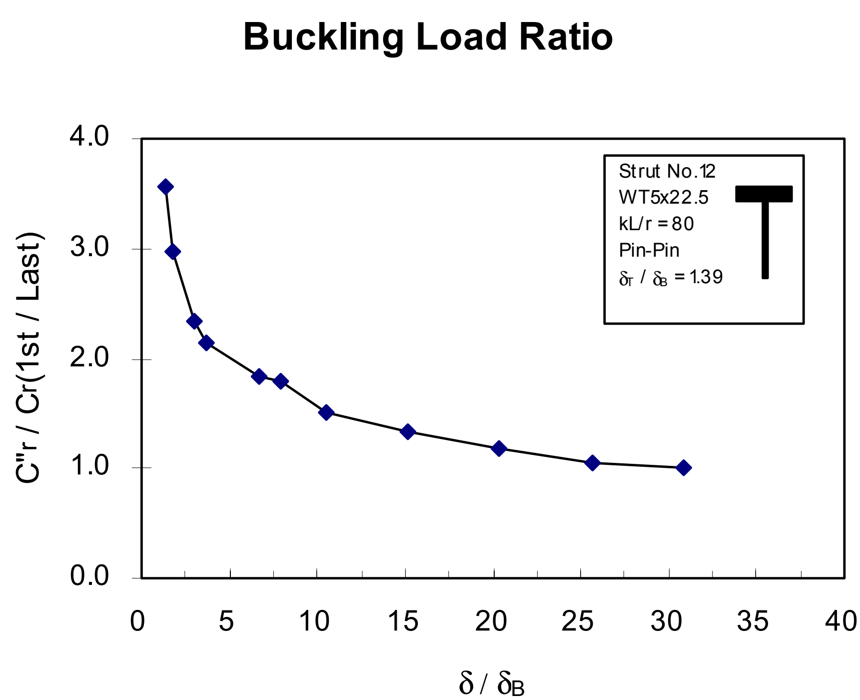

Figure 2.10 Example of normalized maximum compression strength reached upon repeated cycling data, C_r" / C_r (1st / Last)

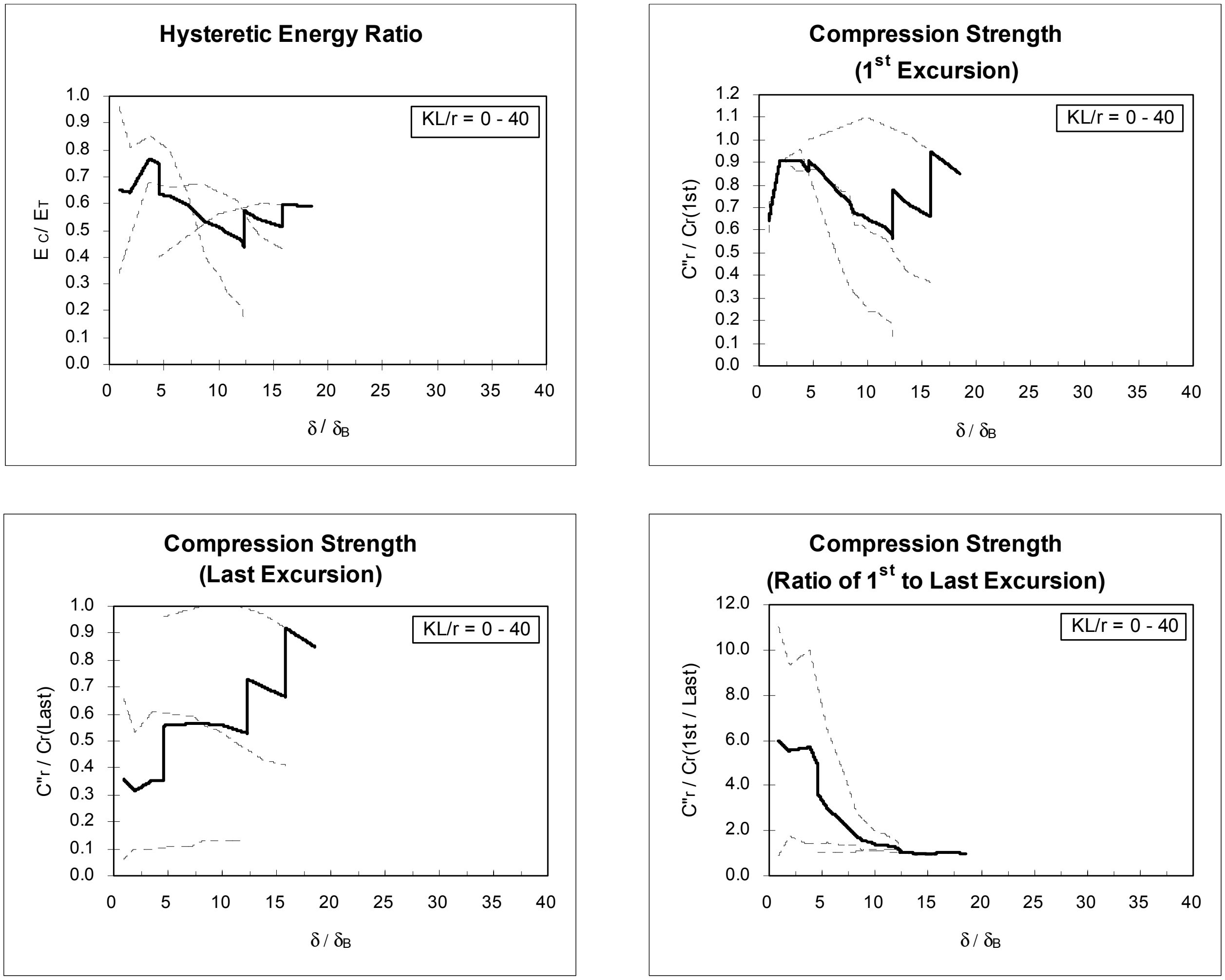

Figure 2.11 All structural shapes with KL/r = 0 to 40 (Average shown by thicker line)

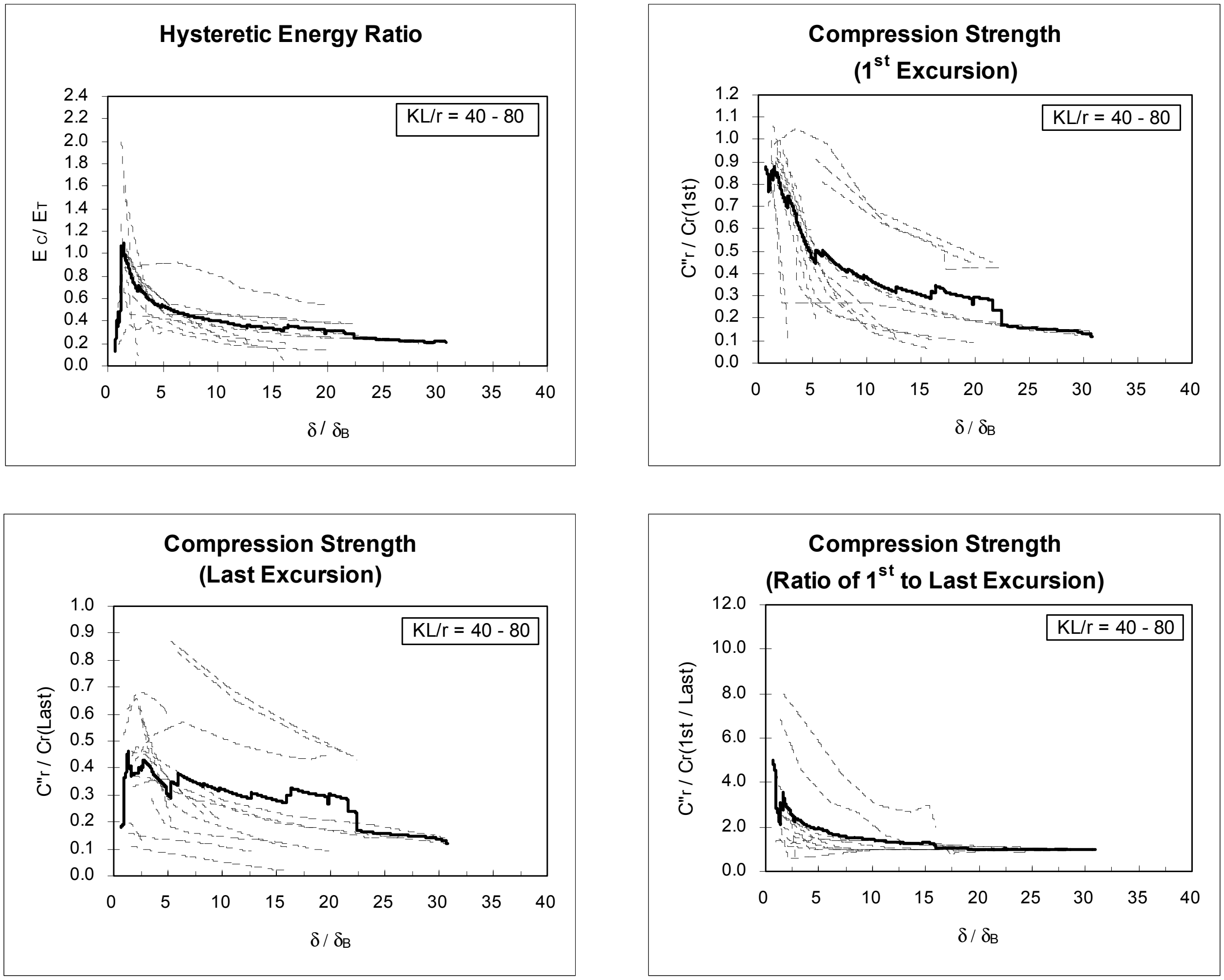

Figure 2.12 All structural shapes with KL/r = 40 to 80 (Average shown by thicker line)

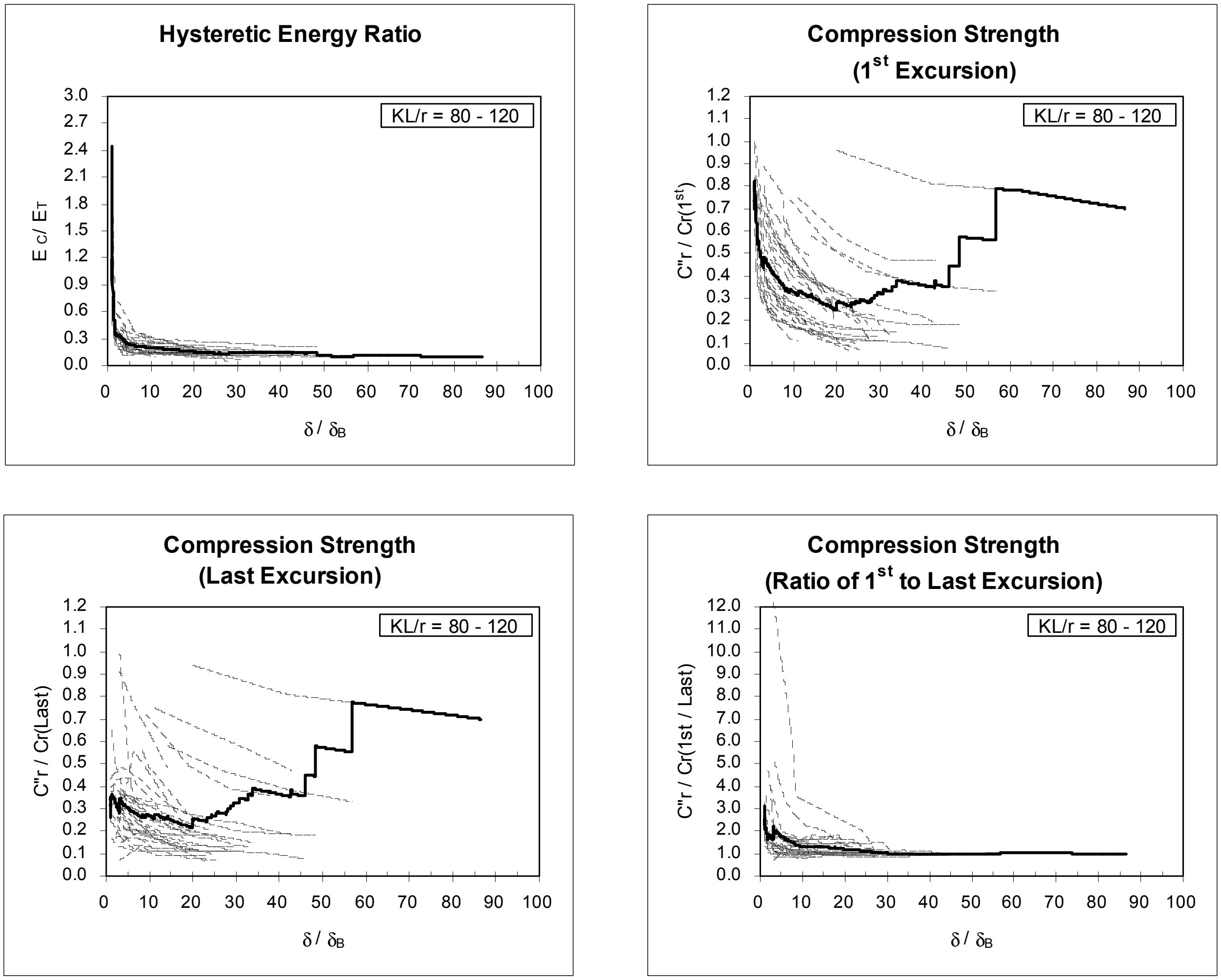

Figure 2.13 All structural shapes with KL/r = 80 to 120 (Average shown by thicker line)

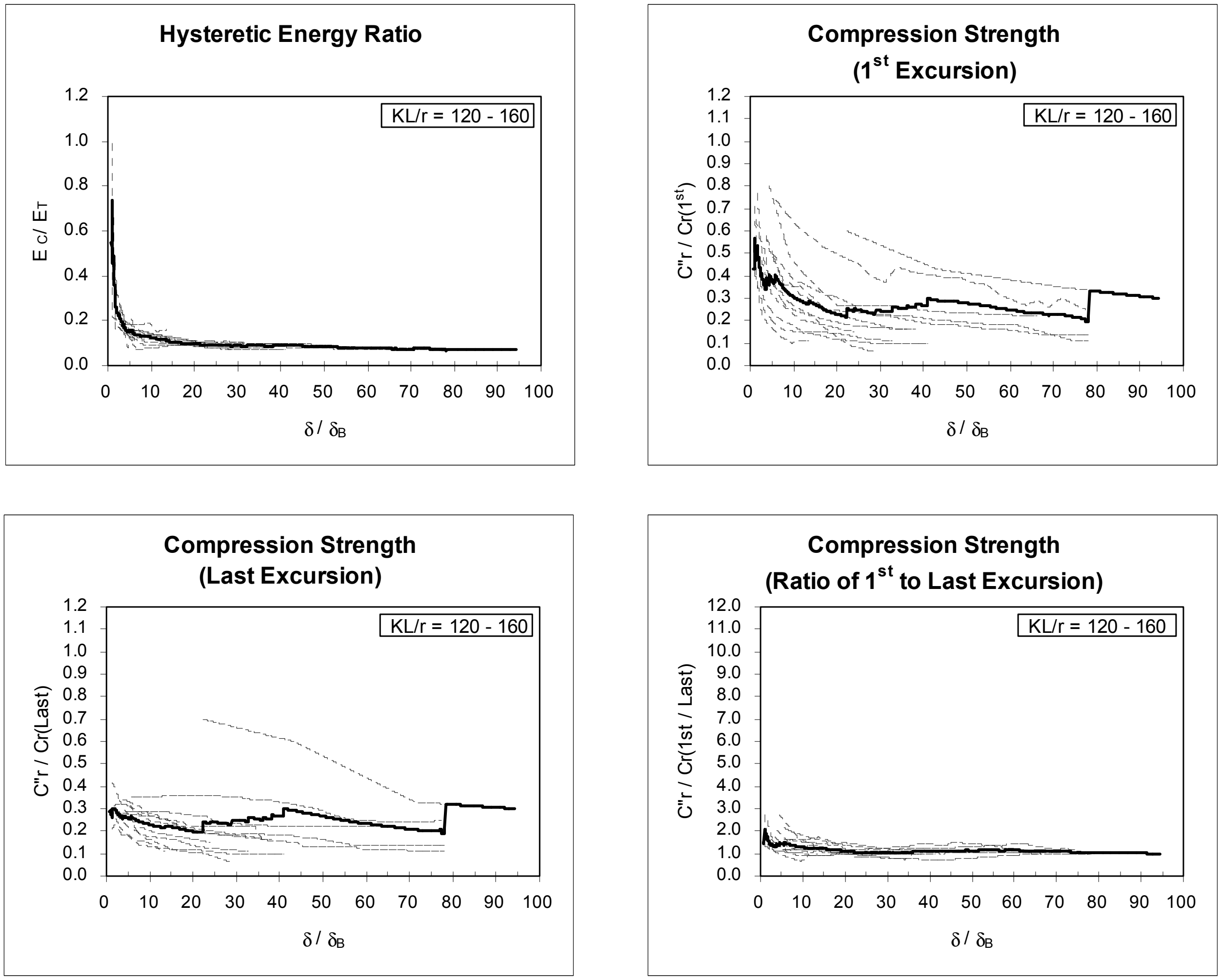

Figure 2.14 All structural shapes with KL/r = 120 to 160 (Average shown by thicker line)

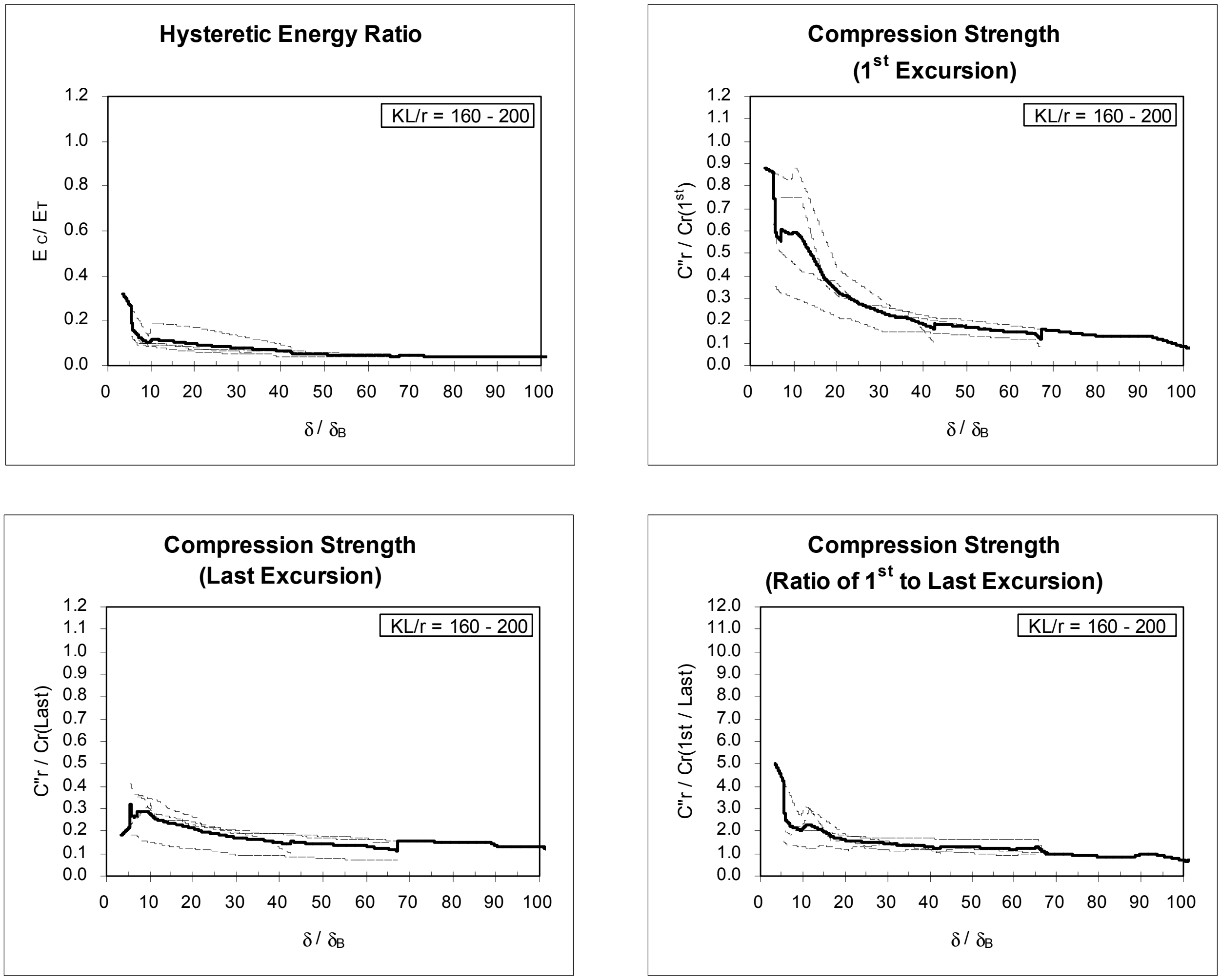

Figure 2.15 All structural shapes with KL/r = 160 to 200 (Average shown by thicker line)

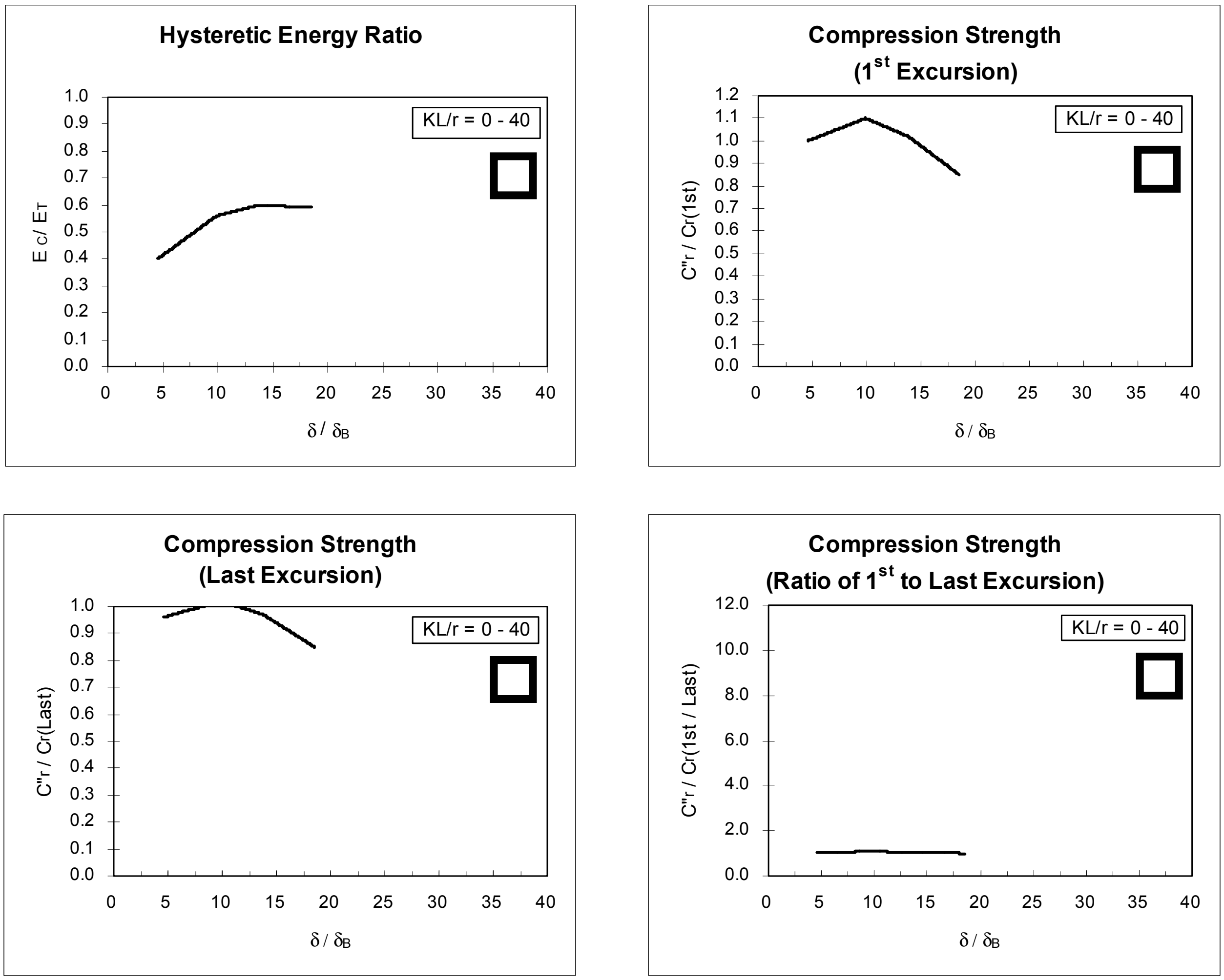

Figure 2.16 Structural Tubes with KL/r = 0 to 40 (Average shown by thicker line)

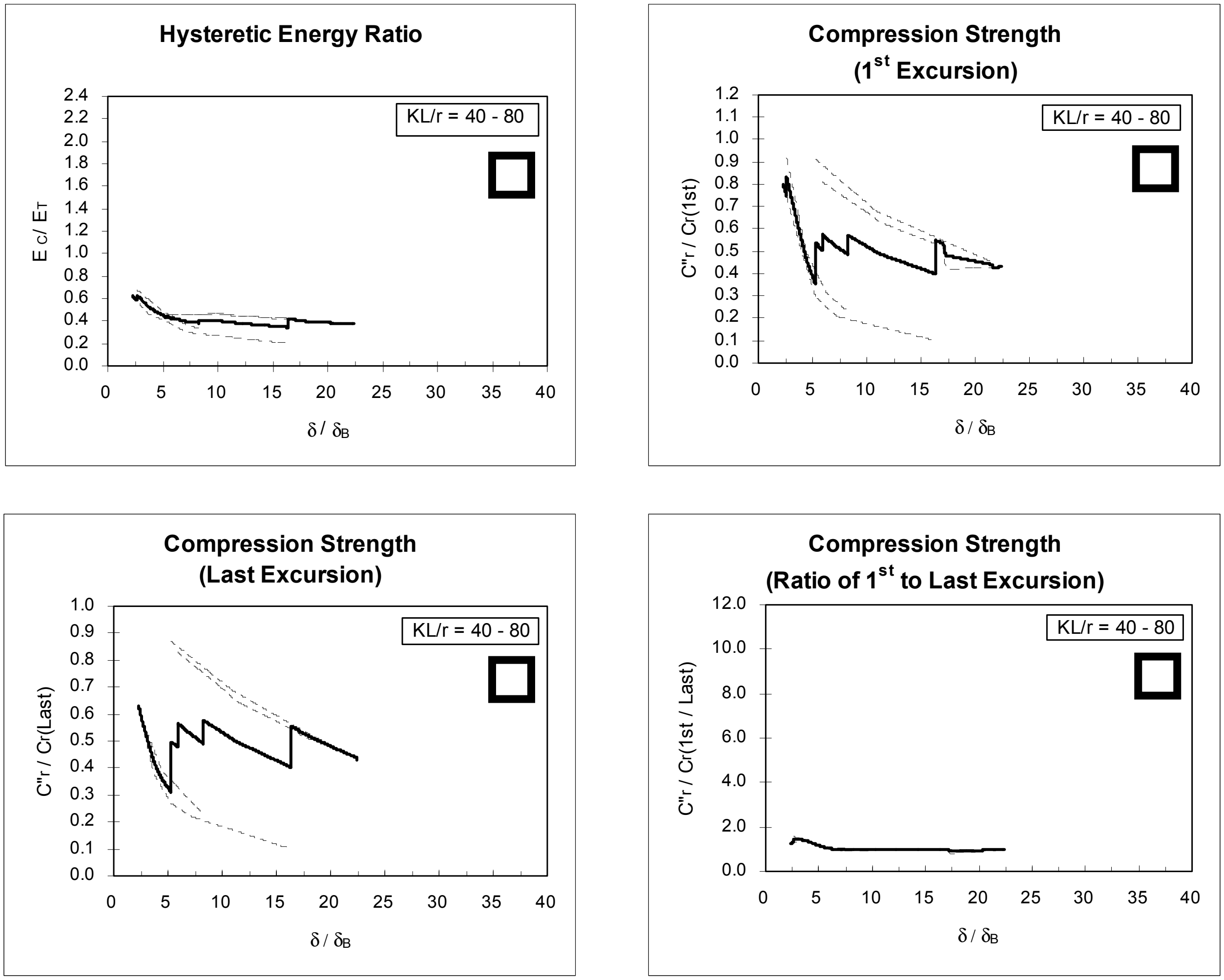

Figure 2.17 Structural Tubes with KL/r = 40 to 80 (Average shown by thicker line)

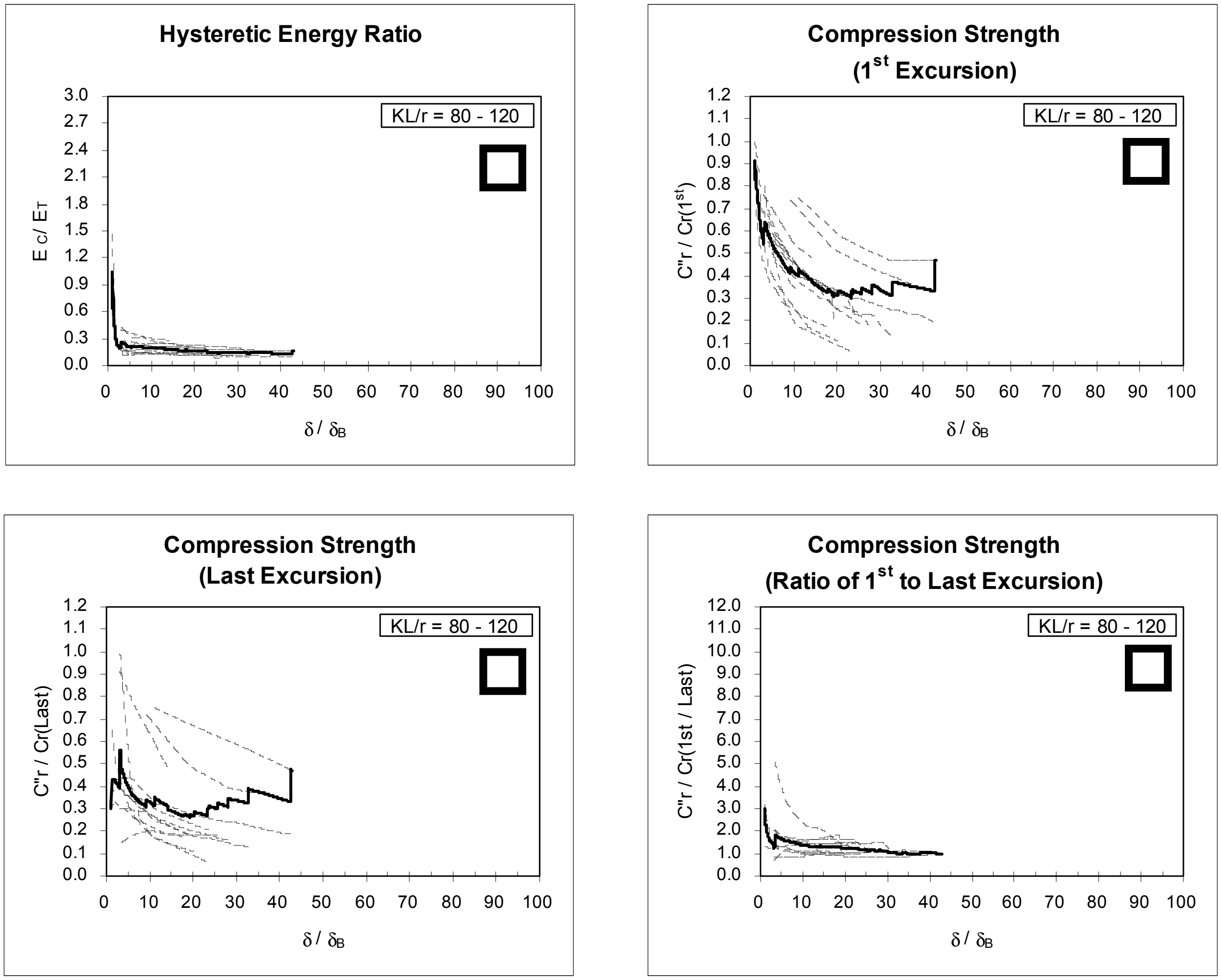

Figure 2.18 Structural Tubes with KL/r = 80 to 120 (Average shown by thicker line)

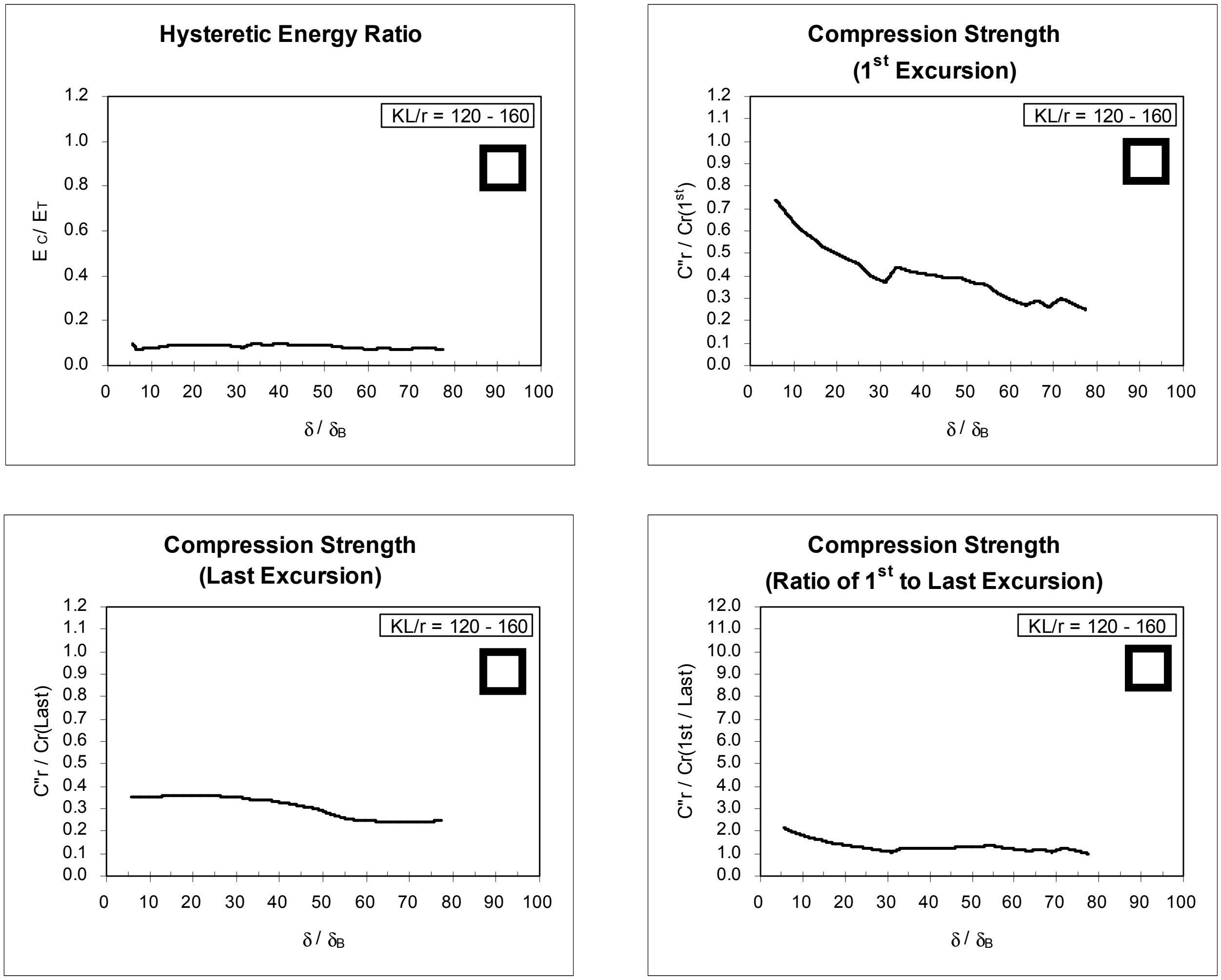

Figure 2.19 Structural Tubes with KL/r = 120 to 160 (Average shown by thicker line)

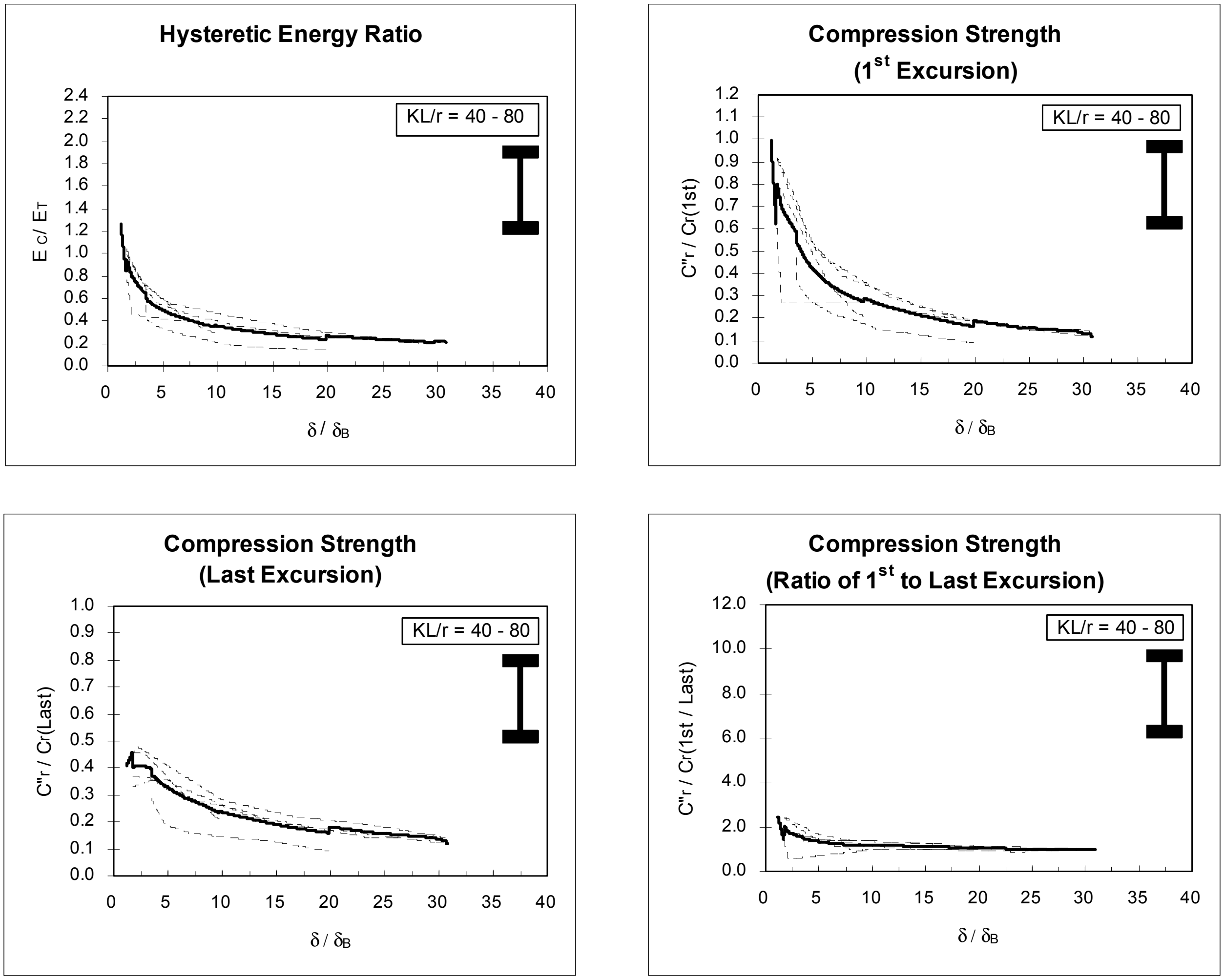

Figure 2.20 Wide Flanges with KL/r = 40 to 80 (Average shown by thicker line)

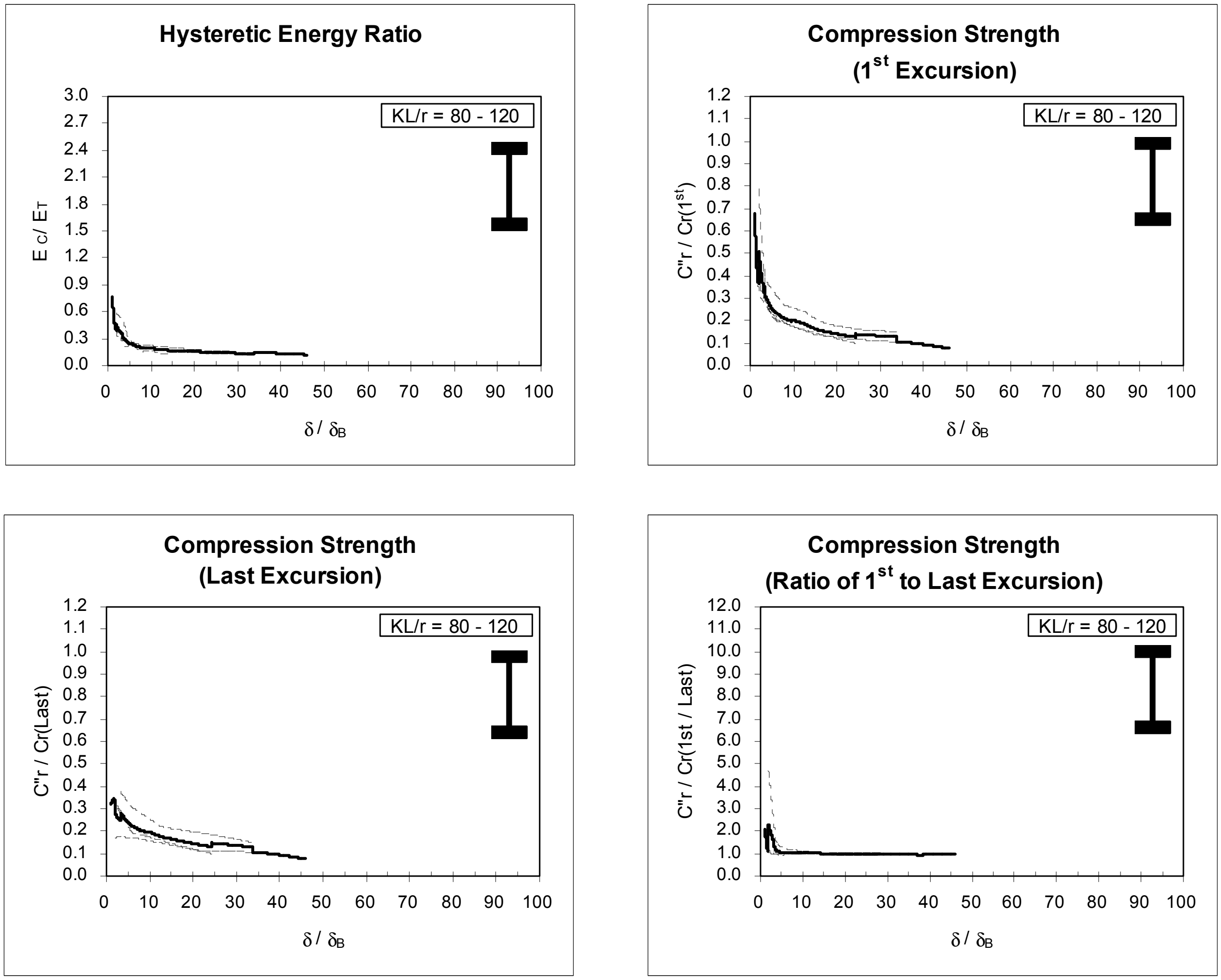

Figure 2.21 Wide Flanges with KL/r = 80 to 120 (Average shown by thicker line)

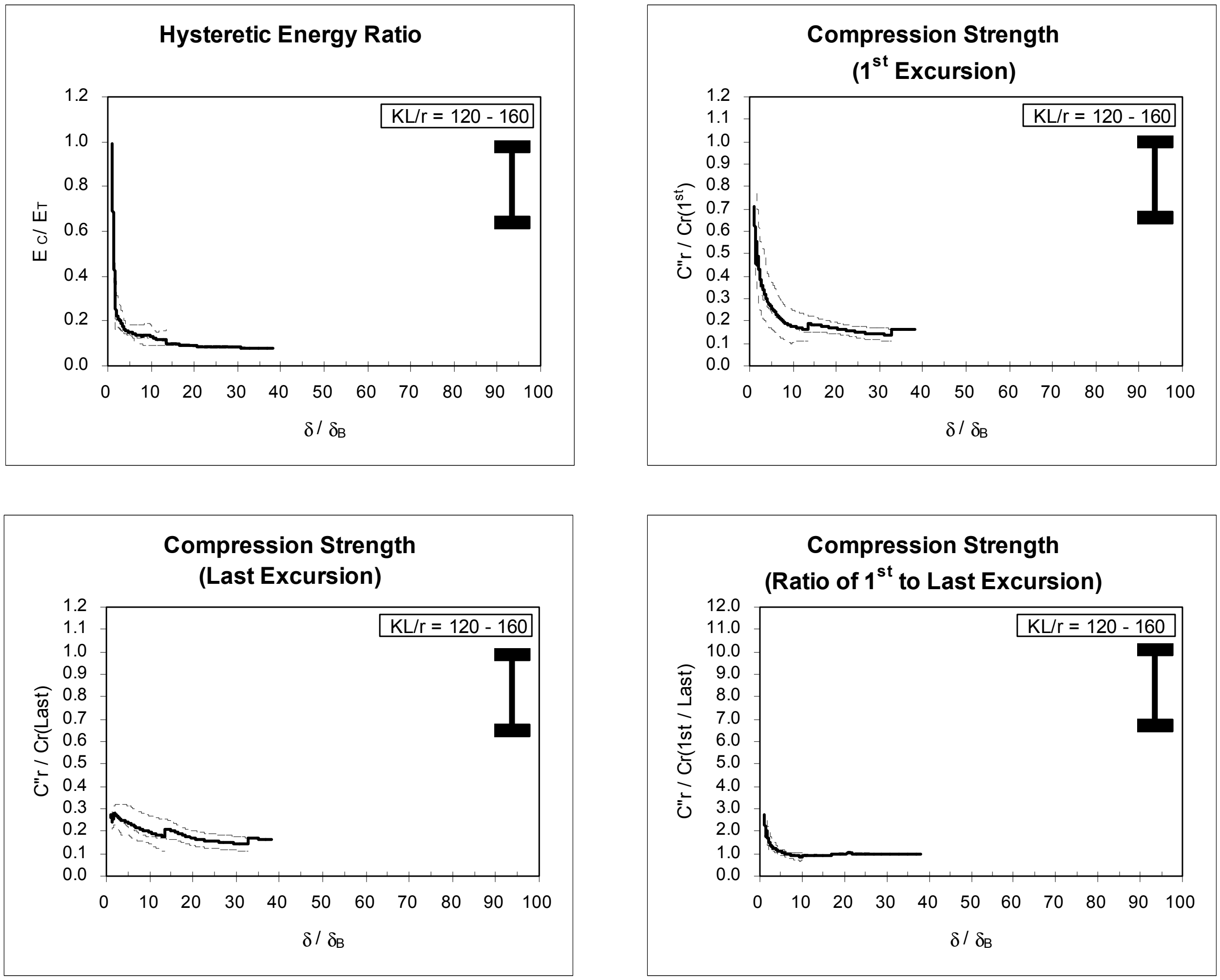

Figure 2.22 Wide Flanges with KL/r = 120 to 160 (Average shown by thicker line)

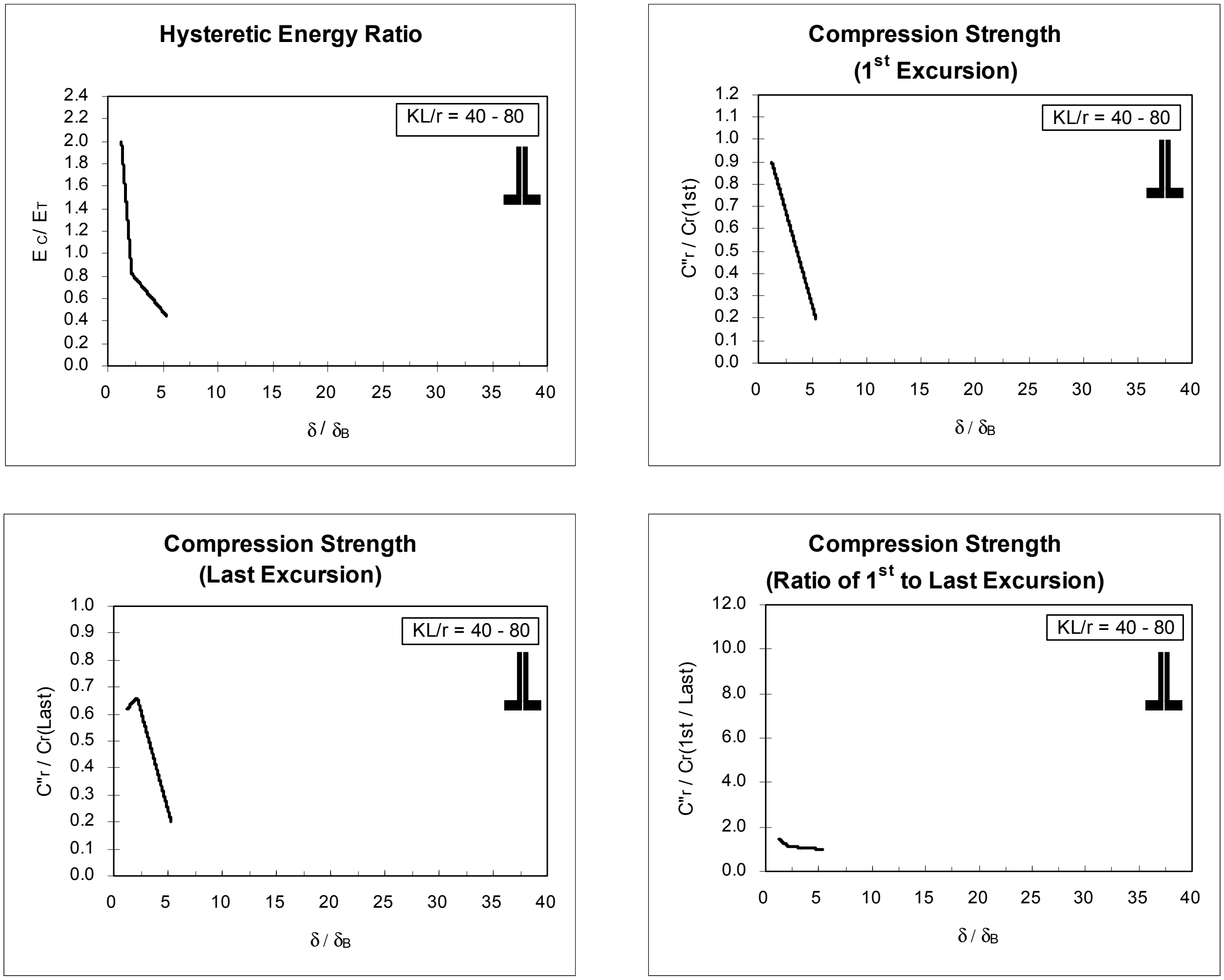

Figure 2.23 Double Angles, back-to-back with KL/r = 40 to 80
(Average shown by thicker line)

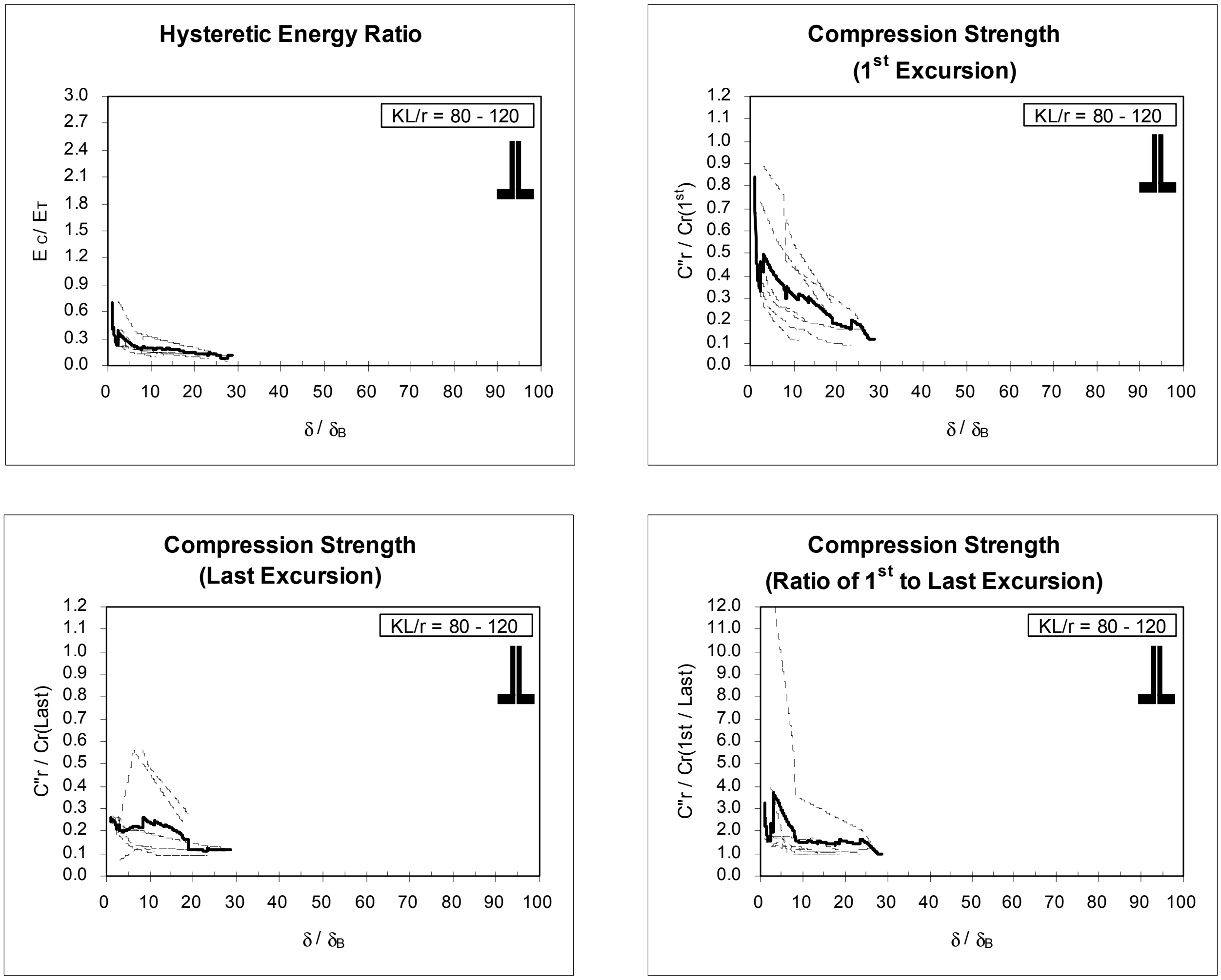

Figure 2.24 Double Angles, back-to-back with KL/r = 80 to 120
(Average shown by thicker line)

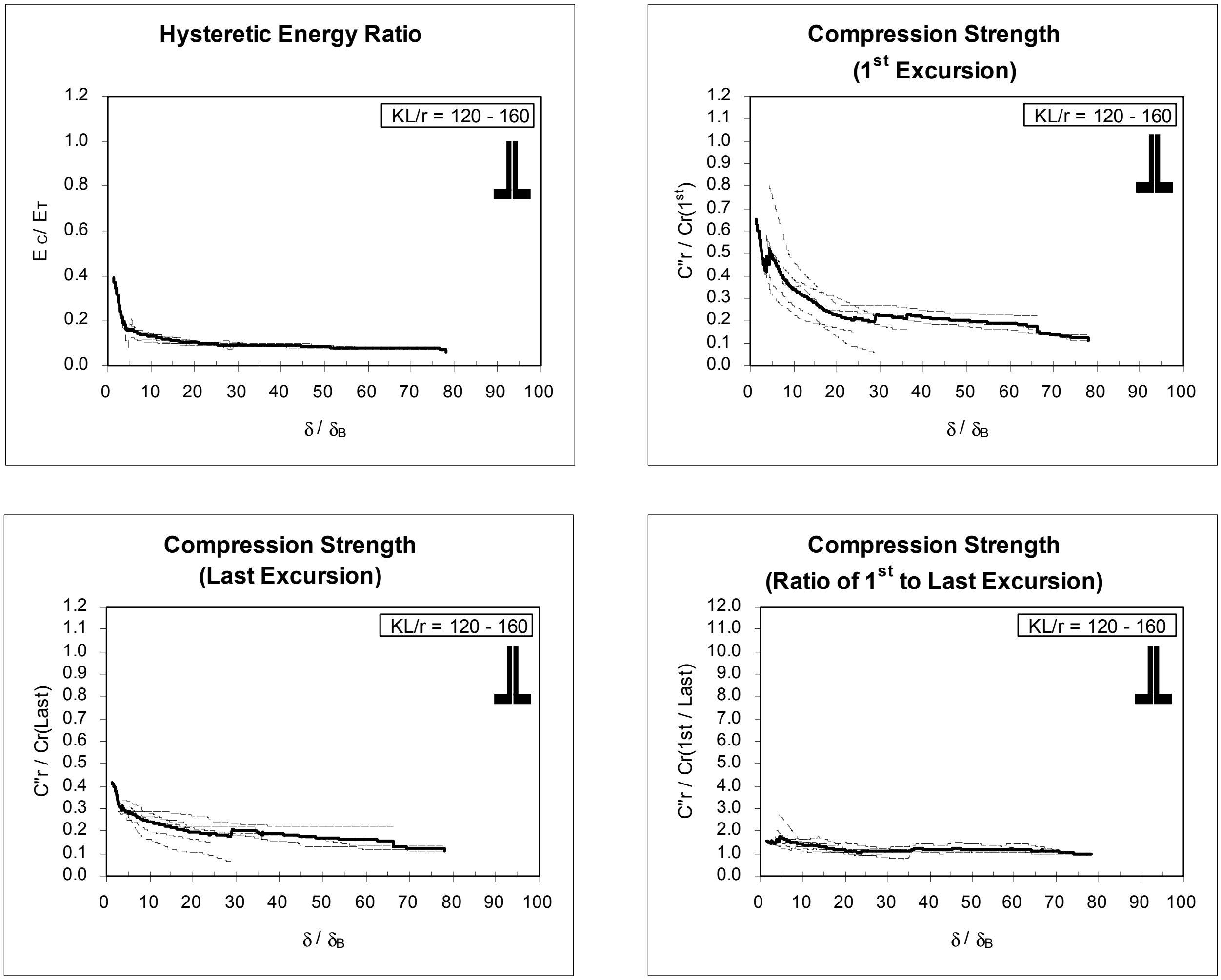

Figure 2.25 Double Angles, back-to-back with KL/r = 120 to 160
(Average shown by thicker line)

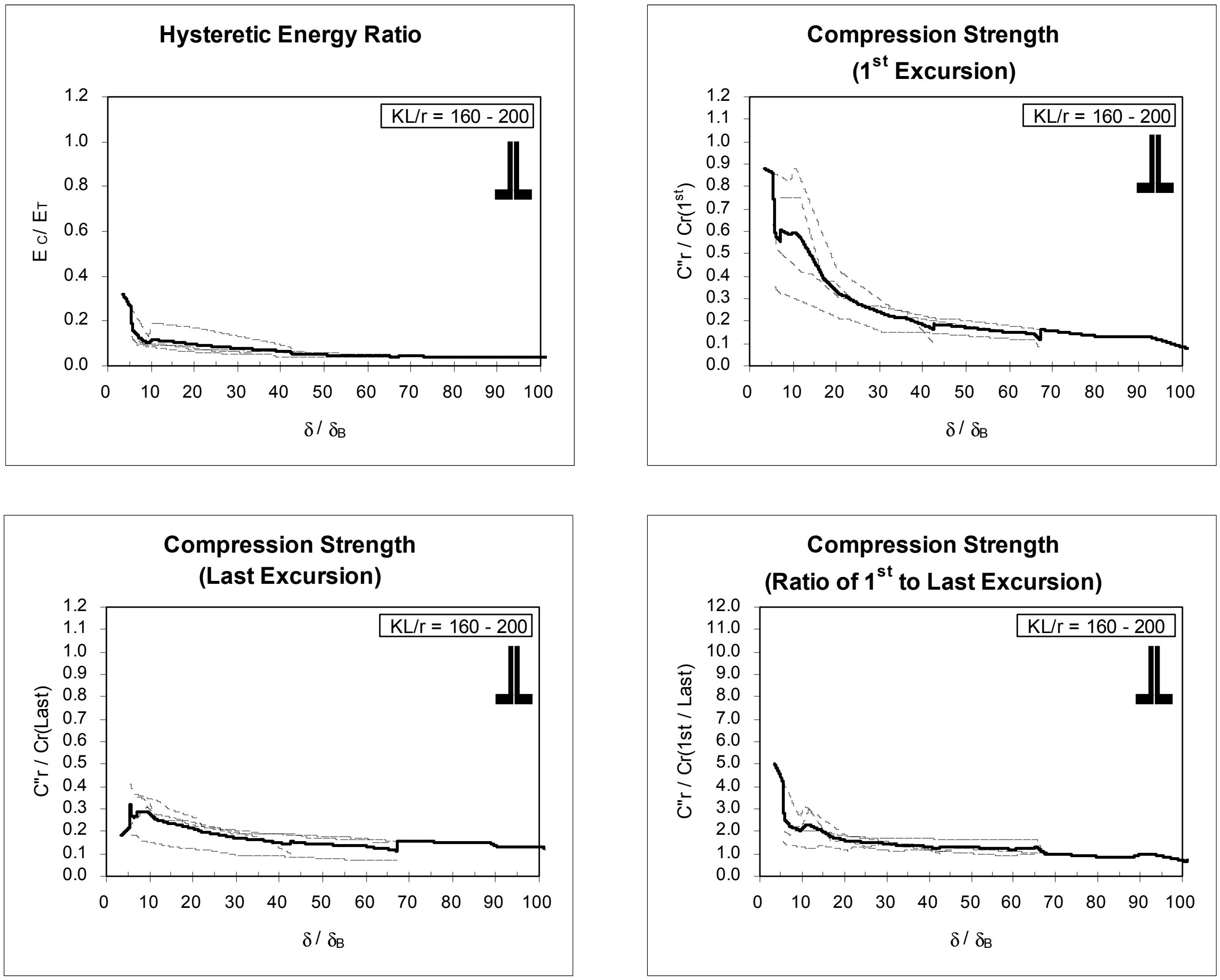

Figure 2.26 Double Angles, back-to-back with KL/r = 160 to 200
(Average shown by thicker line)

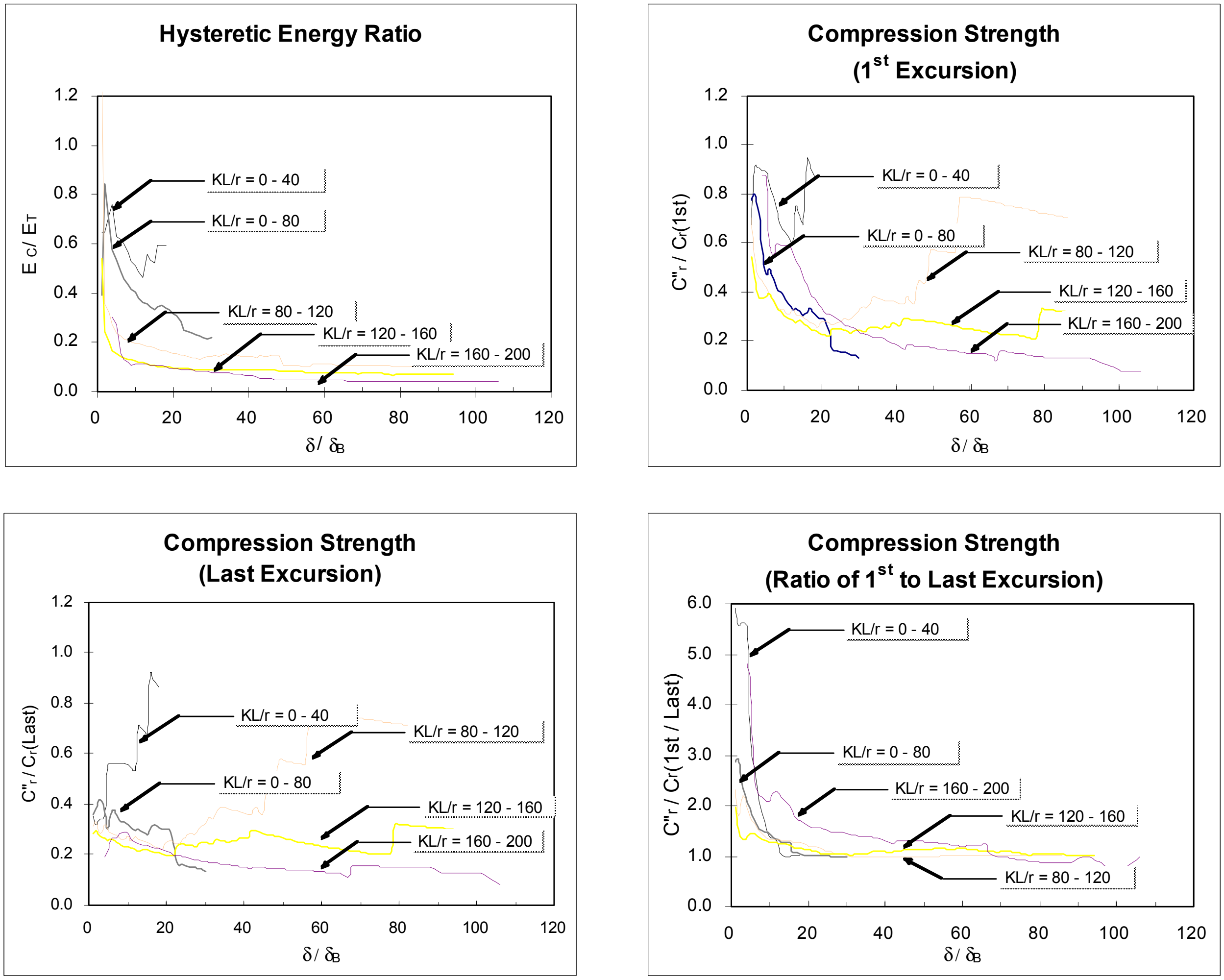

Figure 2.27 Averages of data by KL/r value ranges

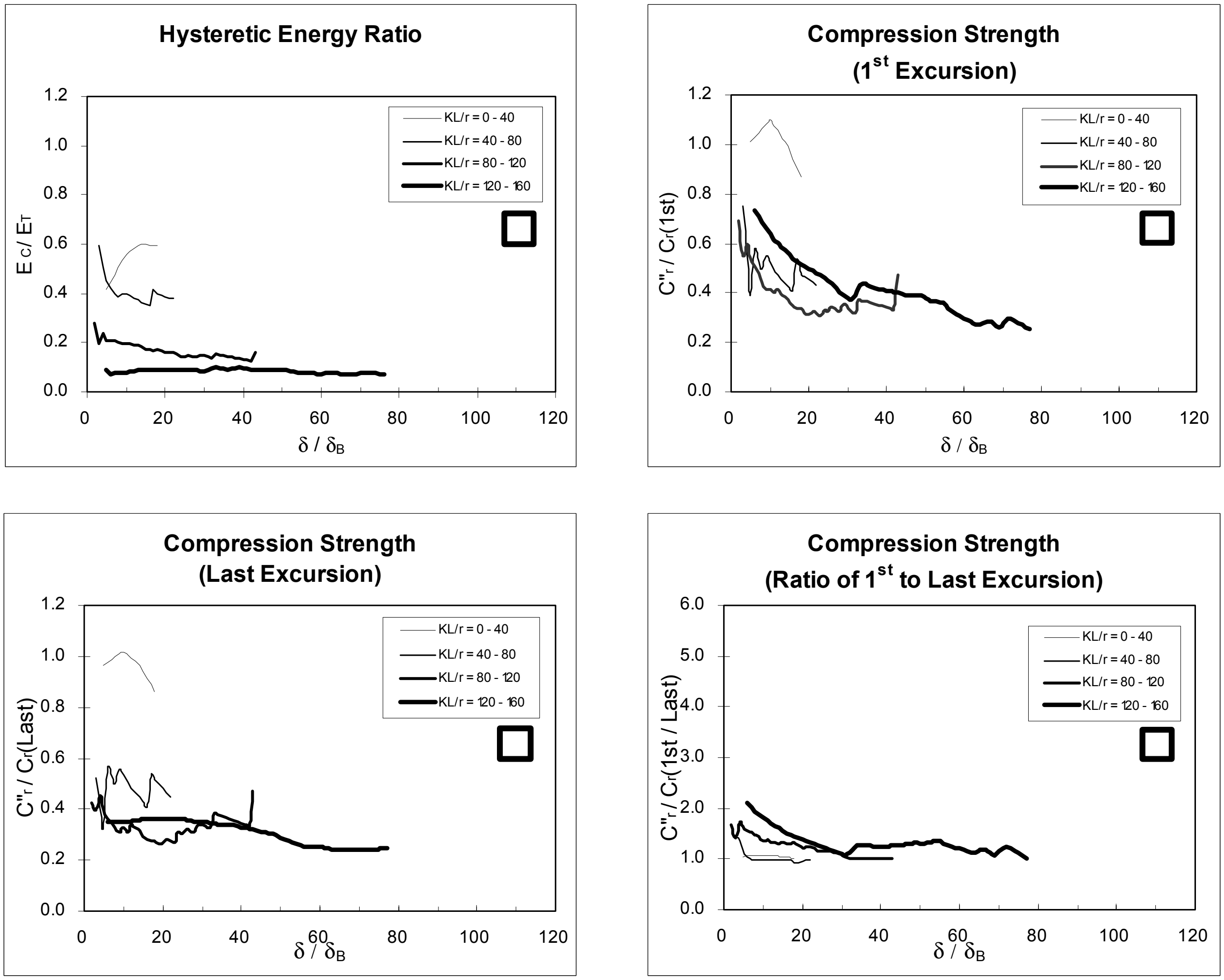

Figure 2.28 Averages of data by KL/r value ranges for tubular sections

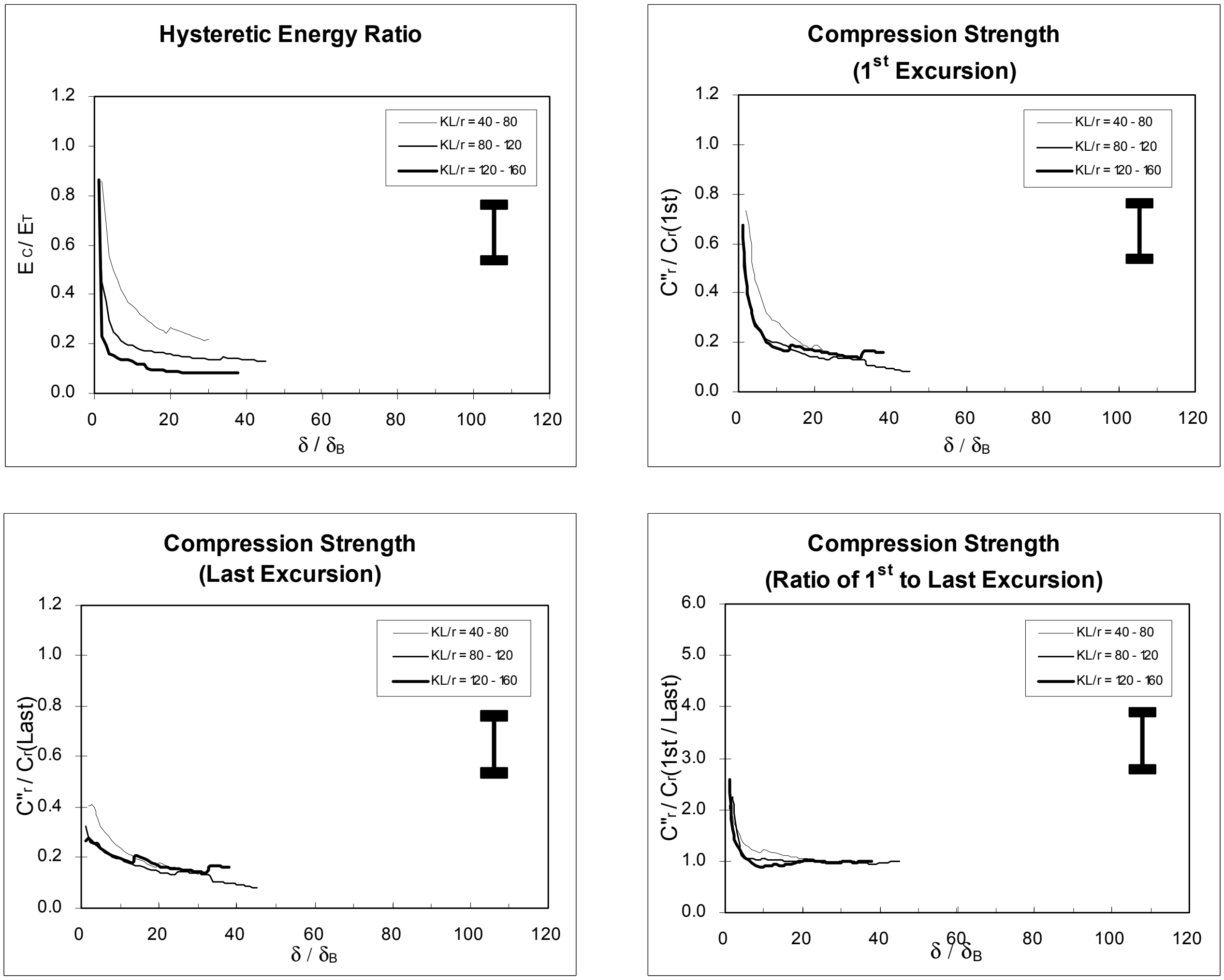

Figure 2.29 Averages of data by KL/r value ranges for wide flange section

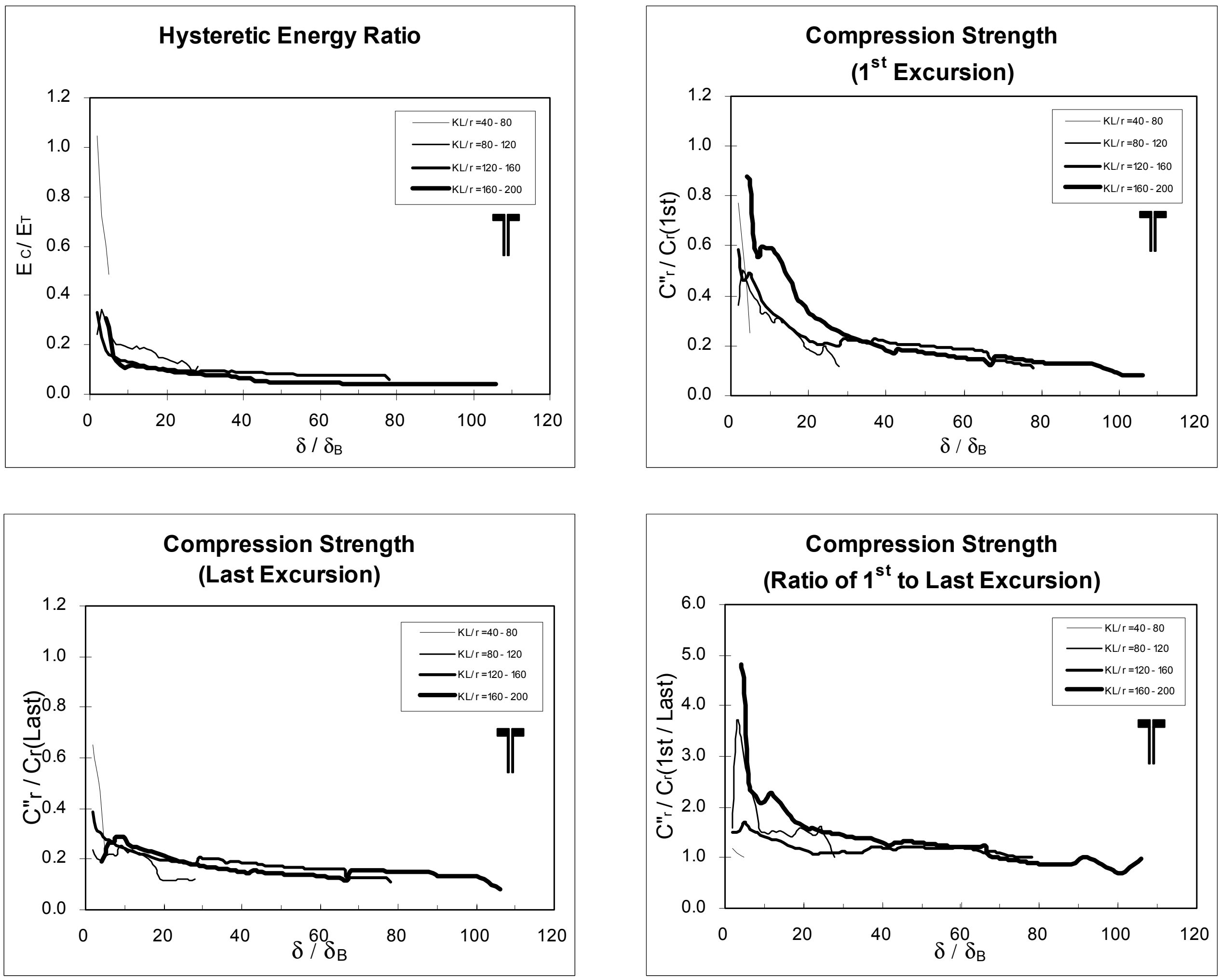

Figure 2.30 Averages of data by KL/r value ranges for double angles, back-to-back

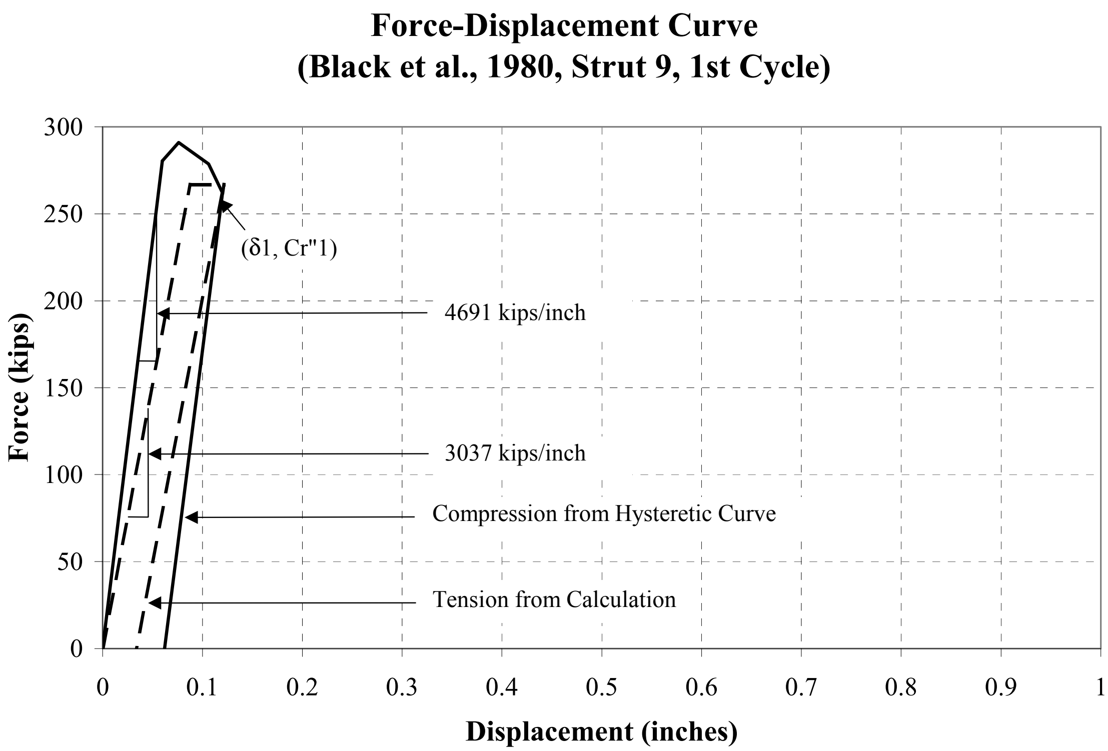

Figure 2.31 Hysteretic energy ratio from the first cycle of strut 9 (Black et al., 1980)

SECTION 3

NON-LINEAR DYNAMIC ANALYSES OF SINGLE STORY BRACED FRAMES

Non-linear dynamic analyses of a single story X-braced bay designed using various R factors and KL/r values were conducted to investigate the demands on the braces and the effects of slenderness on the energy dissipation of the braces. In this section, the specifics of the building analyzed, the brace model considered, the ground motions, and software used are presented. Typical brace force-displacement hysteretic loops for various KL/r and R factors obtained from these analyses are included in Appendix C. The complete set of results will be included on the aforementioned MCEER Users Network. Hysteretic energy calculations made using the results from these non-linear analyses will be used in SECTION 4, along with other parametric studies.

3.1 Specifics of the Building Analyzed

The building used for this study is a single story steel building with 38.5 m x 38.5 m plan dimensions. Lateral bracing is provided by a single braced bay in each exterior frame. As such, this building is identical in geometry to the one designed by Tremblay (1999). The typical floor plan and elevation of this building are shown in Figure 3.1. The height of the braced frame is 3.8 m, its width 7.6 m. Columns were designed to resist gravity dead and live roof loads of 1.0 kPa (20.9 psf) and 1.48 kPa (31.0 psf) respectively. Beams needed not to be designed as the horizontal displacements at the top of columns were constrained to be the same. Braces were designed to resist the seismic loads only. Half of the building floor mass (by tributary area) was assigned to each braced frame to calculate the horizontal seismic design loads. These were also calculated in accordance with Uniform Building Code (ICBO, 1994) procedure, specified as:

$$V = C_s W \tag{3.1}$$

where, V is the base shear, W is the total dead load of 1339 kN (300 kips), and C_s is the seismic coefficient defined as:

$$C_s = \frac{C_e}{R_w} \tag{3.2}$$

where, R_w is the response modification factor (described in SECTION 2) and C_e is called elastic seismic response coefficient and expressed as:

$$C_e = ZIC \tag{3.3}$$

where, Z is the seismic zone factor, I is the importance factor taken as 1.0, and C is the numerical constant, defined as:

$$C = \frac{1.25S}{T_1^{2/3}} \tag{3.2}$$

where, S is the site coefficient taken as 1.0, and T_1 is the fundamental period of the structure (calculated here from dynamic analyses).

Note that Z of 0.20 was used here, to match the design by Tremblay for Vancouver. Also, it is important to realize that based on the procedures described in the following section, the UBC equations only served to give a shape for the elastic design spectra to be divided by R for brace designs using the AISC LRFD format (and not as suggested by Eq. 3.2 which would have been applicable for an Allowable Stress Design approach).

3.2 Bracing Member Design

In this parametric study, as indicated previously, bracing members have been designed with various slenderness ratios (KL/r) and response modification factors (R). Five R factors were used for design and analysis, namely 1, 2, 4, 6, and 8. Note that an R factor of 6 is prescribed by the AISC Provisions (1997) for SCBF (as indicated in SECTION 2). Three values of brace slenderness ratios were considered, namely 50, 100, and 150 to represent stocky, moderate, and slender braces, respectively. As a result, 15 different bracing members were designed (five R values times three KL/r values). These frames have each been subjected to 6 different earthquake excitations, for a total of 90 non-linear dynamic analyses. Earthquakes used for analyses are summarized in Table 3.1.

Table 3.1 Earthquake records used

Event	Station	Comp.	Scaled			Scale Factor
			PHA (mm/s^2)	PHA (g)	PHV (mm/s)	
1940 Imperial Valey, Ca	El Centro	S00E	2406.8	0.25	3.3	0.70
1971 San Fernando, Ca	Hollywood Storage, L.A.	N90E	1962.8	0.20	2.1	0.95
1971 San Fernando, Ca	Hollywood Storage, L.A.	S00W	2282.9	0.23	1.7	1.36
1949 Western Washington, Wa	Olympia, Highway Test lab.	N04W	1598.1	0.16	2.1	0.99
1983 Coalinga aftershock, Ca	Oil Fields Fire Station	N270	2538.6	0.26	1.6	1.20
Simulated Motion, Mw=7.2	R=70km	-	2271.4	0.23	1.9	2.12

The following design procedure (illustrated in Figures 3.2 and 3.3) was followed to ensure that the resulting strength of each braced frame matched its design spectrum value for the corresponding R and KL/r values:

(a) The UBC design spectrum (Figure 3.3) was scaled-down by the target R value.
(b) The maximum specified base shear, V, from that spectrum (i.e. from the short-period plateau of the spectrum) was considered to initiate the design.
(c) For the specified design strength and target KL/r value, the brace area, A, and inertia, I, were determined.
(d) The natural period, T_n, of the resulting braced frame was calculated.
(e) At the calculated period, the required base shear was read from the design spectrum. If this demand was different from the one considered in the previous iteration (or in step (b) for the first iteration), the new specified base shear was therefore considered in step (c) to redesign the brace. If the demand was identical to the one considered, the iteration processed ended.

Square Hollow Structural Sections (HSS), also known as tubes, were selected for all designs, as this was apparently the structural section type that was apparently the most frequently tested (as shown in Table 2.3). Note that member sizes (i.e. width and thickness of the square tubular sections) were selected to provide a strength that perfectly matched the brace forces resulting from the loads applied to the braced frames. These were calculated using the solver function in a spreadsheet program. The corresponding braces are therefore "virtual members" that have the desired properties but that may not correspond to an available shape listed in the AISC Manual (1992). Designs constrained to available structural shapes will be discussed in the following section. Calculation sheets for the 15 bracing members considered here are included in Appendix D.

3.3 Brace Models Considered

Analytical models to represent the cyclic behavior of steel bracing members have been developed by Jain et al. (1977), Gugerli and Goel (1982), Ikeda et al. (1984), Lee and Goel (1987), and Hassan and Goel (1991). These models simulate several important phenomena observed during the inelastic cyclic loading of braces, such as progressive deterioration of the compression buckling strength, and residual elongation due to plasticity. Lee and Goel (1987) and Hassan and Goel (1991) also included a model to compute the number of cycles prior to fracture.

Analytical models for steel bracing members can be classified into three general types, namely: (a) finite element models; (b) phenomenological (empirical) models, and; (c) physical models.

As one would expect, finite element models generally divide the brace into a series of small segments. Although these can provide the most realistic representation of brace behavior, this typically requires a very fine mesh and large-displacement analysis, which makes finite element models too complex for the linear-elastic or non-linear inelastic analysis of actual braced structures.

Phenomenological models of the cyclic behavior of braces have been developed and refined by Jain et al. (1977), Ikeda et al. (1984), Lee and Goel (1987), and Hassan and Goel (1991). These models are based on simplified empirical rules which can mimic the observed axial force-axial displacement hysteretic curves of the bracing members. The axial force, axial stiffness, as well as a number of empirical parameters, are specified to define the hysteretic curve of a given brace. For computational efficiency, these models generally use linear segments to define the hysteretic loops. A schematic of the hysteresis rules used by the Ikeda and Mahin's model (1984) and the Hassan and Goel's model (1991) are shown in Figure 3.4 and 3.5, respectively. Models having fewer number of linear segments tend to be simpler and less computationally demanding, but the models having more segments can replicate more accurately the complex behavior of braces.

Brace models based entirely on physical behavior (physical brace models) were developed by Nonaka (1987), Gugerli and Goel (1982), and Ikeda and Mahin (1984) to simulate the cyclic buckling behavior of steel braces. Taddei (1995) implemented the Ikeda and Mahin model in Drain-2DX. This model is based on an analytical expression of the axial force (P) versus axial displacement (δ), describing the behavior of steel brace members. The P-δ expression still depends on some empirical characteristics, such as knowledge of the P-M interaction curve, value of the tangent modulus as it evolves during testing, and modeling of plastic hinge rotation at midspan.

The model divides a hysteretic cycle into six possible zones of behavior, over which simple formulations are used to approximate the physical characteristics. Figures 3.6 and 3.7 show the member geometry and zones of physical behavior, respectively.

In this study, the refined physical model was used for non-linear dynamic analysis. Though this model requires more computation time than the phenomenological model, it was deemed to capture more accurately the cyclic inelastic behavior of bracing members. Figures 3.8 and 3.9 show comparisons of the results with results obtained with the phenomenological and refined physical model, respectively.

3.4 Non-linear Dynamic Analyses

Six ground motions were used in the non-linear dynamic analyses. The characteristics of these six earthquakes are presented in Table 3.1 and the time histories of the records are plotted in Figures 3.10 to 3.12. With these ground motions, response spectra with 5% damping were constructed and scaled to match the UBC 94 Zone 2B spectra as much as possible over the range of periods from 0 to 3, using least square method. The non-scaled and scaled response spectra are shown in Figures 3.13 and 3.14, respectively.

All non-linear dynamic analyses have been performed using Drain-2DX (Prakash and Powell, 1993), and the Ikeda and Mahin physical brace (element No. 5) implemented in Drain-2DX by Taddei (1995). P-δ effects were included in analyses, and 5% damping was used (mass proportional Rayleigh damping factors are presented in Table 3.2).

Table 3.2 Mass proportional damping factors, α, used in analyses

KL/r	R = 1	R = 2	R = 4	R = 6	R = 8
50	1.8008	1.0076	0.5966	0.4426	0.3563
100	2.3977	1.5391	0.9188	0.6767	0.5458
150	3.5939	2.5426	1.6894	1.2473	1.0062

The hysteresis loops obtained from the analysis of all bracing members considered are attached in Appendix C. The corresponding behaviors inferred from these results as well as from other analyses and parametric studies will be presented in the following section.

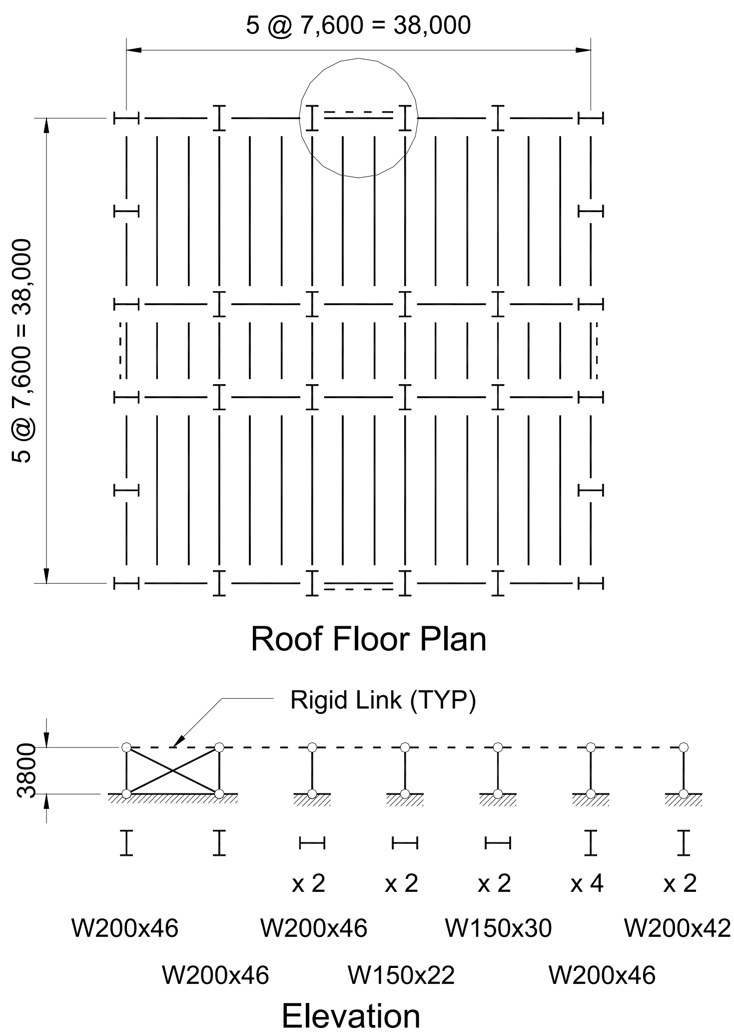

Figure 3.1 Building studied (Tremblay, 1999)

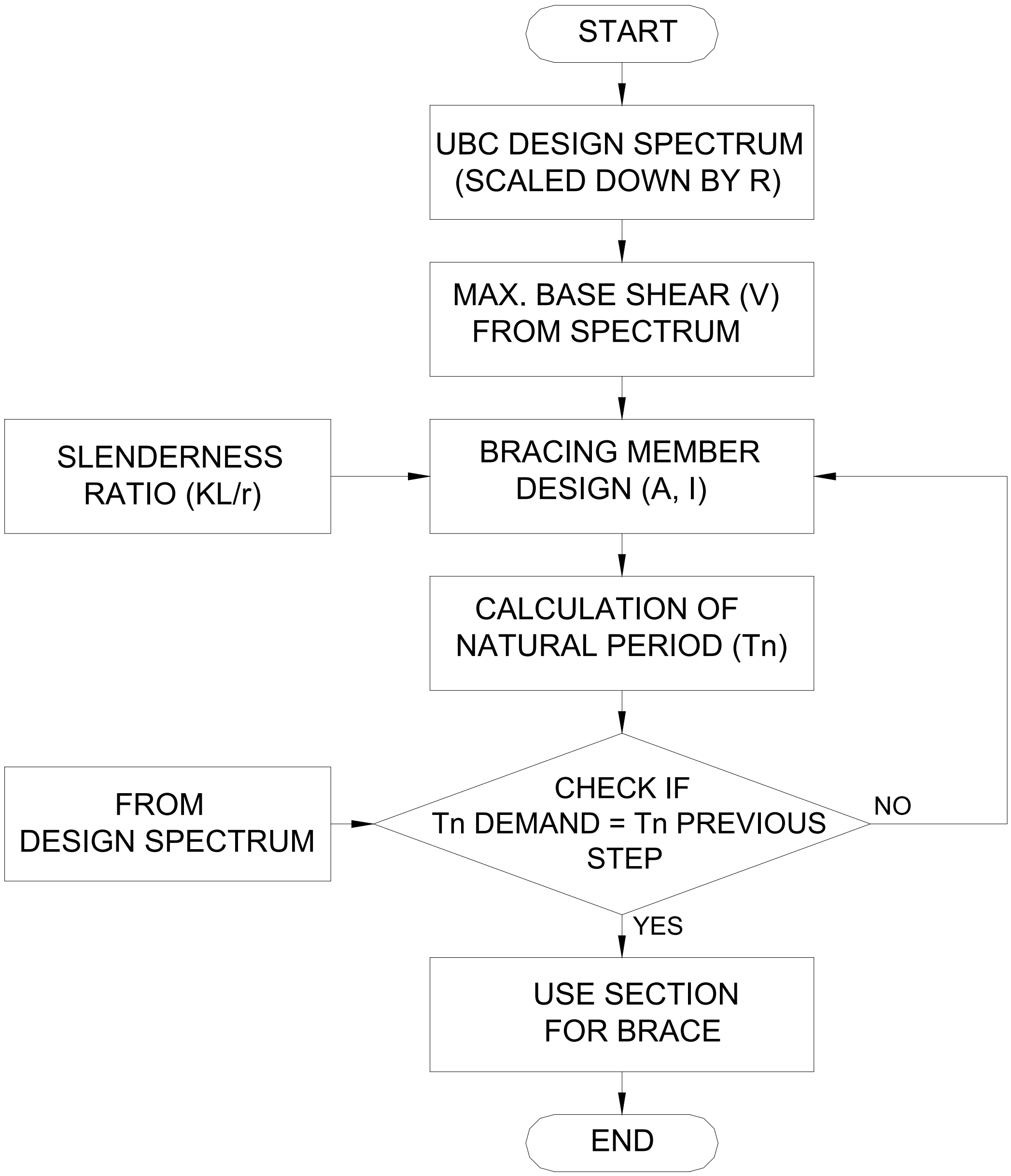

Figure 3.2 Bracing member design

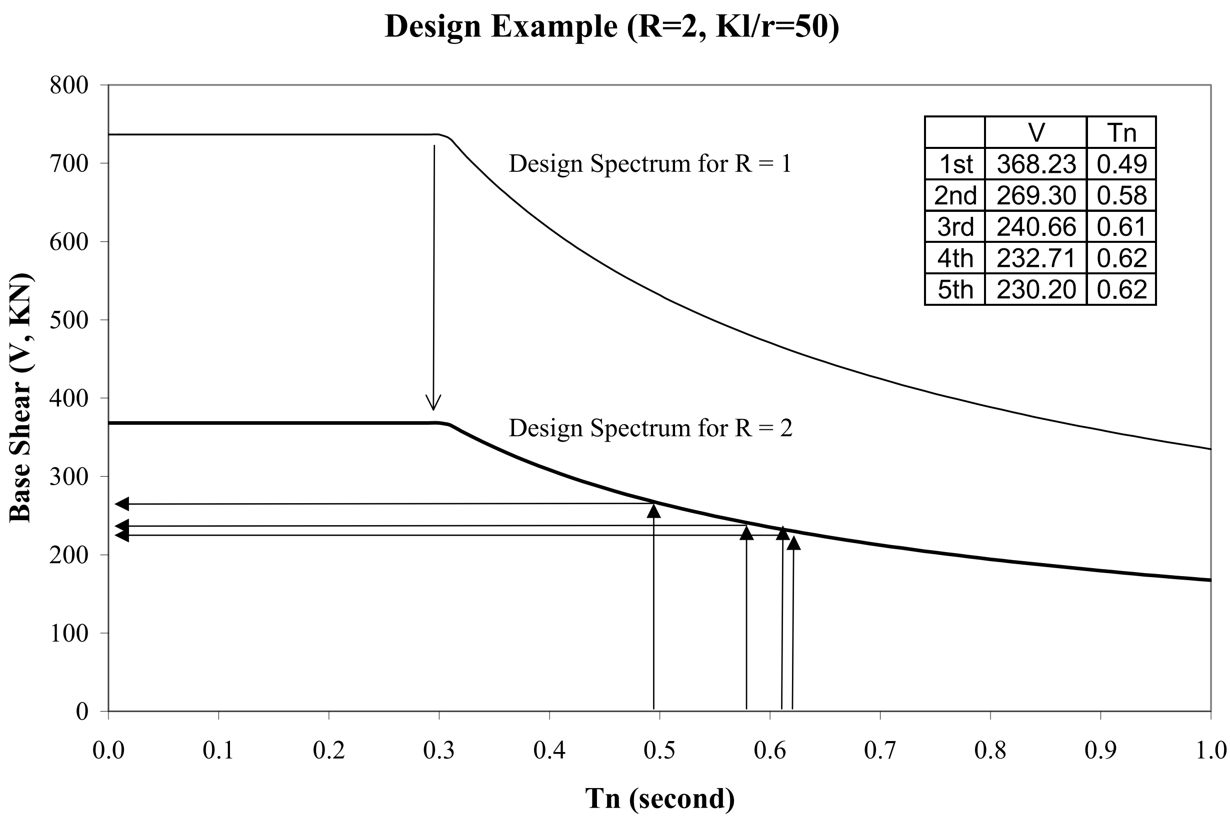

Figure 3.3 Design Example for braced frame with KL/r = 50 and R = 2

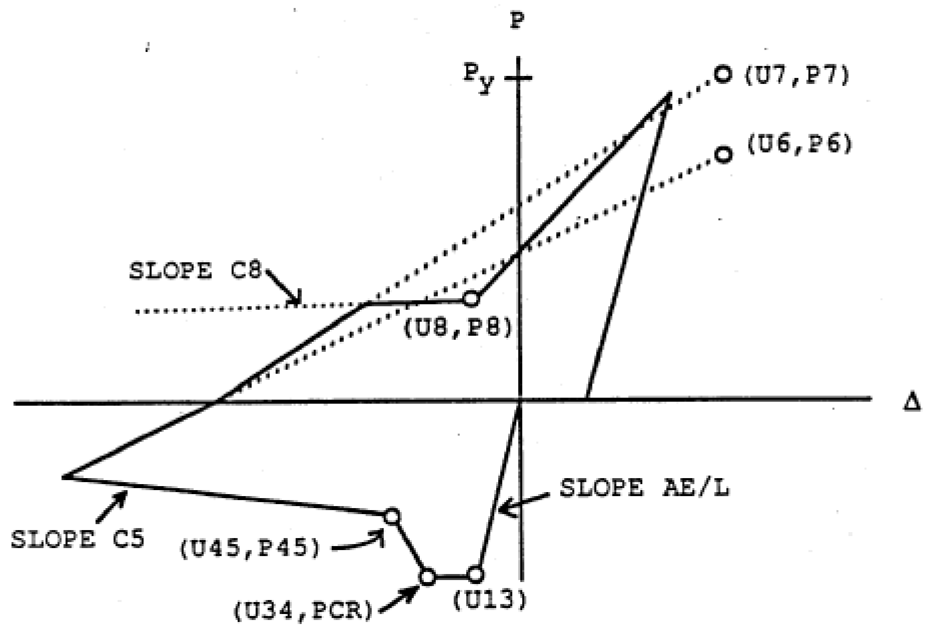

Figure 3.4 Hysteretic rules of Ikeda and Mahin (1984)'s phenomenological model

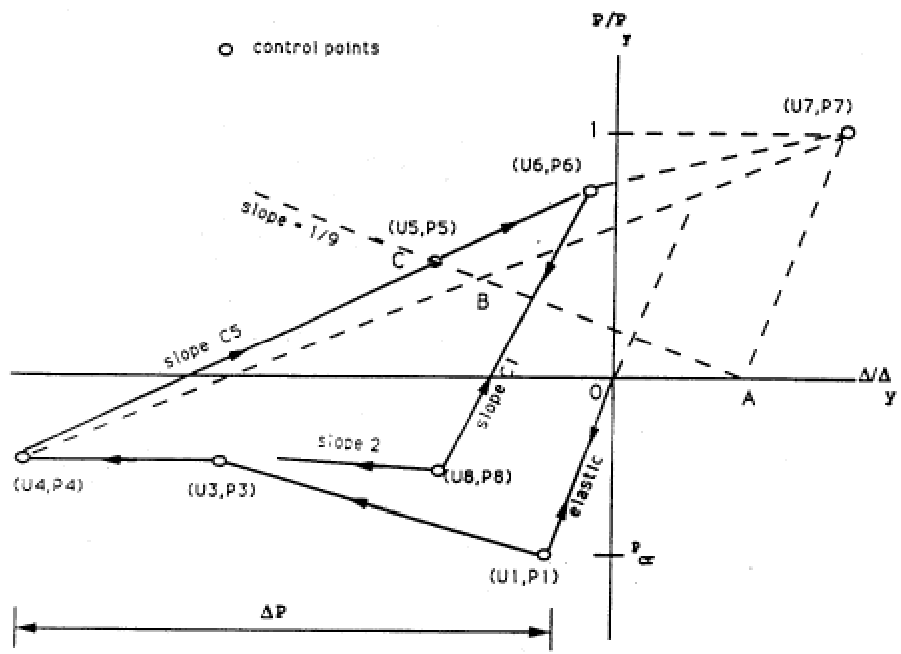

Figure 3.5 Hysteretic rules of Hassan and Goel (1991)'s phenomenological model

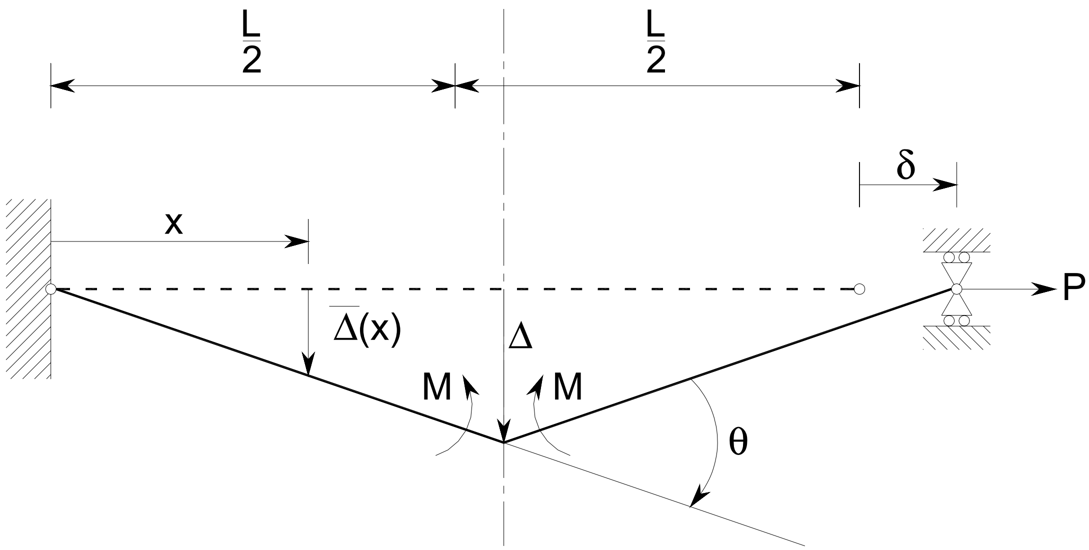

Figure 3.6 Member geometry of refined physical theory model (Ikeda and Mahin, 1984)

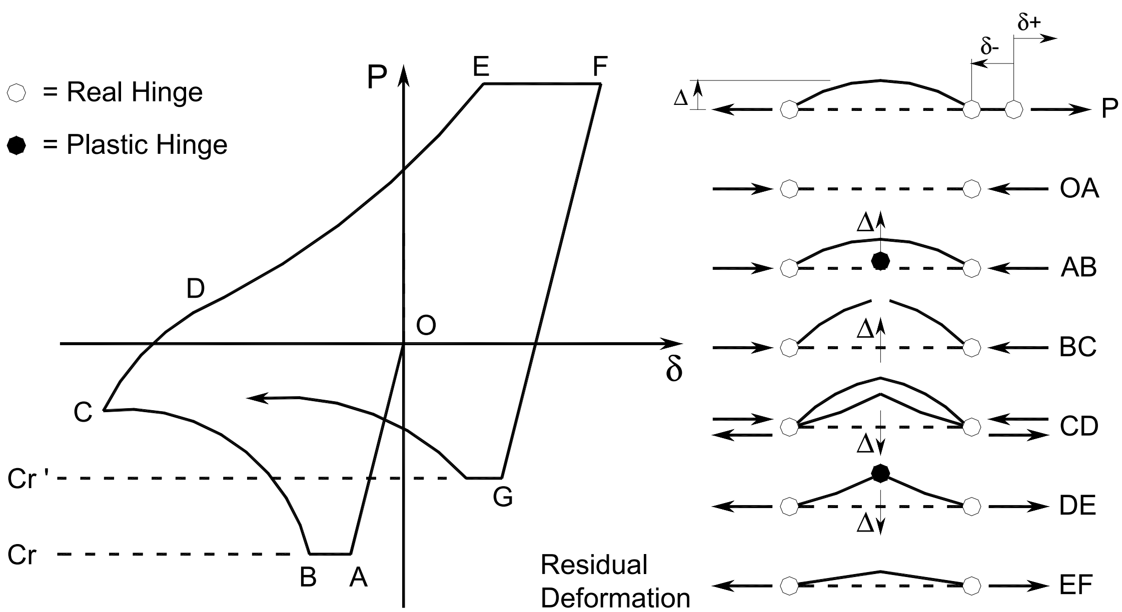

Figure 3.7 Zone definitions of refined physical theory model (Bruneau et al., 1998)

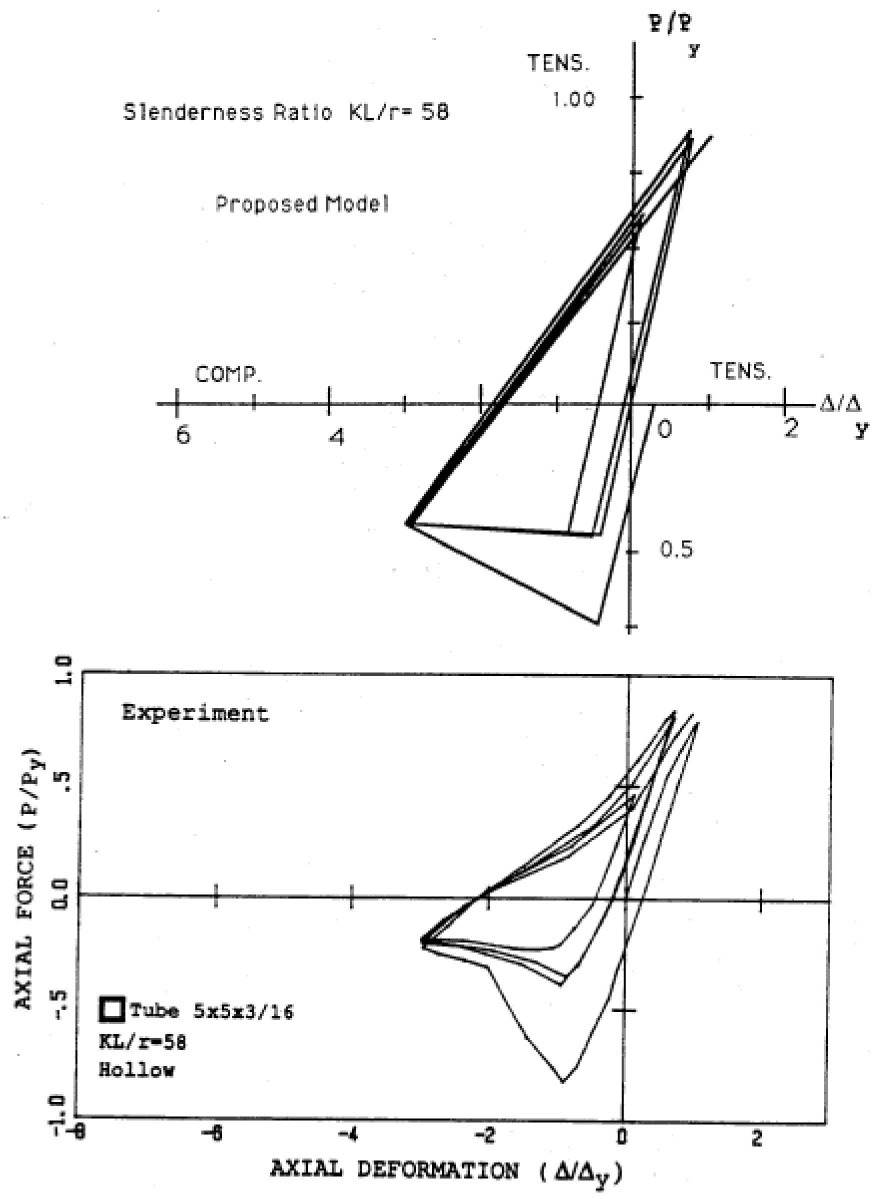

Figure 3.8 Comparison of a test result (below) with results obtained using the phenomenological model (Hassan and Goel, 1991)

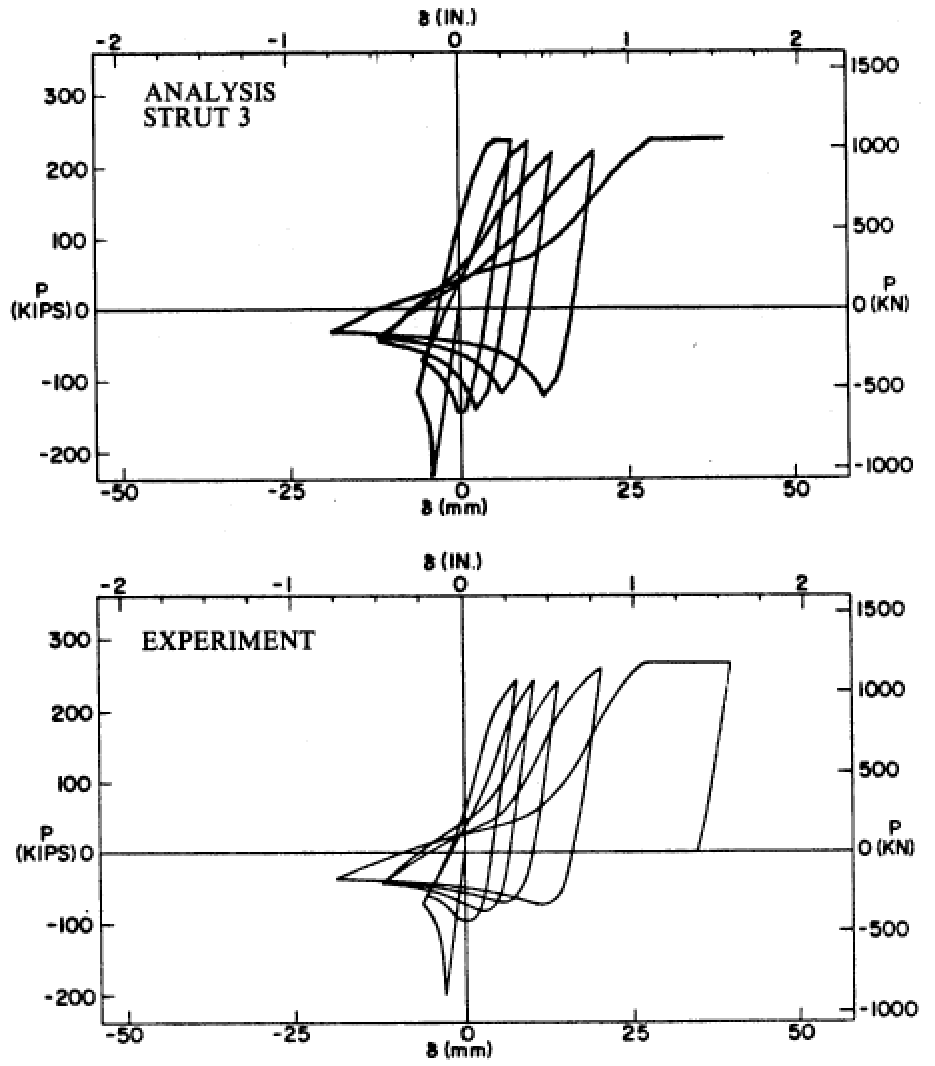

Figure 3.9 Comparison of a test result (below) with results obtained using the refined physical theory model (Ikeda and Mahin, 1984)

GROUND ACCELERATION
EL CENTRO (E1)

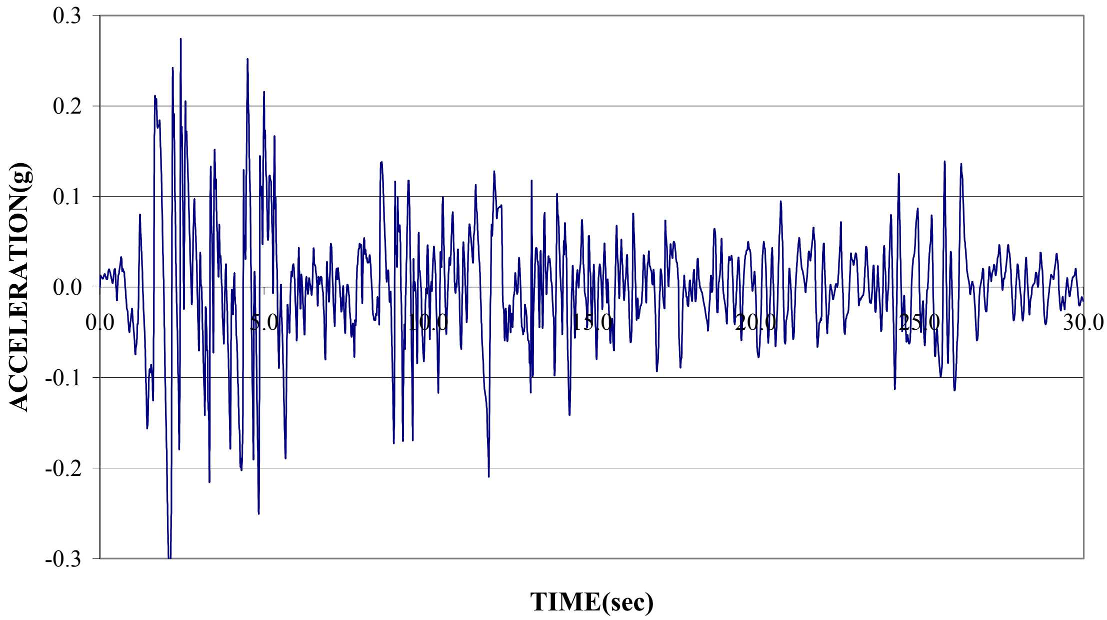

GROUND ACCELERATION
HOLLYWOOD STORAGE, L.A., NE (E2)

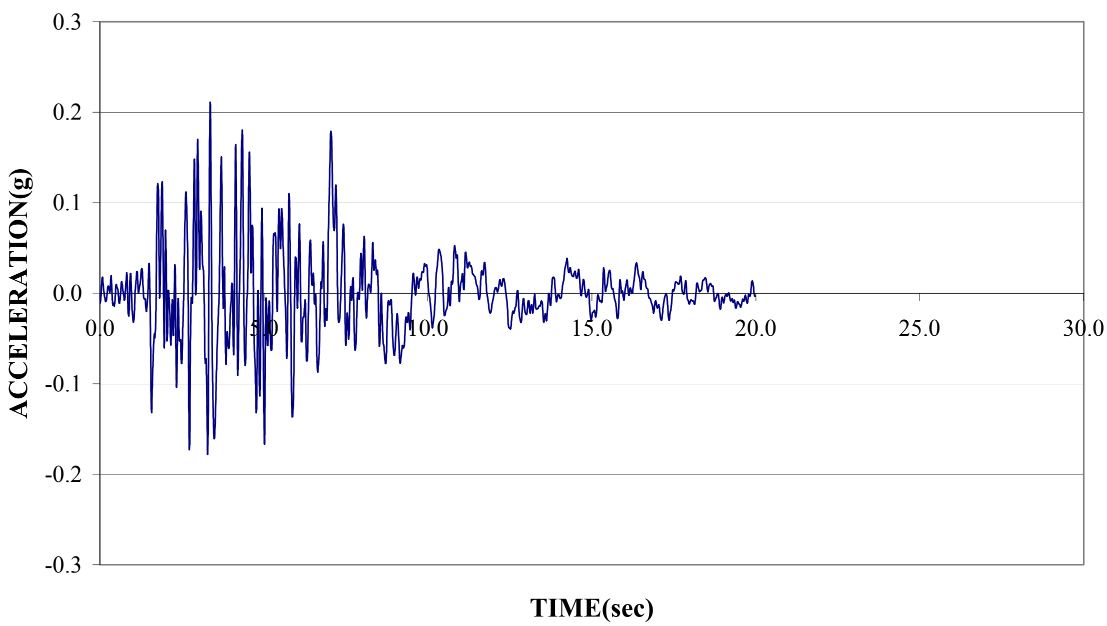

Figure 3.10 Earthquake records

GROUND ACCELERATION
HOLLYWOOD STORAGE, L.A., SW (E3)

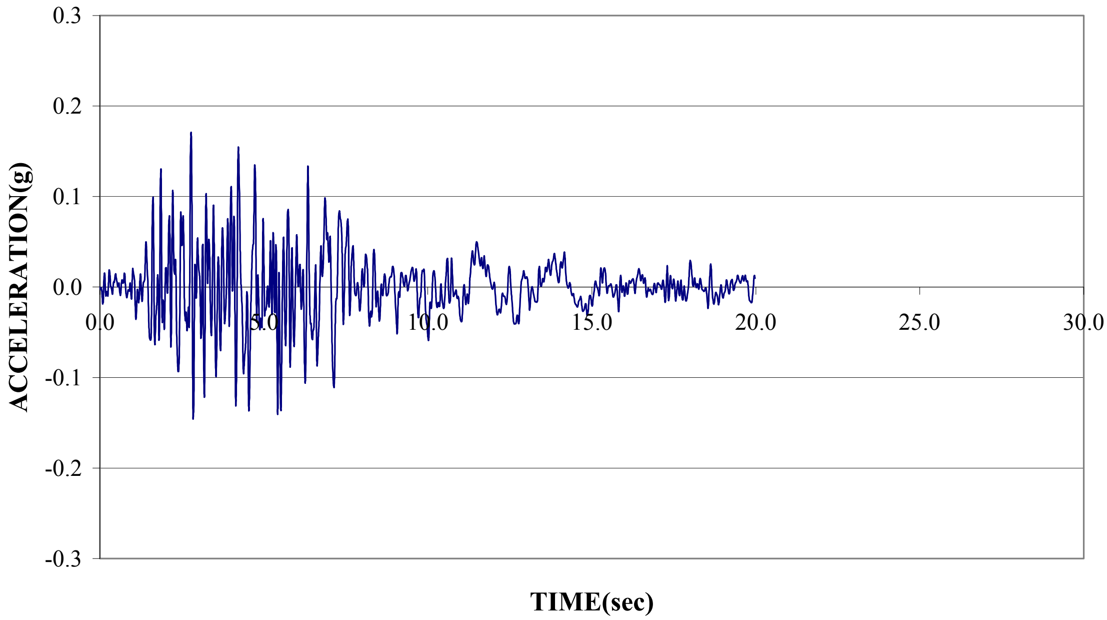

GROUND ACCELERATION
OLYMPIA, HIGHWAY TEST LAB. (E4)

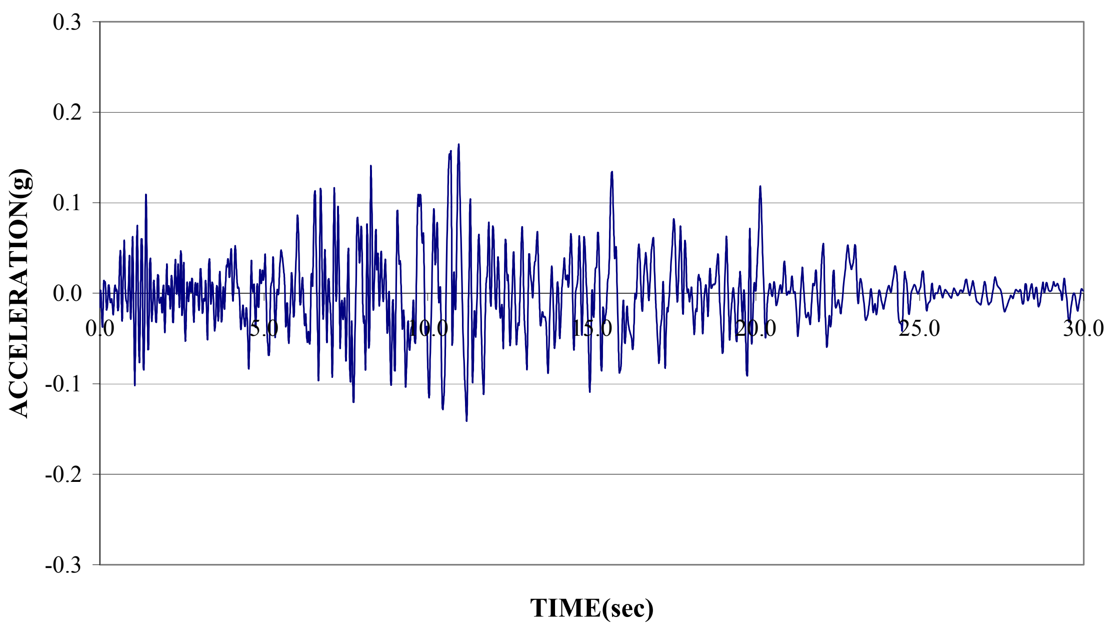

Figure 3.11 Earthquake records (continue)

GROUND ACCELERATION
OIL FIELDS FIRE STATION (E5)

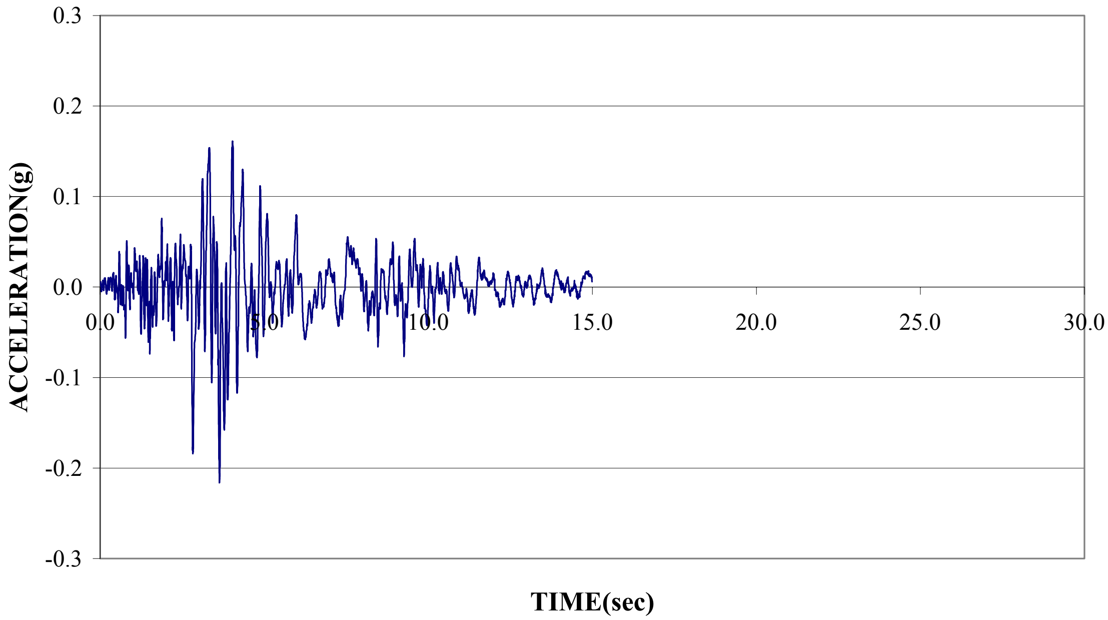

GROUND ACCELERATION
SIMULATED MOTION, R=72km (E6)

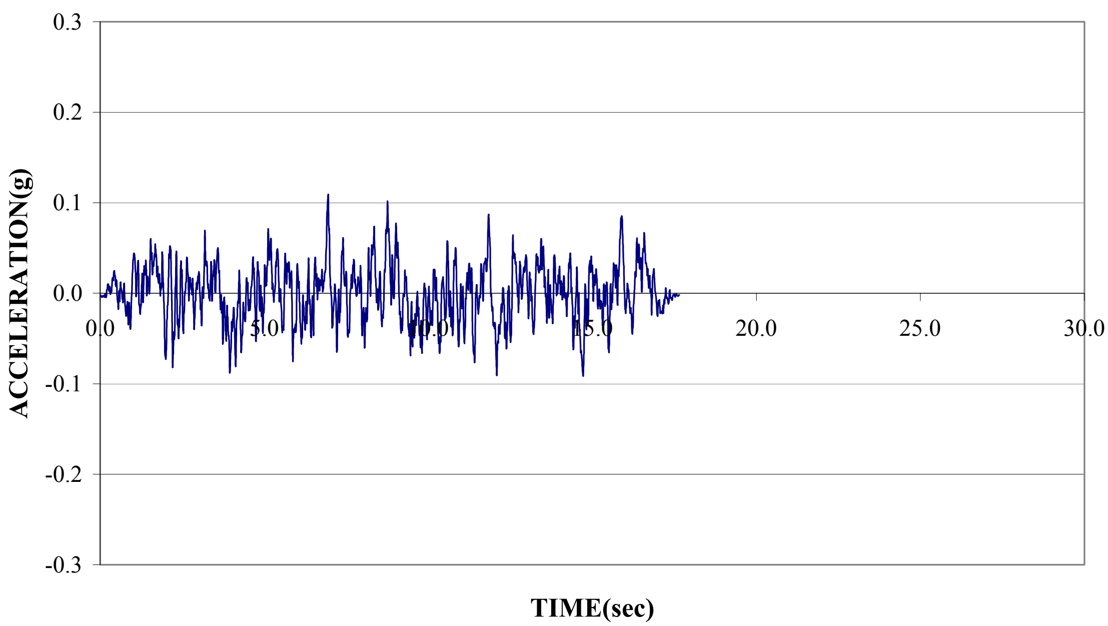

Figure 3.12 Earthquake records (continue)

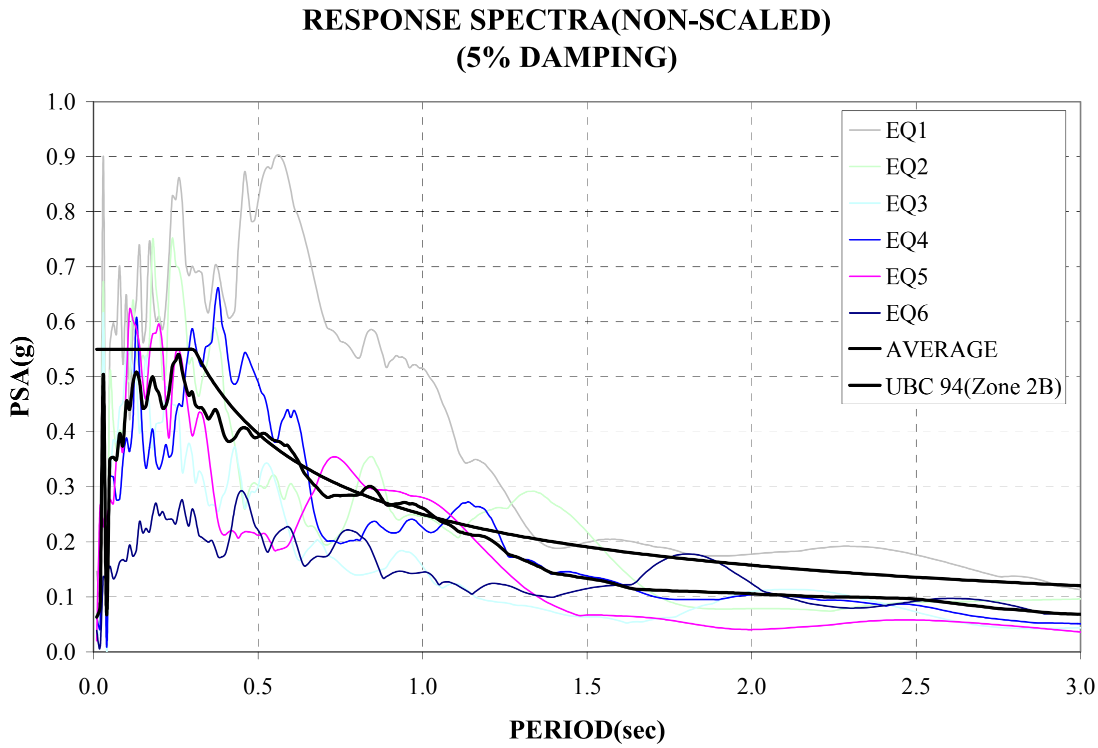

Figure 3.13 Non-scaled response spectra

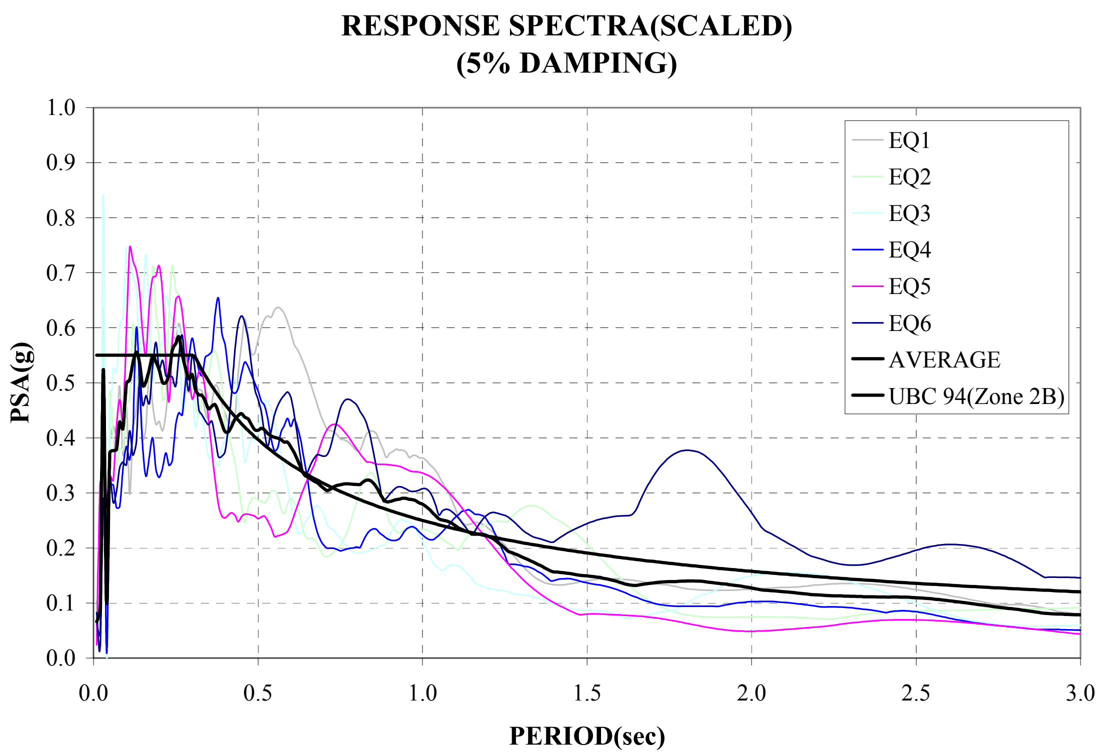

Figure 3.14 Scaled response spectra

SECTION 4

PARAMETRIC AND CASE STUDIES

In this section, results from the non-linear dynamic analyses conducted in the previous section, are investigated and correlated with the experimental data reviewed in SECTION 2. In particular, the hysteretic energy ratios are related to KL/r and R values. Ductile design procedures for CBF and case studies are discussed. Fracture life of tubular bracing members is also reviewed. For reasons indicated in the previous section, this parametric study is limited to structural tubes and pipes.

4.1 Normalized Cumulative Energy Demand Ratios

Normalized cumulative energy demand ratios ($\Sigma E_C / E_T$) from experimental data and results of analyses are summarized in Tables 4.1 and 4.2, respectively. The cumulative energy from analyses of cases having small R values and large KL/r could not be calculated because the bracing members remained in the elastic range, defined as zone OA and AB in Figure 3.7. These cases are noted as N/A in Table 4.2. The normalized cumulative energy ratios as a function of R for the cases having KL/r values of 50 and 150 are presented in Figures 4.1 and 4.2, respectively. The corresponding averages are compared in Figure 4.3. The range of normalized cumulative energy ratios obtained from the experimental data is contained within the shaded area in Figure 4.1. The average results are included in Figures 4.2 and 4.3 (a single experimental data point in the case of Figure 4.2). As shown in Figures 4.1 and 4.2, as R increases, the normalized cumulative energy ratio decreases. It is also observed that all the analysis results obtained are within the range of experimental data available. Figure 4.3 shows that increasing KL/r translates into a decrease in normalized cumulative energy ratios. This means that more slender members undergo less inelastic energy demand than stocky ones, irrespectively of the R value used in design.

Table 4.1 Cumulative energy ratios ($\Sigma E_C / E_T$) from experimental data

KL/r=50 (0 - 75)			KL/r=100 (75 - 125)			KL/r=150 (125 - 200)		
Reference	Specimen I.D.	$\Sigma(E_C/E_T)$	Reference	Specimen I.D.	$\Sigma(E_C/E_T)$	Reference	Specimen I.D.	$\Sigma(E_C/E_T)$
Black et al.(1980)	21	5.90	Black et al.(1980)	17	3.21	Archambault et al.(1995)	S3B	2.28
Zayas et al.(1980)	1	2.61	Black et al.(1980)	18	2.42			
Zayas et al.(1980)	2	4.28	Black et al.(1980)	22	3.50			
Zayas et al.(1980)	3	2.28	Black et al.(1980)	14	4.55			
Zayas et al.(1980)	4	3.02	Black et al.(1980)	15	2.25			
Zayas et al.(1980)	5	6.67	Black et al.(1980)	16	6.11			
Zayas et al.(1980)	6	8.22	Black et al.(1980)	24	4.66			
Jain et al.(1978)	1	4.74	Jain et al.(1978)	6	0.83			
Jain et al.(1978)	4	2.16	Jain et al.(1978)	12A	0.72			
Jain et al.(1978)	9	1.70	Jain et al.(1978)	15	1.32			
Walpole (1996)	2	1.98	Archambault et al.(1995)	S1B	2.22			
Walpole (1996)	3	1.94	Archambault et al.(1995)	S1QB	1.19			
			Archambault et al.(1995)	S2B	2.30			
			Archambault et al.(1995)	S4B	2.26			
			Archambault et al.(1995)	S4QB	0.95			
			Archambault et al.(1995)	S5B	2.44			
			Walpole (1996)	1	1.51			
Average		3.79	Average		2.50	Average		2.28
max		8.22	max		6.11	Max		2.28
min		1.70	min		0.72	Min		2.28

Table 4.2 Cumulative energy ratios ($\Sigma\ E_C\ /\ E_T$) from analysis results

KL/r=50		$\Sigma(E_C/E_T)$				
Earthquake	Element	R=1	R=2	R=4	R=6	R=8
E1	Elem.1	N/A	7.646	5.447	4.666	4.084
E1	Elem.2	N/A	6.923	5.592	5.710	4.520
E2	Elem.1	N/A	1.955	3.359	2.684	2.053
E2	Elem.2	N/A	1.153	3.587	3.150	2.853
E3	Elem.1	N/A	3.225	3.331	2.415	2.062
E3	Elem.2	N/A	2.462	3.082	2.967	2.256
E4	Elem.1	N/A	3.463	5.209	4.563	3.495
E4	Elem.2	N/A	4.364	6.122	5.123	3.789
E5	Elem.1	N/A	2.963	2.552	1.616	1.549
E5	Elem.2	N/A	2.120	2.887	1.876	2.157
E6	Elem.1	N/A	4.929	2.970	2.556	2.350
E6	Elem.2	N/A	5.795	1.843	1.469	1.217
Average		N/A	3.916	3.832	3.233	2.699
KL/r=150		$\Sigma(E_C/E_T)$				
Earthquake	Element	R=1	R=2	R=4	R=6	R=8
E1	Elem.1	N/A	N/A	N/A	3.281	2.956
E1	Elem.2	N/A	N/A	3.649	3.553	3.057
E2	Elem.1	N/A	N/A	N/A	1.536	1.068
E2	Elem.2	N/A	N/A	N/A	1.222	1.354
E3	Elem.1	N/A	N/A	N/A	1.131	1.271
E3	Elem.2	N/A	N/A	N/A	1.347	0.956
E4	Elem.1	N/A	N/A	3.454	2.688	2.366
E4	Elem.2	N/A	N/A	2.219	1.978	2.110
E5	Elem.1	N/A	N/A	N/A	0.889	1.177
E5	Elem.2	N/A	N/A	N/A	0.851	1.042
E6	Elem.1	N/A	N/A	1.505	0.686	1.000
E6	Elem.2	N/A	N/A	1.451	1.617	0.832
Average		N/A	N/A	2.456	1.732	1.599

Normalized cumulative energy ratios as a function of the width-to-thickness ratios (b/t) are presented in Figure 4.4 and Figure 4.5 for KL/r of 50 and 150 respectively. As mentioned in the previous section, the HSS bracing members used for the analyses do not correspond to actual members available in the AISC LRFD Manual of Steel Construction (1994). These virtual tubular members have b/t ratios excessively large and cannot therefore be compared with the experimental data.

4.2 Alternative Approaches for Sensitivity Case Studies

4.2.1 Redesign Following AISC Ductile Design Procedures

Bracing members were designed following ductile design procedures (AISC, 1997; Bruneau et al., 1998). Ductile design starts with a strength design in accordance with the AISC LRFD Specification (1993) and minimum weight as design objective. In that process, tubular braces were selected. Then, members obtained from strength design are evaluated and modified as necessary to guarantee ductile response of the frame, by satisfying the limits on the KL/r and b/t ratios of braces specified for SCBF (AISC, 1997). Calculation sheets, following the ductile design procedures, are attached in Appendix E and resulting brace member sizes are summarized Table 4.3. Essentially, the design procedure follows the same approach as in SECTION 3, with the exception that available structural shapes are used, rather than specified section properties that may not correspond to sections currently produced. All resulting brace members are bigger than those designed following the design procedure outlined in SECTION 3. This is expected as bigger sections are typically obtained for ductile design when compared to strength design. However, because of the requirements for ductile designs, brace members ended up being the same for all cases, regardless of R values (from 1 to 6). As a result, they all behaved elastically, making all comparisons of hysteretic behavior a moot point in this case.

Table 4.3 Strength design and ductile design data

R	Strength Design			Ductile Design			Code Limits	
	Member(U.S.)	KL/r	b/t	Member(U.S.)	KL/r	b/t	KL/r	b/t
1	TS 7 x 7 x 1/4	122.1	26.0	TS 10 x 10 x 5/8	88.5	14.0	101.0	15.4
2	TS 6 x 6 x 1/4	143.6	22.0	TS 10 x 10 x 5/8	88.5	14.0	101.0	15.4
4	TS 5 x 5 x 3/16	171.6	24.7	TS 10 x 10 x 5/8	88.5	14.0	101.0	15.4
6	TS 5 x 5 x 1/8	169.0	38.0	TS 10 x 10 x 5/8	88.5	14.0	101.0	15.4
8	TS 4 1/2 x 4 1/2 x 1/8	187.9	34.0	TS 10 x 10 x 5/8	88.5	14.0	101.0	15.4

4.2.2 *Effects of KL/r on R and b/t ratios*

To investigate the relationship between KL/r, R, and b/t without being constrained to actual available member sizes, bracing members were redesigned.For a desired KL/r ratio corresponding to a given cross-sectional area and member length, member dimensions such as width, depth, and thickness were changed to obtain the necessary radius of gyration, r. The design procedure is otherwise identical to the one described in SECTION 3 and calculation sheets are attached in Appendix F. Results are summarized in Table 4.4 and compared in Figure 4.6 and Figure 4.7. The R values in Table 4.4 and Figure 4.6 were obtained as follows:

(a) The members designed in SECTION 3 for R=1, 2, 4, 6, and 8 and KL/r value of 50 are kept as the "reference members" (i.e., unchanged).
(b) KL/r is increased from 50 to 100 and 150 and the member is redesigned to satisfy the new KL/r value but keeping the cross sectional area and length of member constant and only changing the width, depth, and thickness of the braces to achieve the new slenderness.
(c) The resulting brace member dimensions are used to calculate the brace strength (i.e., the elastic buckling capacity of the bracing member).
(d) From that bracing force, the contribution of the compression member to the base shear of strength of the frame is calculated, and assumed to be equal to the total base shear strength in this case (tension member strength is neglected).
(e) Modal analysis is performed to get the natural frequency (T_n) of the structure.
(f) The corresponding base shear at T_n is found on the elastic design spectrum.
(g) Dividing (f) by (d) gives the corresponding R value resulting from the member size change to have the target KL/r without changing length or cross sectional area of the brace.

Here, strength of the frame is taken as equal to twice the strength of the compression brace which governs the design process when the brace is assumed to resist V/2. This neglects the possible overstrength provided by the tension brace, which would be included however in non-linear time history analysis of the resulting systems.

Table 4.4 Effects of KL/r on R and b/t ratios

KL/r	R				
50	1.0	2.0	4.0	6.0	8.0
100	1.8	3.2	6.3	9.5	12.7
150	4.0	7.1	14.3	21.4	28.5
	b/t				
R	1	2	4	6	8
50	667.1	1884.1	5355.7	9825.7	15115.2
100	166.0	470.3	1338.2	2455.8	3778.3
150	73.2	208.5	594.2	1090.9	1678.7
	T_n				
R	1	2	4	6	8
50	0.37	0.62	1.05	1.42	1.76
100	0.37	0.62	1.05	1.42	1.76
150	0.37	0.62	1.05	1.42	1.76
	I				
R	1	2	4	6	8
50	29959.90	10618.18	3736.70	2037.03	1324.07
100	7489.96	2654.58	934.20	509.23	331.04
150	3328.87	1179.81	415.20	226.32	147.13

In that perspective, R is the ratio of the demand on the elastic response spectra at the period of the system divided by the strength calculated by the above procedure at the same period. Consequently, as KL/r increases, the strength of the compression brace decreases, the corresponding assumed design strength of the frame reduces, and R increases.

As shown in Figure 4.6 and Figure 4.7, following the above procedure, R increases and b/t decreases for increasing values of KL/r. In this context, a larger R means that structures with larger KL/r have a greater ductility demand, and smaller b/t means a higher resistance against local buckling. As seen in the previous section, a structure with a large R value has less normalized cumulative energy dissipation. Since R increases with KL/r, this suggests that increasing KL/r in this case translate into decreasing normalized cumulative energy dissipation demand. These observations are based on the non-linear dynamic analyses reported here for KL/r of 50 and 150, and the assumption that the trends can be interpolated for other values of KL/r.

4.2.3 Effects of member length, L, on R

Another alternative design approach was adopted to investigate the relationship between KL/r and R. In this approach, for each target KL/r value, the bracing member lengths were increased while the member geometry (width, depth, and thickness) was kept constant. Design procedures otherwise followed those presented in SECTION 3 and calculation sheets are attached in Appendix G. The results of designs and R value calculations are summarized in Table 4.5 and Figure 4.8. Though the tensile strengths of bracing members (A_gF_y) remained constant in this case, the buckling strength of the bracing members (C_r) decreased for larger KL/r values. Again, increasing KL/r results in higher R values and thus, higher ductility demands but lower normalized cumulative energy dissipation capability (based on data presented in SECTION 2). Note that these observations are subjected to the same limitations expressed in the previous section.

Table 4.5 Effects of member length (L) on R

KL/r (L)	R				
50	1.00	2.00	4.00	6.00	8.00
100	1.40	2.81	5.62	8.44	11.25
150	2.77	5.51	11.06	16.59	22.12
	T_n				
KL/r (L)	R=1	R=2	R=4	R=6	R=8
50	0.37	0.62	1.05	1.42	1.76
100	0.53	0.88	1.49	2.01	2.49
150	0.64	1.08	1.82	2.46	3.05

4.3 Fracture Life of Tubular Bracing Members

Bracing members may suffer from large cyclic deformations under severe earthquakes. Previous studies (Tang and Goel, 1987 and Archambault et al., 1995) showed that some bracing members designed in full compliance with current code requirements, sometimes do not have sufficient ductility to survive the imposed deformations. The members cracked and fractured early due to severe local buckling in the regions of plastic hinges. In any concentrically braced frame, the braces provide the lateral stiffness and strength to the structure and are the elements that dissipate the seismic energy. Fracture of braces may lead to collapse. In this section, two different fracture criteria of tubular bracing members are reviewed. Note that wherever Δ is used in fracture models, it actually corresponds to the axial elongation of the brace, i.e., δ per the notation used in the rest of the report.

4.3.1 Tang and Goel Model

Tang and Goel (1987) introduced an empirical fracture criterion for rectangular tubular bracing members. This criterion requires a special calculation of the number of cycles that contribute to fatigue life. To count these cycles, Tang and Goel established the following rules applicable to a brace axial deformation time history (referring to Figure 4.9 to help explain some of these concepts):

(a) A full cycle is typically defined from one peak in compression to another. In-between these two compressive peaks, the brace member will typically be subjected to tension (although not always). For this discussion, displacements are taken as negative in the direction of greater compression. For example, in Figure 4.9, full cycles are defined from point 1 to 2, 2 to 3, etc.

(b) Only the half cycles from a compression peak to the point of maximum tension (or minimum compression) in a cycle are counted to contribute to fatigue life. In that perspective, in Figure 4.9, cycle 1-2 contributes a value of 1 to the fatigue life calculation (i.e. a displacement of Δ/Δ_y=+1 from the point 1 at Δ/Δ_y=-1 to the peak displacement in tension at Δ/Δ_y=0).

(c) A standard cycle is defined as the one contributing a value of 1.0 to the fatigue life calculation.

(d) The effect of small deformations cycles (defined as deformations of less than the standard cycle, or, in other words, of less than Δ_y) are deemed to only have a small effect on the fatigue life of bracing members, and are ignored. For example, cycle 0-1 in Figure 4.9 would be ignored.

(e) The amplitude of cycles proportionally contribute to fatigue life. In other words, a cycle with an amplitude of 4Δy is equal to 4 cycles of Δy. For example, in Figure 4.9, cycle 2-3 is equivalent to two cycles 1-2.

Figure 4.10 illustrates how a complex displacement time history is decomposed in a series of standard cycles following the above rules.

Following this criterion, the following fracture life model for tubular bracing members was proposed:

$$N_f = C_s \frac{(B/D)(60)}{[(B-2t)/t]^2} \quad for\ KL/r \leq 60 \tag{4.1a}$$

$$N_f = C_s \frac{(B/D)(KL/r)}{[(B-2t)/t]^2} \quad for\ KL/r > 60 \tag{4.1b}$$

where N_f is the fracture life expressed in terms of standard cycles, C_s is a numerical coefficient obtained from the test results, B and D are respectively the gross width and depth of the section (in inches), and t is thickness of the section (in inches).

Lee and Goel (1987) reformulated this model by considering the effect of F_y and eliminating the dependency on KL/r. In this criterion, Δ_f is used instead of N_f to quantify the fracture life of a tubular bracing member. This method proceeds per the following steps.

(a) The hysteresis curves (P vs. Δ) is converted to a normalized hysteresis curves (P/P_y vs. Δ/Δ_y).

(b) The deformation amplitude (tension excursion in a cycle) is divided into two parts, Δ_1 and Δ_2, defined at the axial load $P_y/3$ point, as illustrated in Figure 4.11. Δ_1 is the tension deformation from the load reversal point to $P_y/3$, while Δ_2 is from that $P_y/3$ point up to the unloading point.

(c) $\Delta_{f,exp}$ is obtained by adding 0.1 times Δ_1 to Δ_2 in each cycle and summary summing up for all cycles up to the failure (i.e., by the equation $\Delta_f = \Sigma(0.1\Delta_1 + \Delta_2)$).

(d) The theoretical fracture life, Δ_f is expressed as follows:

$$\Delta_f = C_s \frac{(46/F_y)^{1.2}}{[(B-2t)/t]^{1.6}}\left(\frac{4B/D+1}{5}\right) \tag{4.2}$$

where C_s is an empirically obtained constant calibrated from test results, and F_y is the yield strength of the brace (ksi). The numerical constant C_s, originally given as 1335 by Lee and Goel (1987), was recalibrated using the test results of Gugerli and Goel (1982) and Lee and Goel (1987), and found to be 1560 by Hassan and Goel (1991). Fracture is assumed to occur when $\Delta_{f,exp} = \Delta_f$.

4.3.2 Archambault et al. Model

Another criterion was presented by Archambault et al. (1995). This criterion re-introduced the effect of slenderness ratio, KL/r, on the basis that, based on a review of previous test results, the Tang and Goel model was noted to underestimate the fracture life of tubular bracing members having large slenderness ratios. Two distinct trends were noted for fracture life of bracing members as a function of KL/r, depending on whether slenderness was lower or higher than 70. They introduced the term, Δ^*_f (to differentiate it from Δ_f used by Tang and Goel), and expressed fatigue life as follows:

$$\Delta^*_f = C_s \frac{(317/F_y)^{1.2}}{[(B-2t)/t]^{0.5}}\left(\frac{4B/D+1}{5}\right)^{0.8} \times (70)^2 \ \ for\ KL/r < 70 \tag{4.3a}$$

$$\Delta^*_f = C_s \frac{(317/F_y)^{1.2}}{[(B-2t)/t]^{0.5}}\left(\frac{4B/D+1}{5}\right)^{0.8} \times (KL/r)^2 \ \ for\ KL/r \geq 70 \tag{4.3b}$$

where the C_s value is empirically determined from the experimental results was given as 0.0257, F_y is in MPa and all dimensions are in mm units.

4.3.3 Effects of KL/r and b/t on the Fracture Life

The graphical expression of the equations for fracture life of tubular bracing members proposed by Tang and Goel and Archambault et al. are presented in Figures 4.12 and 4.13, respectively and further compared in Figure 4.14 and 4.15. As indicated in the previous sections, fracture life of tubular bracing member depends on both slenderness ratio, KL/r, and the width-to-thickness ratio, b/t (where $b/t = (B-2t)/t$ for a square tube). Figure 4.13 and Eq. (4.3) show that fracture life does not depend on KL/r for KL/r < 70, and that intermediate and slender bracing members (KL/r ≥ 70) have a fracture life, rapidly increasing in proportion to the square of KL/r. Width-to-thickness ratio, b/t, also has an impact on fracture life, with bracing members having larger b/t value surviving fewer cycles of large inelastic deformations.

4.4 General Observations

It is well known that inelastic cyclic behavior of CBFs largely depends on their slenderness ratios (KL/r) and width-to-thickness ratios (b/t). It is also generally agreed that width-to-thickness ratio (b/t) also has an impact on the fracture life. Bracing members with larger local b/t values are more prone to develop local buckling and will consequently not survive many cycles of large inelastic deformations. Latest research by others indicate that intermediate and slender bracing members (KL/r ≥ 70) have much superior fracture life, and this improvement rapidly increases in proportion to the square of KL/r value.

A number of new observations can be made from the parametric and case studies conducted in this section. These depend closely on the assumptions used for the parametric studies.

(a) When a bracing member is designed with a bigger R value, then the normalized cumulative energy ratio decreases. At first, this may appear to be counterintuitive, as it is generally expected that a structure designed with a bigger R value will have a greater ductility demand, resulting in more energy dissipation because of this larger deformation demand. However, this can be explained as follows. Recall, as explained in SECTION 2.3.1, that the energy dissipation of a brace in compression, E_C, is obtained by calculating the area under the force-axial deformation curve, i.e., corresponding to the compression force times the axial deformation. E_C is then normalized by the corresponding tensile energy, E_T, and the sum of these values for each cycle, cumulated until the end of cyclic loading history, is defined as the normalized cumulative energy ratio $\Sigma(E_C/E_T)$. This means that the normalized cumulative energy in compression is not only a function of axial deformation, but also of the compression force and tensile yield strength. The earthquake loading history also has an effect on the normalized cumulative energy in compression. Figures 4.16 and 4.17 show the normalized cumulative energy ratios of braces designed with same KL/r and R value, but subjected to different earthquakes. Trends are clear although exceptions occur in some cases. For example, for a KL/r value of 50 and R values increasing from 2 to 4, the normalized cumulative energy ratios decreased when Earthquake 1 was applied, but increased when Earthquake 2 was applied. Taking Earthquake 1 as a case study that is consistent with the general trend, to illustrate the effect of R on behavior, it is first possible to observe, as shown in Figures 4.18 and 4.19, that although the brace designed with the larger R value of 4 deformed more than the brace designed with R of 2, the latter resists bigger forces. As the brace deforms more at R of 4, it suffers more strength degradation which translates into a lower normalized cumulative energy ratio. Exceptions occur when the amount of inelastic cycles for the case with greater R value overcome this effect, as shown in Figures 4.20 and 4.21, where the bigger brace corresponding to the case with an R of 2 undergoes mostly cycles in the elastic range (without dissipating energy).

(b) When a bracing member is designed with larger KL/r value, then the normalized cumulative energy ratio decreases. This is a consequence of the ratio of tensile and compressive strength as a function of KL/r, which translates directly into a lower normalized energy ratio (E_C/E_T) for more slender members. This can be illustrated schematically using Figure 4.22. In this example, the strength degradation of a brace after elastic buckling in compression (Equation 2.2) is considered for all cycles except the first. The normalized energy ratios for the 2^{nd} and following cycles of members with KL/r of 50 and 150 are 0.64 and 0.10, respectively, resulting in normalized cumulative energy ratios of 0.64n and 0.10n respectively after *n* cycles. In this case, the member with KL/r of 150 would have to undergo roughly 6.4 more cycles than the member with KL/r of 50 to have the same resulting normalized cumulative energy ratios. Looking at results from the analyses using actual earthquakes, a similar trend was observed. For example, as shown in Figure 4.23 and Tables 4.6 and 4.7, though the slender brace (designed with KL/r value of 150) experienced more inelastic cycle than the stocky brace (designed with KL/r value of 50), the normalized cumulative energy in compression ($\Sigma(E_C/E_T)$) of the stocky brace is still bigger than for the slender brace. Here, the normalized energy ratio (E_C/E_T) of the stocky and slender brace in the 1st cycle (the 1st cycle with relatively large inelastic deformation) are respectively 0.39 and 0.11, and in the 11th cycle, 0.47 and 0.14, respectively. The normalized cumulative energy ratios ($\Sigma(E_C/E_T)$) are 5.22 and 3.45, respectively, even though the slender brace experienced 1.76 times more inelastic cycles.

Table 4.6 Energy calculation for the brace with R=4, KL/r=50, and Earthquake 4

No	Cycle	δ(mm)	E_C/E_T	E_C	E_T
1	5th	7.71	0.18	23.63	132.58
2	6th	5.31	0.12	9.52	82.38
3	7th	8.56	0.20	30.18	149.90
4	8th	21.47	0.39	207.53	532.79
5	9th	21.77	0.39	214.75	546.54
6	10th	34.34	0.49	600.66	1223.84
7	11th	14.22	0.26	89.59	350.35
8	12th	10.66	0.23	49.92	212.80
9	13th	14.12	0.34	99.11	292.97
10	14th	26.56	0.50	391.33	786.29
11	15th	19.66	0.40	201.58	508.96
12	16th	28.61	0.28	242.25	879.78
13	17th	5.85	0.16	14.13	88.85
14	18th	23.60	0.47	299.35	635.14
15	19th	3.40	0.06	3.10	52.65
16	20th	21.73	0.39	231.20	594.41
17	21st	8.81	0.17	29.92	175.37
18	22nd	1.84	0.02	0.61	25.03
19	23rd	3.69	0.06	3.26	57.39
20	24th	1.86	0.03	0.74	25.23
21	25th	3.52	0.08	6.12	72.76
Σ			5.22	2748.48	7426.01

Table 4.7 Energy calculation for the brace with R=4, KL/r=150, and Earthquake 4

No	Cycle	δ(mm)	E_C/E_T	E_C	E_T
1	28th	22.38	0.11	779.30	7225.05
2	29th	1.23	0.01	3.23	221.70
3	30th	4.84	0.06	65.41	1160.55
4	31st	2.89	0.04	21.58	525.80
5	32nd	2.95	0.05	26.18	504.12
6	33rd	4.37	0.08	72.95	894.23
7	34th	1.31	0.04	4.66	113.71
8	35th	2.79	0.07	23.82	360.01
9	36th	2.33	0.06	14.61	246.19
10	37th	4.56	0.12	103.64	899.04
11	38th	10.89	0.14	442.26	3164.51
12	39th	2.13	0.05	10.86	206.87
13	40th	2.09	0.05	11.04	206.83
14	41st	2.96	0.05	18.25	341.70
15	42nd	0.92	0.03	1.77	70.72
16	43rd	1.41	0.03	4.33	144.25
17	44th	1.62	0.03	5.19	151.77
18	45th	1.90	0.04	8.22	193.37
19	46th	1.41	0.04	5.04	136.33
20	47th	5.81	0.13	167.67	1316.62
21	48th	1.98	0.05	9.06	194.26
22	49th	1.13	0.02	2.28	98.72
23	50th	1.24	0.03	3.30	123.72
24	51st	2.21	0.04	9.84	243.72
25	52nd	0.12	0.00	0.05	12.44
26	53rd	1.78	0.04	6.72	180.83
27	54th	4.50	0.11	93.01	831.49
28	55th	0.99	0.02	1.89	97.10
29	56th	1.70	0.04	6.38	161.53
30	57th	1.36	0.03	4.04	120.52
31	58th	1.01	0.04	2.64	70.98
32	59th	0.74	0.05	2.87	52.54
33	60th	0.62	0.17	3.11	18.21
34	61st	1.24	0.09	9.93	109.95
35	62nd	0.98	0.20	12.17	59.89
36	63rd	0.51	0.88	15.65	17.82
37	64th	0.94	0.41	29.56	72.65
Σ			3.45	2002.51	20549.74

(c) Assuming behavior of the braced frames was driven by behavior of the compression member alone, when the braces are designed with bigger KL/r by changing the member dimensions (i.e., width, depth, and thickness) and keeping cross sectional area and length of the member constant, higher R values and thus, higher ductility demands are obtained. From point (a) above, this would also imply lower normalized cumulative energy demand. This is because these brace members designed with bigger KL/r have a smaller inertia, and corresponding R value are calculated by the procedure described in SECTION 4.2.3.

(d) Following the same design assumptions as in (c), when the bracing member is designed with bigger KL/r value by increasing bracing member lengths but keeping member geometry (width, depth, and thickness) constant, this again results in higher R values and thus, higher ductility demands and lower normalized cumulative energy demands.

(e) When a bracing member is designed by following standard ductile design procedures, then bigger sections are obtained than when designed by following the strength design procedure. Restrictions on KL/r and b/t limitation in the ductile design procedure can lead to selection of member sizes that are totally unrelated to R values. The resulting large braces may in some cases remain elastic throughout the entire earthquake response which somehow renders the special ductile detail provisions paradoxical.

Normalized Cumulative Energy Ratio (KL/r=50)

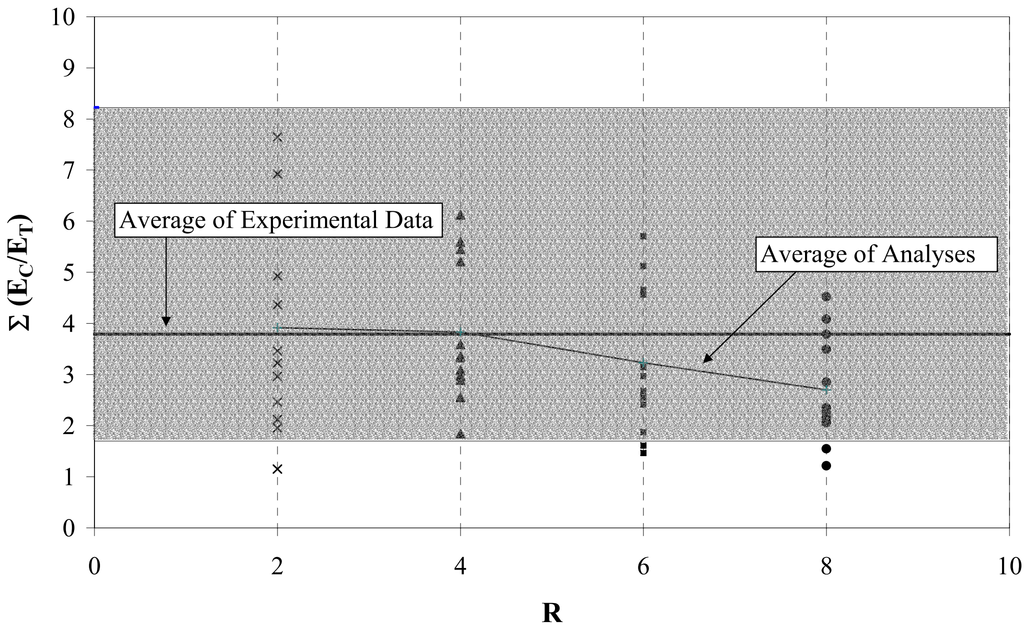

Figure 4.1 Normalized Cumulative Energy Ratios with KL/r = 50

(x, ▲, ■, and ● are analytical results for cases having R of 2, 4, 6, and 8 respectively)

Normalized Cumulative Energy Ratio (KL/r=150)

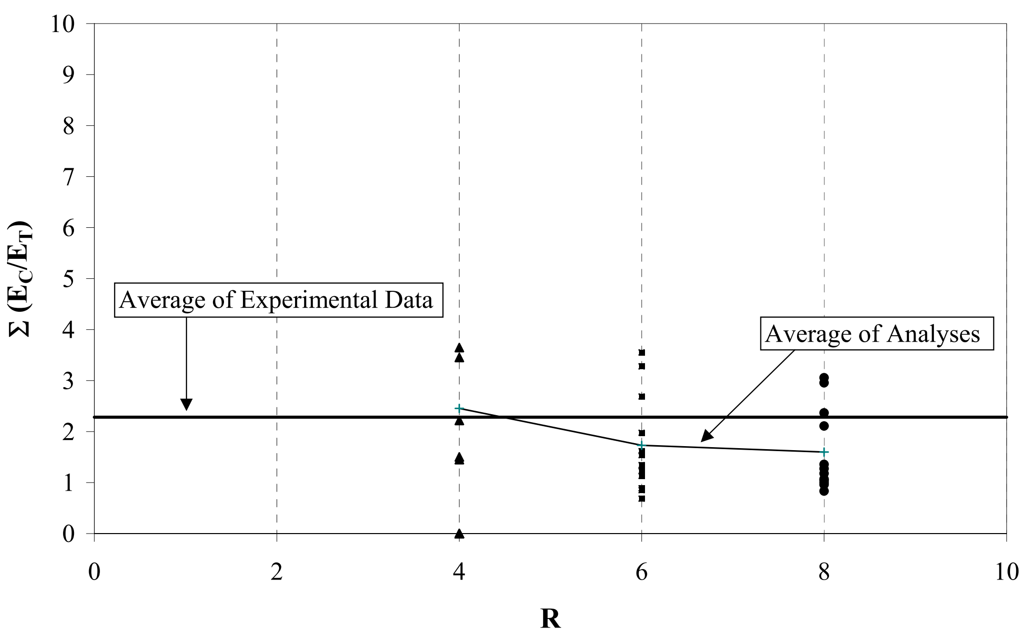

Figure 4.2 Normalized Cumulative Energy Ratios with KL/r = 150

(x, ▲, ■, and ● are analytical results for cases having R of 2, 4, 6, and 8 respectively)

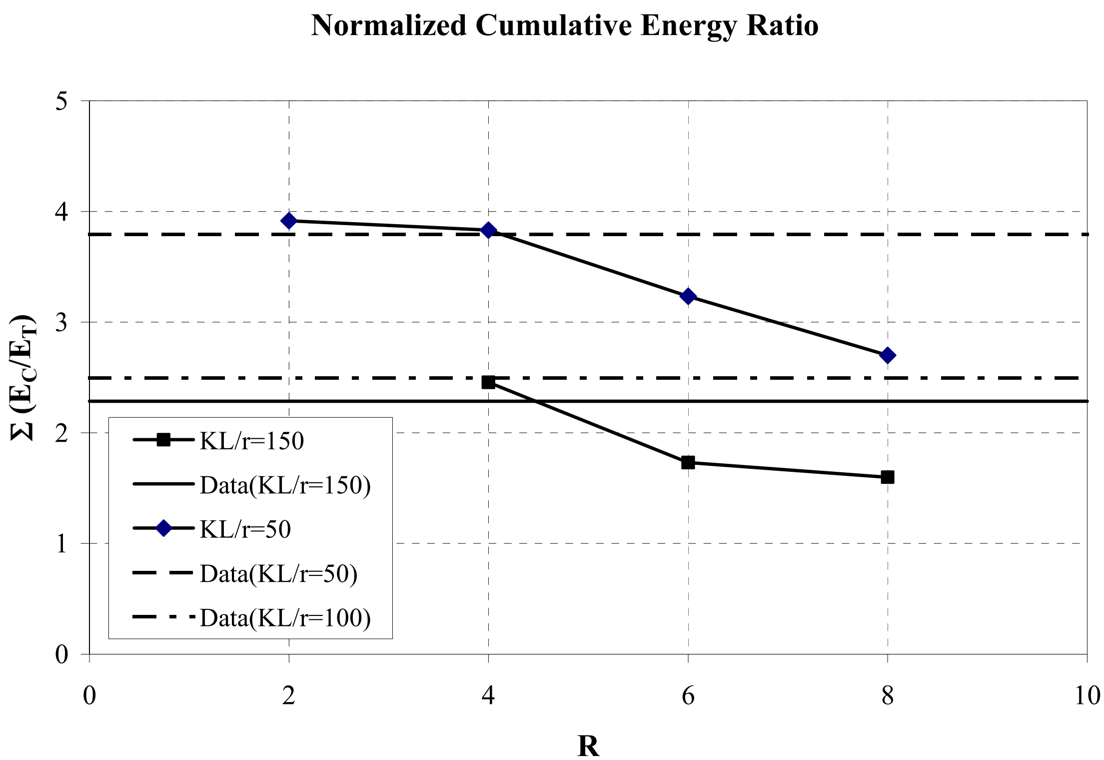

Figure 4.3 Averages of Normalized Cumulative Energy Ratios

Normalized Cumulative Energy Ratio (KL/r=50)

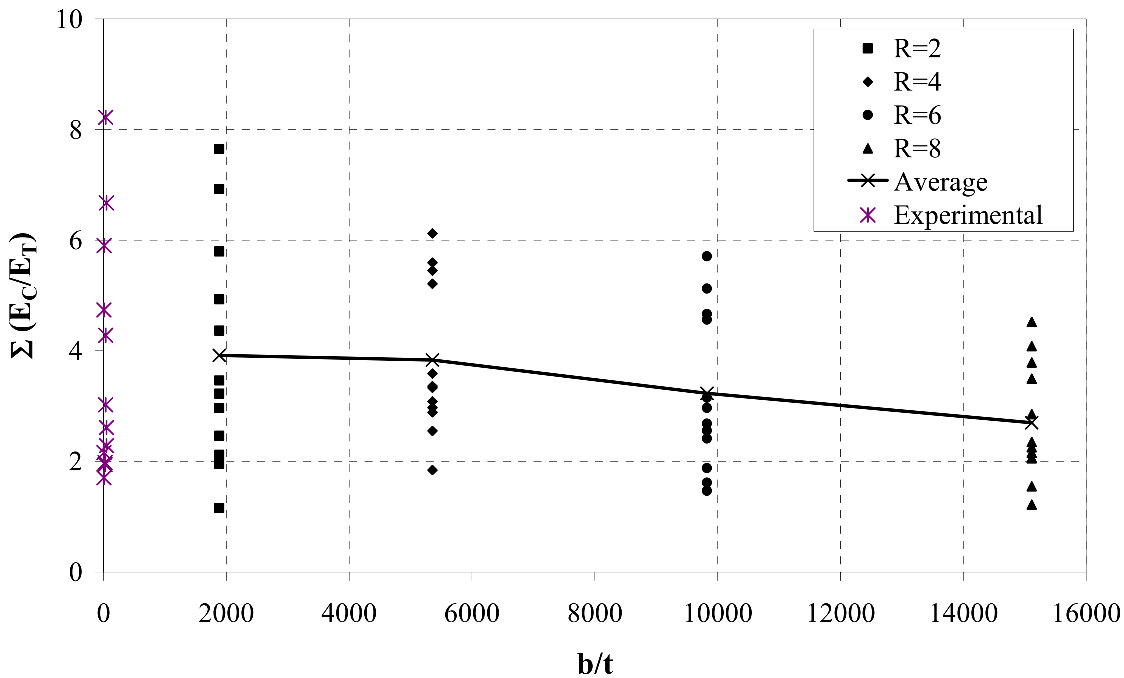

Figure 4.4 Normalized Cumulative Energy Ratios vs. b/t with KL/r = 50

Normalized Cumulative Energy Ratio (KL/r=150)

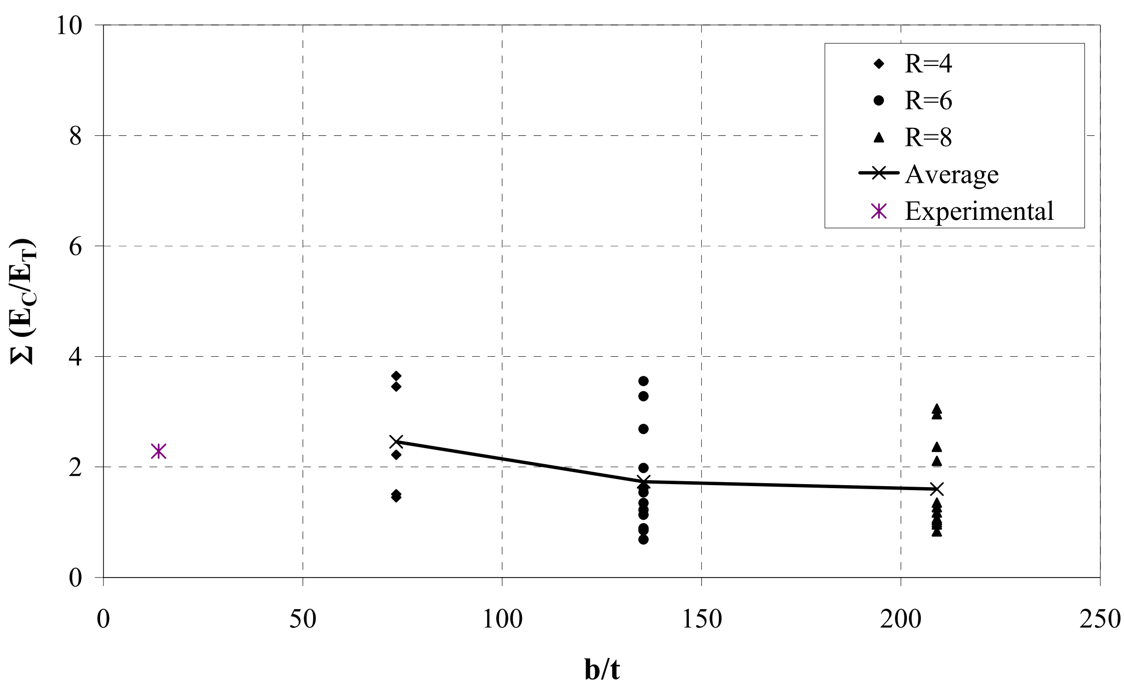

Figure 4.5 Normalized Cumulative Energy Ratios vs. b/t with KL/r = 150

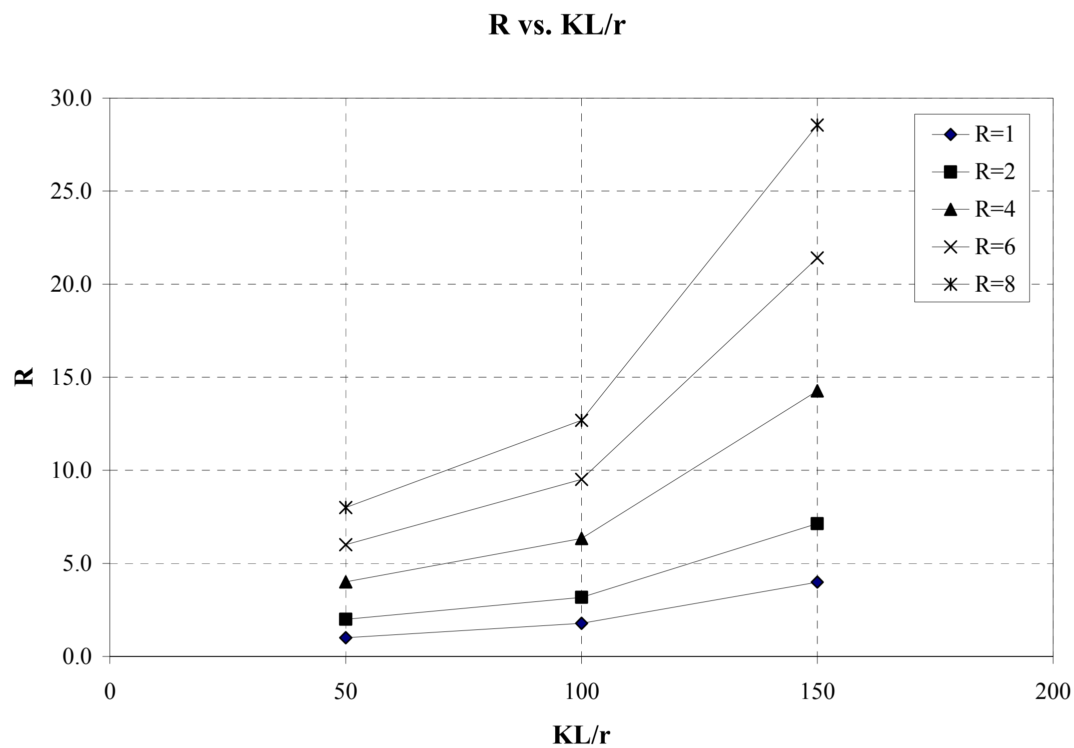

Figure 4.6 Effects of KL/r on R

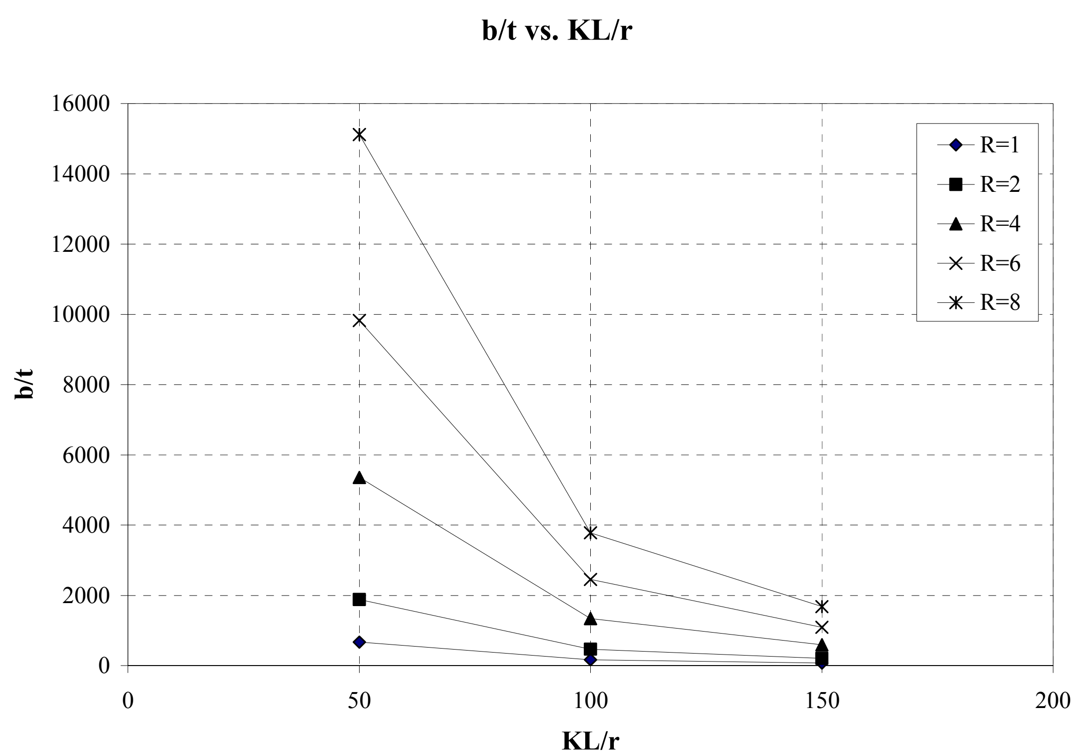

Figure 4.7 Effects of KL/r on b/t ratios

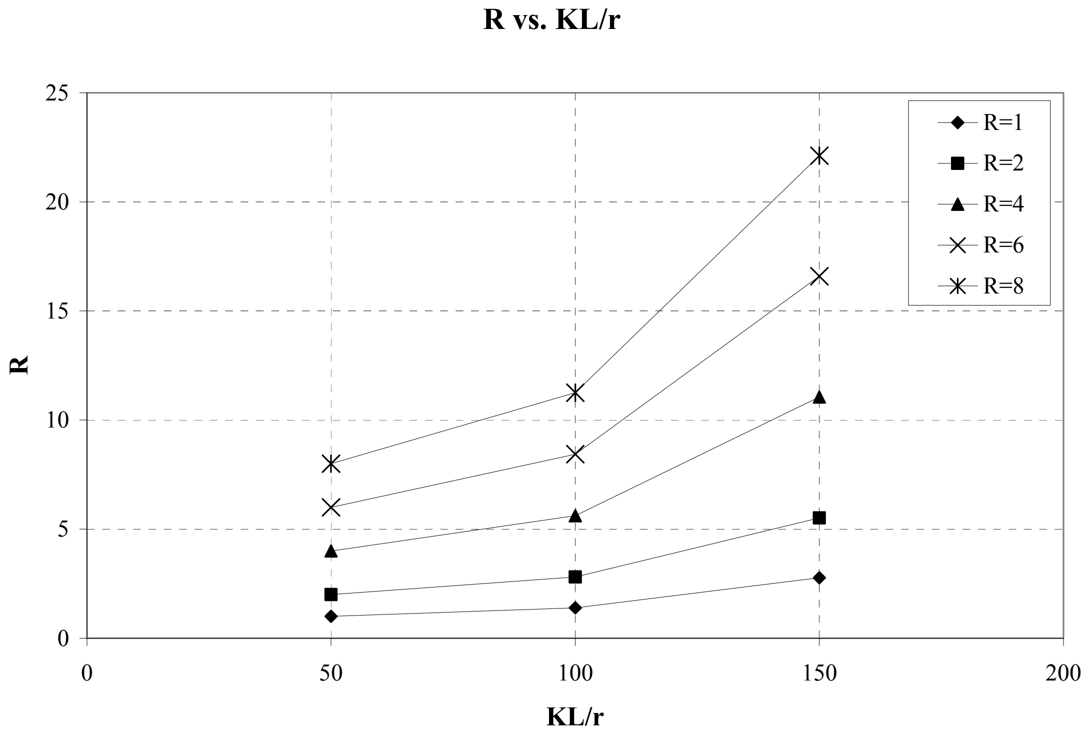

Figure 4.8 Effects of member length (L) on R

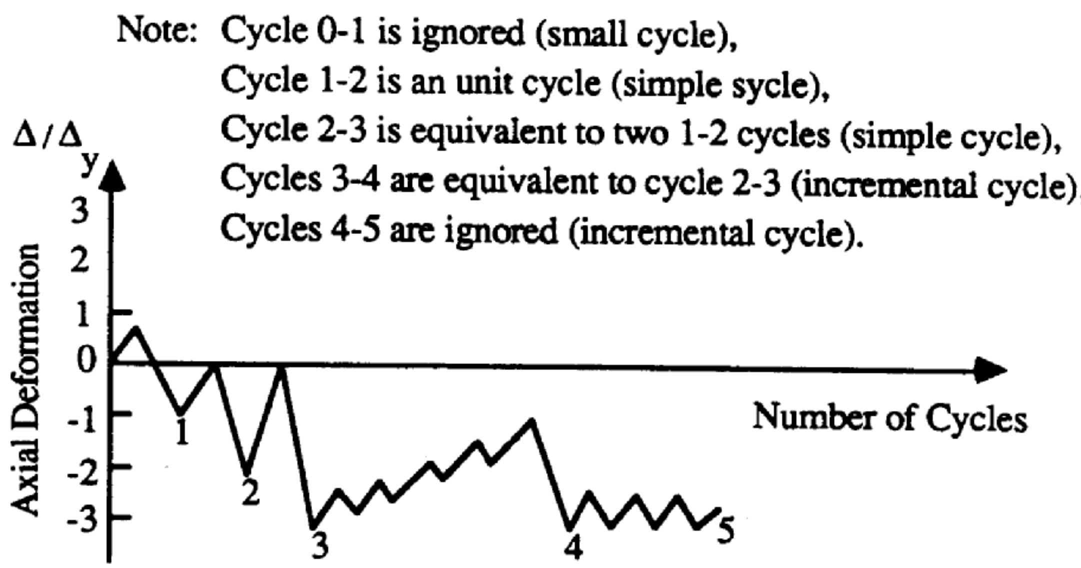

Figure 4.9 Typical cycles in a deformation history of Tang and Goel model (1987)

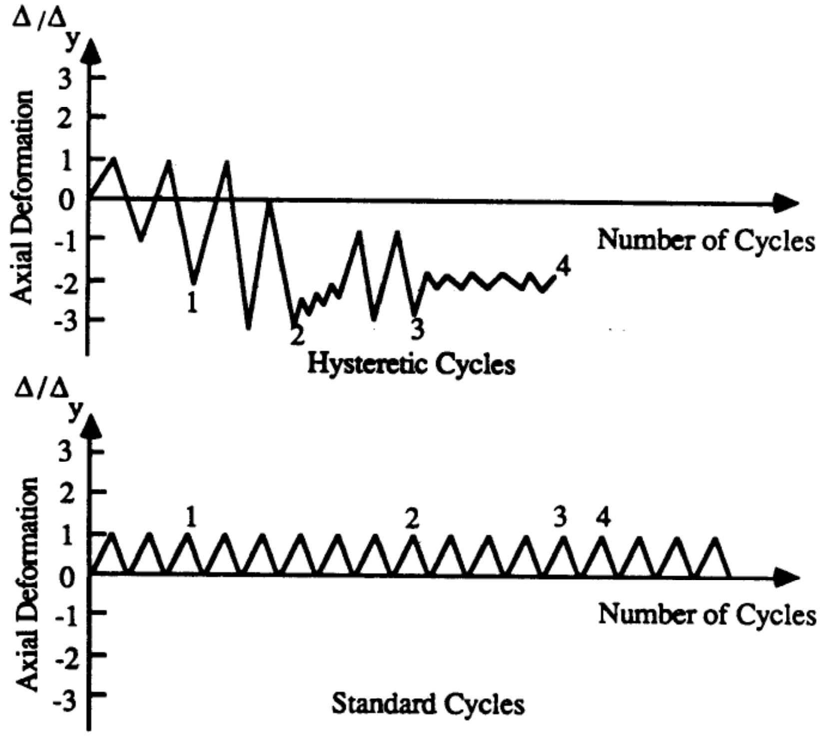

Figure 4.10 Equivalent conversion between hysteretic cycles and the standard cycles of Tang and Goel model (1987)

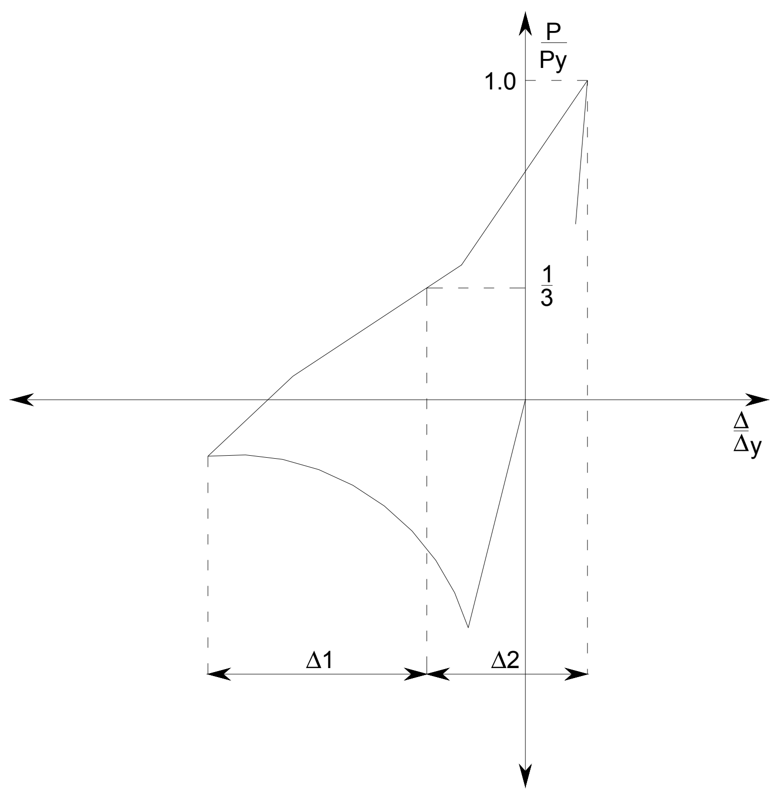

Figure 4.11 Definition of Δ_1 and Δ_2 (Lee and Goel model)

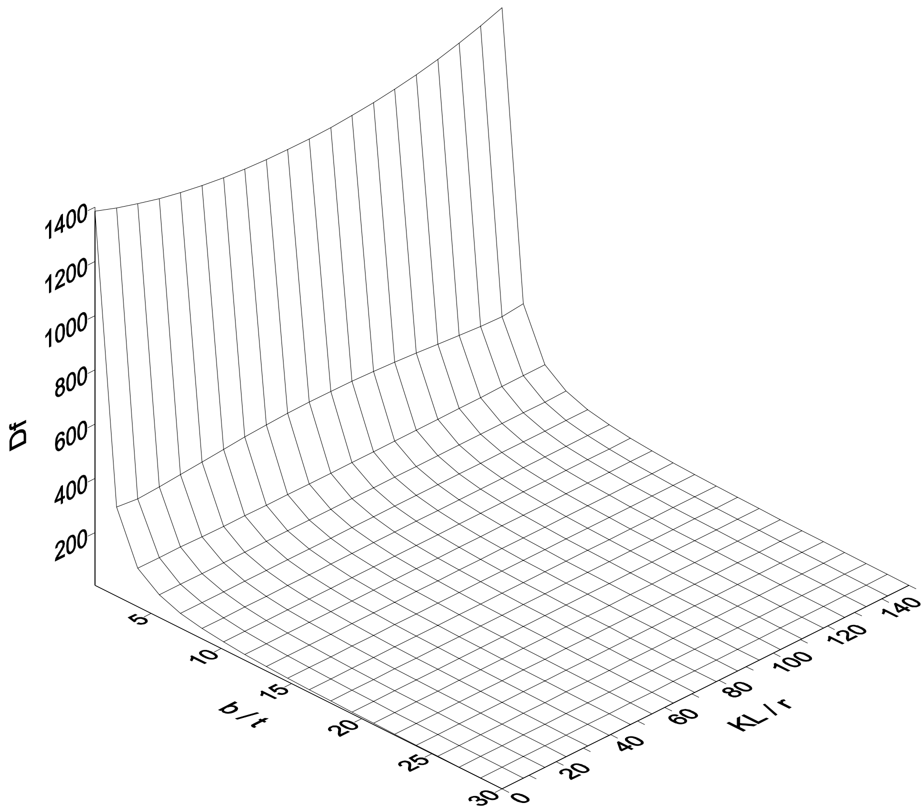

Figure 4.12 Tang and Goel fracture life model

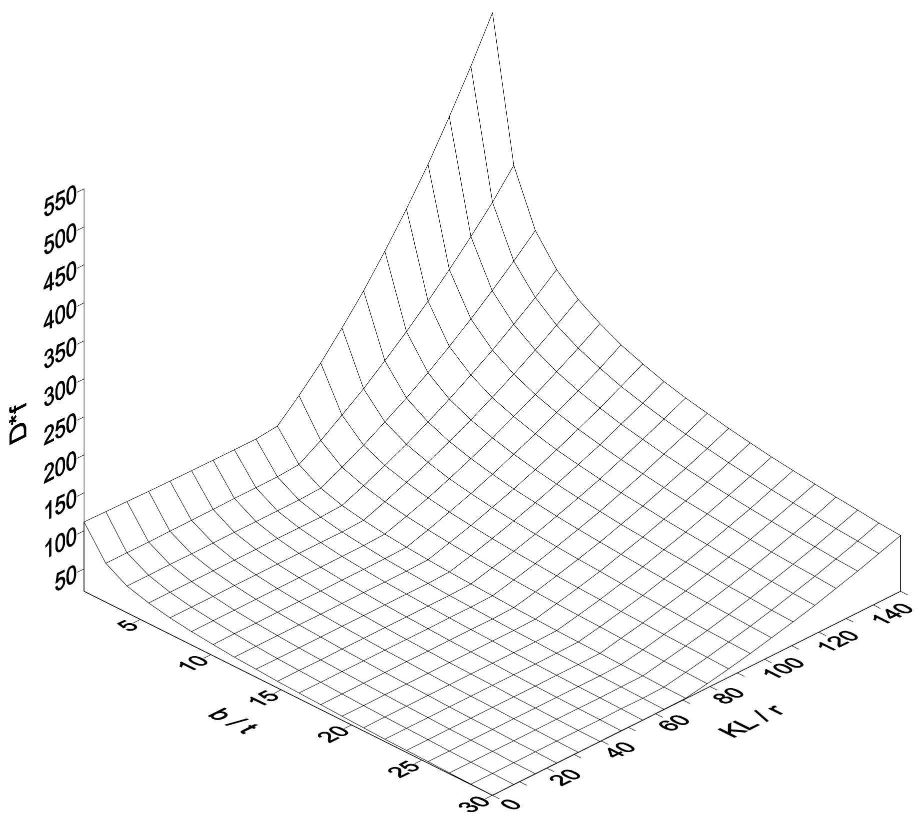

Figure 4.13 Archambault et al. fracture life model

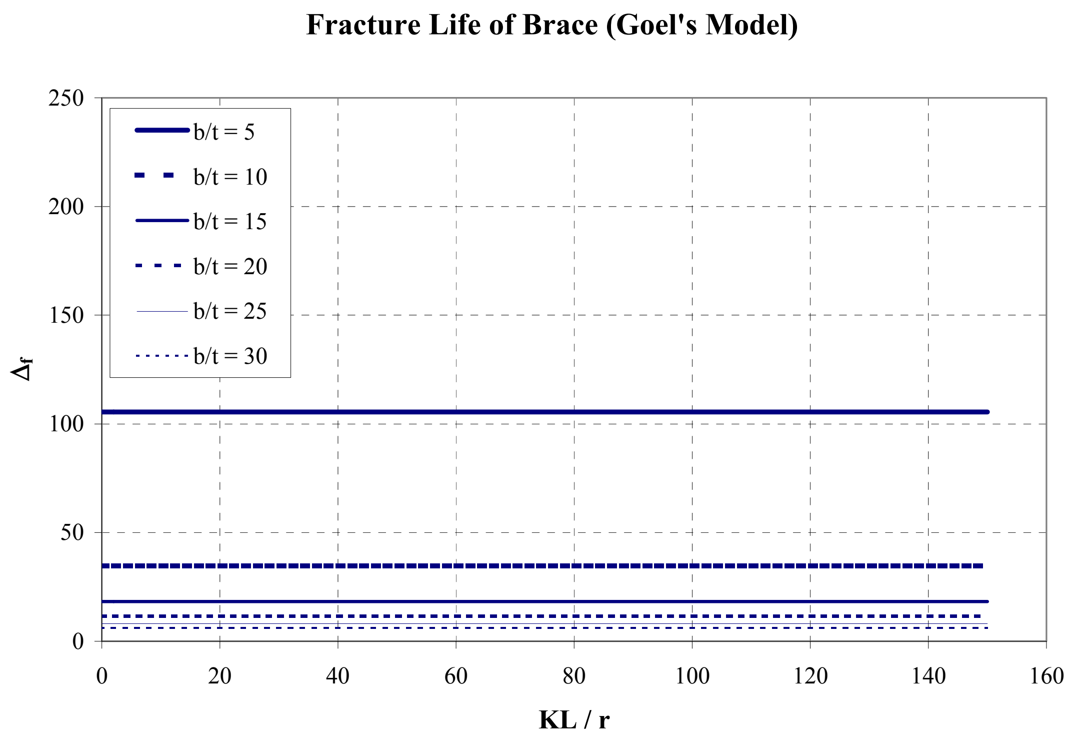

Figure 4.14 Tang and Goel fracture life model by b/t

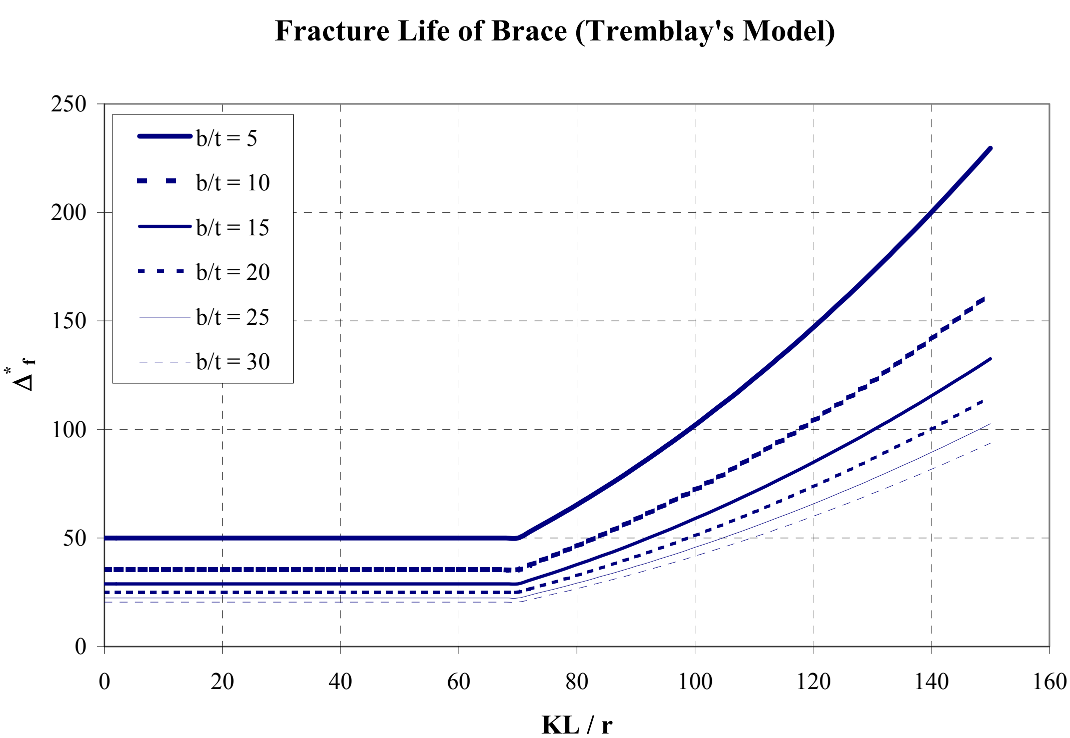

Figure 4.15 Archambault et al. fracture life model by b/t

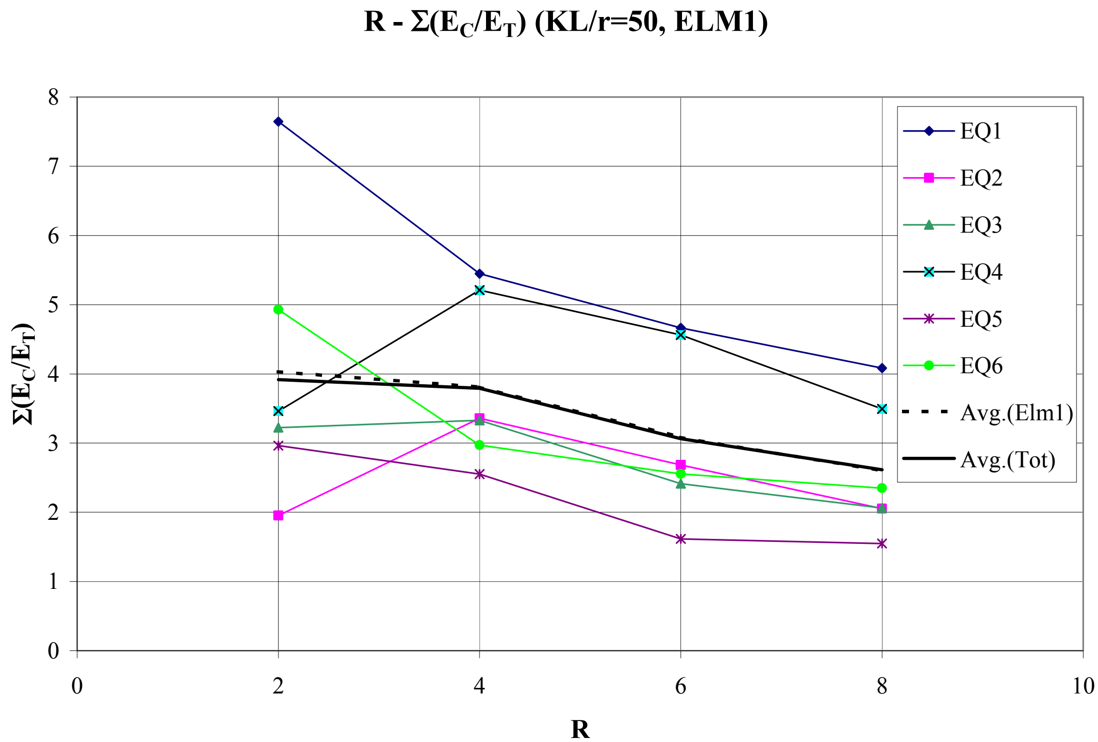

Figure 4.16 $\Sigma(E_C/E_T)$ for a brace in X braced frames with KL/r = 50 (Member 1)

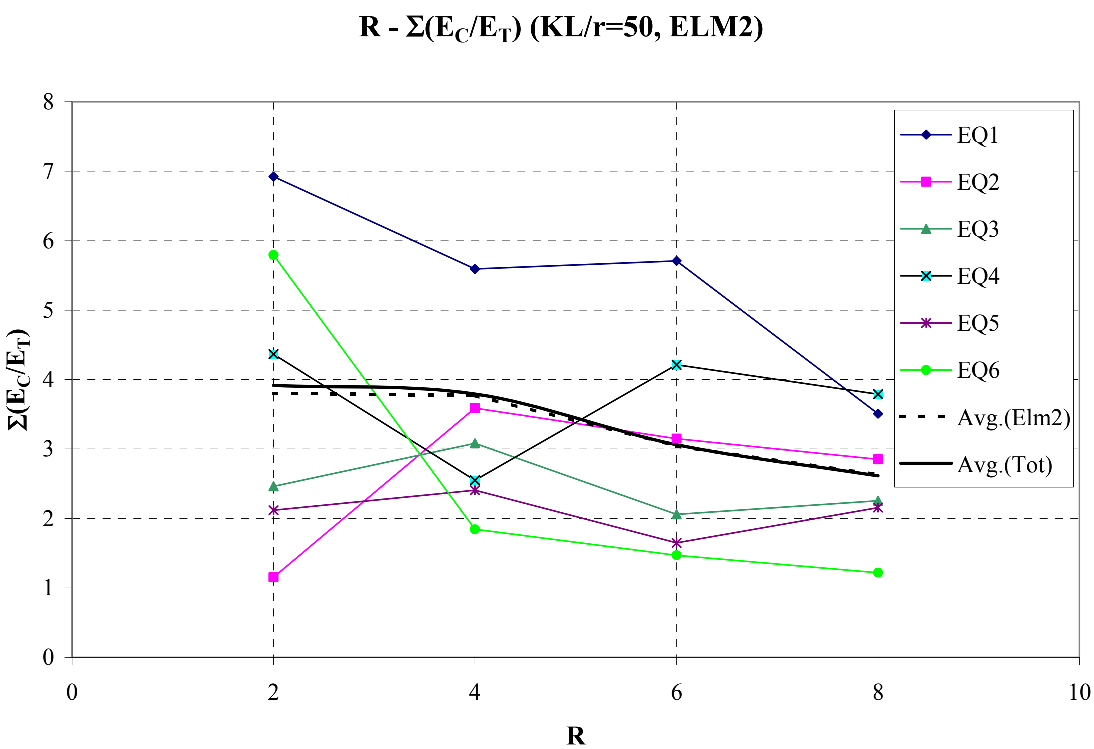

Figure 4.17 $\Sigma(E_C/E_T)$ for a brace in X braced frames with KL/r = 50 (Member 2)

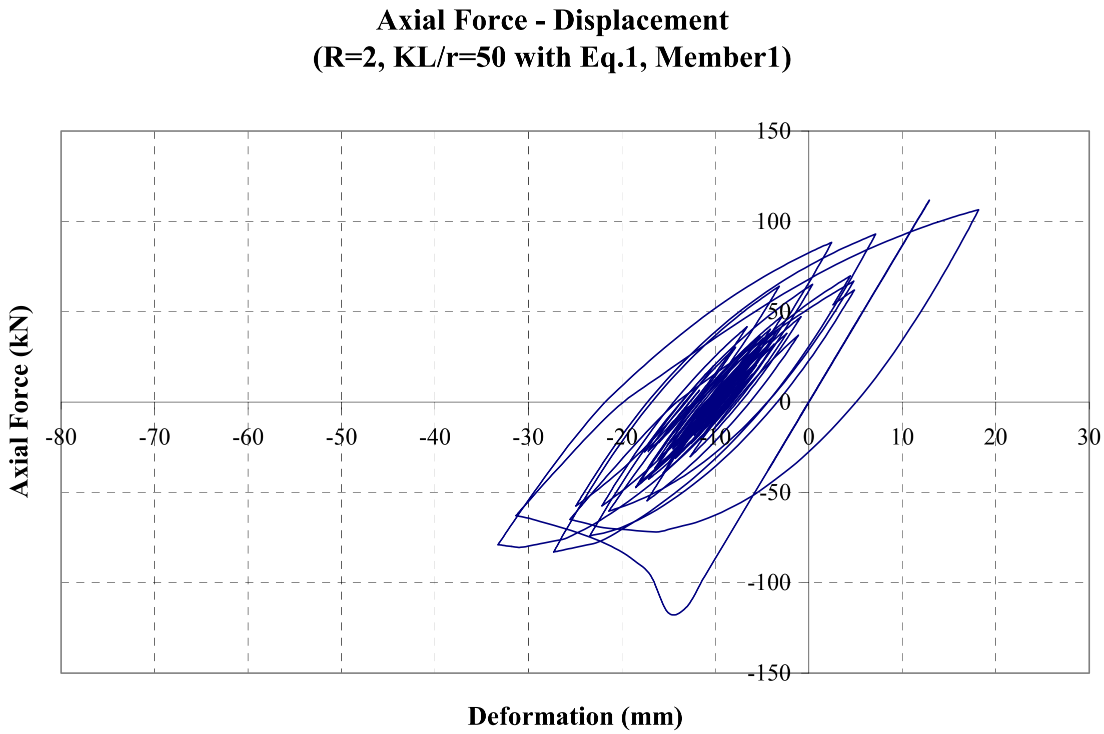

Figure 4.18 Hysteretic curve for the brace designed with R=2 and KL/r=50 (Earthquake 1)

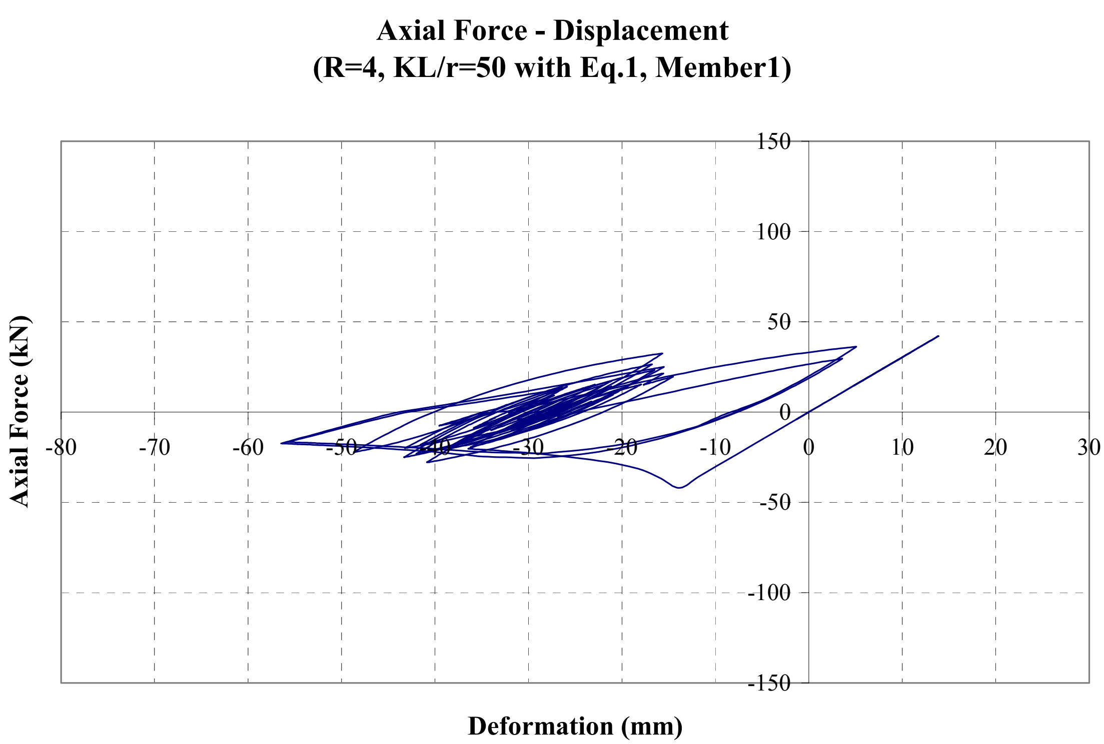

Figure 4.19 Hysteretic curve for the brace designed with R=4 and KL/r=50 (Earthquake 1)

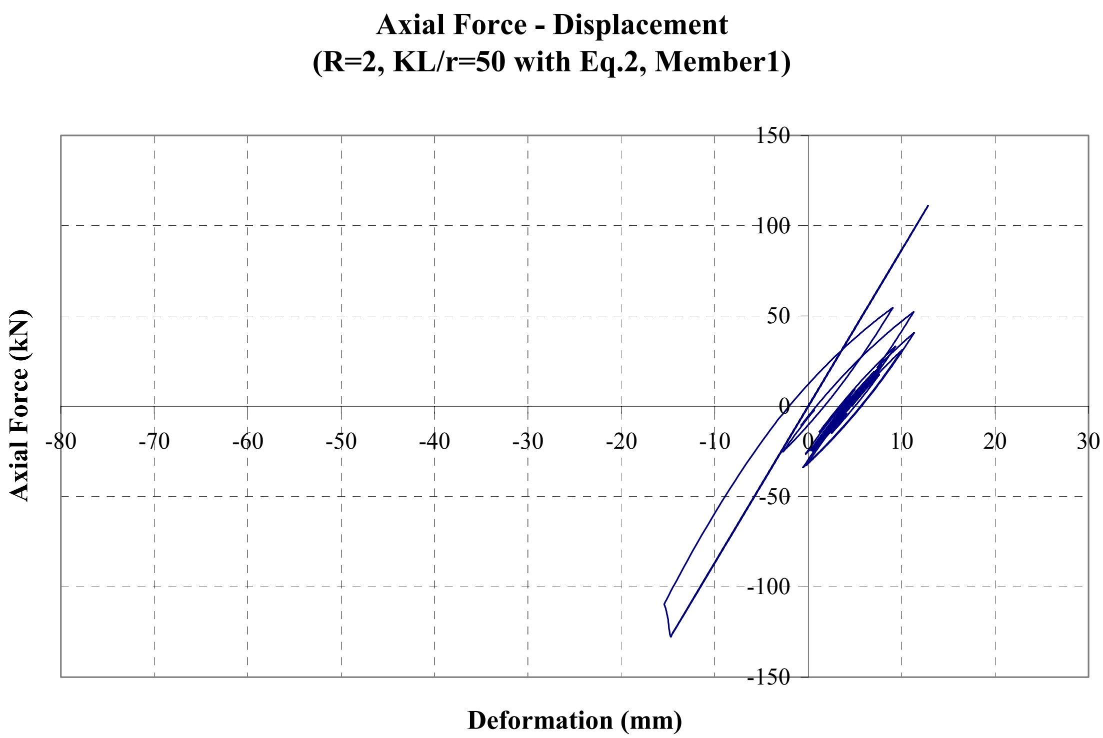

Figure 4.20 Hysteretic curve for the brace designed with R=2 and KL/r=50 (Earthquake 2)

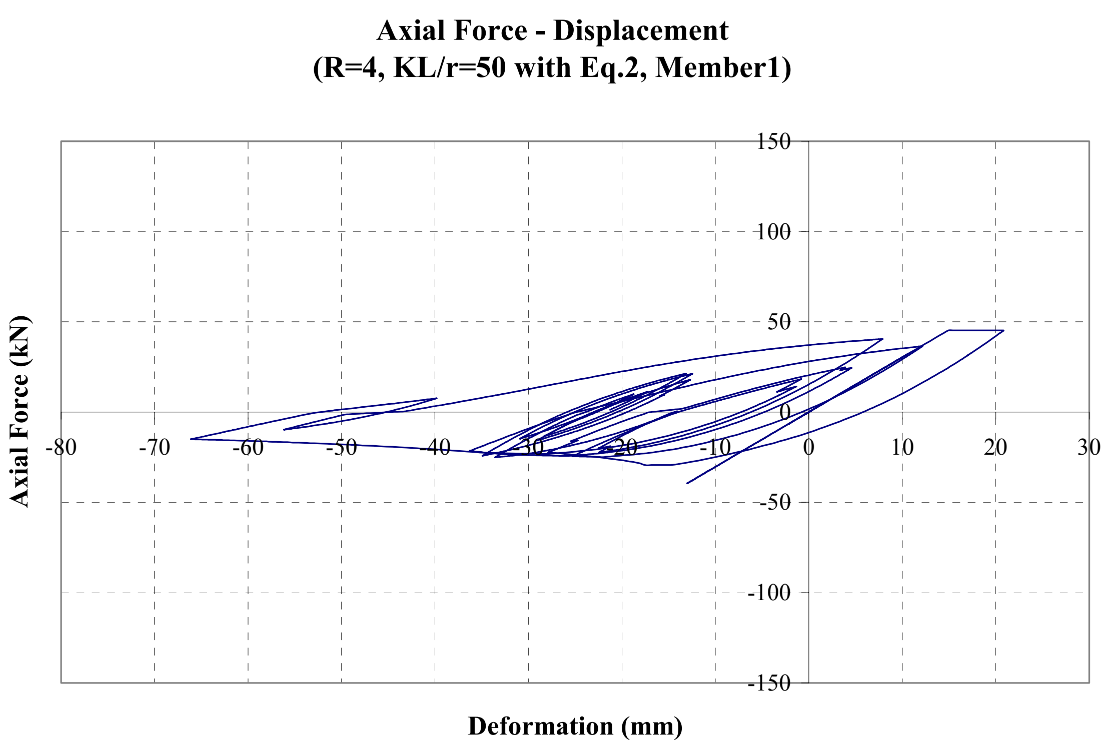

Figure 4.21 Hysteretic curve for the brace designed with R=4 and KL/r=50 (Earthquake 2)

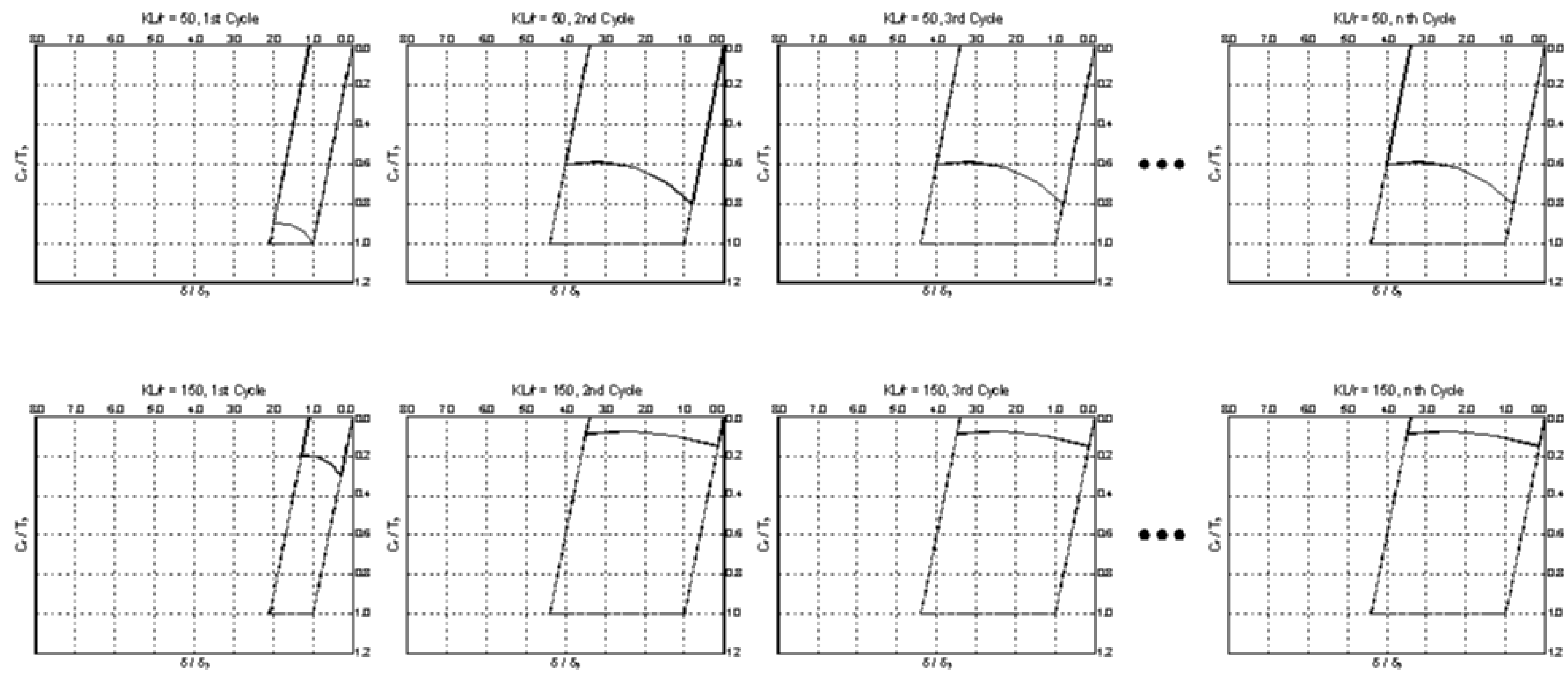

Figure 4.22 Comparison the schematically normalized cumulative energy ratios of braces with KL/r of 50 and 150

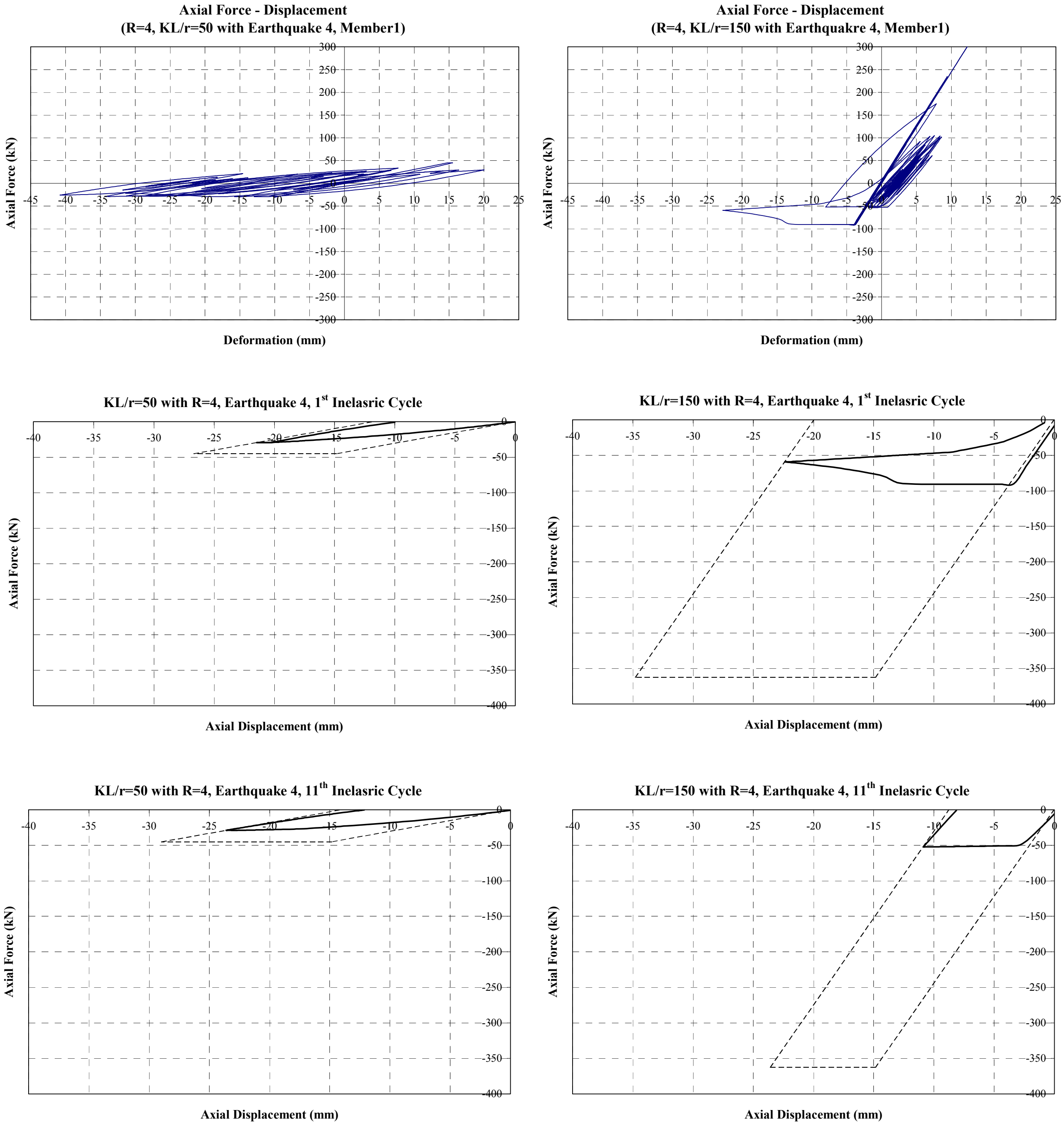

Figure 4.23 Comparison of the normalized cumulative energy ratios of braces analyzed (Braces with R=4, Earthquake 4, and KL/r=50 and 150)

SECTION 5

SUMMARY AND CONCLUSIONS

5.1 Summary

A comprehensive review of regulations and guidelines for the seismic design of CBF showed that design requirements for CBF have changed considerably over the various editions of the AISC Seismic Provisions, from 1992 up until Supplement 2 of the 1997 edition of AISC Seismic Provisions (AISC, 2000). This is in spite of little new test results over that period. Much discussion is currently underway on the requirements that must be specified to achieve satisfactory seismic performance of CBF and an in-depth review of past data is timely.

The objective of this report was to review existing experimental data to assess the extent of hysteretic energy dissipation achieved by bracing members in compression and the extent of the degradation of braces compression strength upon repeated cycling loads. Past experimental results were reviewed to quantify these parameters at various magnitudes of the axial deformation in compression, δ, as a function of KL/r, and for various types of structural shapes. Results will be posted and available on the MCEER Users Network. An extensive database of these quantities was established. The response of single story buildings was also investigated along with a few additional case studies to outline trends in response and to develop a better understanding of the sensitivity of some design parameters on the seismic response of CBF. Issues relevant to fracture life of braces were also considered.

Results from the non-linear dynamic analyses of buildings having X-braced bay and designed using various R factors and KL/r values were correlated with results from the experimental data, database, and observations were made on how normalized cumulative hysteretic energy ratios related to KL/r and R values.

5.2 Conclusions

From the experimental data review and database constructed using results from previous tests, and dynamic analyses of single story braced frames, the following conclusions can be made.

(a) While the normalized energy dissipation E_C/E_T typically decreases with increasing normalized displacements δ/δ_B, the ratios are consistently smaller for larger KL/r values. Braces having moderate KL/r (80 - 120) do not have significantly more normalized energy dissipation in compression than those having a slenderness in excess of 120. This is significant considering the large number of braced frames designed and built with braces having a KL/r of approximately 100. The rapid drop in energy dissipation effectiveness (down to 0.3 or less for braces having KL/r above 80) as the normalized displacement approximately exceed 3 is also significant; this suggests that reliance on the compression brace to dissipate seismic energy, while effective at very low KL/r, may be overly optimistic for the slenderness more commonly encountered in practice.

(b) Reduction in the normalized C_r''/C_r(first) envelope is particularly severe for W-shape braces having KL/r above 80. However, behavior is not worse for KL/r in the 120 to 160 range. In that perspective, tubes perform better, over all slenderness range. The performance of double-angle braces is in between these two extremes. Observation of the results for C_r''/C_r(last) and C_r''/C_r(first/last) show that the compression capacity at low δ/δ_B values drops rapidly upon repeated cycling, and that C_r''/C_r(first) is effectively equal to C_r''/C_r(last) at normalized displacements above 3 in most instances.

(c) When a bracing member is designed with a bigger R value or a bigger KL/r value, then the normalized cumulative energy ratio decreases. Assuming behavior of the braced frames was driven by behavior of the compression member alone, when the braces are designed with bigger KL/r by changing the member dimensions (i.e., width, depth, and thickness) and keeping cross sectional area and length of the member constant, higher R values, and thus higher ductility demands, are obtained. From the point above, this would also imply lower normalized cumulative energy demand. Following the same design assumptions, when the bracing member is designed with bigger KL/r value by increasing bracing member lengths but keeping member geometry (width, depth, and thickness) constant, this again results in higher R values and thus, higher ductility demands and lower normalized cumulative energy demands. When a bracing member is designed by following standard ductile design procedures, then bigger sections are obtained than when designed by following the strength design procedure. Restrictions on KL/r and b/t limitation in the ductile design procedure can lead to selection of member sizes that are totally unrelated to R values. The resulting large braces may in some cases remain elastic throughout the entire earthquake response which somehow renders the special ductile detail provisions paradoxical.

(d) Consensus in the existing literature establishes that smaller width-to-thickness ratios help delay the brittle failure of bracing members; the higher resistance against local buckling translates into a higher cyclic fracture life of members.

SECTION 6

REFERENCES

American Institute of Steel Constructions, Inc. (1992), "Seismic Provisions for Structural Steel Buildings", AISC, Chicago, Illinois.

American Institute of Steel Constructions, Inc. (1993), "Load and Resistance Factor Design Specification for Structural Steel Buildings", AISC, Chicago, Illinois.

American Institute of Steel Constructions, Inc. (1994), "Load and Resistance Factor Design, Manual of Steel Construction", AISC, Chicago, Illinois.

American Institute of Steel Constructions, Inc. (1997), "Seismic Provisions for Structural Steel Buildings", AISC, Chicago, Illinois.

American Institute of Steel Constructions, Inc. (2000), "Seismic Provisions for Structural Steel Buildings (1997) Supplement No. 2", AISC, Chicago, Illinois.

Applied Technology Council (1995), "Structural Response Modification Factors", *Report No. ATC-19*, ATC, Redwood City, California.

Archambault, Marie-Hélène, Tremblay, Robert and Filiatrault, André (1995), Étude du Comportment Séismique des Contreventements Ductiles en X Avec Profilés Tubulaires en Acier", *Rapport No. EPM/GCS-1995-09*, Département de Génie Civil Section Structures, École Polytechnique, Montréal, Quebec, Canada.

Astaneh-Asl, A., Goel, S. C. and Hanson, R. D. (1982), "Cycle Behavior of Double Angle Bracing Members with End Gusset Plates", *Report No. UMEE 82R7*, August, Department of Civil Engineering, The University of Michigan, Ann Arbor, Michigan.

Black, R. G., Wenger, W. A. and Popov, E. P. (1980), "Inelastic Buckling of Steel Struts under Cyclic Load and Reversal", *Report No. UCB/EERC-80/40*, Earthquake Engineering Research Center, University of California, Berkeley, California.

Bruneau, Michel, Uang, Chia-Ming and Whittaker, Andrew (1998), "Ductile Design of Steel Structures", McGraw-Hill, New York, New York.

BSSC (1997), "NEHRP (National Earthquake Hazards Reduction Program) Recommended Provisions for Seismic Regulations for New Buildings", *Report No. FEMA-302-303*, Building Seismic Safety Council, Federal Emergency Management Agency, Washington, D.C.

CSA (1994), "Limit State Design of Structures", *CAN/CSA-S16.1-M94*, Canadian Standard Association, Rexdale, Ontario, Canada.

Goel, Subhash C. and Lee, S. (1992), "A Fracture Criterion for Concrete-Filled Tubular Bracing Members Under Cyclic Loading", *Proceedings of the 1992 ASCE Structures Congress*, pp. 922 – 925, ASCE, Reston, Virginia.

Gugerli, H. and Goel, S. C. (1982), "Inelastic Cyclic Behavior of Steel Bracing Members", *Report No. UMEE 82R1*, January, Department of Civil Engineering, The University of Michigan, Ann Arbor, Michigan.

Hassan, O. F. and Goel, S. C. (1991), "Modeling of Bracing Members and Seismic Behavior of Concentrically Braced Steel Structures", *Report No. UMCE 91-1*, January, Department of Civil Engineering, The University of Michigan, Ann Arbor, Michigan

ICBO (1994), "Uniform Building Code", International Conference of Building Officials, Whittier, California

Ikeda, K., Mahin, S. A. and Dermitzakis, S. N. (1984), “Phenomenological Modeling of Steel Braces under Cyclic Loading”, *Report No. UCB/EERC-84/09*, Earthquake Engineering Research Center, University of California, Berkeley, California.

Ikeda, K. and Mahin, S. A. (1984), “A Refined Physical Theory Model for Predicting the Seismic Behavior of Braced Frames”, *Report No. UCB/EERC-84/12*, Earthquake Engineering Research Center, University of California, Berkeley, California.

Jain, A. K., Goel, S. C. and Hanson, R. D. (1977), “Static and Dynamic Hysteresis Behavior of Steel Tubular Members with Welded Gusset Plates”, *Report No. UMEE 77R3*, June, Department of Civil Engineering, The University of Michigan, Ann Arbor, Michigan.

Jain, A. K., Goel, S. C. and Hanson, R. D. (1978), “Hysteresis Behavior of Bracing Members and Seismic Response of Braced Frames with Different Proportions”, *Report No. UMEE 78R3*, July, Department of Civil Engineering, The University of Michigan, Ann Arbor, Michigan.

Lee, S. and Goel, S. C. (1987), “Seismic Behavior of Hollow and Concrete-Filled Square Tubular Bracing Members”, *Report No. UMEE 87-11*, December, Department of Civil Engineering, The University of Michigan, Ann Arbor, Michigan.

Leowardi, L. Sukendro and Walpole, Warren R. (1996), “Performance of Steel Brace Members”, Department of Civil Engineering, University of Canterbury, Christchurch, New Zealand.

Nonaka, Taijiro (1987), “Formulation of Inelastic Bar Under Repeated Axial and Thermal Loadings”, *Journal of the Engineering Mechanics*, vol. 113, No. 11, August, pp. 1647 – 1664, ASCE, Reston, Virginia.

Prakash, V. and Powell, G. H. (1993), “DRAIN-2DX, DRAIN-3DX and DRAIN-BUILDING, Base Program Design Documentation”, *Report No. UCB/SEMM-93/16*, December, Structural Engineering Mechanics and Materials, University of California, Berkeley, California.

SEAOC (1978), (1990), (1996), (1999), “Tentative Lateral Force Requirement”, Seismology Committee, Structural Engineers Association of California, Sacramento/San Francisco/Los Angeles, California.

Taddei, Pascal (1995), “Implementation of the Refined Physical Theory Model of Braced Steel Frames in NONSPEC and DRAIN-2DX”, August, Department of Civil Engineering, The University of Ottawa, Ottawa, Ontario, Canada.

Tremblay, Robert (1999), Personal Communication, École Polytechnique, Montréal, Quebec, Canada.

Tang, Xiaodong and Goel, Subhash C. (1987), “Seismic Analysis and Design Considerations of Braced Steel Structures”, *Report No. UMCE 87-4*, April, Department of Civil Engineering, The University of Michigan, Ann Arbor, Michigan.

Tang, Xiaodong and Goel, Subhash C. (1989), “Brace Fractures and Analysis of Phase I Structures”, *Journal of the Structural Engineering*, vol. 102, No. 8, August, pp. 1960 – 1976, ASCE, Reston, Virginia.

Walpole, Warren R. (1996), “Behaviour of Cold-Formed Steel RHS Members under Cyclic Loading”, Department of Civil Engineering, University of Canterbury, Christchurch, New Zealand.

Zayas, Victor A., Popop, Egor P. and Mahin, Stephen A. (1980), “Cyclic Inelastic Buckling of Tubular Steel Braces”, *Report No. UCB/EERC-80/16*, Earthquake Engineering Research Center, University of California, Berkeley, California.

APPENDIX A

Example of Detailed Spreadsheet Data

(To Be Made Available on MCEER User's Network)

	Strut 1 (W, p-p)				
	L(in)	δ_B(in)	δ_T(in)	T_y(kips)	C_r(kips)
	150.00	0.08	0.21	248.86	96.61
	KL/r	δ_T/δ_B	δ/δ_T	$\delta/\delta_{B,max}$	f_y(ksi)
	120.00	2.58	14.76	38.02	40.40
Cycle	δ/δ_B	E_C/E_T	C_r''/C_r (1st)	C_r''/C_r (Last)	$1^{st}/L^{ast}$
1	1.56	0.23	0.77	0.31	2.51
2	2.43	0.17	0.56	0.32	1.78
3	3.13	0.16	0.53	0.32	1.62
4	4.25	0.14	0.41	0.32	1.31
5	5.60	0.13	0.36	0.31	1.17
6	6.34	0.11	0.32	0.30	1.06
7	8.42	0.09	0.26	0.28	0.94
8	11.29	0.09	0.24	0.26	0.90
9	14.41	0.09	0.22	0.25	0.89
10	18.32	0.09	0.20	0.21	0.96
11	23.18	0.08	0.18	0.19	0.95
12	28.65	0.08	0.17	0.18	0.95
13	38.02	0.08	0.16	0.16	1.00
14	x	x	x	x	x
15	x	x	x	x	x

	Strut 2 (W, p-p)				
	L(in)	δ_B(in)	δ_T(in)	T_y(kips)	C_r(kips)
	61.20	0.07	0.09	309.75	251.06
	KL/r	δ_T/δ_B	δ/δ_T	$\delta/\delta_{B,max}$	f_y(ksi)
	40.00	1.23	24.11	29.75	42.20
Cycle	δ/δ_B	E_C/E_T	C_r''/C_r (1st)	C_r''/C_r (Last)	$1^{st}/L^{ast}$
1	1.75	0.98	0.92	0.37	2.45
2	3.69	0.65	0.71	0.36	1.98
3	4.47	0.56	0.57	0.33	1.72
4	7.73	0.45	0.39	0.28	1.42
5	12.05	0.35	0.31	0.24	1.30
6	14.53	0.32	0.26	0.20	1.29
7	19.64	0.25	0.19	0.17	1.15
8	23.72	0.24	0.16	0.14	1.09
9	29.75	0.19	0.15	0.15	1.00
10	x	x	x	x	x
11	x	x	x	x	x
12	x	x	x	x	x
13	x	x	x	x	x
14	x	x	x	x	x
15	x	x	x	x	x

	Strut 3 (W, p-p)				
	L(in)	δ_B(in)	δ_T(in)	T_y(kips)	C_r(kips)
	120.84	0.14	0.17	235.97	200.85
	KL/r	δ_T/δ_B	δ/δ_T	$\delta/\delta_{B,max}$	f_y(ksi)
	80.00	1.17	8.11	9.53	40.20
Cycle	δ/δ_B	E_C/E_T	C_r''/C_r (1st)	C_r''/C_r (Last)	$1^{st}/L^{ast}$
1	1.70	0.43	0.36	0.35	1.04
2	2.57	0.32	0.30	0.30	1.00
3	5.09	0.23	0.22	0.22	1.00
4	6.03	0.21	0.20	0.19	1.07
5	9.53	0.19	0.18	0.18	1.00
6	x	x	x	x	x
7	x	x	x	x	x
8	x	x	x	x	x
9	x	x	x	x	x
10	x	x	x	x	x
11	x	x	x	x	x
12	x	x	x	x	x
13	x	x	x	x	x
14	x	x	x	x	x
15	x	x	x	x	x

	Strut 4 (W, p-p)			
	L(in)	δ_B(in)	δ_T(in)	T_y(kips
	120.84	0.14	0.18	247.71
	KL/r	δ_T/δ_B	δ/δ_T	$\delta/\delta_{B,max}$
	80.00	1.22	19.94	24.28
Cycle	δ/δ_B	E_C/E_T	C_r''/C_r (1st)	C_r''/C_r (Last)
1	0.94	0.77	0.68	0.32
2	1.56	0.45	0.42	0.34
3	2.37	0.30	0.34	0.32
4	4.45	0.26	0.24	0.25
5	8.75	0.20	0.18	0.18
6	16.07	0.16	0.14	0.14
7	24.28	0.14	0.10	0.10
8	x	x	x	x
9	x	x	x	x
10	x	x	x	x
11	x	x	x	x
12	x	x	x	x
13	x	x	x	x
14	x	x	x	x
15	x	x	x	x

	Strut 5 (W, p-p)				
	L(in)	δ_B(in)	δ_T(in)	T_y(kips)	C_r(kips)
	120.84	0.11	0.18	247.71	152.11
	KL/r	δ_T/δ_B	δ/δ_T	$\delta_T/\delta_{B,max}$	f_y(ksi)
	80.00	1.63	20.75	33.79	42.20
Cycle	δ/δ_B	E_C/E_T	C_r''/C_r (1st)	C_r''/C_r (Last)	$1^{st}/L^{ast}$
1	3.25	0.36	0.43	0.38	1.12
2	3.48	0.21	0.38	0.37	1.04
3	5.72	0.23	0.32	0.31	1.03
4	7.86	0.15	0.27	0.28	0.97
5	9.55	0.17	0.26	0.26	1.00
6	12.67	0.13	0.24	0.22	1.06
7	15.57	0.15	0.20	0.21	0.98
8	18.98	0.15	0.18	0.20	0.91
9	25.54	0.13	0.16	0.18	0.92
10	33.79	0.12	0.15	0.15	1.00
11	x	x	x	x	x
12	x	x	x	x	x
13	x	x	x	x	x
14	x	x	x	x	x
15	x	x	x	x	x

	Strut 6 (W, p-p)				
	L(in)	δ_B(in)	δ_T(in)	T_y(kips)	C_r(kips)
	116.04	0.10	0.18	211.88	115.34
	KL/r	δ_T/δ_B	δ/δ_T	$\delta/\delta_{B,max}$	f_y(ksi)
	120.00	1.84	17.78	32.66	44.70
Cycle	δ/δ_B	E_C/E_T	C_r''/C_r (1st)	C_r''/C_r (Last)	$1^{st}/L^{ast}$
1	0.87	0.99	0.71	0.26	2.77
2	1.74	0.16	0.47	0.30	1.60
3	2.76	0.17	0.32	0.26	1.23
4	3.41	0.15	0.28	0.25	1.12
5	5.08	0.14	0.24	0.22	1.09
6	7.77	0.12	0.19	0.19	1.03
7	8.78	0.13	0.19	0.18	1.06
8	12.34	0.11	0.15	0.17	0.91
9	16.26	0.10	0.15	0.16	0.94
10	21.05	0.09	0.14	0.13	1.08
11	26.71	0.09	0.12	0.12	1.00
12	32.66	0.08	0.11	0.11	1.00
13	x	x	x	x	x
14	x	x	x	x	x
15	x	x	x	x	x

	Strut 7 (W, p-p)				
	L(in)	δ_B(in)	δ_T(in)	T_y(kips)	C_r(kips)
	58.44	0.09	0.10	229.50	203.45
	KL/r	δ_T/δ_B	δ/δ_T	$\delta/\delta_{B,max}$	f_y(ksi)
	40.00	1.13	17.61	19.87	50.00
Cycle	δ/δ_B	E_C/E_T	C_r''/C_r (1st)	C_r''/C_r (Last)	$1^{st}/L^{ast}$
1	3.47	0.68	0.47	0.29	1.65
2	3.55	0.41	0.36	0.28	1.27
3	4.73	0.34	0.28	0.19	1.50
4	6.86	0.28	0.22	0.16	1.37
5	8.99	0.23	0.19	0.15	1.22
6	11.04	0.19	0.15	0.14	1.09
7	14.51	0.16	0.13	0.13	1.00
8	19.87	0.14	0.09	0.09	1.00
9	x	x	x	x	x
10	x	x	x	x	x
11	x	x	x	x	x
12	x	x	x	x	x
13	x	x	x	x	x
14	x	x	x	x	x
15	x	x	x	x	x

	Strut 8 (DA, back to back, p-p)			
	L(in)	δ_B(in)	δ_T(in)	T_y(kips
	111.24	0.11	0.16	279.07
	KL/r	δ_T/δ_B	δ/δ_T	$\delta/\delta_{B,max}$
	80.00	1.40	16.77	23.40
Cycle	δ/δ_B	E_C/E_T	C_r''/C_r (1st)	C_r''/C_r (Last)
1	1.11	0.70	0.84	0.26
2	1.14	0.41	0.71	0.24
3	1.68	0.31	0.42	0.23
4	2.15	0.24	0.37	0.21
5	2.72	0.21	0.33	0.19
6	4.30	0.20	0.26	0.15
7	5.82	0.19	0.23	0.13
8	8.60	0.16	0.19	0.11
9	9.11	0.15	0.17	0.11
10	12.39	0.14	0.16	0.09
11	15.68	0.12	0.12	0.09
12	18.97	0.10	0.10	0.09
13	23.40	0.08	0.09	0.09
14	x	x	x	x
15	x	x	x	x

Figure A.1 Example of Results for specimens tested by Black et al., 1980

APPENDIX B

Investigation of Bracing Information

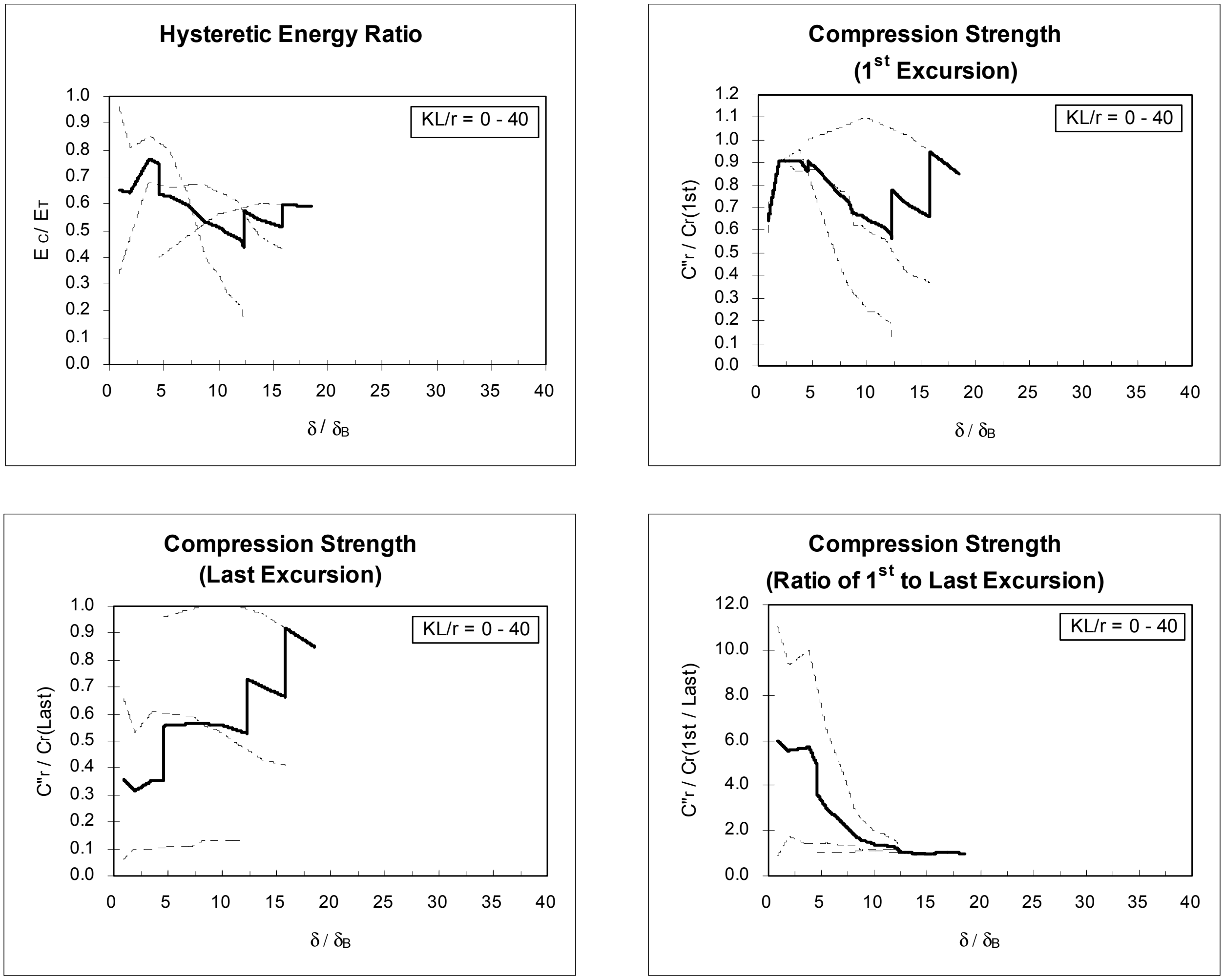

Figure B.1 All structural shapes with KL/r = 0 to 40 (Average shown by thicker line)

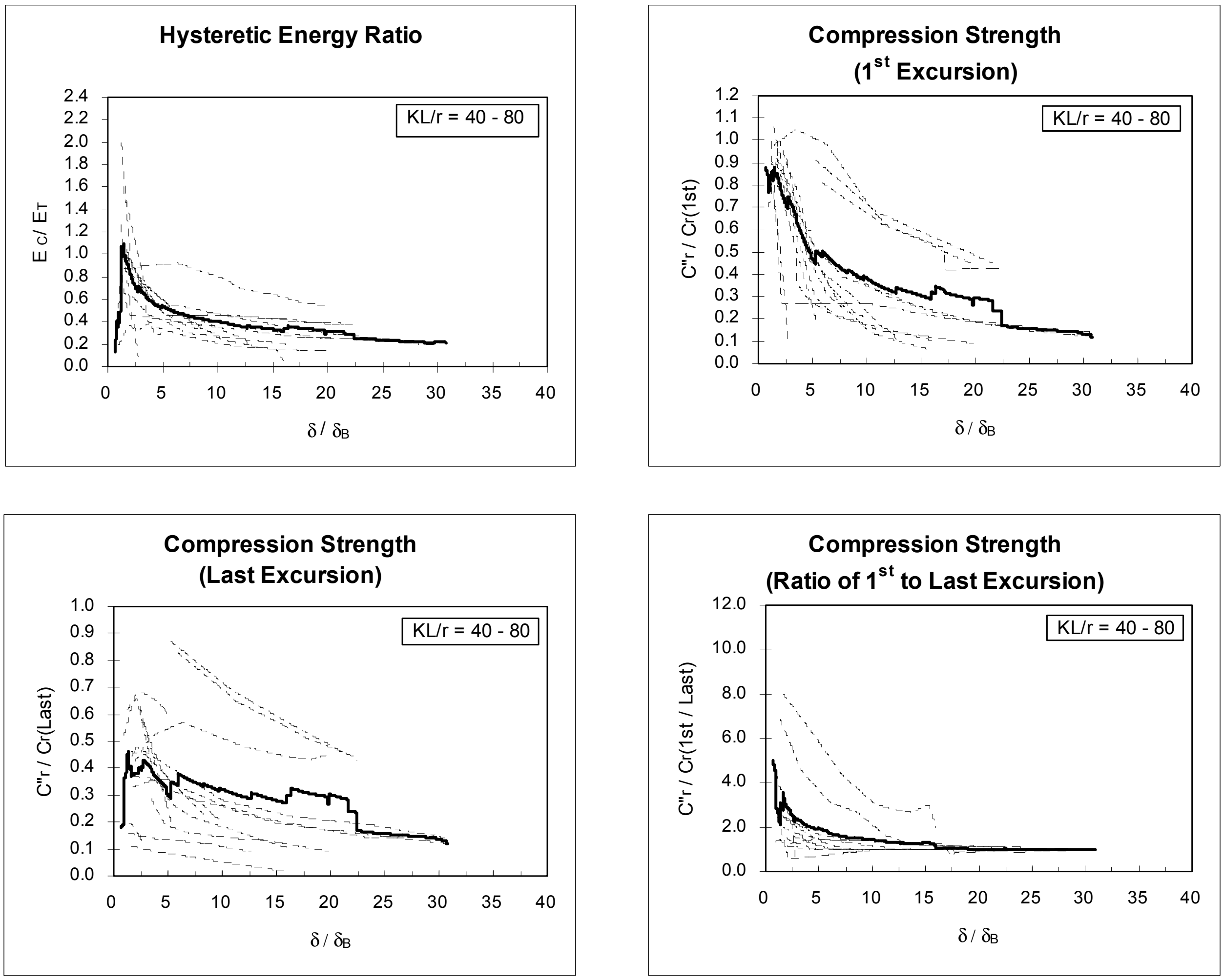

Figure B.2 All structural shapes with KL/r = 40 to 80 (Average shown by thicker line)

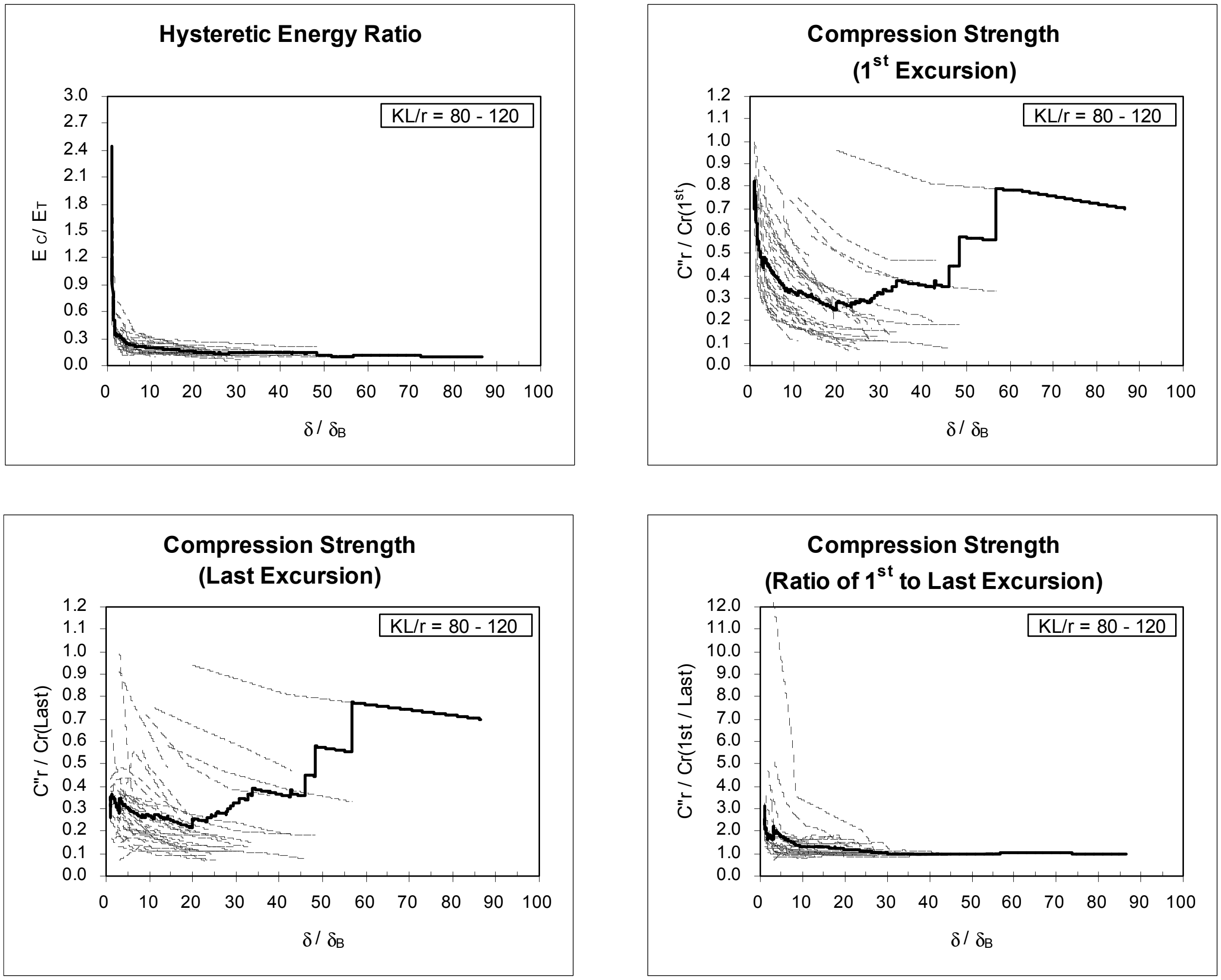

Figure B.3 All structural shapes with KL/r = 80 to 120 (Average shown by thicker line)

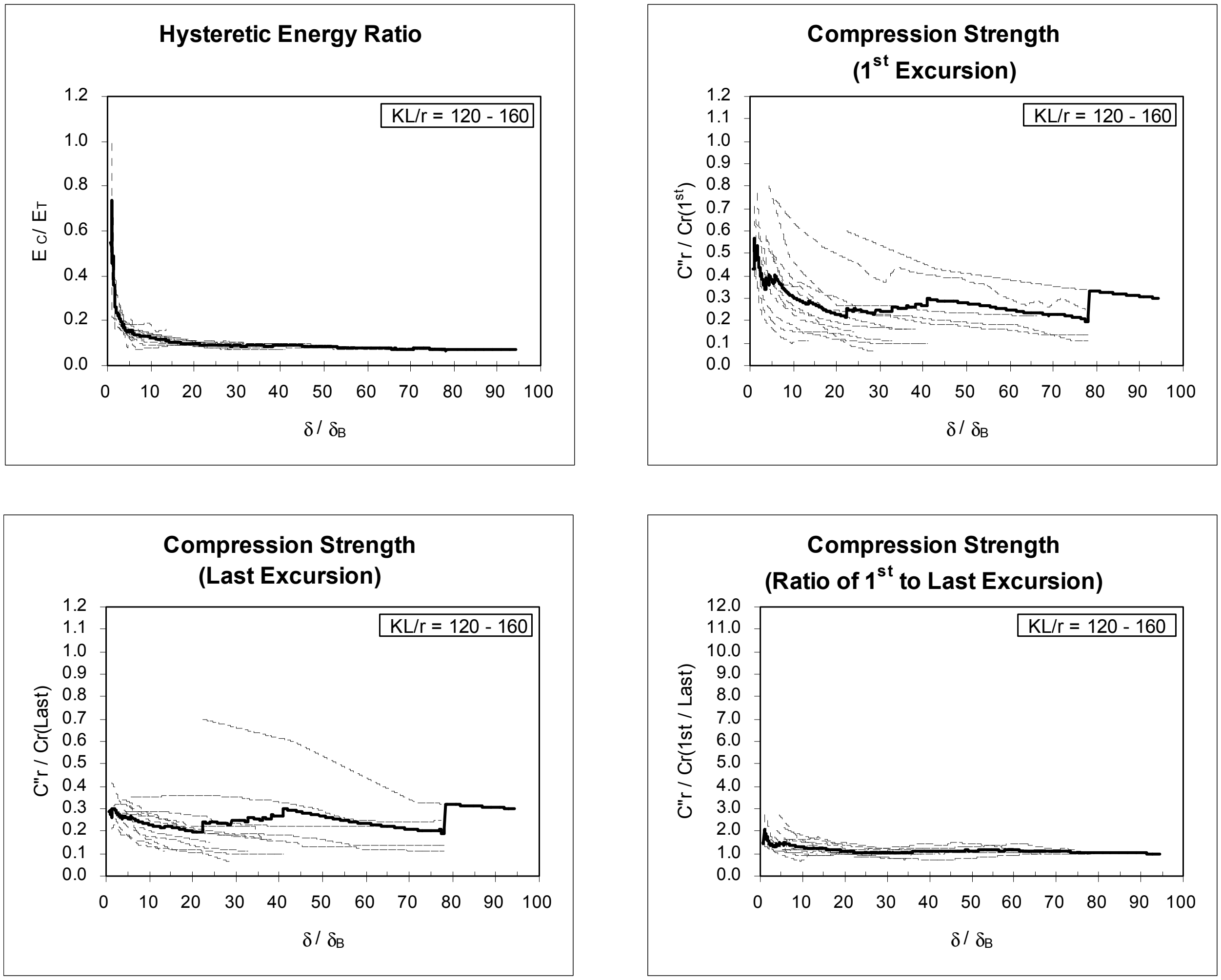

Figure B.4 All structural shapes with KL/r = 120 to 160 (Average shown by thicker line)

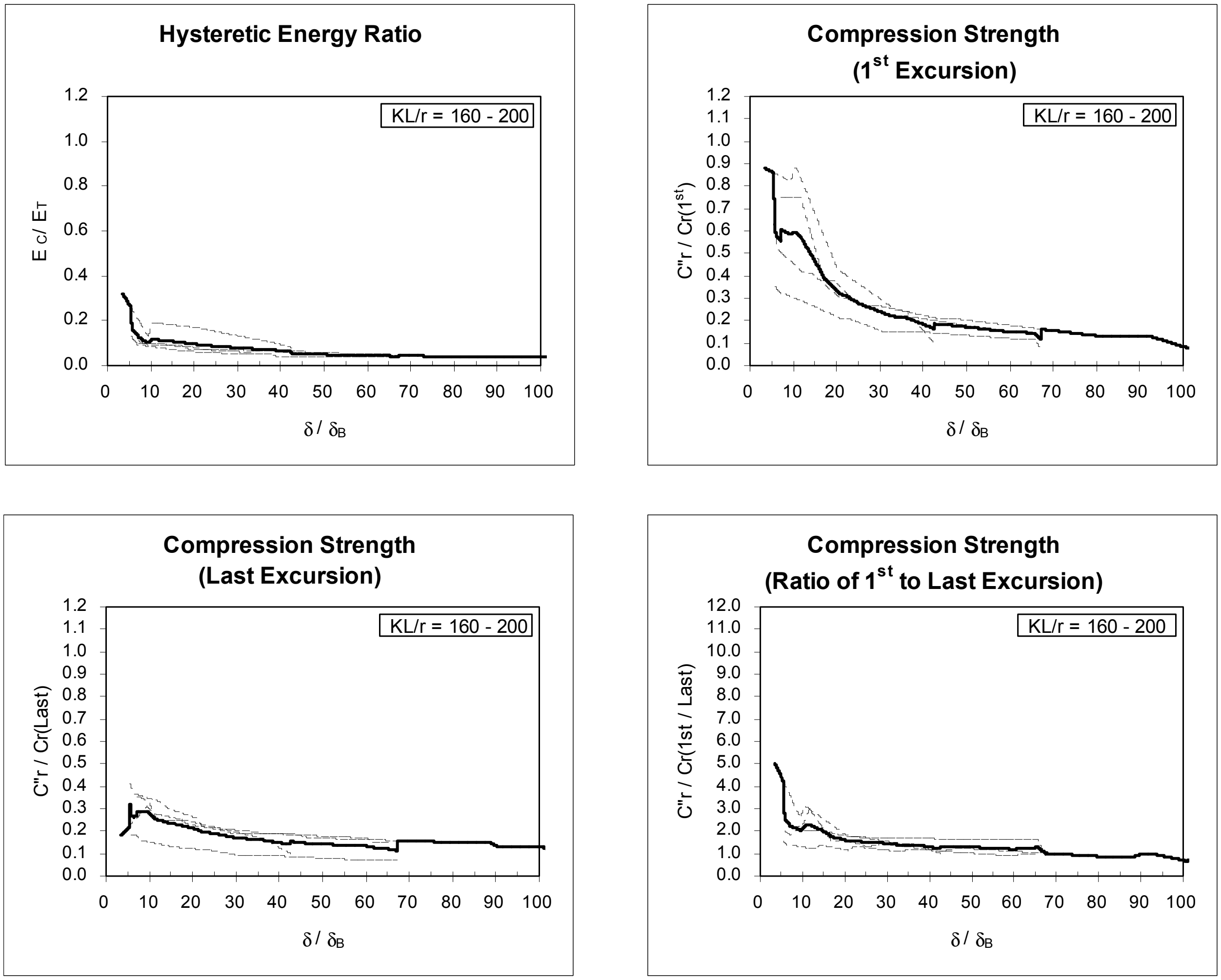

Figure B.5 All structural shapes with KL/r = 160 to 200 (Average shown by thicker line)

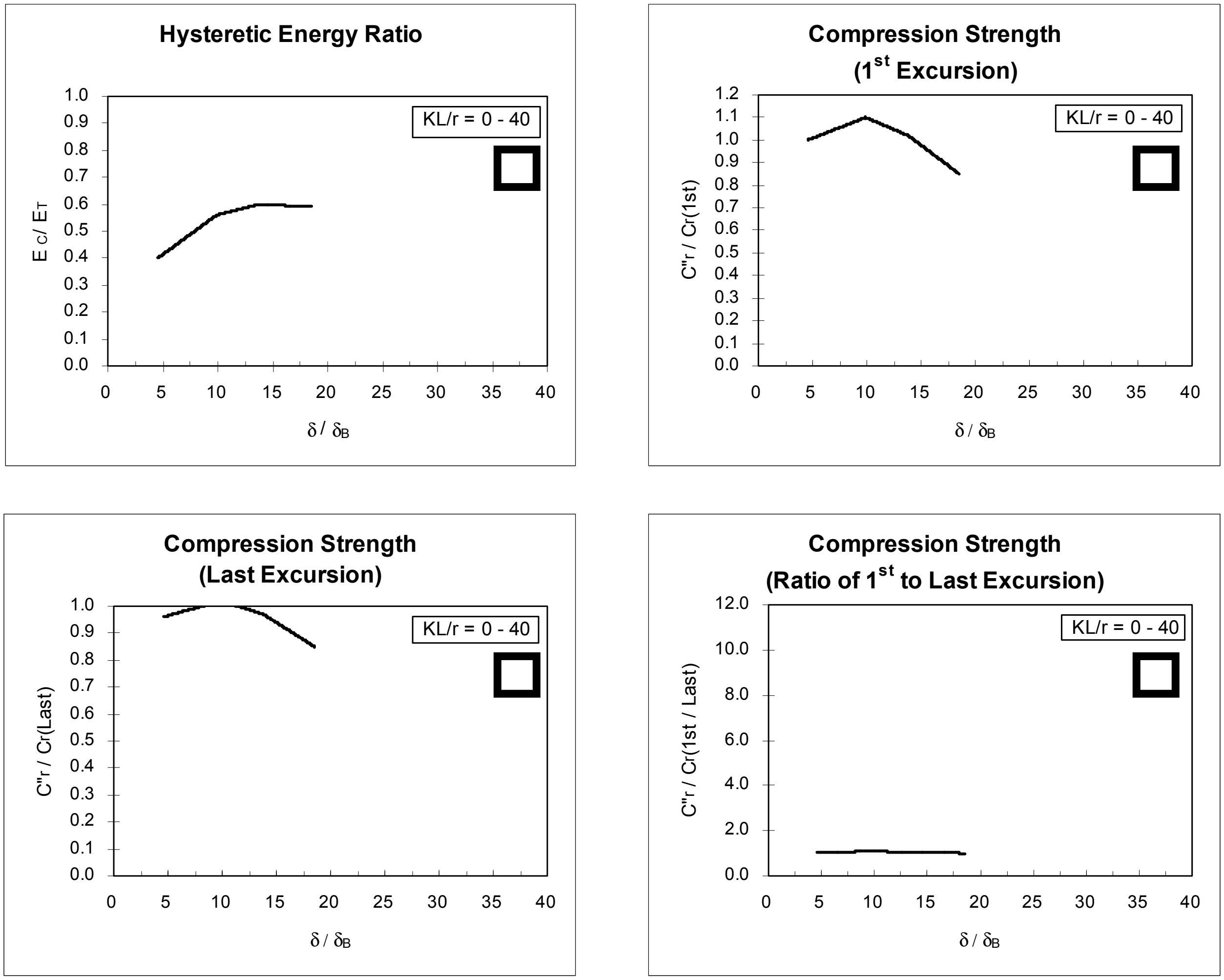

Figure B.6 Structural Tubes with KL/r = 0 to 40 (Average shown by thicker line)

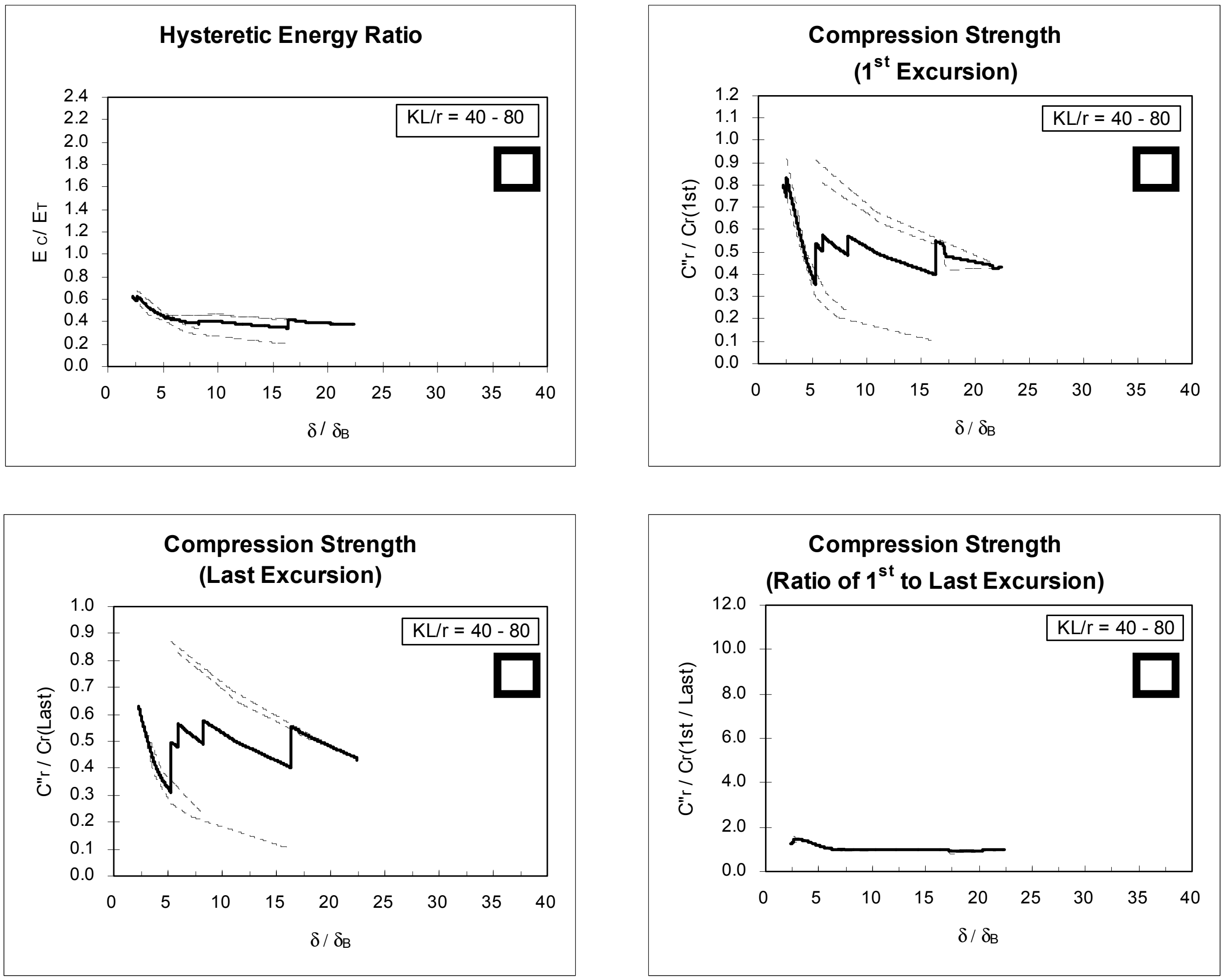

Figure B.7 Structural Tubes with KL/r = 40 to 80 (Average shown by thicker line)

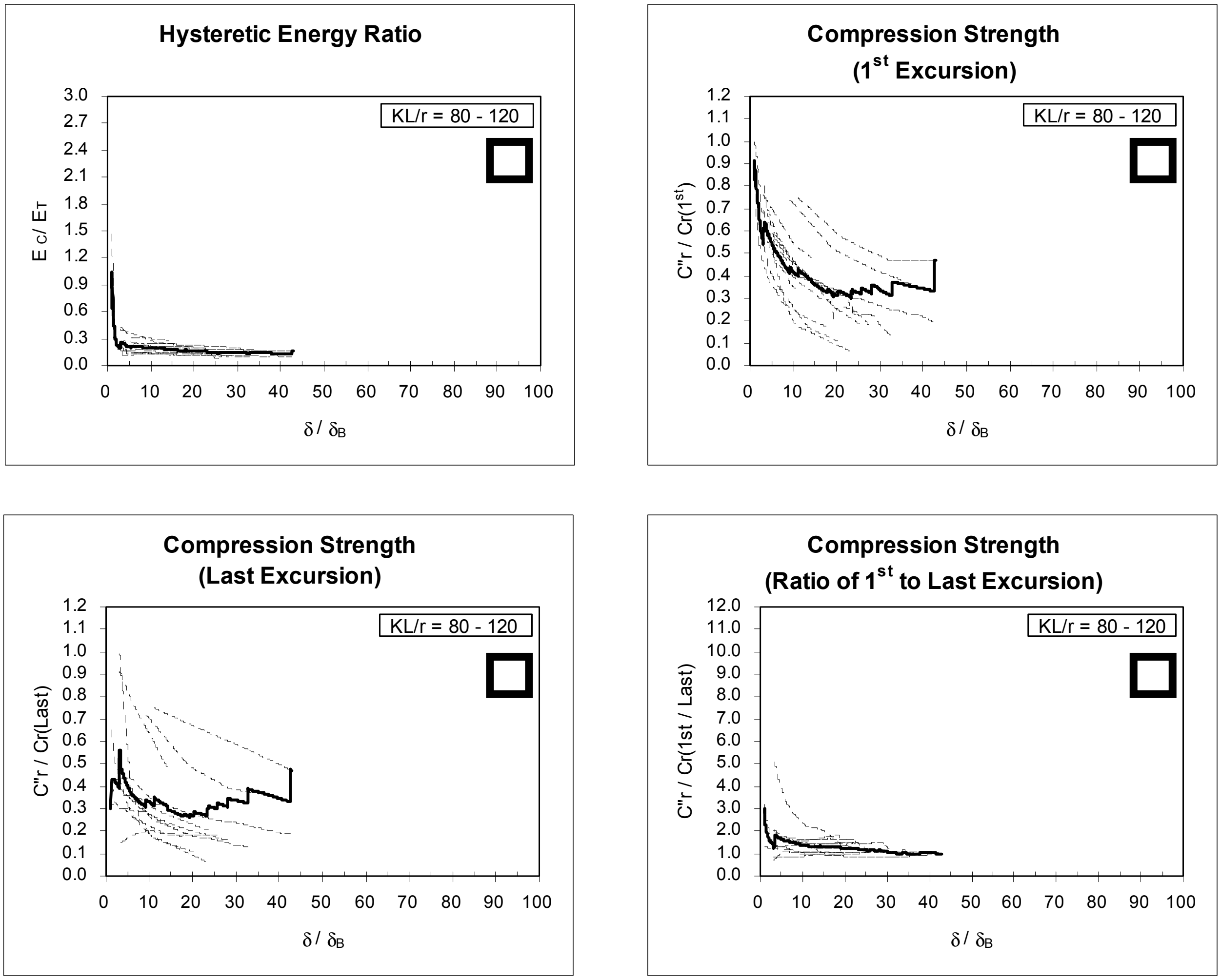

Figure B.8 Structural Tubes with KL/r = 80 to 120 (Average shown by thicker line)

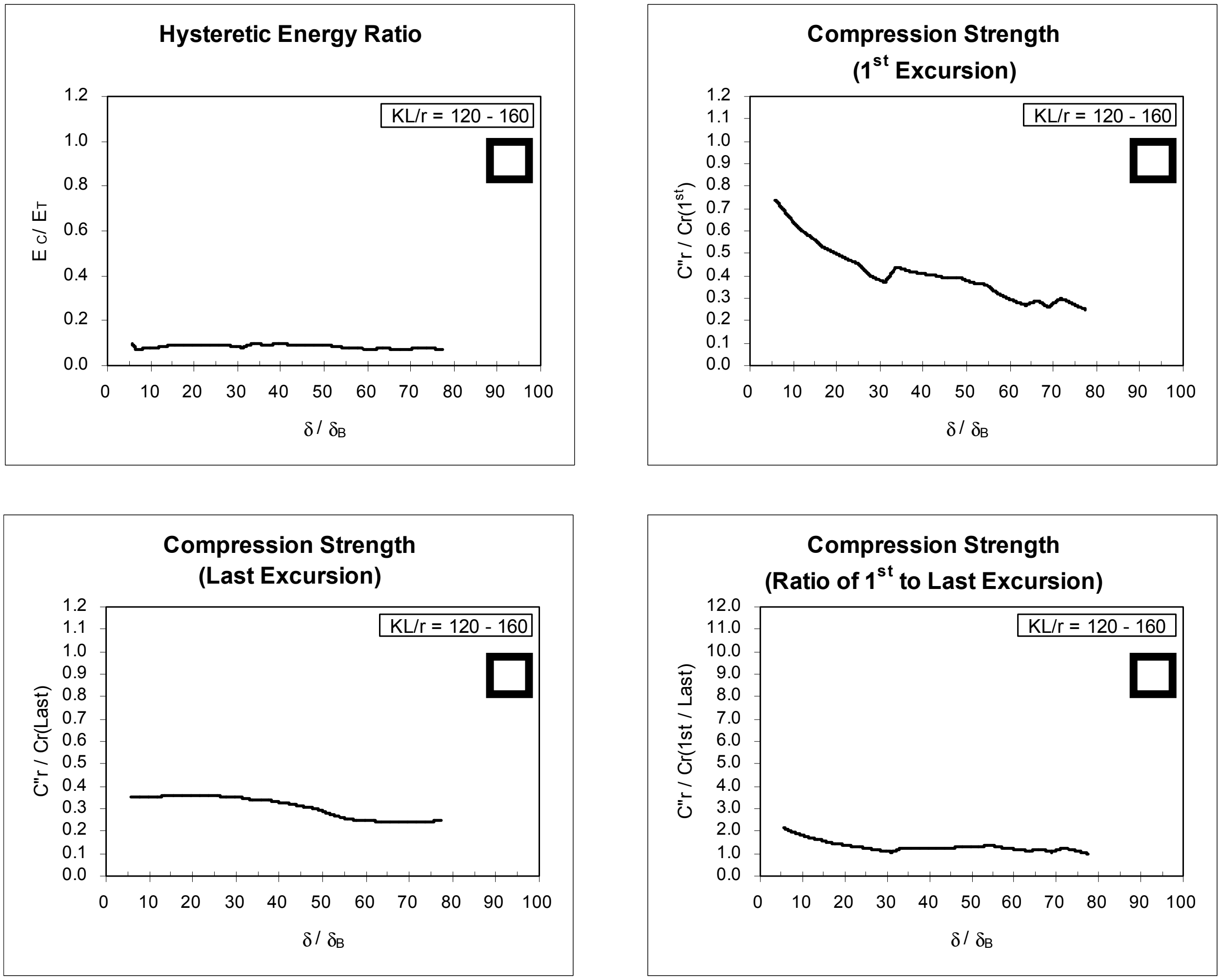

Figure B.9 Structural Tubes with KL/r = 120 to 160 (Average shown by thicker line)

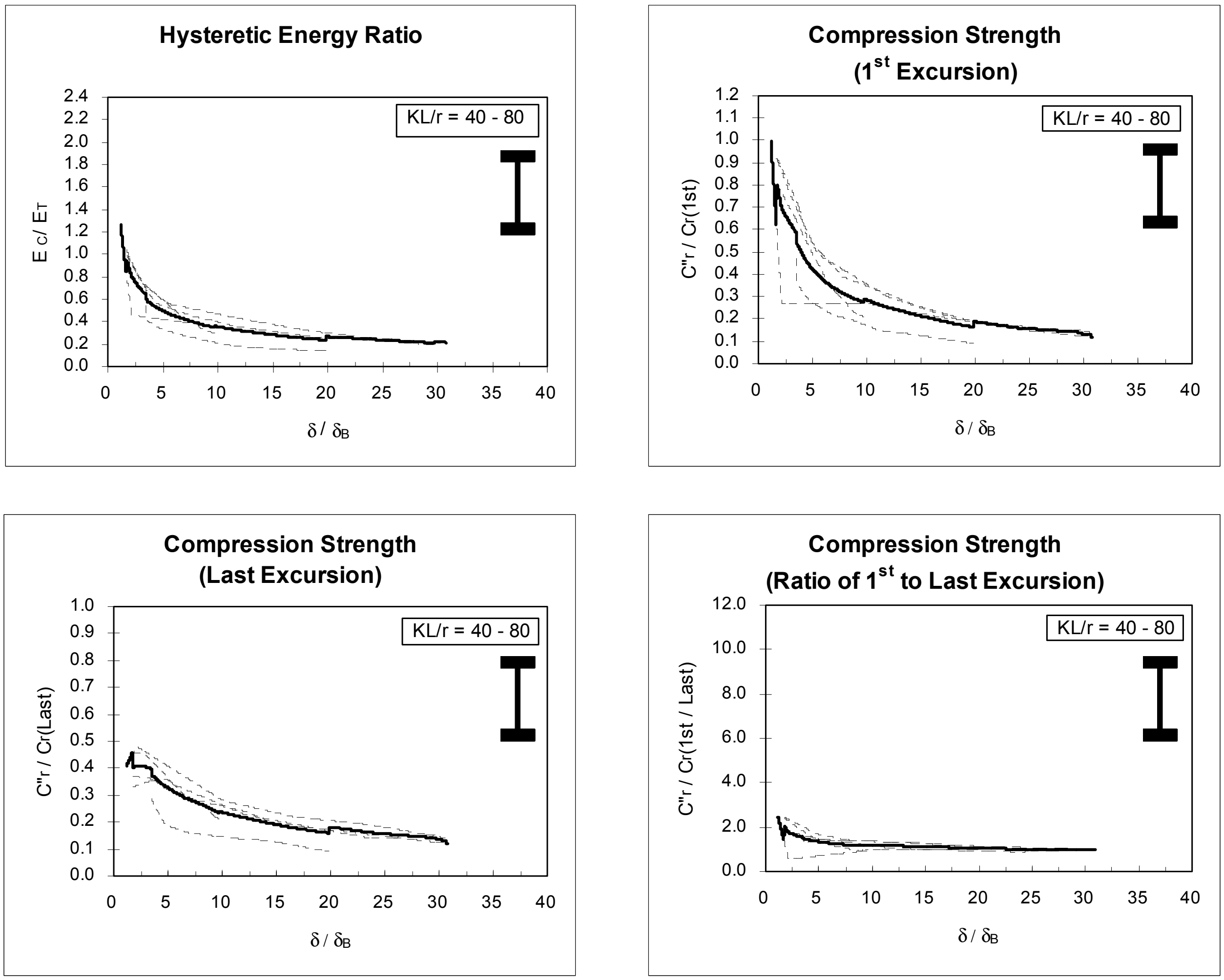

Figure B.10 Wide Flanges with KL/r = 40 to 80 (Average shown by thicker line)

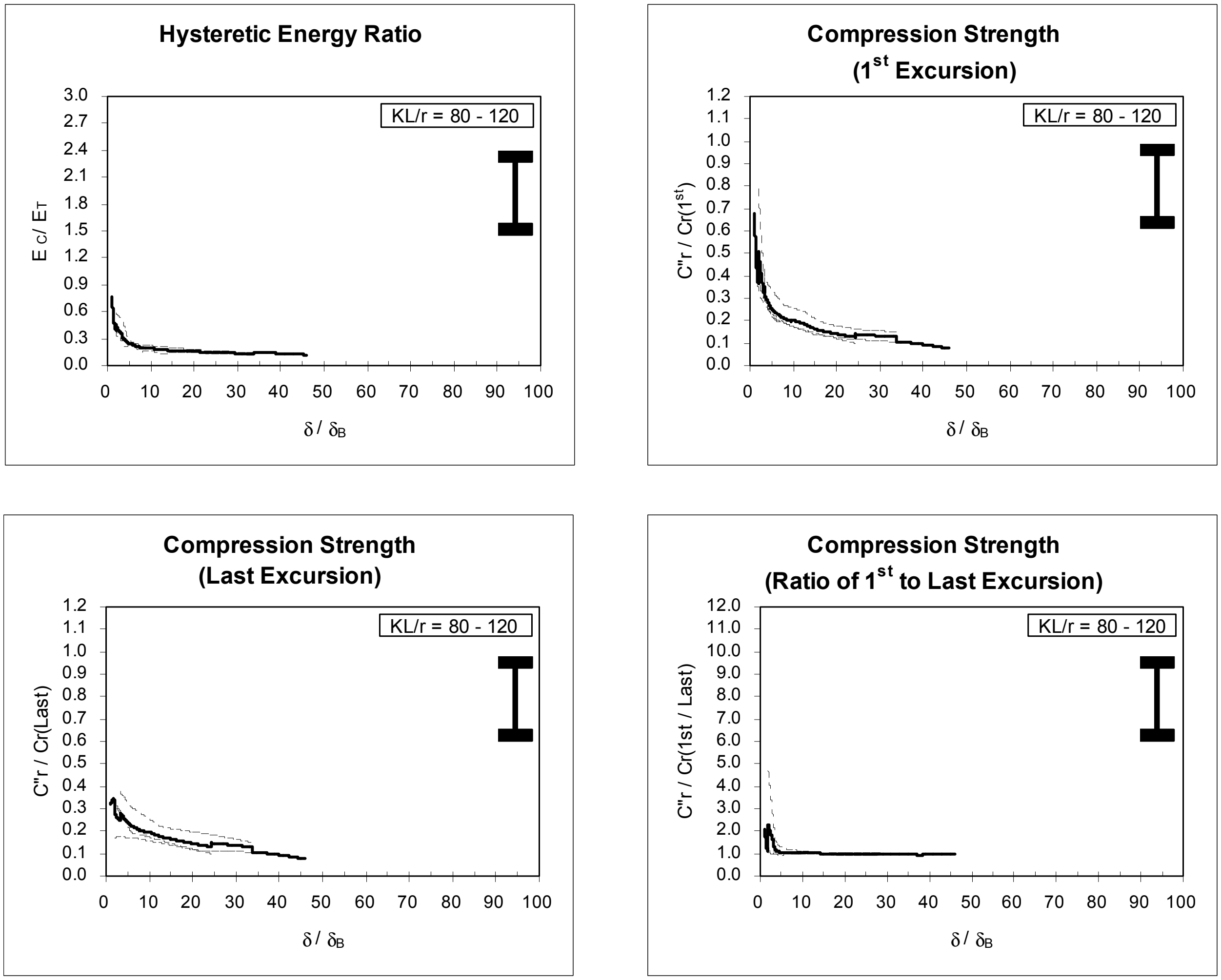

Figure B.11 Wide Flanges with KL/r = 80 to 120 (Average shown by thicker line)

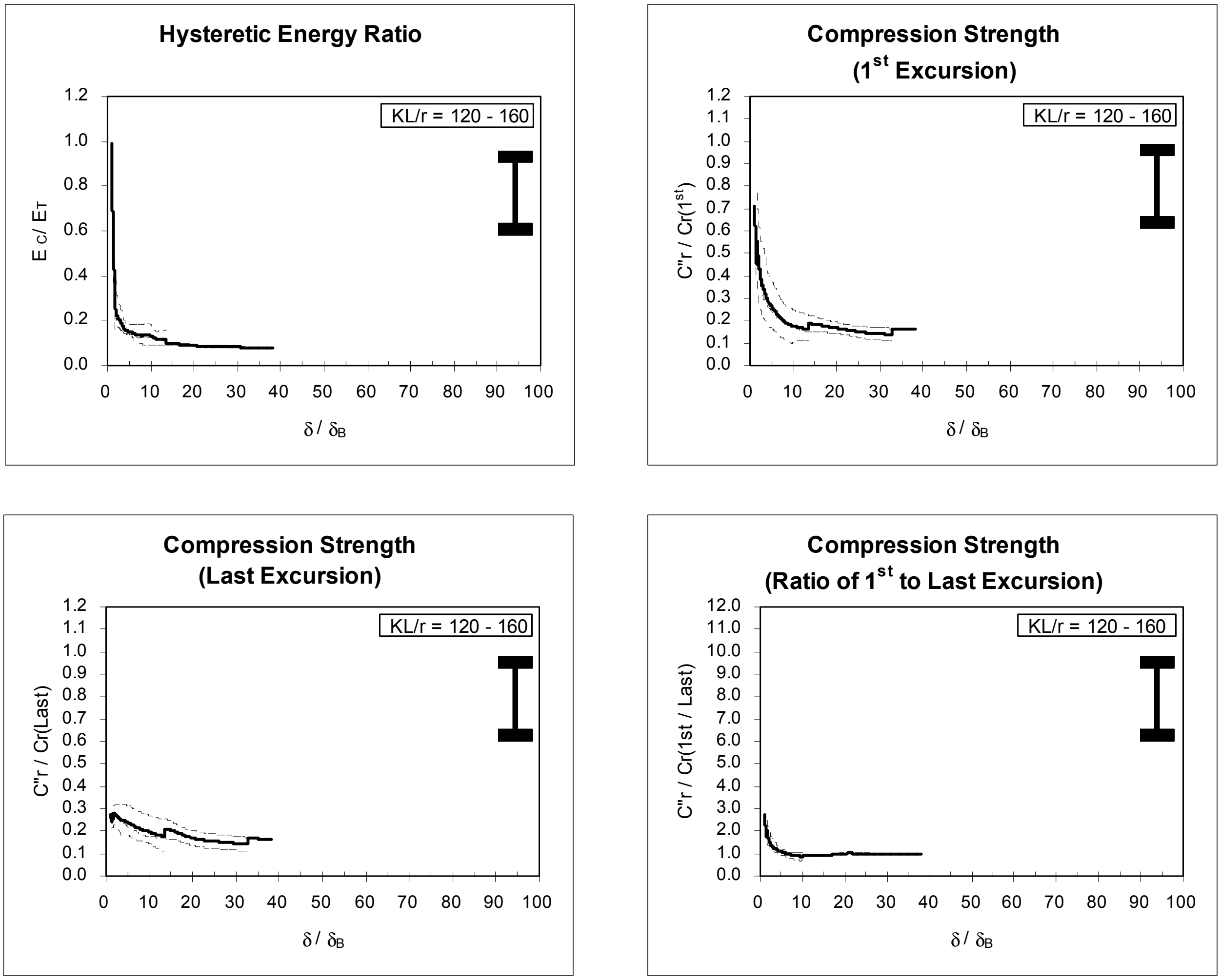

Figure B.12 Wide Flanges with KL/r = 120 to 160 (Average shown by thicker line)

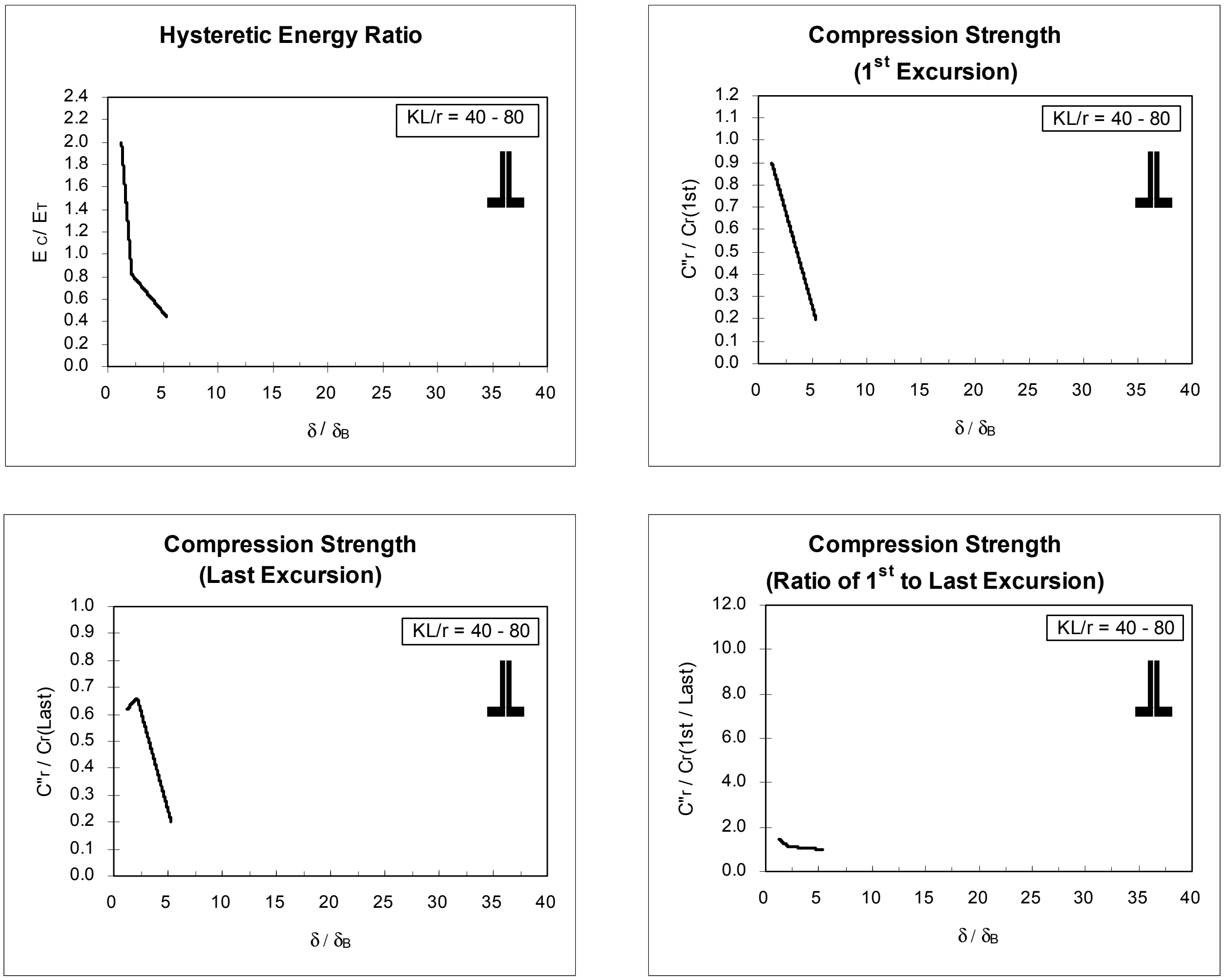

Figure B.13 Double Angles, back-to-back with KL/r = 40 to 80
(Average shown by thicker line)

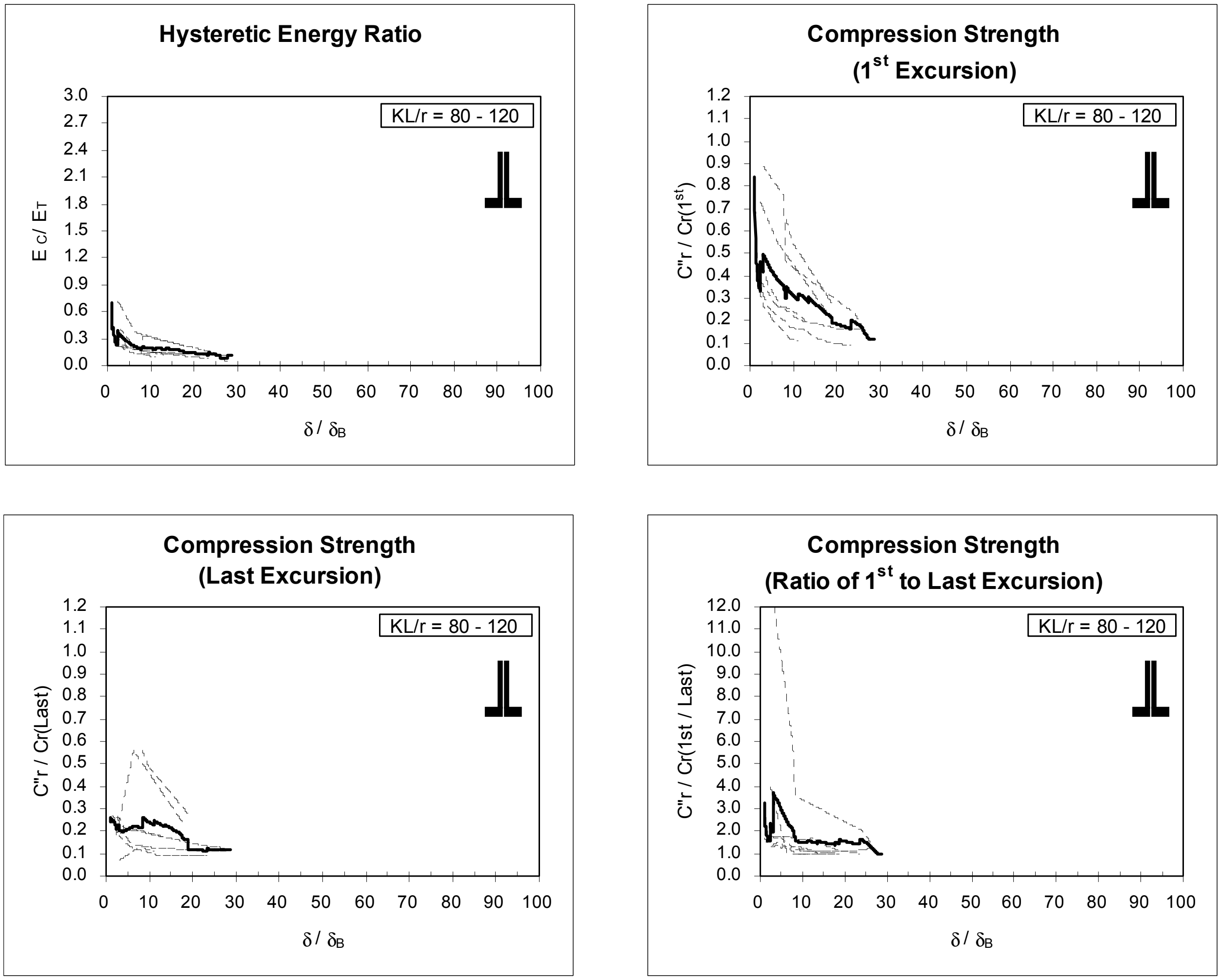

Figure B.14 Double Angles, back-to-back with KL/r = 80 to 120
(Average shown by thicker line)

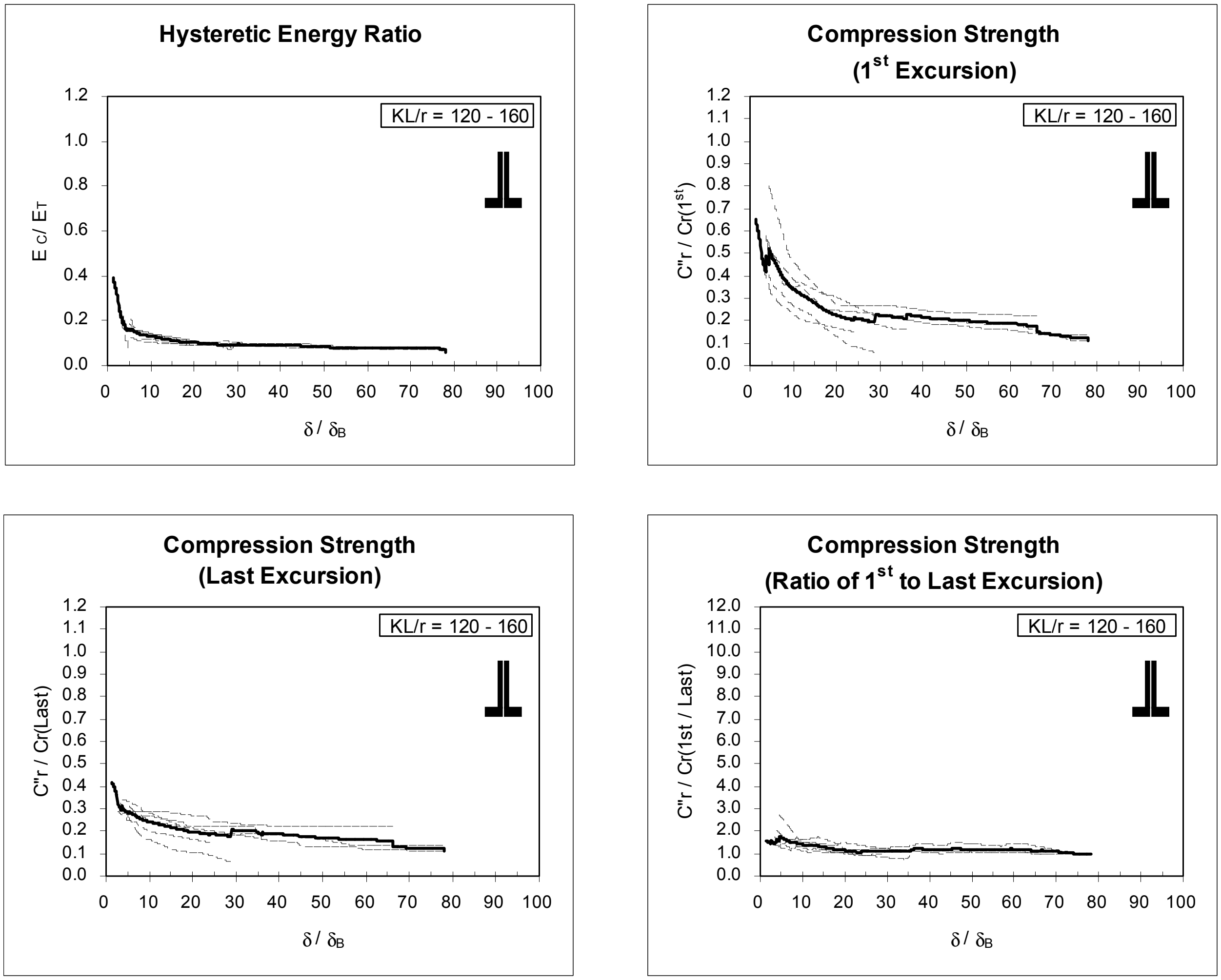

Figure B.15 Double Angles, back-to-back with KL/r = 120 to 160
(Average shown by thicker line)

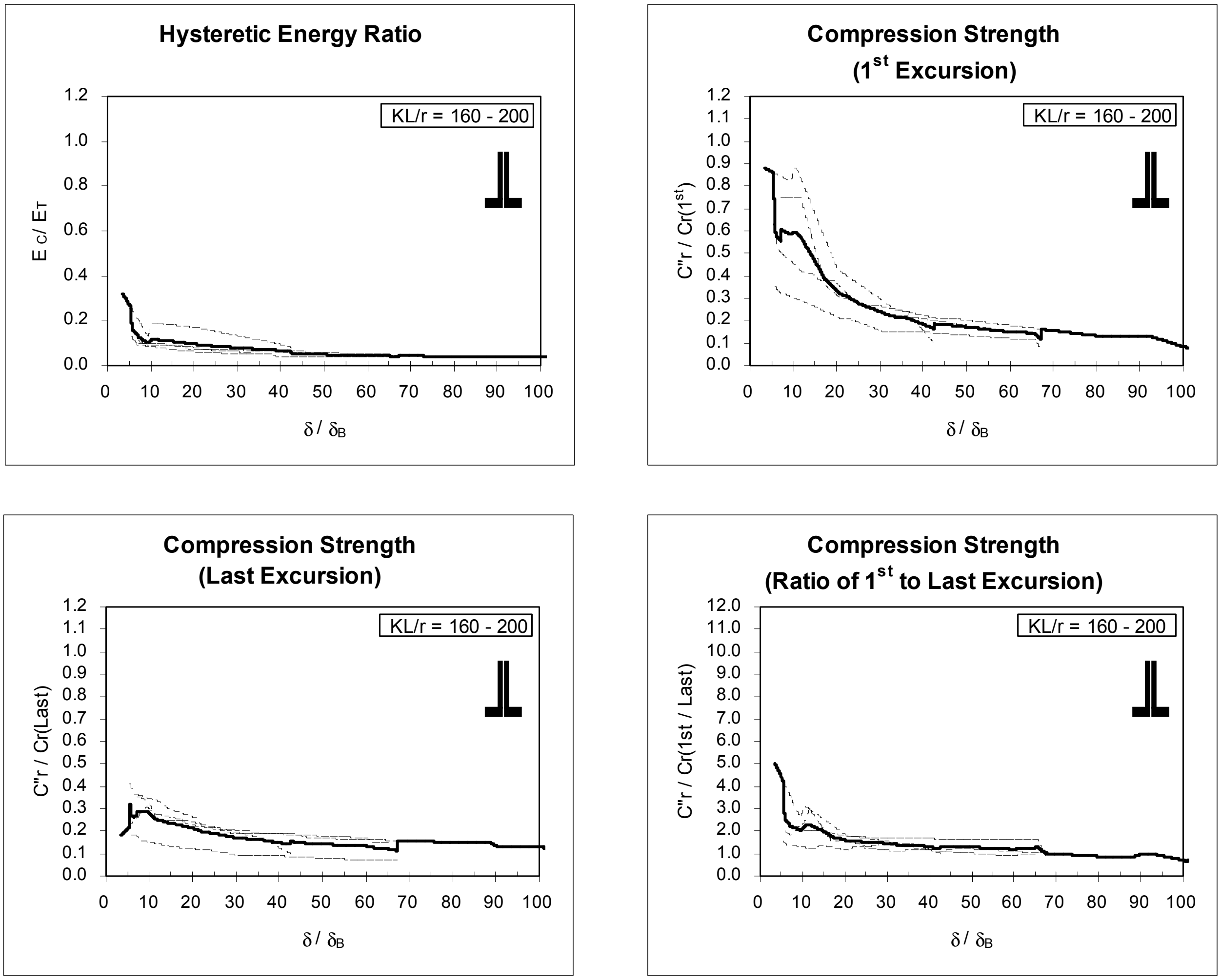

Figure B.16 Double Angles, back-to-back with KL/r = 160 to 200
(Average shown by thicker line)

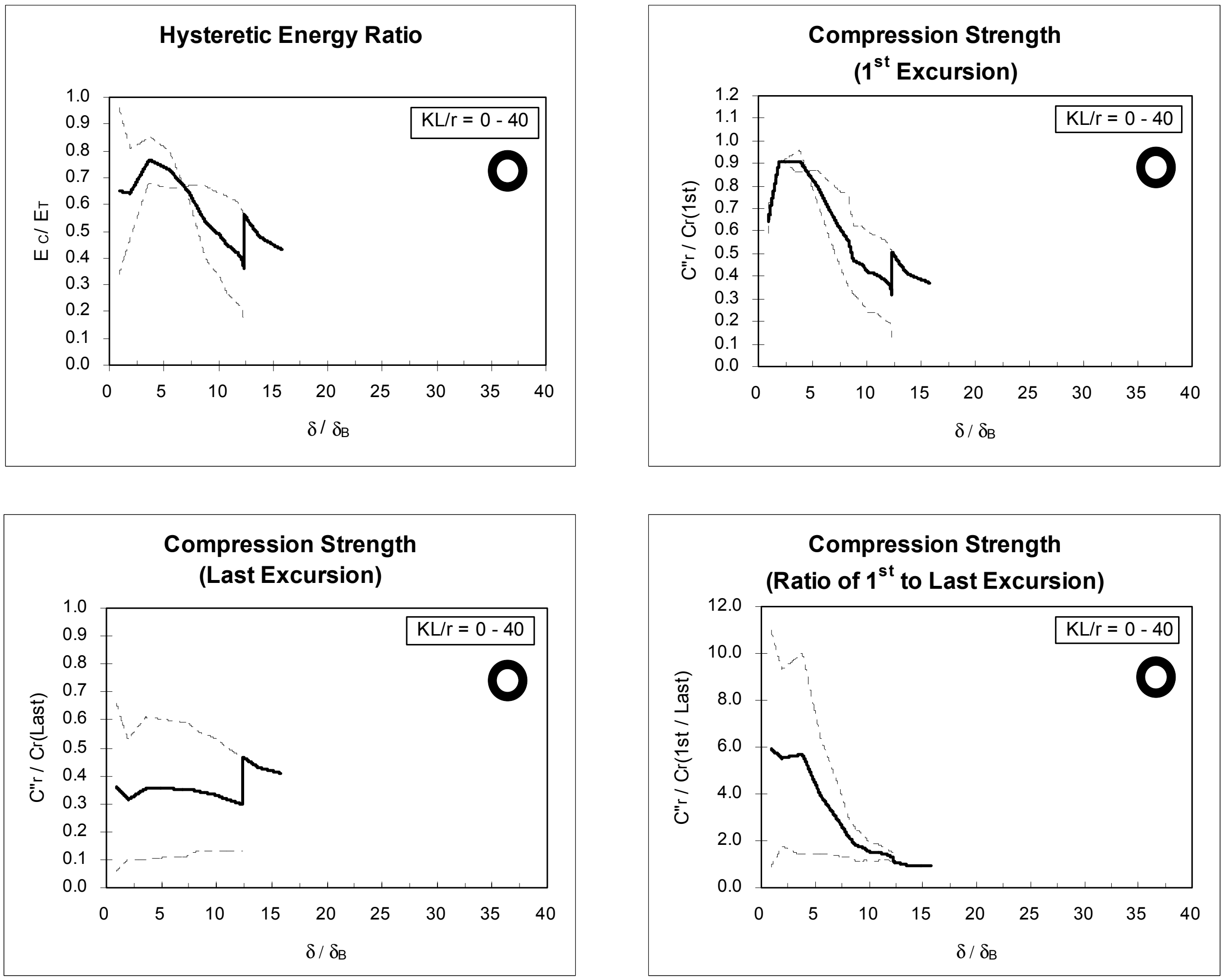

Figure B.17 Structural Pipes with KL/r = 0 to 40 (Average shown by thicker line)

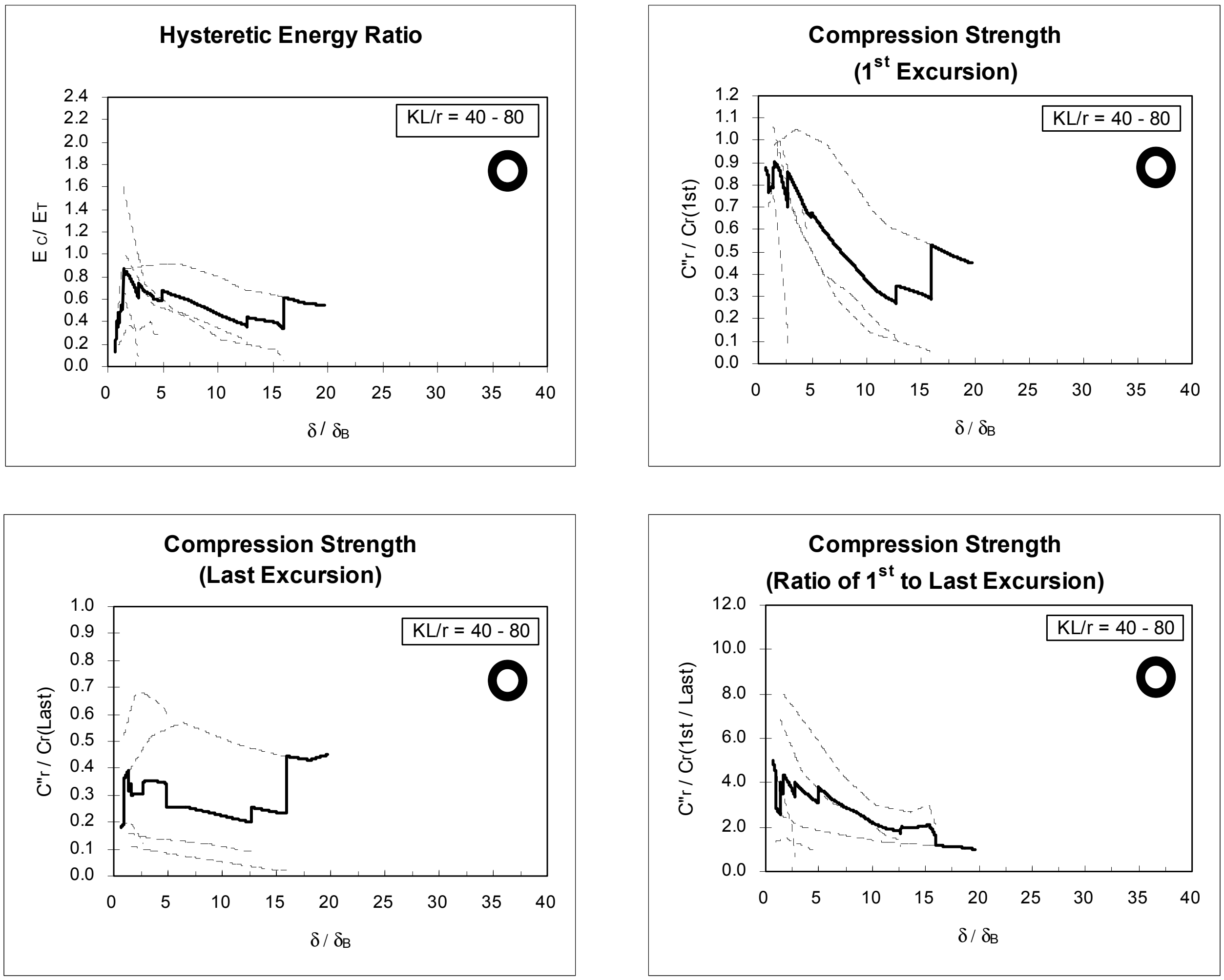

Figure B.18 Structural Pipes with KL/r = 40 to 80 (Average shown by thicker line)

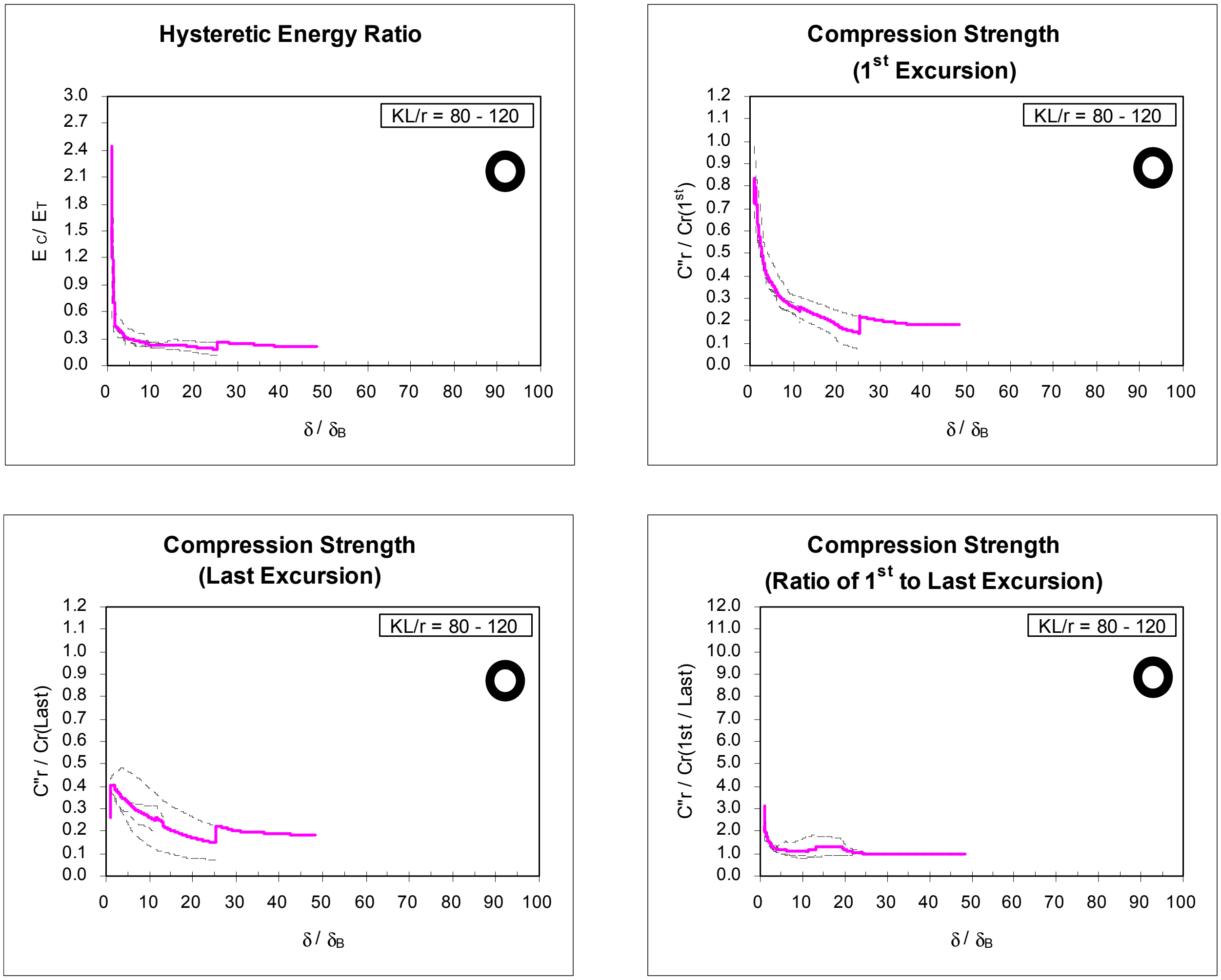

Figure B.19 Structural Pipes with KL/r = 80 to 120 (Average shown by thicker line)

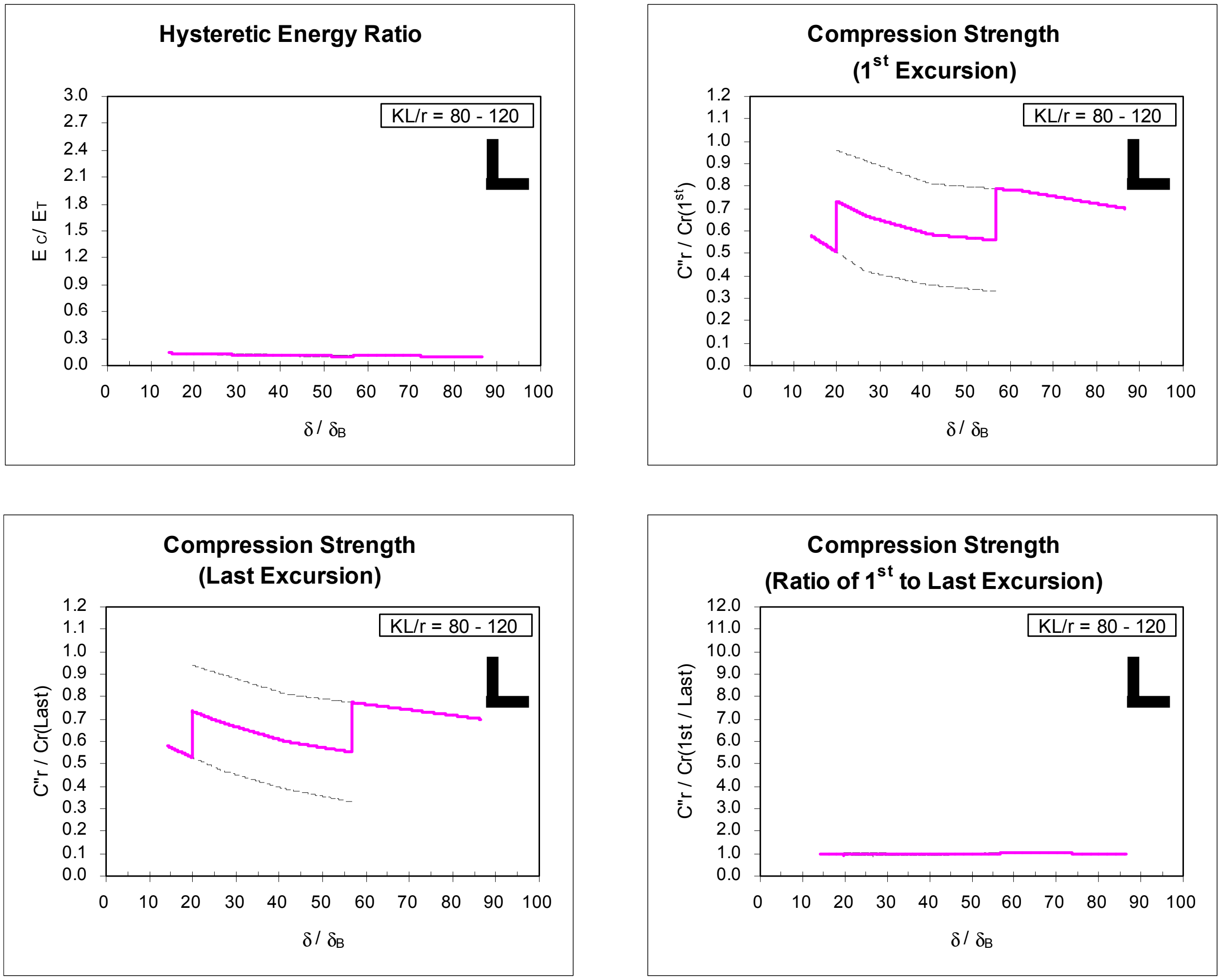

Figure B.20 Single Angles with KL/r = 80 to 120 (Average shown by thicker line)

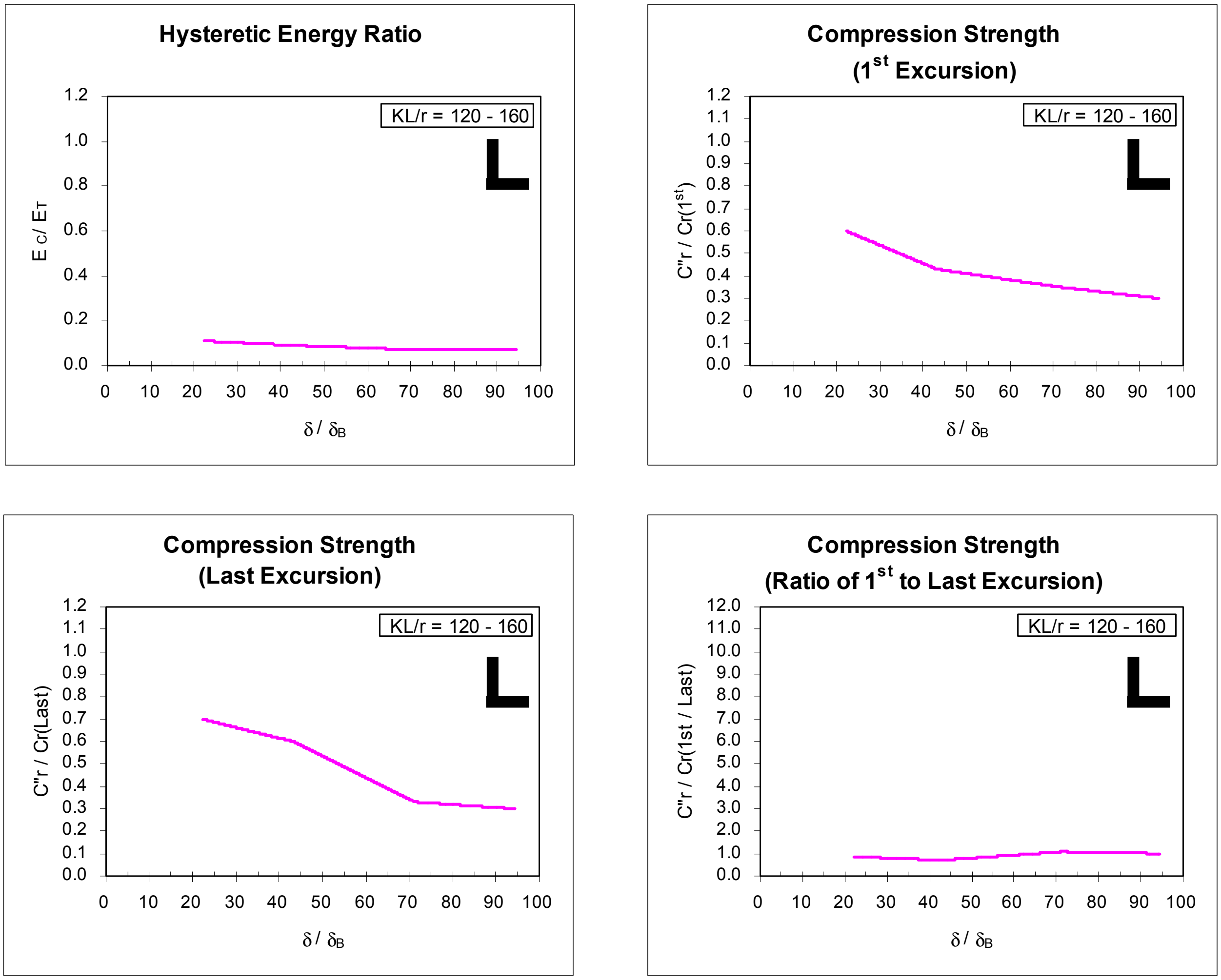

Figure B.21 Single Angles with KL/r = 120 to 160 (Average shown by thicker line)

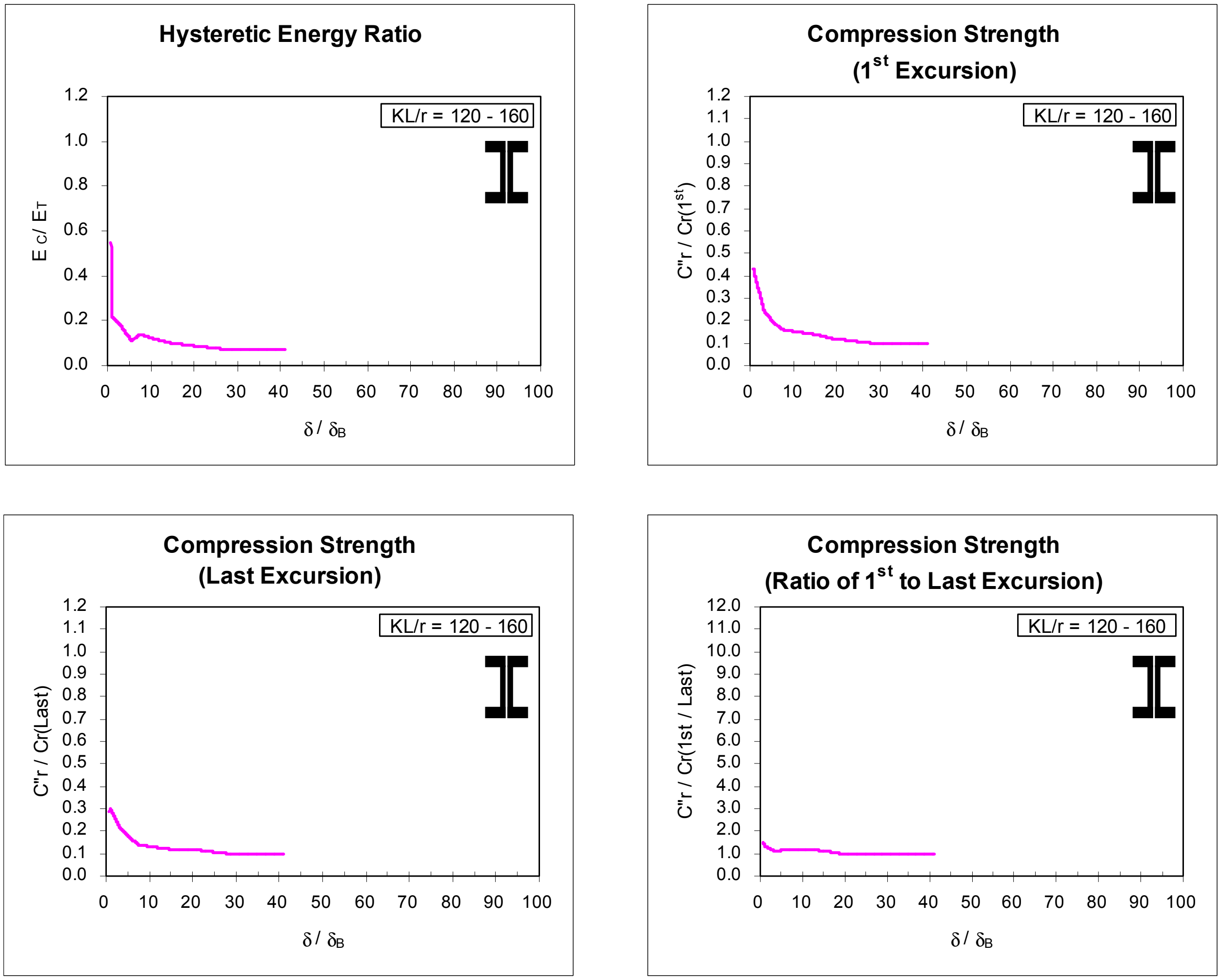

Figure B.22 Double Channels, back to back with KL/r = 120 to 160
(Average shown by thicker line)

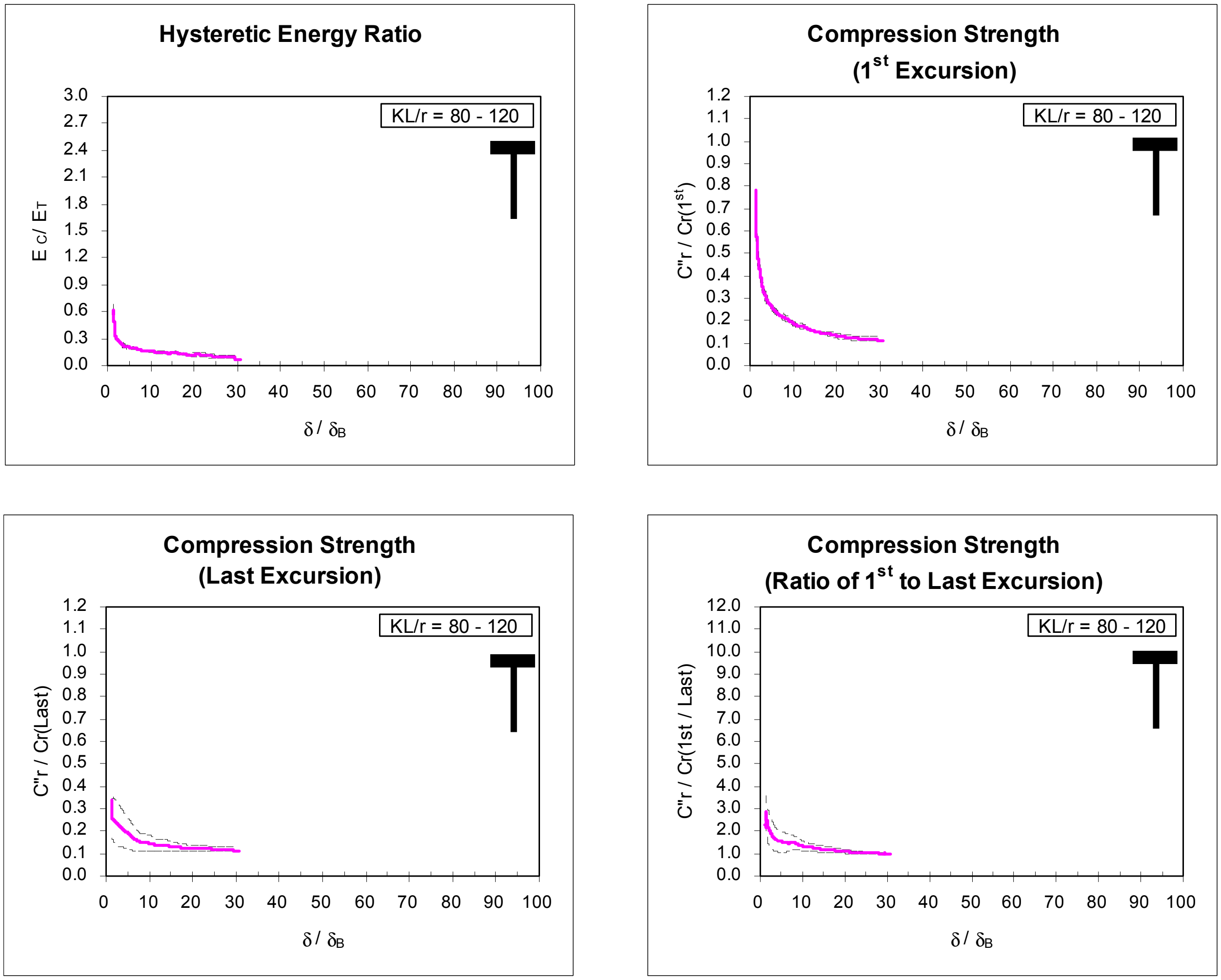

Figure B.23 Structural Tees with KL/r = 80 to 120 (Average shown by thicker line)

APPENDIX C

Hysteretic Curves

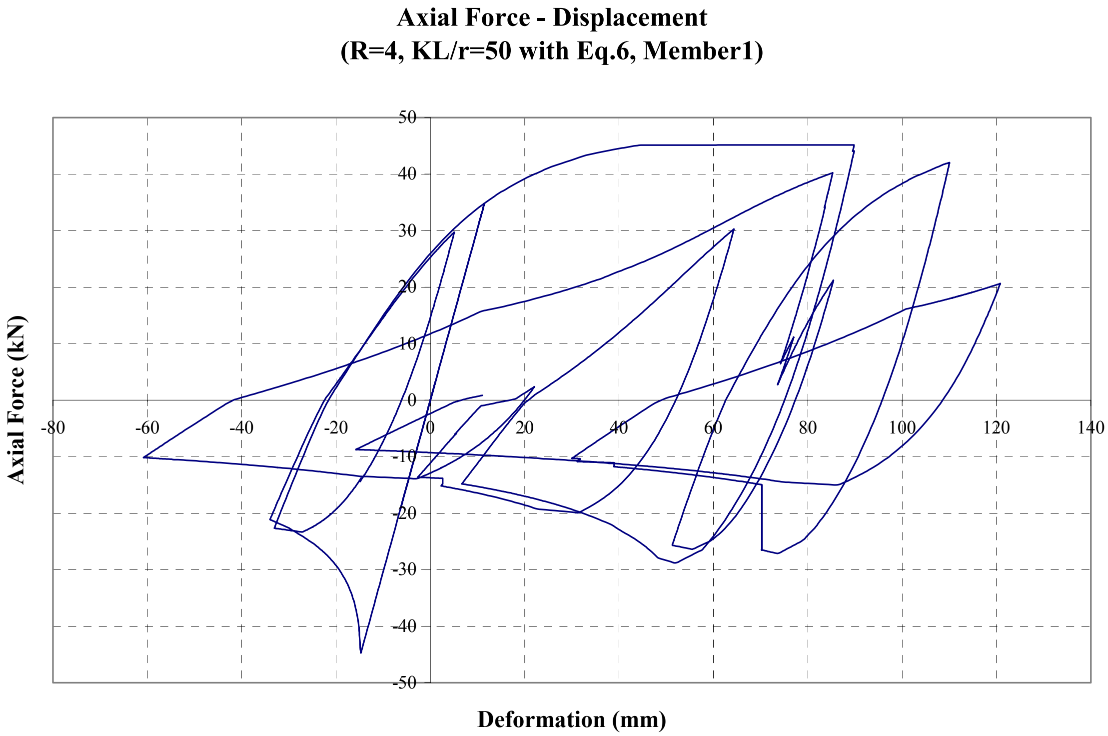

Figure C.1 Axial Force – Displacement Curve with R=4, KL/r=50 and EQ. 6 Member1

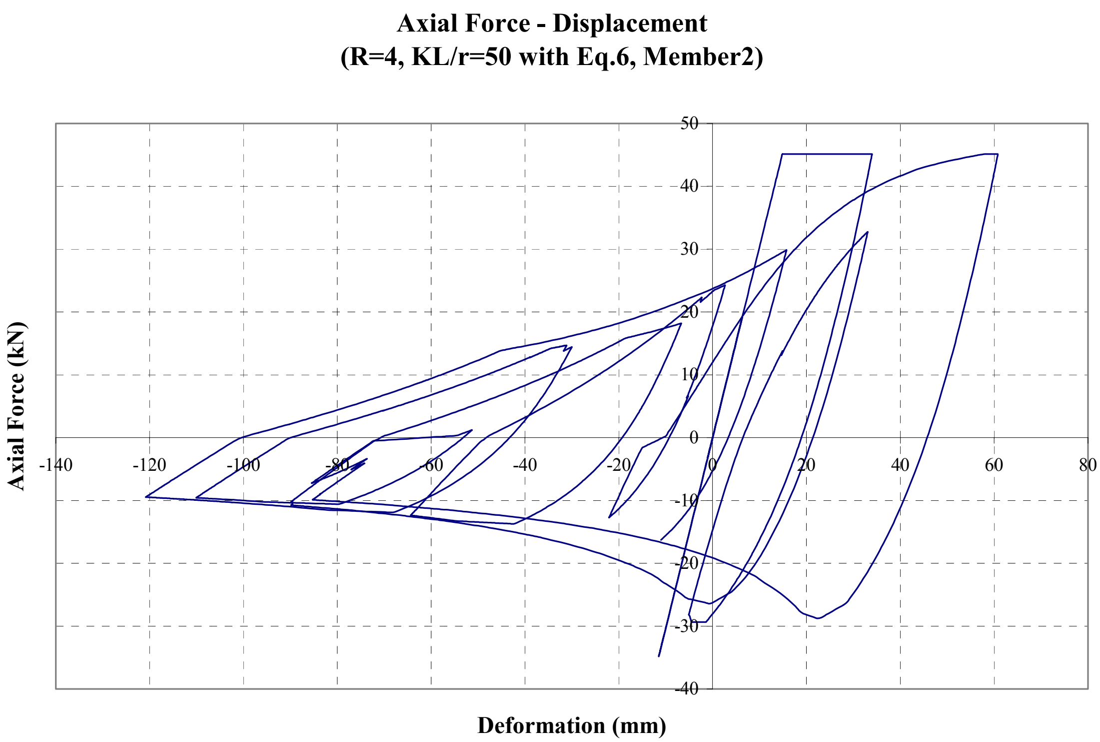

Figure C.2 Axial Force – Displacement Curve with R=4, KL/r=50 and EQ. 6 Member2

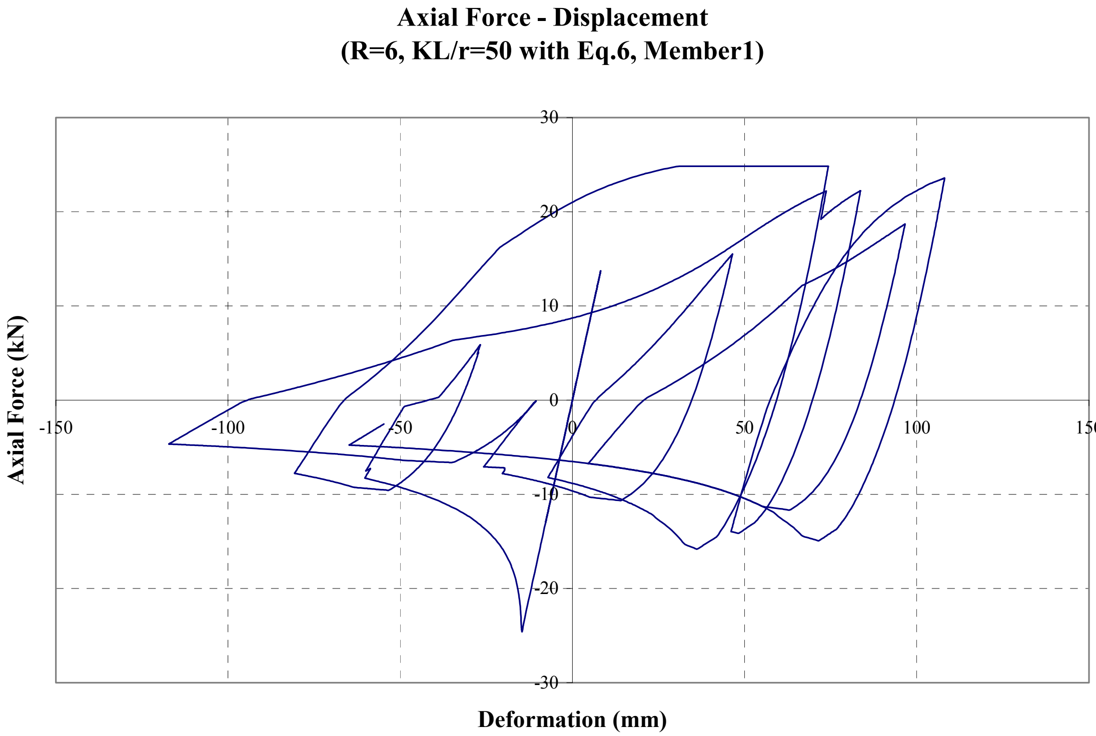

Figure C.3 Axial Force – Displacement Curve with R=6, KL/r=50 and EQ. 6 Member1

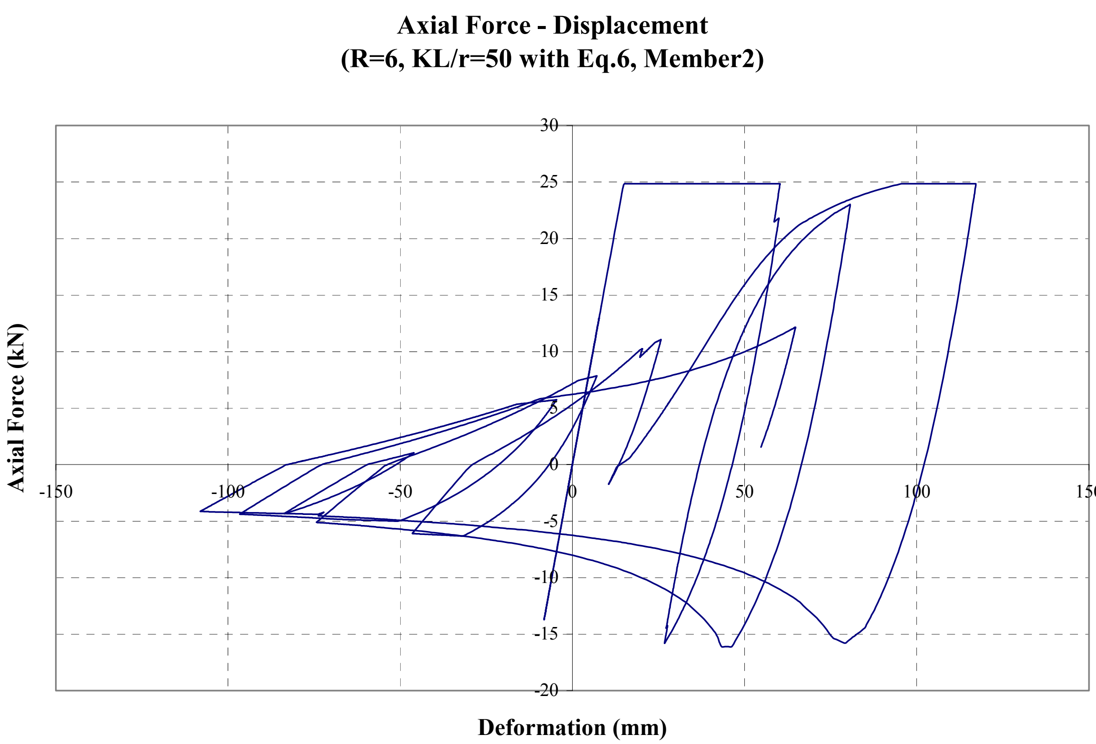

Figure C.4 Axial Force – Displacement Curve with R=6, KL/r=50 and EQ. 6 Member2

APPENDIX D

Bracing Member Design Calculation Sheets

Outcomes of Calculations Below

T/C,	Pbr =	363.09	(kN)	Fy =	35.0	(kN/cm^2)								
R=1	E =	20000.0	(kN/cm^2)	L =	849.7	(cm)								
	B(cm)	D(cm)	t(cm)	B-2t(cm)	A(cm^2)	Areq'd(cm^2)	I_y(cm^4)	$I_{y,req'd}$(cm^4)	r_y(cm)	$r_{y,req'd}$(cm)	Z_y(cm^3)	L/r	Py	Pcr
L/r=50	41.7	41.7	0.06	41.6	10.3739	10.3739	2995.99	2995.99	16.99	16.99	161.94	50	363.09	819.09

Detailed Calculations

1) Bracing Members for Element #5 in DRAIN-2DX)

Control Information

One Line	nmbt(I) 1

Property Types

1st Line	itt(I) 1	Area(R) 10.37	RI(R) 2995.99	Effek(R) 1.0	Plamom(R) 5667.83	Yiestr(R) 35.0	E0(R) 20000.0	Harden(R) 0.0
2nd Line	Theta0(R) 0.0							
3rd Line	isec(I) 31	itemax(I) 100	tol(R) 0.00001	styp(R) 0.00001				
4th Line	Beta(R) 1.2	E1(R) 0.05	E2(R) 0.9	E3(R) 1.25	E4(R) -0.25			
5th Line	P12(R) 0.5	a1(R) 1.0	b1(R) 0.0	c1(R) -1.33	a2(R) 1.33	b2(R) -1.33	c2(R) 0	
6th Line	Ratet(R) 1.0	Ratec(R) 1.0						

2) Design Iterations

R=1

KL/r=50	V(kN)	Pbr(kN)	Tn(sec.)
1st	736.45	411.69	0.35
2nd	674.02	376.79	0.36
3rd	661.48	369.78	0.37
4th	649.51	363.09	0.37

θ = 0.46364761

Figure D.1 Outcomes of Calculations for R=1 and KL/r=50

Outcomes of Calculations Below

T/C, R=1	Pbr =	411.69	(kN)	Fy =	35.0	(kN/cm^2)								
	E =	20000.0	(kN/cm^2)	L =	849.7	(cm)								
	B(cm)	D(cm)	t(cm)	B-2t(cm)	A(cm^2)	Areq'd(cm^2)	I_y(cm^4)	$I_{y,req'd}$(cm^4)	r_y(cm)	$r_{y,req'd}$(cm)	Z_y(cm^3)	L/r	Py	Pcr
L/r=100	21.1	21.1	0.25	20.6	20.8564	20.8564	1505.83	1505.83	8.50	8.50	162.78	100	729.97	411.69

Detailed Calculations

1) Bracing Members for Element #5 in DRAIN-2DX)

Control Information

One Line	nmbt(I)
	1

Property Types

1st Line	itt(I)	Area(R)	RI(R)	Effek(R)	Plamom(R)	Yiestr(R)	E0(R)	Harden(R)
	1	20.86	1505.83	1.0	5697.33	35.0	20000.0	0.0
2nd Line	Theta0(R)							
	0.0							
3rd Line	isec(I)	itemax(I)	tol(R)	styp(R)				
	31	100	0.00001	0.00001				
4th Line	Beta(R)	E1(R)	E2(R)	E3(R)	E4(R)			
	1.2	0.05	0.9	1.25	-0.25			
5th Line	P12(R)	a1(R)	b1(R)	c1(R)	a2(R)	b2(R)	c2(R)	
	0.5	1.0	0.0	-1.33	1.33	-1.33	0	
6th Line	Ratet(R)	Ratec(R)						
	1.0	1.0						

2) Design Iterations

R=1	KL/r=100	V(kN)	Pbr(kN)	Tn(sec.)	θ =	0.46364761
	1st	736.45	411.69	0.26	< 0.3	

Figure D.2 Outcomes of Calculations for R=1 and KL/r=100

Outcomes of Calculations Below

T/C, R=1	Pbr =	411.69	(kN)	Fy =	35.0	(kN/cm^2)								
	E =	20000.0	(kN/cm^2)	L =	849.7	(cm)								
	B(cm)	D(cm)	t(cm)	B-2t(cm)	A(cm^2)	Areq'd(cm^2)	I_y(cm^4)	$I_{y,req'd}$(cm^4)	r_y(cm)	$r_{y,req'd}$(cm)	Z_y(cm^3)	L/r	Py	Pcr
L/r=150	14.7	14.7	0.85	13.0	46.9268	46.9268	1505.83	1505.83	5.66	5.66	244.03	150	1642.44	411.69

Detailed Calculations

1) Bracing Members for Element #5 in DRAIN-2DX)

Control Information

One Line	nmbt(I)
	1

Property Types

1st Line	itt(I)	Area(R)	RI(R)	Effek(R)	Plamom(R)	Yiestr(R)	E0(R)	Harden(R)
	1	46.93	1505.83	1.0	8540.90	35.0	20000.0	0.0
2nd Line	Theta0(R)							
	0.0							
3rd Line	isec(I)	itemax(I)	tol(R)	styp(R)				
	31	100	0.00001	0.00001				
4th Line	Beta(R)	E1(R)	E2(R)	E3(R)	E4(R)			
	1.2	0.05	0.9	1.25	-0.25			
5th Line	P12(R)	a1(R)	b1(R)	c1(R)	a2(R)	b2(R)	c2(R)	
	0.5	1.0	0.0	-1.33	1.33	-1.33	0	
6th Line	Ratet(R)	Ratec(R)						
	1.0	1.0						

2) Design Iterations

R=1	KL/r=150	V(kN)	Pbr(kN)	Tn(sec.)	θ =	0.46364761
	1st	736.45	411.69	0.17	< 0.3	

Figure D.3 Outcomes of Calculations for R=1 and KL/r=150

Outcomes of Calculations Below

T/C, R=2	Pbr =	128.68	(kN)	Fy =	35.0	(kN/cm^2)								
	E =	20000.0	(kN/cm^2)	L =	849.7	(cm)								
	B(cm)	D(cm)	t(cm)	B-2t(cm)	A(cm^2)	Areq'd(cm^2)	I_y(cm^4)	$I_{y,req'd}$(cm^4)	r_y(cm)	$r_{y,req'd}$(cm)	Z_y(cm^3)	L/r	Py	Pcr
L/r=50	41.6	41.6	0.02	41.6	3.6767	3.6767	1061.82	1061.82	16.99	16.99	57.39	50	128.68	290.30

Detailed Calculations

1) Bracing Members for Element #5 in DRAIN-2DX)

Control Information

One Line	nmbt(I)
	1

Property Types

1st Line	itt(I)	Area(R)	RI(R)	Effek(R)	Plamom(R)	Yiestr(R)	E0(R)	Harden(R)
	1	3.68	1061.82	1.0	2008.76	35.0	20000.0	0.0
2nd Line	Theta0(R)							
	0.0							
3rd Line	isec(I)	itemax(I)	tol(R)	styp(R)				
	31	100	0.00001	0.00001				
4th Line	Beta(R)	E1(R)	E2(R)	E3(R)	E4(R)			
	1.2	0.05	0.9	1.25	-0.25			
5th Line	P12(R)	a1(R)	b1(R)	c1(R)	a2(R)	b2(R)	c2(R)	
	0.5	1.0	0.0	-1.33	1.33	-1.33	0	
6th Line	Ratet(R)	Ratec(R)						
	1.0	1.0						

2) Design Iterations

R=2

KL/r=50	V(kN)	Pbr(kN)	Tn(sec.)
1st	368.23	205.84	0.49
2nd	269.30	150.54	0.58
3rd	240.66	134.53	0.61
4th	232.71	130.09	0.62
5th	230.20	128.68	0.62

θ = 0.46364761

Figure D.4 Outcomes of Calculations for R=2 and KL/r=50

Outcomes of Calculations Below

T/C, R=2	Pbr =	169.54	(kN)	Fy =	35.0	(kN/cm^2)								
	E =	20000.0	(kN/cm^2)	L =	849.7	(cm)								
	B(cm)	D(cm)	t(cm)	B-2t(cm)	A(cm^2)	Areq'd(cm^2)	I_y(cm^4)	$I_{y,req'd}$(cm^4)	r_y(cm)	$r_{y,req'd}$(cm)	Z_y(cm^3)	L/r	Py	Pcr
L/r=100	20.9	20.9	0.10	20.7	8.5887	8.5887	620.11	620.11	8.50	8.50	67.04	100	300.61	169.54

Detailed Calculations

1) Bracing Members for Element #5 in DRAIN-2DX)

Control Information

One Line	nmbt(I)
	1

Property Types

1st Line	itt(I)	Area(R)	RI(R)	Effek(R)	Plamom(R)	Yiestr(R)	E0(R)	Harden(R)
	1	8.59	620.11	1.0	2346.24	35.0	20000.0	0.0
2nd Line	Theta0(R)							
	0.0							
3rd Line	isec(I)	itemax(I)	tol(R)	styp(R)				
	31	100	0.00001	0.00001				
4th Line	Beta(R)	E1(R)	E2(R)	E3(R)	E4(R)			
	1.2	0.05	0.9	1.25	-0.25			
5th Line	P12(R)	a1(R)	b1(R)	c1(R)	a2(R)	b2(R)	c2(R)	
	0.5	1.0	0.0	-1.33	1.33	-1.33	0	
6th Line	Ratet(R)	Ratec(R)						
	1.0	1.0						

2) Design Iterations

R=2

KL/r=100	V(kN)	Pbr(kN)	Tn(sec.)
1st	368.23	205.84	0.37
2nd	324.76	181.54	0.39
3rd	308.31	172.35	0.40
4th	303.27	169.54	0.41

θ = 0.46364761

Figure D.5 Outcomes of Calculations for R=2 and KL/r=100

Outcomes of Calculations Below

T/C, R=2	Pbr =	205.84	(kN)	Fy =	35.0	(kN/cm^2)								
	E =	20000.0	(kN/cm^2)	L =	849.7	(cm)								
	B(cm)	D(cm)	t(cm)	B-2t(cm)	A(cm^2)	Areq'd(cm^2)	I_y(cm^4)	$I_{y,req'd}$(cm^4)	r_y(cm)	$r_{y,req'd}$(cm)	Z_y(cm^3)	L/r	Py	Pcr
L/r=150	14.3	14.3	0.42	13.4	23.4634	23.4634	752.91	752.91	5.66	5.66	122.07	150	821.22	205.84

Detailed Calculations

1) Bracing Members for Element #5 in DRAIN-2DX)

Control Information

One Line	nmbt(I)
	1

Property Types

1st Line	itt(I)	Area(R)	RI(R)	Effek(R)	Plamom(R)	Yiestr(R)	E0(R)	Harden(R)
	1	23.46	752.91	1.0	4272.44	35.0	20000.0	0.0
2nd Line	Theta0(R)							
	0.0							
3rd Line	isec(I)	itemax(I)	tol(R)	styp(R)				
	31	100	0.00001	0.00001				
4th Line	Beta(R)	E1(R)	E2(R)	E3(R)	E4(R)			
	1.2	0.05	0.9	1.25	-0.25			
5th Line	P12(R)	a1(R)	b1(R)	c1(R)	a2(R)	b2(R)	c2(R)	
	0.5	1.0	0.0	-1.33	1.33	-1.33	0	
6th Line	Ratet(R)	Ratec(R)						
	1.0	1.0						

2) Design Iterations

R=2	KL/r=150	V(kN)	Pbr(kN)	Tn(sec.)	θ =	0.46364761
	1st	368.23	205.84	0.25	< 0.3	

Figure D.6 Outcomes of Calculations for R=2 and KL/r=150

Outcomes of Calculations Below

T/C, R=4	Pbr =	45.29	(kN)	Fy =	35.0	(kN/cm^2)								
	E =	20000.0	(kN/cm^2)	L =	849.7	(cm)								
	B(cm)	D(cm)	t(cm)	B-2t(cm)	A(cm^2)	Areq'd(cm^2)	I_y(cm^4)	$I_{y,req'd}$(cm^4)	r_y(cm)	$r_{y,req'd}$(cm)	Z_y(cm^3)	L/r	Py	Pcr
L/r=50	41.6	41.6	0.01	41.6	1.2939	1.2939	373.67	373.67	16.99	16.99	20.20	50	45.29	102.16

Detailed Calculations

1) Bracing Members for Element #5 in DRAIN-2DX)

Control Information

One Line	nmbt(I)
	1

Property Types

1st Line	itt(I)	Area(R)	RI(R)	Effek(R)	Plamom(R)	Yiestr(R)	E0(R)	Harden(R)
	1	1.29	373.67	1.0	706.92	35.0	20000.0	0.0
2nd Line	Theta0(R)							
	0.0							
3rd Line	isec(I)	itemax(I)	tol(R)	styp(R)				
	31	100	0.00001	0.00001				
4th Line	Beta(R)	E1(R)	E2(R)	E3(R)	E4(R)			
	1.2	0.05	0.9	1.25	-0.25			
5th Line	P12(R)	a1(R)	b1(R)	c1(R)	a2(R)	b2(R)	c2(R)	
	0.5	1.0	0.0	-1.33	1.33	-1.33	0	
6th Line	Ratet(R)	Ratec(R)						
	1.0	1.0						

2) Design Iterations

R=4

KL/r=50	V(kN)	Pbr(kN)	Tn(sec.)
1st	184.11	102.92	0.70
2nd	106.15	59.34	0.92
3rd	88.47	49.46	1.01
4th	83.13	46.47	1.04
5th	81.53	45.58	1.05
6th	81.01	45.29	1.05

θ = 0.46364761

Figure D.7 Outcomes of Calculations for R=4 and KL/r=50

Outcomes of Calculations Below

T/C, R=4	Pbr =	60.50	(kN)	Fy =	35.0	(kN/cm^2)								
	E =	20000.0	(kN/cm^2)	L =	849.7	(cm)								
	B(cm)	D(cm)	t(cm)	B-2t(cm)	A(cm^2)	Areq'd(cm^2)	I_y(cm^4)	$I_{y,req'd}$(cm^4)	r_y(cm)	$r_{y,req'd}$(cm)	Z_x(cm^3)	L/r	Py	Pcr
L/r=100	20.9	20.9	0.04	20.8	3.0649	3.0649	221.29	221.29	8.50	8.50	23.92	100	107.27	60.50

Detailed Calculations

1) Bracing Members for Element #5 in DRAIN-2DX)

Control Information

One Line	nmbt(I)
	1

Property Types

1st Line	itt(I)	Area(R)	RI(R)	Effek(R)	Plamom(R)	Yiestr(R)	E0(R)	Harden(R)
	1	3.06	221.29	1.0	837.26	35.0	20000.0	0.0
2nd Line	Theta0(R)							
	0.0							
3rd Line	isec(I)	itemax(I)	tol(R)	styp(R)				
	31	100	0.00001	0.00001				
4th Line	Beta(R)	E1(R)	E2(R)	E3(R)	E4(R)			
	1.2	0.05	0.9	1.25	-0.25			
5th Line	P12(R)	a1(R)	b1(R)	c1(R)	a2(R)	b2(R)	c2(R)	
	0.5	1.0	0.0	-1.33	1.33	-1.33	0	
6th Line	Ratet(R)	Ratec(R)						
	1.0	1.0						

2) Design Iterations

R=4

KL/r=100	V(kN)	Pbr(kN)	Tn(sec.)
1st	184.11	102.92	0.52
2nd	129.42	72.35	0.62
3rd	115.10	64.34	0.66
4th	110.40	61.71	0.68
5th	108.22	60.50	0.68

θ = 0.46364761

Figure D.8 Outcomes of Calculations for R=4 and KL/r=100

Outcomes of Calculations Below

T/C, R=4	Pbr =	90.77	(kN)	Fy =	35.0	(kN/cm^2)								
	E =	20000.0	(kN/cm^2)	L =	849.7	(cm)								
	B(cm)	D(cm)	t(cm)	B-2t(cm)	A(cm^2)	Areq'd(cm^2)	I_y(cm^4)	$I_{y,req'd}$(cm^4)	r_y(cm)	$r_{y,req'd}$(cm)	Z_y(cm^3)	L/r	Py	Pcr
L/r=150	14.1	14.1	0.19	13.7	10.3467	10.3467	332.02	332.02	5.66	5.66	53.84	150	362.14	90.77

Detailed Calculations

1) Bracing Members for Element #5 in DRAIN-2DX)

Control Information

One Line	nmbt(I)
	1

Property Types

1st Line	itt(I)	Area(R)	RI(R)	Effek(R)	Plamom(R)	Yiestr(R)	E0(R)	Harden(R)
	1	10.35	332.02	1.0	1884.27	35.0	20000.0	0.0
2nd Line	Theta0(R)							
	0.0							
3rd Line	isec(I)	itemax(I)	tol(R)	styp(R)				
	31	100	0.00001	0.00001				
4th Line	Beta(R)	E1(R)	E2(R)	E3(R)	E4(R)			
	1.2	0.05	0.9	1.25	-0.25			
5th Line	P12(R)	a1(R)	b1(R)	c1(R)	a2(R)	b2(R)	c2(R)	
	0.5	1.0	0.0	-1.33	1.33	-1.33	0	
6th Line	Ratet(R)	Ratec(R)						
	1.0	1.0						

2) Design Iterations

R=4

KL/r=150	V(kN)	Pbr(kN)	Tn(sec.)
1st	184.11	102.92	0.35
2nd	168.51	94.20	0.37
3rd	162.38	90.77	0.37

θ = 0.46364761

Figure D.9 Outcomes of Calculations for R=4 and KL/r=150

Outcomes of Calculations Below

T/C, R=6	Pbr =	24.69	(kN)	Fy =	35.0	(kN/cm^2)								
	E =	20000.0	(kN/cm^2)	L =	849.7	(cm)								
	B(cm)	D(cm)	t(cm)	B-2t(cm)	A(cm^2)	Areq'd(cm^2)	I_y(cm^4)	$I_{y,req'd}$(cm^4)	r_y(cm)	$r_{y,req'd}$(cm)	Z_y(cm^3)	L/r	Py	Pcr
L/r=50	41.6	41.6	0.00	41.6	0.7053	0.7053	203.70	203.70	16.99	16.99	11.01	50	24.69	55.69

Detailed Calculations

1) Bracing Members for Element #5 in DRAIN-2DX)

Control Information

One Line	nmbt(I)
	1

Property Types

1st Line	itt(I)	Area(R)	RI(R)	Effek(R)	Plamom(R)	Yiestr(R)	E0(R)	Harden(R)
	1	0.71	203.70	1.0	385.37	35.0	20000.0	0.0
2nd Line	Theta0(R)							
	0.0							
3rd Line	isec(I)	itemax(I)	tol(R)	styp(R)				
	31	100	0.00001	0.00001				
4th Line	Beta(R)	E1(R)	E2(R)	E3(R)	E4(R)			
	1.2	0.05	0.9	1.25	-0.25			
5th Line	P12(R)	a1(R)	b1(R)	c1(R)	a2(R)	b2(R)	c2(R)	
	0.5	1.0	0.0	-1.33	1.33	-1.33	0	
6th Line	Ratet(R)	Ratec(R)						
	1.0	1.0						

2) Design Iterations

R=6

KL/r=50	V(kN)	Pbr(kN)	Tn(sec.)
1st	122.74	68.61	0.85
2nd	62.18	34.76	1.20
3rd	49.41	27.62	1.35
4th	45.68	25.53	1.40
5th	44.58	24.92	1.42
6th	44.16	24.69	1.42

θ = 0.46364761

Figure D.10 Outcomes of Calculations for R=6 and KL/r=50

Outcomes of Calculations Below

T/C, R=6	Pbr =	32.73	(kN)	Fy =	35.0	(kN/cm^2)								
	E =	20000.0	(kN/cm^2)	L =	849.7	(cm)								
	B(cm)	D(cm)	t(cm)	B-2t(cm)	A(cm^2)	Areq'd(cm^2)	I_y(cm^4)	$I_{y,req'd}$(cm^4)	r_y(cm)	$r_{y,req'd}$(cm)	Z_x(cm^3)	L/r	Py	Pcr
L/r=100	20.8	20.8	0.02	20.8	1.6583	1.6583	119.73	119.73	8.50	8.50	12.94	100	58.04	32.73

Detailed Calculations

1) Bracing Members for Element #5 in DRAIN-2DX)

Control Information

One Line	nmbt(I)
	1

Property Types

1st Line	itt(I)	Area(R)	RI(R)	Effek(R)	Plamom(R)	Yiestr(R)	E0(R)	Harden(R)
	1	1.66	119.73	1.0	453.02	35.0	20000.0	0.0
2nd Line	Theta0(R)							
	0.0							
3rd Line	isec(I)	itemax(I)	tol(R)	styp(R)				
	31	100	0.00001	0.00001				
4th Line	Beta(R)	E1(R)	E2(R)	E3(R)	E4(R)			
	1.2	0.05	0.9	1.25	-0.25			
5th Line	P12(R)	a1(R)	b1(R)	c1(R)	a2(R)	b2(R)	c2(R)	
	0.5	1.0	0.0	-1.33	1.33	-1.33	0	
6th Line	Ratet(R)	Ratec(R)						
	1.0	1.0						

2) Design Iterations

R=6

KL/r=100	V(kN)	Pbr(kN)	Tn(sec.)
1st	122.74	68.61	0.64
2nd	75.12	42.00	0.82
3rd	63.68	35.60	0.89
4th	60.30	33.71	0.91
5th	59.41	33.21	0.92
6th	58.98	32.97	0.93
7th	58.56	32.73	0.93

θ = 0.46364761

Figure D.11 Outcomes of Calculations for R=6 and KL/r=100

Outcomes of Calculations Below

T/C, R=6	Pbr =	49.51	(kN)	Fy =	35.0	(kN/cm^2)								
	E =	20000.0	(kN/cm^2)	L =	849.7	(cm)								
	B(cm)	D(cm)	t(cm)	B-2t(cm)	A(cm^2)	Areq'd(cm^2)	I_y(cm^4)	$I_{y,req'd}$(cm^4)	r_y(cm)	$r_{y,req'd}$(cm)	Z_y(cm^3)	L/r	Py	Pcr
L/r=150	14.0	14.0	0.10	13.8	5.6433	5.6433	181.09	181.09	5.66	5.66	29.36	150	197.52	49.51

Detailed Calculations

1) Bracing Members for Element #5 in DRAIN-2DX)

Control Information

One Line	nmbt(I)
	1

Property Types

1st Line	itt(I)	Area(R)	RI(R)	Effek(R)	Plamom(R)	Yiestr(R)	E0(R)	Harden(R)
	1	5.64	181.09	1.0	1027.74	35.0	20000.0	0.0
2nd Line	Theta0(R)							
	0.0							
3rd Line	isec(I)	itemax(I)	tol(R)	styp(R)				
	31	100	0.00001	0.00001				
4th Line	Beta(R)	E1(R)	E2(R)	E3(R)	E4(R)			
	1.2	0.05	0.9	1.25	-0.25			
5th Line	P12(R)	a1(R)	b1(R)	c1(R)	a2(R)	b2(R)	c2(R)	
	0.5	1.0	0.0	-1.33	1.33	-1.33	0	
6th Line	Ratet(R)	Ratec(R)						
	1.0	1.0						

2) Design Iterations

R=6

KL/r=150	V(kN)	Pbr(kN)	Tn(sec.)
1st	122.74	68.61	0.43
2nd	97.93	54.75	0.48
3rd	91.01	50.87	0.50
4th	88.56	49.51	0.50

θ = 0.46364761

Figure D.12 Outcomes of Calculations for R=6 and KL/r=150

Outcomes of Calculations Below

T/C, R=8	Pbr =	16.05	(kN)	Fy =	35.0	(kN/cm^2)								
	E =	20000.0	(kN/cm^2)	L =	849.7	(cm)								
	B(cm)	D(cm)	t(cm)	B-2t(cm)	A(cm^2)	Areq'd(cm^2)	I_y(cm^4)	$I_{y,req'd}$(cm^4)	r_y(cm)	$r_{y,req'd}$(cm)	Z_y(cm^3)	L/r	Py	Pcr
L/r=50	41.6	41.6	0.00	41.6	0.4585	0.4585	132.41	132.41	16.99	16.99	7.16	50	16.05	36.20

Detailed Calculations

1) Bracing Members for Element #5 in DRAIN-2DX)

Control Information

One Line	nmbt(I)
	1

Property Types

1st Line	itt(I)	Area(R)	RI(R)	Effek(R)	Plamom(R)	Yiestr(R)	E0(R)	Harden(R)
	1	0.46	132.41	1.0	250.50	35.0	20000.0	0.0
2nd Line	Theta0(R)							
	0.0							
3rd Line	isec(I)	itemax(I)	tol(R)	styp(R)				
	31	100	0.00001	0.00001				
4th Line	Beta(R)	E1(R)	E2(R)	E3(R)	E4(R)			
	1.2	0.05	0.9	1.25	-0.25			
5th Line	P12(R)	a1(R)	b1(R)	c1(R)	a2(R)	b2(R)	c2(R)	
	0.5	1.0	0.0	-1.33	1.33	-1.33	0	
6th Line	Ratet(R)	Ratec(R)						
	1.0	1.0						

2) Design Iterations

R=8

KL/r=50	V(kN)	Pbr(kN)	Tn(sec.)
1st	92.06	51.46	0.99
2nd	42.13	23.55	1.46
3rd	32.51	18.18	1.66
4th	29.85	16.68	1.73
5th	29.04	16.23	1.76
6th	28.70	16.05	1.76

θ = 0.46364761

Figure D.13 Outcomes of Calculations for R=8 and KL/r=50

Outcomes of Calculations Below

T/C, R=8	Pbr =	21.31	(kN)	Fy =	35.0	(kN/cm^2)								
	E =	20000.0	(kN/cm^2)	L =	849.7	(cm)								
	B(cm)	D(cm)	t(cm)	B-2t(cm)	A(cm^2)	Areq'd(cm^2)	I_y(cm^4)	$I_{y,req'd}$(cm^4)	r_y(cm)	$r_{y,req'd}$(cm)	Z_y(cm^3)	L/r	Py	Pcr
L/r=100	20.8	20.8	0.01	20.8	1.0796	1.0796	77.95	77.95	8.50	8.50	8.43	100	37.79	21.31

Detailed Calculations

1) Bracing Members for Element #5 in DRAIN-2DX)

Control Information

One Line	nmbt(I)
	1

Property Types

1st Line	itt(I)	Area(R)	RI(R)	Effek(R)	Plamom(R)	Yiestr(R)	E0(R)	Harden(R)
	1	1.08	77.95	1.0	294.92	35.0	20000.0	0.0
2nd Line	Theta0(R)							
	0.0							
3rd Line	isec(I)	itemax(I)	tol(R)	styp(R)				
	31	100	0.00001	0.00001				
4th Line	Beta(R)	E1(R)	E2(R)	E3(R)	E4(R)			
	1.2	0.05	0.9	1.25	-0.25			
5th Line	P12(R)	a1(R)	b1(R)	c1(R)	a2(R)	b2(R)	c2(R)	
	0.5	1.0	0.0	-1.33	1.33	-1.33	0	
6th Line	Ratet(R)	Ratec(R)						
	1.0	1.0						

2) Design Iterations

R=8

KL/r=100	V(kN)	Pbr(kN)	Tn(sec.)
1st	92.06	51.46	0.74
2nd	51.15	28.59	0.99
3rd	42.13	23.55	1.10
4th	39.27	21.95	1.14
5th	38.34	21.43	1.15
6th	38.12	21.31	1.15

θ = 0.46364761

Figure D.14 Outcomes of Calculations for R=8 and KL/r=100

Outcomes of Calculations Below

T/C,	Pbr =	32.17	(kN)	Fy =	35.0	(kN/cm^2)								
R=8	E =	20000.0	(kN/cm^2)	L =	849.7	(cm)								
	B(cm)	D(cm)	t(cm)	B-2t(cm)	A(cm^2)	Areq'd(cm^2)	I_x(cm^4)	$I_{y,req'd}$(cm^4)	r_y(cm)	$r_{y,req'd}$(cm)	Z_x(cm^3)	L/r	Py	Pcr
L/r=150	13.9	13.9	0.07	13.8	3.6670	3.6670	117.67	117.67	5.66	5.66	19.08	150	128.35	32.17

Detailed Calculations

1) Bracing Members for Element #5 in DRAIN-2DX)

Control Information

One Line	nmbt(I)
	1

Property Types

1st Line	itt(I)	Area(R)	RI(R)	Effek(R)	Plamom(R)	Yiestr(R)	E0(R)	Harden(R)
	1	3.67	117.67	1.0	667.83	35.0	20000.0	0.0
2nd Line	Theta0(R)							
	0.0							
3rd Line	isec(I)	itemax(I)	tol(R)	styp(R)				
	31	100	0.00001	0.00001				
4th Line	Beta(R)	E1(R)	E2(R)	E3(R)	E4(R)			
	1.2	0.05	0.9	1.25	-0.25			
5th Line	P12(R)	a1(R)	b1(R)	c1(R)	a2(R)	b2(R)	c2(R)	
	0.5	1.0	0.0	-1.33	1.33	-1.33	0	
6th Line	Ratet(R)	Ratec(R)						
	1.0	1.0						

2) Design Iterations

R=8

KL/r=150	V(kN)	Pbr(kN)	Tn(sec.)
1st	92.06	51.46	0.49
2nd	67.32	37.63	0.58
3rd	60.17	33.63	0.61
4th	58.18	32.52	0.62
5th	57.55	32.17	0.62

$\theta =$ 0.46364761

Figure D.15 Outcomes of Calculations for R=8 and KL/r=150

APPENDIX E

Ductile Design Procedures

Outcomes of Calculations Below

Detailed Calculations

1) Strength Design

T/C,	Pbr =	411.69	(kN)	Fy =	35.0	(kN/cm^2)			
R=1	E =	20000.0	(kN/cm^2)	L =	849.7	(cm)			
	B(cm)	D(cm)	t(cm)	B-2t(cm)	(B-2t)/t	A(cm^2)	I_y(cm^4)	r_y(cm)	Z_y(cm^3)
	17.780	17.780	0.635	16.510	26.0	42.516	2056.18	6.96	270.39
Try	7	7	0.25	6.5	26.0	6.59	49.40	2.74	16.50
Pbr =	92.51	(kips)							
KL =	27.9	(ft)							
LRFD p. #3-41									

Checking KL/r and b/t

KL/r =	122.0912	>	KL/r,limit =	101.0	(720/sqrt(Fy)), in ksi	N.G.
b/t =	26.0	>	b/t,limit =	15.4	(110/sqrt(Fy)), in ksi	N.G.

2) Ductile Design (lightest section satisfying criteria shown below)

	B(cm)	D(cm)	t(cm)	B-2t(cm)	(B-2t)/t	A(cm^2)	I_y(cm^4)	r_y(cm)	Z_y(cm^3)
	25.400	25.400	1.588	22.225	14.0	144.516	13361.03	9.60	1271.64
Try	10	10	0.625	8.750	14.0	22.40	321.00	3.78	77.60
r >=	3.31	(in)							
t >=	0.574	(in)							
LRFD p. #3-40									

Checking KL/r and b/t

KL/r =	88.49998	<	KL/r,limit =	101.0	(720/sqrt(Fy)), in ksi	O.K.
b/t =	14.0	<	b/t,limit =	15.4	(720/sqrt(Fy)), in ksi	O.K.

Figure E.1 Outcomes of Calculations for R=1

Outcomes of Calculations Below

Detailed Calculations

1) Strength Design

T/C, R=2	Pbr =	205.84	(kN)	Fy =	35.0	(kN/cm^2)			
	E =	20000.0	(kN/cm^2)	L =	849.7	(cm)			
	B(cm)	D(cm)	t(cm)	B-2t(cm)	(B-2t)/t	A(cm^2)	I_x(cm^4)	r_x(cm)	Z_x(cm^3)
	15.240	15.240	0.635	13.970	22.0	36.064	1261.18	5.92	195.01
Try	6	6	0.25	5.5	22.0	5.59	30.30	2.33	11.90
Pbr =	46.26	(kips)							
KL =	27.9	(ft)							
LRFD p. #3-41									

Checking KL/r and b/t

KL/r =	143.5751	>	KL/r,limit =	101.0	(720/sqrt(Fy)), in ksi	N.G.
b/t =	22.0	>	b/t,limit =	15.4	(720/sqrt(Fy)), in ksi	N.G.

2) Ductile Design (lightest section satisfying criteria shown below)

	B(cm)	D(cm)	t(cm)	B-2t(cm)	(B-2t)/t	A(cm^2)	I_x(cm^4)	r_x(cm)	Z_x(cm^3)
	25.400	25.400	1.588	22.225	14.0	144.516	13361.03	9.60	1271.64
Try	10	10	0.625	8.750	14.0	22.40	321.00	3.78	77.60
r >=	3.31	(in)							
t >=	0.574	(in)							
LRFD p. #3-40									

Checking KL/r and b/t

KL/r =	88.49998	<	KL/r,limit =	101.0	(720/sqrt(Fy)), in ksi	O.K.
b/t =	14.0	<	b/t,limit =	15.4	(720/sqrt(Fy)), in ksi	O.K.

Figure E.2 Outcomes of Calculations for R=2

Outcomes of Calculations Below

Detailed Calculations

1) Strength Design

T/C,	Pbr =	102.92	(kN)	Fy =	35.0	(kN/cm^2)			
R=4	E =	20000.0	(kN/cm^2)	L =	849.7	(cm)			
	B(cm)	D(cm)	t(cm)	B-2t(cm)	(B-2t)/t	A(cm^2)	I_x(cm^4)	r_x(cm)	Z_x(cm^3)
	12.700	12.700	0.476	11.748	24.7	22.710	557.75	4.95	103.07
Try	5	5	0.1875	4.6	24.7	3.52	13.40	1.95	6.29
Pbr =	23.13	(kips)							
KL =	27.9	(ft)							
LRFD p. #3-41									

Checking KL/r and b/t

KL/r =	171.5538	>	KL/r,limit =	101.0	(720/sqrt(Fy)), in ksi	N.G.
b/t =	24.7	>	b/t,limit =	15.4	(720/sqrt(Fy)), in ksi	N.G.

2) Ductile Design (lightest section satisfying criteria shown below)

	B(cm)	D(cm)	t(cm)	B-2t(cm)	(B-2t)/t	A(cm^2)	I_x(cm^4)	r_x(cm)	Z_x(cm^3)
	25.400	25.400	1.588	22.225	14.0	144.516	13361.03	9.60	1271.64
Try	10	10	0.625	8.750	14.0	22.40	321.00	3.78	77.60
r >=	3.31	(in)							
t >=	0.574	(in)							
LRFD p. #3-40									

Checking KL/r and b/t

KL/r =	88.49998	<	KL/r,limit =	101.0	(720/sqrt(Fy)), in ksi	O.K.
b/t =	14.0	<	b/t,limit =	15.4	(720/sqrt(Fy)), in ksi	O.K.

Figure E.3 Outcomes of Calculations for R=4

Outcomes of Calculations Below

Detailed Calculations

1) Strength Design

T/C, R=6	Pbr =	68.61	(kN)	Fy =	35.0	(kN/cm^2)			
	E =	20000.0	(kN/cm^2)	L =	849.7	(cm)			
	B(cm)	D(cm)	t(cm)	B-2t(cm)	(B-2t)/t	A(cm^2)	I_x(cm^4)	r_x(cm)	Z_x(cm^3)
	12.700	12.700	0.318	12.065	38.0	15.484	391.67	5.03	71.45
Try	5	5	0.125	4.8	38.0	2.40	9.41	1.98	4.36
Pbr =	15.42	(kips)							
KL =	27.9	(ft)							
LRFD p. #3-41									

Checking KL/r and b/t

KL/r =	168.9545	>	KL/r,limit =	101.0	(720/sqrt(Fy)), in ksi	N.G.
b/t =	38.0	>	b/t,limit =	15.4	(720/sqrt(Fy)), in ksi	N.G.

2) Ductile Design (lightest section satisfying criteria shown below)

	B(cm)	D(cm)	t(cm)	B-2t(cm)	(B-2t)/t	A(cm^2)	I_x(cm^4)	r_x(cm)	Z_x(cm^3)
	25.400	25.400	1.588	22.225	14.0	144.516	13361.03	9.60	1271.64
Try	10	10	0.625	8.750	14.0	22.40	321.00	3.78	77.60
r >=	3.31	(in)							
t >=	0.574	(in)							
LRFD p. #"3-40									

Checking KL/r and b/t

KL/r =	88.49998	<	KL/r,limit =	101.0	(720/sqrt(Fy)), in ksi	O.K.
b/t =	14.0	<	b/t,limit =	15.4	(720/sqrt(Fy)), in ksi	O.K.

Figure E.4 Outcomes of Calculations for R=6

Outcomes of Calculations Below

Detailed Calculations

1) Strength Design

T/C, R=8	Pbr =	51.46	(kN)	Fy =	35.0	(kN/cm^2)			
	E =	20000.0	(kN/cm^2)	L =	849.7	(cm)			
	B(cm)	D(cm)	t(cm)	B-2t(cm)	(B-2t)/t	A(cm^2)	I_x(cm^4)	r_x(cm)	Z_x(cm^3)
	11.430	11.430	0.318	10.795	34.0	13.871	282.20	4.52	57.35
Try	4.5	4.5	0.125	4.3	34.0	2.15	6.78	1.78	3.50
Pbr =	11.56	(kips)							
KL =	27.9	(ft)							
LRFD p. #3-41									

Checking KL/r and b/t

KL/r =	187.9382	>	KL/r,limit =	101.0	(720/sqrt(Fy)), in ksi	N.G.
b/t =	34.0	>	b/t,limit =	15.4	(720/sqrt(Fy)), in ksi	N.G.

2) Ductile Design (lightest section satisfying criteria shown below)

	B(cm)	D(cm)	t(cm)	B-2t(cm)	(B-2t)/t	A(cm^2)	I_x(cm^4)	r_x(cm)	Z_x(cm^3)
	25.400	25.400	1.588	22.225	14.0	144.516	13361.03	9.60	1271.64
Try	10	10	0.625	8.750	14.0	22.40	321.00	3.78	77.60
r >=	3.31	(in)							
t >=	0.574	(in)							
LRFD p. #3-40									

Checking KL/r and b/t

KL/r =	88.49998	<	KL/r,limit =	101.0	(720/sqrt(Fy)), in ksi	O.K.
b/t =	14.0	<	b/t,limit =	15.4	(720/sqrt(Fy)), in ksi	O.K.

Figure E.5 Outcomes of Calculations for R=8

APPENDIX F

Case Study 1

(Effects of KL/r on R and b/t ratios)

Outcomes of Calculations Below

T/C, R=1	Pbr =	363.09	(kN)	Fy =	35.0	(kN/cm^2)								
	E =	20000.0	(kN/cm^2)	L =	849.7	(cm)								
	B(cm)	D(cm)	t(cm)	B-2t(cm)	A(cm^2)	Areq'd(cm^2)	I_y(cm^4)	$I_{y,req'd}$(cm^4)	r_y(cm)	$r_{y,req'd}$(cm)	Z_y(cm^3)	L/r	Py	Pcr
L/r=50	41.7	41.7	0.06	41.6	10.3739	10.3739	2995.99	2995.99	16.99	16.99	161.94	50	363.09	819.09

Detailed Calculations

1) Bracing Members for Element #5 in DRAIN-2DX)

Control Information

One Line	nmbt(I)
	1

Property Types

1st Line	itt(I)	Area(R)	RI(R)	Effek(R)	Plamom(R)	Yiestr(R)	E0(R)	Harden(R)
	1	10.37	2995.99	1.0	5667.83	35.0	20000.0	0.0
2nd Line	Theta0(R)							
	0.0							
3rd Line	isec(I)	itemax(I)	tol(R)	styp(R)				
	31	100	0.00001	0.00001				
4th Line	Beta(R)	E1(R)	E2(R)	E3(R)	E4(R)			
	1.2	0.05	0.9	1.25	-0.25			
5th Line	P12(R)	a1(R)	b1(R)	c1(R)	a2(R)	b2(R)	c2(R)	
	0.5	1.0	0.0	-1.33	1.33	-1.33	0	
6th Line	Ratet(R)	Ratec(R)						
	1.0	1.0						

2) Design Iterations

R=1

KL/r=50	V(kN)	Pbr(kN)	Tn(sec.)
1st	736.45	411.69	0.35
2nd	674.02	376.79	0.36
3rd	661.48	369.78	0.37
4th	649.51	363.09	0.37

θ = 0.46364761

R= 1

Figure F.1 Outcomes of Calculations for R=1 and KL/r=50

Outcomes of Calculations Below

T/C, R=1	Pbr = / E =	363.09 / 20000.0	(kN) / (kN/cm^2)	Fy = / L =	35.0 / 849.7	(kN/cm^2) / (cm)							
	B(cm)	D(cm)	t(cm)	B-2t(cm)	A(cm^2)	I_y(cm^4)	$I_{y,reqd}$(cm^4)	r_y(cm)	$r_{y,reqd}$(cm	Z_y(cm^3)	L/r	Py	Pcr
L/r=100	20.9	20.9	0.12	20.7	10.3739	749.00	749.00	8.50	8.50	80.97	100	363.09	204.77

Detailed Calculations

1) Bracing Members for Element #5 in DRAIN-2DX)

Control Information

One Line	nmbt(I)
	1

Property Types

1st Line	itt(I)	Area(R)	RI(R)	Effek(R)	Plamom(R)	Yiestr(R)	E0(R)	Harden(R)
	1	10.37	749.00	1.0	2833.89	35.0	20000.0	0.0
2nd Line	Theta0(R)							
	0.0							
3rd Line	isec(I)	itemax(I)	tol(R)	styp(R)				
	31	100	0.00001	0.00001				
4th Line	Beta(R)	E1(R)	E2(R)	E3(R)	E4(R)			
	1.2	0.05	0.9	1.25	-0.25			
5th Line	P12(R)	a1(R)	b1(R)	c1(R)	a2(R)	b2(R)	c2(R)	
	0.5	1.0	0.0	-1.33	1.33	-1.33	0	
6th Line	Ratet(R)	Ratec(R)						
	1.0	1.0						

2) Design Iterations

R=1

KL/r=100	V(kN)	Pbr(kN)	Tn(sec.)
1st	736.45	411.69	0.35
2nd	674.02	376.79	0.36
3rd	661.48	369.78	0.37
4th	649.51	363.09	0.37
5th			
6th	366.31	204.77	0.37
7th	649.51		

θ = 0.46364761

R= 1.7731248

Figure F.2 Outcomes of Calculations for R=1 and KL/r=100

Outcomes of Calculations Below

T/C, R=1	Pbr =	363.09	(kN)	Fy =	35.0	(kN/cm^2)							
	E =	20000.0	(kN/cm^2)	L =	849.7	(cm)							
	B(cm)	D(cm)	t(cm)	B-2t(cm)	A(cm^2)	I_y(cm^4)	$I_{y,req'd}$(cm^4)	r_y(cm)	$r_{y,req'd}$(cm	Z_y(cm^3)	L/r	Py	Pcr
L/r=150	14.1	14.1	0.19	13.7	10.3739	332.89	332.89	5.66	5.66	53.98	150	363.09	91.01

Detailed Calculations

1) Bracing Members for Element #5 in DRAIN-2DX)

Control Information

One Line	nmbt(I)
	1

Property Types

1st Line	itt(I)	Area(R)	RI(R)	Effek(R)	Plamom(R)	Yiestr(R)	E0(R)	Harden(R)
	1	10.37	332.89	1.0	1889.21	35.0	20000.0	0.0
2nd Line	Theta0(R)							
	0.0							
3rd Line	isec(I)	itemax(I)	tol(R)	styp(R)				
	31	100	0.00001	0.00001				
4th Line	Beta(R)	E1(R)	E2(R)	E3(R)	E4(R)			
	1.2	0.05	0.9	1.25	-0.25			
5th Line	P12(R)	a1(R)	b1(R)	c1(R)	a2(R)	b2(R)	c2(R)	
	0.5	1.0	0.0	-1.33	1.33	-1.33	0	
6th Line	Ratet(R)	Ratec(R)						
	1.0	1.0						

2) Design Iterations

R=1

KL/r=150	V(kN)	Pbr(kN)	Tn(sec.)
1st	736.45	411.69	0.35
2nd	674.02	376.79	0.36
3rd	661.48	369.78	0.37
4th	649.51	363.09	0.37
5th			
6th	162.80	91.01	0.37
7th	649.51		

θ = 0.46364761

R= 3.98953087

Figure F.3 Outcomes of Calculations for R=1 and KL/r=150

Outcomes of Calculations Below

T/C, R=2	Pbr =	128.68	(kN)	Fy =	35.0	(kN/cm^2)								
	E =	20000.0	(kN/cm^2)	L =	849.7	(cm)								
	B(cm)	D(cm)	t(cm)	B-2t(cm)	A(cm^2)	Areq'd(cm^2)	I_x(cm^4)	$I_{y,req'd}$(cm^4)	r_x(cm)	$r_{y,req'd}$(cm)	Z_x(cm^3)	L/r	Py	Pcr
L/r=50	41.6	41.6	0.02	41.6	3.6767	3.6767	1061.82	1061.82	16.99	16.99	57.39	50	128.68	290.30

Detailed Calculations

1) Bracing Members for Element #5 in DRAIN-2DX)

Control Information

One Line	nmbt(I)
	1

Property Types

1st Line	itt(I)	Area(R)	RI(R)	Effek(R)	Plamom(R)	Yiestr(R)	E0(R)	Harden(R)
	1	3.68	1061.82	1.0	2008.76	35.0	20000.0	0.0
2nd Line	Theta0(R)							
	0.0							
3rd Line	isec(I)	itemax(I)	tol(R)	styp(R)				
	31	100	0.00001	0.00001				
4th Line	Beta(R)	E1(R)	E2(R)	E3(R)	E4(R)			
	1.2	0.05	0.9	1.25	-0.25			
5th Line	P12(R)	a1(R)	b1(R)	c1(R)	a2(R)	b2(R)	c2(R)	
	0.5	1.0	0.0	-1.33	1.33	-1.33	0	
6th Line	Ratet(R)	Ratec(R)						
	1.0	1.0						

2) Design Iterations

R=2

KL/r=50	V(kN)	Pbr(kN)	Tn(sec.)
1st	368.23	205.84	0.49
2nd	269.30	150.54	0.58
3rd	240.66	134.53	0.61
4th	232.71	130.09	0.62
5th	230.20	128.68	0.62

θ = 0.46364761

R= 2

Figure F.4 Outcomes of Calculations for R=2 and KL/r=50

Outcomes of Calculations Below

T/C, R=2	Pbr =	128.68	(kN)	Fy =	35.0	(kN/cm^2)							
	E =	20000.0	(kN/cm^2)	L =	849.7	(cm)							
	B(cm)	D(cm)	t(cm)	B-2t(cm)	A(cm^2)	I_y(cm^4)	$I_{y,req'd}$(cm^4)	r_y(cm)	$r_{y,req'd}$(cm)	Z_y(cm^3)	L/r	Py	Pcr
L/r=100	20.9	20.9	0.04	20.8	3.6767	265.46	265.46	8.50	8.50	28.70	100	128.68	72.58

Detailed Calculations

1) Bracing Members for Element #5 in DRAIN-2DX)

Control Information

One Line	nmbt(I)
	1

Property Types

1st Line	itt(I)	Area(R)	RI(R)	Effek(R)	Plamom(R)	Yiestr(R)	E0(R)	Harden(R)
	1	3.68	265.46	1.0	1004.39	35.0	20000.0	0.0
2nd Line	Theta0(R)							
	0.0							
3rd Line	isec(I)	itemax(I)	tol(R)	styp(R)				
	31	100	0.00001	0.00001				
4th Line	Beta(R)	E1(R)	E2(R)	E3(R)	E4(R)			
	1.2	0.05	0.9	1.25	-0.25			
5th Line	P12(R)	a1(R)	b1(R)	c1(R)	a2(R)	b2(R)	c2(R)	
	0.5	1.0	0.0	-1.33	1.33	-1.33	0	
6th Line	Ratet(R)	Ratec(R)						
	1.0	1.0						

2) Design Iterations

R=2

KL/r=100	V(kN)	Pbr(kN)	Tn(sec.)
1st	368.23	205.84	0.49
2nd	269.30	150.54	0.58
3rd	240.66	134.53	0.61
4th	232.71	130.09	0.62
5th	230.20	128.68	0.62
6th			
7th	145.15	72.58	0.62
8th	460.39		

θ = 0.46364761

R= 3.17181752

Figure F.5 Outcomes of Calculations for R=2 and KL/r=100

Outcomes of Calculations Below

T/C, R=2	Pbr =	128.68	(kN)	Fy =	35.0	(kN/cm^2)							
	E =	20000.0	(kN/cm^2)	L =	849.7	(cm)							
	B(cm)	D(cm)	t(cm)	B-2t(cm)	A(cm^2)	I_x(cm^4)	$I_{y,eqv}$(cm^4)	r_x(cm)	$r_{y,eqv}$(cm)	Z_x(cm^3)	L/r	Py	Pcr
L/r=150	13.9	13.9	0.07	13.8	3.6767	117.98	117.98	5.66	5.66	19.13	150	128.68	32.26

Detailed Calculations

1) Bracing Members for Element #5 in DRAIN-2DX)

Control Information

One Line	nmbt(I)
	1

Property Types

1st Line	itt(I)	Area(R)	RI(R)	Effek(R)	Plamom(R)	Yiestr(R)	E0(R)	Harden(R)
	1	3.68	117.98	1.0	669.59	35.0	20000.0	0.0
2nd Line	Theta0(R)							
	0.0							
3rd Line	isec(I)	itemax(I)	tol(R)	styp(R)				
	31	100	0.00001	0.00001				
4th Line	Beta(R)	E1(R)	E2(R)	E3(R)	E4(R)			
	1.2	0.05	0.9	1.25	-0.25			
5th Line	P12(R)	a1(R)	b1(R)	c1(R)	a2(R)	b2(R)	c2(R)	
	0.5	1.0	0.0	-1.33	1.33	-1.33	0	
6th Line	Ratet(R)	Ratec(R)						
	1.0	1.0						

2) Design Iterations

R=2

KL/r=150	V(kN)	Pbr(kN)	Tn(sec.)
1st	368.23	205.84	0.49
2nd	269.30	150.54	0.58
3rd	240.66	134.53	0.61
4th	232.71	130.09	0.62
5th	230.20	128.68	0.62
6th			
7th	64.51	32.26	0.62
8th	460.39		

θ = 0.46364761

R= 7.13658919

Figure F.6 Outcomes of Calculations for R=2 and KL/r=150

Outcomes of Calculations Below

T/C, R=4	Pbr =	45.29	(kN)	Fy =	35.0	(kN/cm^2)								
	E =	20000.0	(kN/cm^2)	L =	849.7	(cm)								
	B(cm)	D(cm)	t(cm)	B-2t(cm)	A(cm^2)	Areq'd(cm^2)	I_y(cm^4)	$I_{y,req'd}$(cm^4)	r_y(cm)	$r_{y,req'd}$(cm)	Z_y(cm^3)	L/r	Py	Pcr
L/r=50	41.6	41.6	0.01	41.6	1.2939	1.2939	373.67	373.67	16.99	16.99	20.20	50	45.29	102.16

Detailed Calculations

1) Bracing Members for Element #5 in DRAIN-2DX)

Control Information

One Line	nmbt(I)
	1

Property Types

1st Line	itt(I) 1	Area(R) 1.29	RI(R) 373.67	Effek(R) 1.0	Plamom(R) 706.92	Yiestr(R) 35.0	E0(R) 20000.0	Harden(R) 0.0
2nd Line	Theta0(R) 0.0							
3rd Line	isec(I) 31	itemax(I) 100	tol(R) 0.00001	styp(R) 0.00001				
4th Line	Beta(R) 1.2	E1(R) 0.05	E2(R) 0.9	E3(R) 1.25	E4(R) -0.25			
5th Line	P12(R) 0.5	a1(R) 1.0	b1(R) 0.0	c1(R) -1.33	a2(R) 1.33	b2(R) -1.33	c2(R) 0	
6th Line	Ratet(R) 1.0	Ratec(R) 1.0						

2) Design Iterations

R=4

KL/r=50	V(kN)	Pbr(kN)	Tn(sec.)
1st	184.11	102.92	0.70
2nd	106.15	59.34	0.92
3rd	88.47	49.46	1.01
4th	83.13	46.47	1.04
5th	81.53	45.58	1.05
6th	81.01	45.29	1.05

θ = 0.46364761

R= 4

Figure F.7 Outcomes of Calculations for R=4 and KL/r=50

Outcomes of Calculations Below

T/C, R=4	Pbr =	45.58	(kN)	Fy =	35.0	(kN/cm^2)							
	E =	20000.0	(kN/cm^2)	L =	849.7	(cm)							
	B(cm)	D(cm)	t(cm)	B-2t(cm)	A(cm^2)	I_y(cm^4)	$I_{y,req'd}$(cm^4)	r_y(cm)	$r_{y,req'd}$(cm)	Z_y(cm^3)	L/r	Py	Pcr
L/r=100	20.8	20.8	0.02	20.8	1.2939	93.42	93.42	8.50	8.50	10.10	100	45.29	25.54

Detailed Calculations

1) Bracing Members for Element #5 in DRAIN-2DX)

Control Information

One Line	nmbt(I)
	1

Property Types

1st Line	itt(I)	Area(R)	RI(R)	Effek(R)	Plamom(R)	Yiestr(R)	E0(R)	Harden(R)
	1	1.29	93.42	1.0	353.46	35.0	20000.0	0.0
2nd Line	Theta0(R)							
	0.0							
3rd Line	isec(I)	itemax(I)	tol(R)	styp(R)				
	31	100	0.00001	0.00001				
4th Line	Beta(R)	E1(R)	E2(R)	E3(R)	E4(R)			
	1.2	0.05	0.9	1.25	-0.25			
5th Line	P12(R)	a1(R)	b1(R)	c1(R)	a2(R)	b2(R)	c2(R)	
	0.5	1.0	0.0	-1.33	1.33	-1.33	0	
6th Line	Ratet(R)	Ratec(R)						
	1.0	1.0						

2) Design Iterations

R=4

KL/r=100	V(kN)	Pbr(kN)	Tn(sec.)
1st	184.11	102.92	0.70
2nd	106.15	59.34	0.92
3rd	88.47	49.46	1.01
4th	83.13	46.47	1.04
5th	81.53	45.58	1.05
6th	81.01	45.29	1.05
7th			
8th	51.08	25.54	1.05
9th	324.04		

θ = 0.46364761

R= 6.34357074

Figure F.8 Outcomes of Calculations for R=4 and KL/r=100

Outcomes of Calculations Below

T/C,	Pbr =	45.58	(kN)	Fy =	35.0	(kN/cm^2)							
R=4	E =	20000.0	(kN/cm^2)	L =	849.7	(cm)							
	B(cm)	D(cm)	t(cm)	B-2t(cm)	A(cm^2)	I_y(cm^4)	$I_{y,eqv}$(cm^4)	r_y(cm)	$r_{y,eqv}$(cm)	Z_y(cm^3)	L/r	Py	Pcr
L/r=150	13.9	13.9	0.02	13.9	1.2939	41.52	41.52	5.66	5.66	6.73	150	45.29	11.35

Detailed Calculations

1) Bracing Members for Element #5 in DRAIN-2DX)

Control Information

One Line	nmbt(I)
	1

Property Types

1st Line	itt(I)	Area(R)	RI(R)	Effek(R)	Plamom(R)	Yiestr(R)	E0(R)	Harden(R)
	1	1.29	41.52	1.0	235.64	35.0	20000.0	0.0
2nd Line	Theta0(R)							
	0.0							
3rd Line	isec(I)	itemax(I)	tol(R)	styp(R)				
	31	100	0.00001	0.00001				
4th Line	Beta(R)	E1(R)	E2(R)	E3(R)	E4(R)			
	1.2	0.05	0.9	1.25	-0.25			
5th Line	P12(R)	a1(R)	b1(R)	c1(R)	a2(R)	b2(R)	c2(R)	
	0.5	1.0	0.0	-1.33	1.33	-1.33	0	
6th Line	Ratet(R)	Ratec(R)						
	1.0	1.0						

2) Design Iterations

R=4

KL/r=150	V(kN)	Pbr(kN)	Tn(sec.)
1st	184.11	102.92	0.70
2nd	106.15	59.34	0.92
3rd	88.47	49.46	1.01
4th	83.13	46.47	1.04
5th	81.53	45.58	1.05
6th	81.01	45.29	1.05
7th			
8th	22.70	11.35	1.05
9th	324.04		

θ = 0.46364761

R= 14.2730336

Figure F.9 Outcomes of Calculations for R=4 and KL/r=150

Outcomes of Calculations Below

T/C, R=6	Pbr =	24.69	(kN)	Fy =	35.0	(kN/cm^2)								
	E =	20000.0	(kN/cm^2)	L =	849.7	(cm)								
	B(cm)	D(cm)	t(cm)	B-2t(cm)	A(cm^2)	Areq'd(cm^2)	I_y(cm^4)	$I_{y,req'd}$(cm^4)	r_y(cm)	$r_{y,req'd}$(cm)	Z_y(cm^3)	L/r	Py	Pcr
L/r=50	41.6	41.6	0.00	41.6	0.7053	0.7053	203.70	203.70	16.99	16.99	11.01	50	24.69	55.69

Detailed Calculations

1) Bracing Members for Element #5 in DRAIN-2DX)

Control Information

One Line	nmbt(I)
	1

Property Types

1st Line	itt(I)	Area(R)	RI(R)	Effek(R)	Plamom(R)	Yiestr(R)	E0(R)	Harden(R)
	1	0.71	203.70	1.0	385.37	35.0	20000.0	0.0
2nd Line	Theta0(R)							
	0.0							
3rd Line	isec(I)	itemax(I)	tol(R)	styp(R)				
	31	100	0.00001	0.00001				
4th Line	Beta(R)	E1(R)	E2(R)	E3(R)	E4(R)			
	1.2	0.05	0.9	1.25	-0.25			
5th Line	P12(R)	a1(R)	b1(R)	c1(R)	a2(R)	b2(R)	c2(R)	
	0.5	1.0	0.0	-1.33	1.33	-1.33	0	
6th Line	Ratet(R)	Ratec(R)						
	1.0	1.0						

2) Design Iterations

R=6

KL/r=50	V(kN)	Pbr(kN)	Tn(sec.)
1st	122.74	68.61	0.85
2nd	62.18	34.76	1.20
3rd	49.41	27.62	1.35
4th	45.68	25.53	1.40
5th	44.58	24.92	1.42
6th	44.16	24.69	1.42

θ = 0.46364761

R= 6

Figure F.10 Outcomes of Calculations for R=6 and KL/r=50

Outcomes of Calculations Below

T/C, R=6	Pbr =	24.69	(kN)	Fy =	35.0	(kN/cm^2)							
	E =	20000.0	(kN/cm^2)	L =	849.7	(cm)							
	B(cm)	D(cm)	t(cm)	B-2t(cm)	A(cm^2)	I_y(cm^4)	$I_{y,req'd}$(cm^4)	r_y(cm)	$r_{y,req'd}$(cm)	Z_y(cm^3)	L/r	Py	Pcr
L/r=100	20.8	20.8	0.01	20.8	0.7053	50.92	50.92	8.50	8.50	5.50	100	24.69	13.92

Detailed Calculations

1) Bracing Members for Element #5 in DRAIN-2DX)

Control Information

One Line	nmbt(I)
	1

Property Types

1st Line	itt(I)	Area(R)	RI(R)	Effek(R)	Plamom(R)	Yiestr(R)	E0(R)	Harden(R)
	1	0.71	50.92	1.0	192.67	35.0	20000.0	0.0
2nd Line	Theta0(R)							
	0.0							
3rd Line	isec(I)	itemax(I)	tol(R)	styp(R)				
	31	100	0.00001	0.00001				
4th Line	Beta(R)	E1(R)	E2(R)	E3(R)	E4(R)			
	1.2	0.05	0.9	1.25	-0.25			
5th Line	P12(R)	a1(R)	b1(R)	c1(R)	a2(R)	b2(R)	c2(R)	
	0.5	1.0	0.0	-1.33	1.33	-1.33	0	
6th Line	Ratet(R)	Ratec(R)						
	1.0	1.0						

2) Design Iterations

R=6

KL/r=100	V(kN)	Pbr(kN)	Tn(sec.)
1st	122.74	68.61	0.85
2nd	62.18	34.76	1.20
3rd	49.41	27.62	1.35
4th	45.68	25.53	1.40
5th	44.58	24.92	1.42
6th	44.16	24.69	1.42
7th			
8th	27.84	13.92	1.42
9th	264.97		

θ = 0.46364761

R= 9.51614935

Figure F.11 Outcomes of Calculations for R=6 and KL/r=100

Outcomes of Calculations Below

T/C,	Pbr =	24.92	(kN)	Fy =	35.0	(kN/cm^2)							
R=6	E =	20000.0	(kN/cm^2)	L =	849.7	(cm)							
	B(cm)	D(cm)	t(cm)	B-2t(cm)	A(cm^2)	I_y(cm^4)	$I_{y,eq'd}$(cm^4)	r_y(cm)	$r_{y,eq'd}$(cm)	Z_y(cm^3)	L/r	Py	Pcr
L/r=150	13.9	13.9	0.01	13.9	0.7053	22.63	22.63	5.66	5.66	3.67	150	24.69	6.19

Detailed Calculations

1) Bracing Members for Element #5 in DRAIN-2DX)

Control Information

One Line	nmbt(I) 1

Property Types

1st Line	itt(I) 1	Area(R) 0.71	RI(R) 22.63	Effek(R) 1.0	Plamom(R) 128.45	Yiestr(R) 35.0	E0(R) 20000.0	Harden(R) 0.0
2nd Line	Theta0(R) 0.0							
3rd Line	isec(I) 31	itemax(I) 100	tol(R) 0.00001	styp(R) 0.00001				
4th Line	Beta(R) 1.2	E1(R) 0.05	E2(R) 0.9	E3(R) 1.25	E4(R) -0.25			
5th Line	P12(R) 0.5	a1(R) 1.0	b1(R) 0.0	c1(R) -1.33	a2(R) 1.33	b2(R) -1.33	c2(R) 0	
6th Line	Ratet(R) 1.0	Ratec(R) 1.0						

2) Design Iterations

R=6

KL/r=150	V(kN)	Pbr(kN)	Tn(sec.)
1st	122.74	68.61	0.85
2nd	62.18	34.76	1.20
3rd	49.41	27.62	1.35
4th	45.68	25.53	1.40
5th	44.58	24.92	1.42
6th	44.16	24.69	1.42
7th			
8th	12.38	6.19	1.42
9th	264.97		

θ = 0.46364761

R= 21.411335

Figure F.12 Outcomes of Calculations for R=6 and KL/r=150

Outcomes of Calculations Below

T/C, R=8	Pbr =	16.05	(kN)	Fy =	35.0	(kN/cm^2)								
	E =	20000.0	(kN/cm^2)	L =	849.7	(cm)								
	B(cm)	D(cm)	t(cm)	B-2t(cm)	A(cm^2)	Areq'd(cm^2)	I_y(cm^4)	$I_{y,req'd}$(cm^4)	r_y(cm)	$r_{y,req'd}$(cm)	Z_y(cm^3)	L/r	Py	Pcr
L/r=50	41.6	41.6	0.00	41.6	0.4585	0.4585	132.41	132.41	16.99	16.99	7.16	50	16.05	36.20

Detailed Calculations

1) Bracing Members for Element #5 in DRAIN-2DX)

Control Information

One Line	nmbt(I)
	1

Property Types

1st Line	itt(I)	Area(R)	RI(R)	Effek(R)	Plamom(R)	Yiestr(R)	E0(R)	Harden(R)
	1	0.46	132.41	1.0	250.50	35.0	20000.0	0.0
2nd Line	Theta0(R)							
	0.0							
3rd Line	isec(I)	itemax(I)	tol(R)	styp(R)				
	31	100	0.00001	0.00001				
4th Line	Beta(R)	E1(R)	E2(R)	E3(R)	E4(R)			
	1.2	0.05	0.9	1.25	-0.25			
5th Line	P12(R)	a1(R)	b1(R)	c1(R)	a2(R)	b2(R)	c2(R)	
	0.5	1.0	0.0	-1.33	1.33	-1.33	0	
6th Line	Ratet(R)	Ratec(R)						
	1.0	1.0						

2) Design Iterations

R=8

KL/r=50	V(kN)	Pbr(kN)	Tn(sec.)
1st	92.06	51.46	0.99
2nd	42.13	23.55	1.46
3rd	32.51	18.18	1.66
4th	29.85	16.68	1.73
5th	29.04	16.23	1.76
6th	28.70	16.05	1.76

θ = 0.46364761

R= 8

Figure F.13 Outcomes of Calculations for R=8 and KL/r=50

Outcomes of Calculations Below

T/C,	Pbr =	16.05	(kN)	Fy =	35.0	(kN/cm^2)							
R=8	E =	20000.0	(kN/cm^2)	L =	849.7	(cm)							
	B(cm)	D(cm)	t(cm)	B-2t(cm)	A(cm^2)	I_y(cm^4)	$I_{y,eq'd}$(cm^4)	r_y(cm)	$r_{y,eq'd}$(cm)	Z_y(cm^3)	L/r	Py	Pcr
L/r=100	20.8	20.8	0.01	20.8	0.4585	33.10	33.10	8.50	8.50	3.58	100	16.05	9.05

Detailed Calculations

1) Bracing Members for Element #5 in DRAIN-2DX)

Control Information

One Line	nmbt(I)
	1

Property Types

1st Line	itt(I) 1	Area(R) 0.46	RI(R) 33.10	Effek(R) 1.0	Plamom(R) 125.25	Yiestr(R) 35.0	E0(R) 20000.0	Harden(R) 0.0
2nd Line	Theta0(R) 0.0							
3rd Line	isec(I) 31	itemax(I) 100	tol(R) 0.00001	styp(R) 0.00001				
4th Line	Beta(R) 1.2	E1(R) 0.05	E2(R) 0.9	E3(R) 1.25	E4(R) -0.25			
5th Line	P12(R) 0.5	a1(R) 1.0	b1(R) 0.0	c1(R) -1.33	a2(R) 1.33	b2(R) -1.33	c2(R) 0	
6th Line	Ratet(R) 1.0	Ratec(R) 1.0						

2) Design Iterations

R=8

KL/r=100	V(kN)	Pbr(kN)	Tn(sec.)
1st	92.06	51.46	0.99
2nd	42.13	23.55	1.46
3rd	32.51	18.18	1.66
4th	29.85	16.68	1.73
5th	29.04	16.23	1.76
6th	28.70	16.05	1.76
7th			
8th	18.10	9.05	1.76
9th	229.64		

θ = 0.46364761

R= 12.6866291

Figure F.14 Outcomes of Calculations for R=8 and KL/r=100

Outcomes of Calculations Below

T/C, R=8	Pbr =	16.05	(kN)	Fy =	35.0	(kN/cm^2)							
	E =	20000.0	(kN/cm^2)	L =	849.7	(cm)							
	B(cm)	D(cm)	t(cm)	B-2t(cm)	A(cm^2)	I_y(cm^4)	$I_{y,req'd}$(cm^4)	r_y(cm)	$r_{y,req'd}$(cm)	Z_y(cm^3)	L/r	Py	Pcr
L/r=150	13.9	13.9	0.01	13.9	0.4585	14.71	14.71	5.66	5.66	2.39	150	16.05	4.02

Detailed Calculations

1) Bracing Members for Element #5 in DRAIN-2DX)

Control Information

One Line	nmbt(I)
	1

Property Types

1st Line	itt(I)	Area(R)	RI(R)	Effek(R)	Plamom(R)	Yiestr(R)	E0(R)	Harden(R)
	1	0.46	14.71	1.0	83.50	35.0	20000.0	0.0
2nd Line	Theta0(R)							
	0.0							
3rd Line	isec(I)	itemax(I)	tol(R)	styp(R)				
	31	100	0.00001	0.00001				
4th Line	Beta(R)	E1(R)	E2(R)	E3(R)	E4(R)			
	1.2	0.05	0.9	1.25	-0.25			
5th Line	P12(R)	a1(R)	b1(R)	c1(R)	a2(R)	b2(R)	c2(R)	
	0.5	1.0	0.0	-1.33	1.33	-1.33	0	
6th Line	Ratet(R)	Ratec(R)						
	1.0	1.0						

2) Design Iterations

R=8

KL/r=150	V(kN)	Pbr(kN)	Tn(sec.)
1st	92.06	51.46	0.99
2nd	42.13	23.55	1.46
3rd	32.51	18.18	1.66
4th	29.85	16.68	1.73
5th	29.04	16.23	1.76
6th	28.70	16.05	1.76
7th			
8th	8.04	4.02	1.76
9th	229.64		

θ = 0.46364761

R= 28.5449142

Figure F.15 Outcomes of Calculations for R=8 and KL/r=150

APPENDIX G

Case Study 2

(Effects of Member Length (L) on R)

Outcomes of Calculations Below

T/C, R=1	Pbr =	363.09	(kN)	Fy =	35.0	(kN/cm^2)								
	E =	20000.0	(kN/cm^2)	L =	849.7	(cm)								
	B(cm)	D(cm)	t(cm)	B-2t(cm)	A(cm^2)	Areq'd(cm^2)	I_x(cm^4)	$I_{y,eq'd}$(cm^4)	r_x(cm)	$r_{y,eq'd}$(cm)	Z_x(cm^3)	L/r	Py	Pcr
L/r=50	41.7	41.7	0.06	41.6	10.3739	10.3739	2995.99	2995.99	16.99	16.99	161.94	50	363.09	819.09
												100	363.09	204.77
												150	363.09	91.01

Detailed Calculations

1) Bracing Members for Element #5 in DRAIN-2DX)

Control Information

One Line	nmbt(I) 1

Property Types

1st Line	itt(I) 1	Area(R) 10.37	RI(R) 2995.99	Effek(R) 1.0	Plamom(R) 5667.83	Yiestr(R) 35.0	E0(R) 20000.0	Harden(R) 0.0
2nd Line	Theta0(R) 0.0							
3rd Line	isec(I) 31	itemax(I) 100	tol(R) 0.00001	styp(R) 0.00001				
4th Line	Beta(R) 1.2	E1(R) 0.05	E2(R) 0.9	E3(R) 1.25	E4(R) -0.25			
5th Line	P12(R) 0.5	a1(R) 1.0	b1(R) 0.0	c1(R) -1.33	a2(R) 1.33	b2(R) -1.33	c2(R) 0	
6th Line	Ratet(R) 1.0	Ratec(R) 1.0						

2) Design Iterations

R=1

KL/r=50	V(kN)	Pbr(kN)	Tn(sec.)
1st	736.45	411.69	0.35
2nd	674.02	376.79	0.36
3rd	661.48	369.78	0.37
4th	649.51	363.09	0.37
5th			
6th			
7th			
8th		363.09	0.37
9th			
10th	366.31	204.77	0.53
11th	511.14		
12th	162.80	91.01	0.64
13th	450.75		

θ = 0.46364761

KL/r	R	B	D	L
50	1.00	760.00	380.00	849.71
100	1.40	1520.00	760.00	1699.41
150	2.77	2280.00	1140.00	2549.12

Figure G.1 Outcomes of Calculations for R=1

Outcomes of Calculations Below

T/C, R=2	Pbr =	128.68	(kN)	Fy =	35.0	(kN/cm²)								
	E =	20000.0	(kN/cm²)	L =	849.7	(cm)								
	B(cm)	D(cm)	t(cm)	B-2t(cm)	A(cm²)	Areq'd(cm²)	I_y(cm⁴)	$I_{y,req'd}$(cm⁴)	r_y(cm)	$r_{y,req'd}$(cm)	Z_y(cm³)	L/r	Py	Pcr
L/r=50	41.6	41.6	0.02	41.6	3.6767	3.6767	1061.82	1061.82	16.99	16.99	57.39	50	128.68	290.30
												100	128.68	72.58
												150	128.68	32.26

Detailed Calculations

1) Bracing Members for Element #5 in DRAIN-2DX)

Control Information

One Line	nmbt(I)
	1

Property Types

1st Line	itt(I)	Area(R)	RI(R)	Effek(R)	Plamom(R)	Yiestr(R)	E0(R)	Harden(R)
	1	3.68	1061.82	1.0	2008.76	35.0	20000.0	0.0
2nd Line	Theta0(R)							
	0.0							
3rd Line	isec(I)	itemax(I)	tol(R)	styp(R)				
	31	100	0.00001	0.00001				
4th Line	Beta(R)	E1(R)	E2(R)	E3(R)	E4(R)			
	1.2	0.05	0.9	1.25	-0.25			
5th Line	P12(R)	a1(R)	b1(R)	c1(R)	a2(R)	b2(R)	c2(R)	
	0.5	1.0	0.0	-1.33	1.33	-1.33	0	
6th Line	Ratet(R)	Ratec(R)						
	1.0	1.0						

2) Design Iterations

R=2

KL/r=50	V(kN)	Pbr(kN)	Tn(sec.)
1st	368.23	205.84	0.49
2nd	269.30	150.54	0.58
3rd	240.66	134.53	0.61
4th	232.71	130.09	0.62
5th	230.20	128.68	0.62
6th			
7th			
8th		128.68	0.62
9th			
10th	129.83	72.58	0.88
11th	364.53		
12th	57.70	32.26	1.08
13th	318.01		

θ = 0.46364761

KL/r	R	B	D	L
50	2.00	760.00	380.00	849.71
100	2.81	1520.00	760.00	1699.41
150	5.51	2280.00	1140.00	2549.12

Figure G.2 Outcomes of Calculations for R=2

Outcomes of Calculations Below

T/C, R=4	Pbr =	45.29	(kN)	Fy =	35.0	(kN/cm^2)								
	E =	20000.0	(kN/cm^2)	L =	849.7	(cm)								
	B(cm)	D(cm)	t(cm)	B-2t(cm)	A(cm^2)	Areq'd(cm^2)	I_y(cm^4)	$I_{y,eq'd}$(cm^4)	r_y(cm)	$r_{y,eq'd}$(cm)	Z_y(cm^3)	L/r	Py	Pcr
L/r=50	41.6	41.6	0.01	41.6	1.2939	1.2939	373.67	373.67	16.99	16.99	20.20	50	45.29	102.16
												100	45.29	25.54
												150	45.29	11.35

Detailed Calculations

1) Bracing Members for Element #5 in DRAIN-2DX)

Control Information

One Line	nmbt(I)
	1

Property Types

1st Line	itt(I)	Area(R)	RI(R)	Effek(R)	Plamom(R)	Yiestr(R)	E0(R)	Harden(R)
	1	1.29	373.67	1.0	706.92	35.0	20000.0	0.0
2nd Line	Theta0(R)							
	0.0							
3rd Line	isec(I)	itemax(I)	tol(R)	styp(R)				
	31	100	0.00001	0.00001				
4th Line	Beta(R)	E1(R)	E2(R)	E3(R)	E4(R)			
	1.2	0.05	0.9	1.25	-0.25			
5th Line	P12(R)	a1(R)	b1(R)	c1(R)	a2(R)	b2(R)	c2(R)	
	0.5	1.0	0.0	-1.33	1.33	-1.33	0	
6th Line	Ratet(R)	Ratec(R)						
	1.0	1.0						

2) Design Iterations

R=4

KL/r=50	V(kN)	Pbr(kN)	Tn(sec.)
1st	184.11	102.92	0.70
2nd	106.15	59.34	0.92
3rd	88.47	49.46	1.01
4th	83.13	46.47	1.04
5th	81.53	45.58	1.05
6th	81.01	45.29	1.05
7th			
8th		45.29	1.05
9th			
10th	45.69	25.54	1.49
11th	256.60		
12th	20.31	11.35	1.82
13th	224.56		

θ = 0.46364761

KL/r	R	B	D	L
50	4.00	760.00	380.00	849.71
100	5.62	1520.00	760.00	1699.41
150	11.06	2280.00	1140.00	2549.12

Figure G.3 Outcomes of Calculations for R=4

Outcomes of Calculations Below

T/C, R=6	Pbr =	24.69	(kN)	Fy =	35.0	(kN/cm^2)								
	E =	20000.0	(kN/cm^2)	L =	849.7	(cm)								
	B(cm)	D(cm)	t(cm)	B-2t(cm)	A(cm^2)	Areq'd(cm^2)	I_y(cm^4)	$I_{y,req'd}$(cm^4)	r_y(cm)	$r_{y,req'd}$(cm)	Z_y(cm^3)	L/r	Py	Pcr
L/r=50	41.6	41.6	0.00	41.6	0.7053	0.7053	203.70	203.70	16.99	16.99	11.01	50	24.69	55.69
												100	24.69	13.92
												150	24.69	6.19

Detailed Calculations

1) Bracing Members for Element #5 in DRAIN-2DX)

Control Information

One Line	nmbt(I)
	1

Property Types

1st Line	itt(I)	Area(R)	RI(R)	Effek(R)	Plamom(R)	Yiestr(R)	E0(R)	Harden(R)
	1	0.71	203.70	1.0	385.37	35.0	20000.0	0.0
2nd Line	Theta0(R)							
	0.0							
3rd Line	isec(I)	itemax(I)	tol(R)	styp(R)				
	31	100	0.00001	0.00001				
4th Line	Beta(R)	E1(R)	E2(R)	E3(R)	E4(R)			
	1.2	0.05	0.9	1.25	-0.25			
5th Line	P12(R)	a1(R)	b1(R)	c1(R)	a2(R)	b2(R)	c2(R)	
	0.5	1.0	0.0	-1.33	1.33	-1.33	0	
6th Line	Ratet(R)	Ratec(R)						
	1.0	1.0						

2) Design Iterations

R=6	KL/r=50	V(kN)	Pbr(kN)	Tn(sec.)
	1st	122.74	68.61	0.85
	2nd	62.18	34.76	1.20
	3rd	49.41	27.62	1.35
	4th	45.68	25.53	1.40
	5th	44.58	24.92	1.42
	6th	44.16	24.69	1.42
	7th			
	8th		24.69	1.42
	9th			
	10th	24.91	13.92	2.01
	11th	210.18		
	12th	11.07	6.19	2.46
	13th	183.69		

θ = 0.46364761

KL/r	R	B	D	L
50	6.00	760.00	380.00	849.71
100	8.44	1520.00	760.00	1699.41
150	16.59	2280.00	1140.00	2549.12

Figure G.4 Outcomes of Calculations for R=6

Outcomes of Calculations Below

T/C, R=8	Pbr =	16.05	(kN)	Fy =	35.0	(kN/cm^2)								
	E =	20000.0	(kN/cm^2)	L =	849.7	(cm)								
	B(cm)	D(cm)	t(cm)	B-2t(cm)	A(cm^2)	Areq'd(cm^2)	I_y(cm^4)	$I_{y,req'd}$(cm^4)	r_y(cm)	$r_{y,req'd}$(cm)	Z_y(cm^3)	L/r	Py	Pcr
L/r=50	41.6	41.6	0.00	41.6	0.4585	0.4585	132.41	132.41	16.99	16.99	7.16	50	16.05	36.20
												100	16.05	9.05
												150	16.05	4.02

Detailed Calculations

1) Bracing Members for Element #5 in DRAIN-2DX)

Control Information

One Line	nmbt(I)
	1

Property Types

1st Line	itt(I)	Area(R)	RI(R)	Effek(R)	Plamom(R)	Yiestr(R)	E0(R)	Harden(R)
	1	0.46	132.41	1.0	250.50	35.0	20000.0	0.0
2nd Line	Theta0(R)							
	0.0							
3rd Line	isec(I)	itemax(I)	tol(R)	styp(R)				
	31	100	0.00001	0.00001				
4th Line	Beta(R)	E1(R)	E2(R)	E3(R)	E4(R)			
	1.2	0.05	0.9	1.25	-0.25			
5th Line	P12(R)	a1(R)	b1(R)	c1(R)	a2(R)	b2(R)	c2(R)	
	0.5	1.0	0.0	-1.33	1.33	-1.33	0	
6th Line	Ratet(R)	Ratec(R)						
	1.0	1.0						

2) Design Iterations

R=8

KL/r=50	V(kN)	Pbr(kN)	Tn(sec.)
1st	92.06	51.46	0.99
2nd	42.13	23.55	1.46
3rd	32.51	18.18	1.66
4th	29.85	16.68	1.73
5th	29.04	16.23	1.76
6th	28.70	16.05	1.76
7th			
8th		16.05	1.76
9th			
10th	16.19	9.05	2.49
11th	182.22		
12th	7.20	4.02	3.05
13th	159.17		

θ = 0.46364761

KL/r	R	B	D	L
50	8.00	760.00	380.00	849.71
100	11.25	1520.00	760.00	1699.41
150	22.12	2280.00	1140.00	2549.12

Figure G.5 Outcomes of Calculations for R=8

MCEER
MULTIDISCIPLINARY CENTER FOR EARTHQUAKE ENGINEERING RESEARCH
A National Center of Excellence in Advanced Technology Applications

University at Buffalo, State University of New York
Red Jacket Quadrangle ■ Buffalo, New York 14261-0025
Phone: 716/645-3391 ■ Fax: 716/645-3399
E-mail: mceer@acsu.buffalo.edu ■ WWW Site: http://mceer.buffalo.edu

University at Buffalo *The State University of New York*

ISSN 1520-295X